Physiological and morphological analysis of a coordinating circuit

Inaugural-Dissertation

zur

Erlangung des Doktorgrades

der Mathematisch-Naturwissenschaftlichen Fakultät

der Universität zu Köln

vorgelegt von

Felix Blumenthal

aus Bonn

Köln 2018

Berichterstatter:

Dr. Carmen Wellmann

Prof. Dr. Ansgar Büschges

Tag der mündlichen Prüfung:

03.09.2018

Table of Contents

Zusammenfassung

Während des Schwimmens werden die vier paarigen Pleopoden (Swimmerets), die sich am Abdomen des Flusskrebses befinden, von posterior nach anterior in einer metachronalen Welle mit einer Phasenverzögerung von 23 ± 7% zwischen jedem Segment koordiniert. Dabei wird jeweils jeder einzelne Pleopod von Motorneuronen innerviert, die von einem individuellen, lokalen zentralen Mustergenerator (CPG), gesteuert werden. Die intersegmentale Koordination der CPGs wird durch drei Neurone in jedem Hemisegment erreicht, die ein koordinierendes Netzwerk bilden. Ein aufsteigendes (ASC_E) und ein absteigendes (DSC) koordinierendes Neuron kodieren die Information über den Aktivitätsstatus ihres eigenen Moduls und projizieren diese Information zu den anderen Ganglien. Das Kommissurale Interneuron 1 (ComInt1), ein Neuron das keine Aktionspotenziale generiert, dekodiert diese Information, die von den drei koordinierenden Neuronen mit einem Gradienten an synaptischer Stärke übertragen wird. Dabei wird das größte erregende postsynaptische Potenzial (EPSP) von den direkt benachbarten koordinierenden Neuronen hervorgerufen, die kleinsten von den koordinierenden Neuronen deren Ursprung am weitesten entfernet ist. Dabei sind die EPSPs von ASC_E immer größer als die von DSC.

Die koordinierenden Neurone adaptieren an das Erregungslevel des Systems, indem sie ihre Kodierungseigenschaften an das Erregungslevel anpassen und so große Unterschiede in der Burststärke durch einen engen Bereich von Aktionspotenzialen kodieren können. Dieser Befund führte zu der Hypothese, dass ComInt1 seine Dekodierungseigenschaften ebenfalls an das Erregungslevel des Systems anpasst. Aus diesem Grund habe ich die intrazellulär gemessene Aktivität von ComInt1 aufgenommen und das Erregungsniveau des Systems geändert, indem ich Carbachol (CCh, ein cholinerger Agonist), das Peptid Crustacean Cardiocative Peptide (CCAP, ein muskarinischer Agonist) oder Edrophoniumchlorid (EdCl, ein Acetylcholinesterase-Inhibitor) appliziert habe. Um die direkten und indirekten Wirkungen der Chemikalien zu untersuchen, analysierte ich die Membranpotentialoszillationen und die EPSPs von ComInt1, zusammengefasst als C1-Intensität. Außerdem habe ich die Membranpotentialänderungen von ComInt1 analysiert, sowie den Eingangswiderstand der Membran in einem intakten Netzwerk und im isolierten Neuron gemessen. ComInt1

adaptierte an das Erregungslevel seines eignen CPGs, von dem es über eine elektrische Synapse kontinuierlich die Aktivität erfasste. Zudem empfing ComInt1 über chemische Synapsen periodische Eingänge von den koordinierenden Neuronen. Daher ist ComInt1 in der Lage, Informationen der anderen drei CPGs zu dekodieren, zu integrieren und Fehlanpassungen zwischen den Aktivitätszuständen aller vier ipsilateral gekoppelten Oszillatoren zu erkennen und diese Aktivitäten miteinander zu synchronisieren.

In dem zweiten Teil meiner Arbeit untersuchte ich, wie der Gradient der synaptischen Stärke in ComInt1 erreicht wird. Ich stellte die Hypothese auf, dass die unterschiedlich großen EPSPs auf Unterschiede in der Anzahl der Synapsen oder auf die Größe der Synapsen zurückzuführen sind, die die koordinierenden Neurone und ComInt1 bilden. Um diese Hypothese zu untersuchen, habe ich ComInt1 und einzelne koordinierende Neurone iontophoretisch mit Fluoreszenzfarbstoffen gefärbt und präsynaptische Endigungen der koordinierenden Neurone immunohistochemisch mit Anti-Synapsin markiert. Ich identifizierte Synapsen von koordinierenden Neuronen dorsal an der Mittelline. In diesem Bereich hat ComInt1 einen aufsteigenden und absteigenden dendritischen Ast und die Axone der koordinierenden Neurone passieren hier die Ganglien. Ich berechnete das Volumen der kolokalisierten Bereiche der farbstoffgefüllten koordinierenden Neurone und immunohistochemisch markierten präsynaptischen Endigungen, die den ersten Hinweis dafür lieferten, dass der Gradient der synaptischen Stärke seinen Ursprung in der synaptischen Zusammensetzung hat.

Abstract

During swimming the four paired swimmerets on the crayfish's abdomen are coordinated in an anteriorly proceeding metachronal wave with a phase lag of 23 ± 7% between each segment. Each swimmeret is innervated by motor neurons which are driven by local interneurons of the central pattern generator (CPG). The intersegmental coordination of the CPGs is achieved by three neurons located in each hemisegment that form a coordinating circuit. One ascending (ASC_E) and one descending (DSC) Coordinating Neuron encode the information about the status of their home module and project it to other ganglia. A nonspiking neuron, Commissural Interneuron 1 (ComInt1), decodes this information transmitted by three Coordinating Neurons with a gradient of synaptic strength. The largest excitatory postsynaptic potential (EPSP) is elicited by the directly adjacent Coordinating Neurons, the smallest of the Coordinating Neurons whose origin is the most distant. Thereby, EPSPs elicited by ASC_E are always larger than those of DSC.

Coordinating Neurons adapt to the system's excitation level by tuning their encoding properties, so that large differences in burst strength are encoded by a narrow range of spikes. This finding led to the hypothesis that ComInt1 also adapts to the level of excitation by similarly tuning its decoding abilities. Therefore, I recorded intracellularly from ComInt1 and changed the excitation level by bath application of carbachol (CCh; cholinergic agonist), crustacean cardioactive peptide (CCAP, muscarinic agonist), or edrophonium chloride (EdCl; acetylcholine esterase inhibitor). To investigate direct and indirect actions of the drugs, I analyzed ComInt1's membrane oscillations and its EPSP shapes, resulting in the C1 intensity. Moreover, I analyzed its membrane potential changes and measured input resistance with the network intact and in the isolated neuron. ComInt1 adapts to the excitation level of its own CPG. Moreover, ComInt1 continuously samples the activity of its own microcircuit via an electrical synapse and receives perturbations transmitted via chemical synapses from the Coordinating Neurons. Therefore, it is capable to decode and to integrate information of the other three CPGs and to detect mismatches between the states of activity of all four ipsilateral coupled oscillators to synchronize those activities to each other.

Secondly, I investigated how the gradient of synaptic strength in ComInt1 is achieved. I hypothesized that the different sized EPSPs are due to differences in the number of synapses or in the size of synapses the Coordinating Neurons form onto ComInt1. Therefore, I iontophoretically filled ComInt1 and single Coordinating Neurons with fluorescence dyes and immunohistochemically labeled presynaptic boutons of Coordinating Neurons with Anti-Synapsin. I identified synapses of Coordinating Neurons at the dorsal midline region, where ComInt1 has one ascending and descending dendritic branch. Moreover, the axons of the Coordinating Neurons pass through the other ganglia in this region. I calculated the volume of the colocalized areas of dye-filled Coordinating Neurons and immunohistochemically labeled presynaptic boutons, which provided the first evidence that the gradient of synaptic strengths has its origin in the synaptic composition.

1.Introduction

The investigation of the control and coordination of the body, motor control, is one of the most studied branches of research in neuroscience. The questions researchers address in this field of neuroscience are how the central nervous system (CNS) generates behavior as measured by the only observable output: movements. The capability to move is the absolute requirement for an animal, including humans, to survive. Movements can be subdivided in non-locomotory and locomotory. On the non-locomotory side are i.a. the motor control of respiration (Smith et al. 1991), chewing and digestion (Harris-Warrick et al. 1992). Locomotion evolved in order for animals to navigate through the environment they inhabit and to that they have to adjust their locomotion type. Walking and crawling is observable in terrestrial animals, swimming is preferred by aquatic animals, whereas aerial animals fly. All types of locomotion are goal directed in order to find food, to mate with other conspecifics, to escape predators, or to avoid poor environmental conditions. That means that locomotion is not only essential for individual animals to survive, but rather essential for a species to avoid extinction.

The board of control of motor patterns is located at relatively low levels of the CNS, in both, vertebrates and invertebrates that produce alternating and rhythmic movements of the body or appendages. Movements are driven by central pattern generators (CPG), which are located in vertebrate spinal cord segments, and in the segmented invertebrate ventral nerve cord, respectively (Delcomyn 1980; Marder and Calabrese 1996; Pearson 2000). CPGs produce rhythmic motor activity by either reciprocal inhibition or excitatory connections between two neurons or two neuronal groups that in turn drive alternating activity of antagonistic motor neuron groups, which innervate antagonistic muscles to generate movements. In all animals, CPGs require the precise timing of their activity to precisely execute meaningful movements that control body segments, limbs, or limb joints for goal directed locomotion. CPGs, and therefore locomotion, can be activated by descending inputs. However, throughout the movement, the locomotor networks have to continuously adjust their outputs, monitored by sense organs or corollary discharge neurons, to maintain body posture, body height or speed, to fulfill the motor task. There are several systems in which CPGs for locomotion are identified: leech swimming (Kristan and Calabrese 1976), insect walking (Pearson and Iles 1970), locust flight

(Wilson 1961), lamprey swimming (Cohen and Wallen 1980) or mouse walking (Smith and Feldman 1987). The advantage of using invertebrate model systems is that the motor pattern, in form of fictive locomotion, can be initiated at the level of the ventral nerve cord with sufficient sensory input or even without sensory input, while descending inputs are absent. Furthermore, the invertebrate CNS is constituted of fewer neurons than vertebrate CNS preparations. The neurons that form CPGs are mostly identified and are more accessible, additionally.

For this reason, invertebrate model systems are suitable to study the coordination of segmentally distributed CPGs. The coordination of distributed neural oscillators is essential for the generation of motor outputs to produce meaningful behaviors. However, the knowledge about the mechanisms of coordination is sparse. For example, in stick insect walking, sensory feedback is crucial for intra- and interleg coordination (Bässler and Büschges 1998; Büschges 1995). In leech swimming, sensory inputs are more homogenous as in the stick insect. Here, coordination is predominantly mediated by direct interactions of CPGs or indirectly by Coordinating Neurons (Friesen and Hocker 2001; Pearce and Friesen 1984; Pearce and Friesen 1985; 1988). In both, stick insect and leech, the networks coordinating the oscillators in different segments or leg joints, are not understood on the cellular level. In contrast, the crayfish swimmeret system is an excellent model to investigate neural mechanisms of coordination because its modular CPGs are anatomically separated and distributed across different segments. In each module the neurons of the CPGs are identified. During swimming, these CPGs are coordinated. Neurons of the intersegmental coordinating circuit are identified as well (Mulloney et al. 2006; Namba and Mulloney 1999; Smarandache et al. 2009; Tschuluun et al. 2001). Furthermore, the coordination is independent of sensory feedback (Ikeda and Wiersma 1964), enabling to investigate fictive locomotion in the isolated CNS, which eases the access to nerves and neurons, as well as for neuromodulators to modulate their targets.

1.1. The crayfish swimmeret system

In this thesis, I used the swimmeret system of the signal crayfish, *Pacifastacus. leniusculus* (Fig. 1), to analyze the coordination of four bilateral pairs of CPGs, and the cellular properties of one particular neuron, under different levels of excitation. Swimmerets are four paired limbs on the abdomen of the crayfish (Fig. 1) that are used, among other functions, for forward swimming (Huxley 1880). They are located on the abdominal segments 2 (green) to 5 (cyan). The swimmerets move in cycles of alternating power-strokes (PS; retraction) and return-strokes (RS; protraction). The most posterior pair starts the movement and the anterior ones follow with a phase lag of 23 ± 7% between segments (Fig. 2 B) (Blumenthal and Smarandache-Wellmann in preparation; Davis 1968; Mulloney and Smarandache-Wellmann 2012). Each pair of swimmerets is innervated by neurons from the ganglion of the same segment. Each swimmeret is driven by its own local CPG (Fig. 2 A) (Hughes and Wiersma 1960; Mulloney and Smarandache 2010; Mulloney et al. 2003; Murchison et al. 1993).

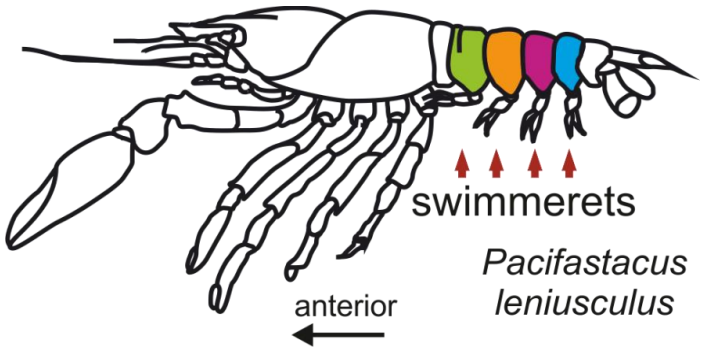

Figure 1: Schematic drawing of a crayfish. The swimmerets are paired limbs attached on the 2nd (green) to the 5th (cyan) segment of the abdomen. Swimmerets are marked by red arrows. Modified from Smarandache et al. (2009)

Each CPG consists of five non-spiking interneurons. Three of these interneurons are inhibitors of PS (IPS), which inhibit the PS motor neurons, and two are inhibitors of RS (IRS), which inhibit the RS motor neurons (Mulloney et al. 2003; Smarandache-Wellmann et al. 2013). IPS and IRS reciprocally inhibit each other (Fig. 3) (Skinner and Mulloney 1998), forming the hemiganglion's CPG. The membrane potentials of IPS and IRS oscillate in antiphase, driving hereby the alternating activity of PS and RS motor

neurons (Mulloney et al. 2003; Paul and Mulloney 1985; Skinner and Mulloney 1998; Smarandache-Wellmann et al. 2013). The cycles of alternating PS and RS movements are driven by the alternating bursting activity of the PS and RS motor neurons, whose axons project through the segmental nerve 1 (N1) to the swimmeret musculature. The axons of RS motor neurons project through the anterior branch and the axons of PS motor neurons through the posterior branch of N1 (Fig. 2 A) (Mulloney and Hall 2000; Mulloney and Smarandache-Wellmann 2012).

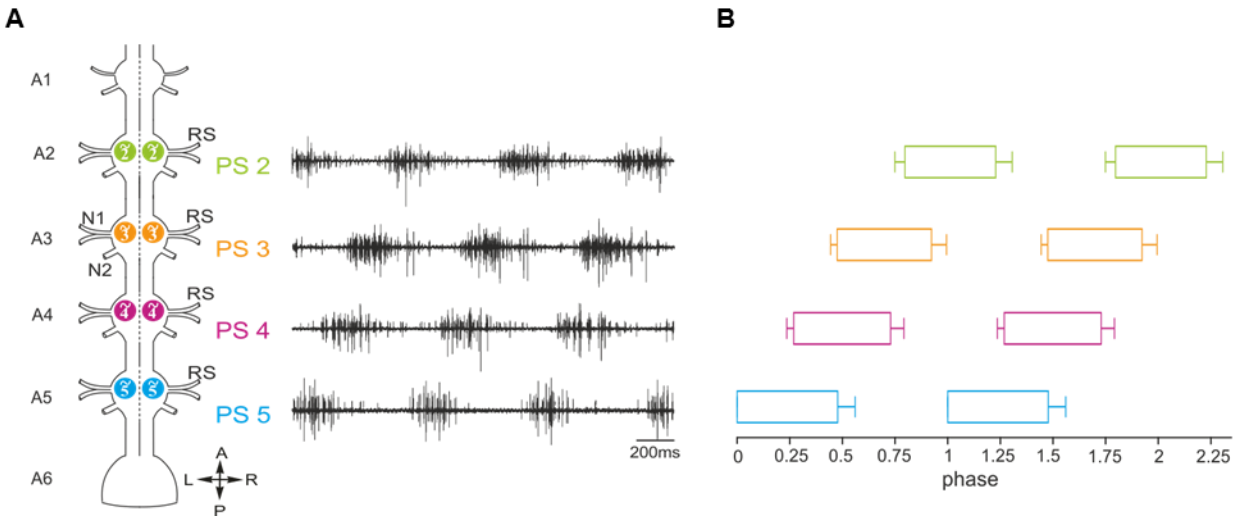

Figure 2: **A:** The abdominal nerve cord of the crayfish nervous system. Swimmerets are innervated by the segmental nerve 1 (N1) throughout the second (A2; green) to the fifth ganglion (A5; cyan). Power-stroke (PS) muscles are innervated via the axons projecting through the posterior branch of N1. The extracellular recordings depict the characteristic rhythmic activity. Each cycle starts with a burst in the most posterior ganglion (PS5; cyan) and the anterior ones (PS4, purple; PS3, orange; PS2, green) follow with a phase lag of 23 ± 7%. **B:** A phase diagram of the rhythmic activity seen in A. The phases refer to the on-set of PS5. The colors refer to the respective PS. Modified from Smarandache et al. (2009) and Smarandache-Wellmann and Grätsch (2014).

Since PS and RS are alternatingly active, it is sufficient to study coordination between segments with the help of either PS or RS movements in this case. Henceforth, I will focus only on the PS activity. PS activity from the fifth abdominal ganglion is termed as PS5. The same applies for A4 (PS in A4 ≙ PS4), A3 (PS in A3 ≙ PS3), and A2 (PS in A2 ≙ PS2).

The activity of PS motor neurons in each ganglion can be recorded extracellularly from the posterior branch of N1, showing the posterior to anterior progression with a phase lag of approximately 23% between the PS bursts (Fig. 2 A & B) (Blumenthal and Smarandache-Wellmann in preparation). As *in vivo,* the phase lag between segments is independent of the frequency of the rhythm in the isolated swimmeret system (Acevedo et al. 1994; Braun and Mulloney 1995; Ikeda and Wiersma 1964). Coordination is considered to be maintained when segment to segment phase lags vary between 16 to 30% (Blumenthal and Smarandache-Wellmann in preparation).

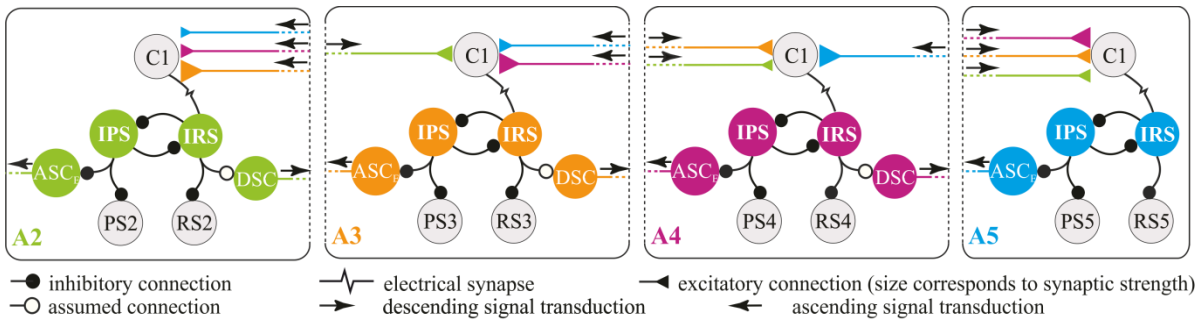

Figure 3: Summary of the ipsilateral connections in the swimmeret system. The Inhibitors of PS (IPS) and the Inhibitors of RS (IRS) form the kernel of the CPG, which are connected via reciprocal inhibition. IPS inhibits the PS motor neurons and ASC_E. IRS inhibits the RS motor neurons and DSC. Thus, a rhythmic alternating rhythm of PS and RS movements is achieved. The ascending Coordinating Neuron (ASC_E) is active when PS motor neurons are active, encodes information about timing, duration, and strength of PS bursts in its home module and projects to anterior ganglia. The descending Coordinating Neuron (DSC) is active when RS motor neurons are active, encodes the information about timing, duration, and strength of RS bursts in its home module and projects to posterior ganglia. DSC does not exist in A5. In every module, the information of all other ASC_E's and DSC's converge on a single interneuron called Commissural Interneuron 1 (C1, ComInt1), which decodes the information and affects the activity of the CPG in its home module. Comint1 is connected to IRS via an electrical synapse. Modified from Smarandache-Wellmann and Grätsch (2014).

The posterior to anterior progression is maintained by a coordinating network consisting of three neurons in each hemiganglion: two Coordinating Neurons, the ascending Coordinating Neuron (ASC_E) and the descending Coordinating Neuron (DSC), and one Commissural Interneuron 1 (ComInt1) (Fig. 3). ASC_E is located in each hemiganglion. Its activity is shaped via direct inhibitory input from IPS. It projects to anterior ganglia and encodes information about timing, duration, and relative strength of PS bursts in its home module (Fig. 3) (Namba and Mulloney 1999; Schneider 2017; Schneider et al. in preparation; Smarandache-Wellmann and Grätsch 2014). DSC is

located in every microcircuit of A2 to A4, but not in A5. Its activity is shaped via direct inhibitory input from IRS. It projects to posterior ganglia and encodes information about timing, duration, and relative strength of RS bursts in its home module (Fig. 3) (Mulloney et al. 2006; Namba and Mulloney 1999; Smarandache-Wellmann and Grätsch 2014).

The coordinating information transmitted by three different Coordinating Neurons, encoded as bursts of spikes, converges simultaneously in a single nonspiking interneuron located in each microcircuit, ComInt1 (Fig. 3 & Fig. 4 A) (Mulloney and Hall 2003). Each spike transmitted by the axons of Coordinating Neurons elicits one excitatory postsynaptic potential (EPSP) in ComInt1 (Fig. 4 A & B), using most probably acetylcholine (ACh) as neurotransmitter (Schneider et al. 2018). These excitatory inputs arrive in ComInt1 with a gradient of synaptic strength (Fig. 4 B & C) (Smarandache et al. 2009). Largest EPSPs are elicited by coordinating information from the immediate neighboring ganglia. EPSPs elicited by ASC_E are always larger than EPSPs elicited by DSC. ComInt1 in A4 and A3 receive mixed input from both ASC_E and DSC, ComInt1 in A2 receives only ASC_E input, whereas ComInt1 in A5 receives only DSC input. The strength of inputs decreases with the distance between the ganglion of origin and the target ganglion. Therefore, every ComInt1 receives a unique mix of inputs that encode information about the status of all other ganglia (Smarandache et al. 2009). This information is decoded by each ComInt1 and integrated into its own microcircuit via an electrical synapse to IRSh, one type of IRS neurons, belonging to the kernel of the CPG (Fig. 3 & 4 D) (Mulloney and Hall 2003; Smarandache-Wellmann et al. 2014). The electrical synapse between ComInt1 and IRSh allows ComInt1 to continuously vary the activity of its own CPG and vice versa. Currents injected into ComInt1 cause direct deflections of the membrane potential (V_m) of IRSh, whereby currents injected in IRSh cause direct deflections of the V_m of ComInt1 (Fig. 4 D). Moreover, the electrical synapse enables ComInt1 to indirectly modulate the PS motor output of its home module, demonstrated by current injections into ComInt1. Hyperpolarizing currents into ComInt1 inhibit the PS motor output, whereas depolarizing currents enhance PS bursts (Fig. 4 E).

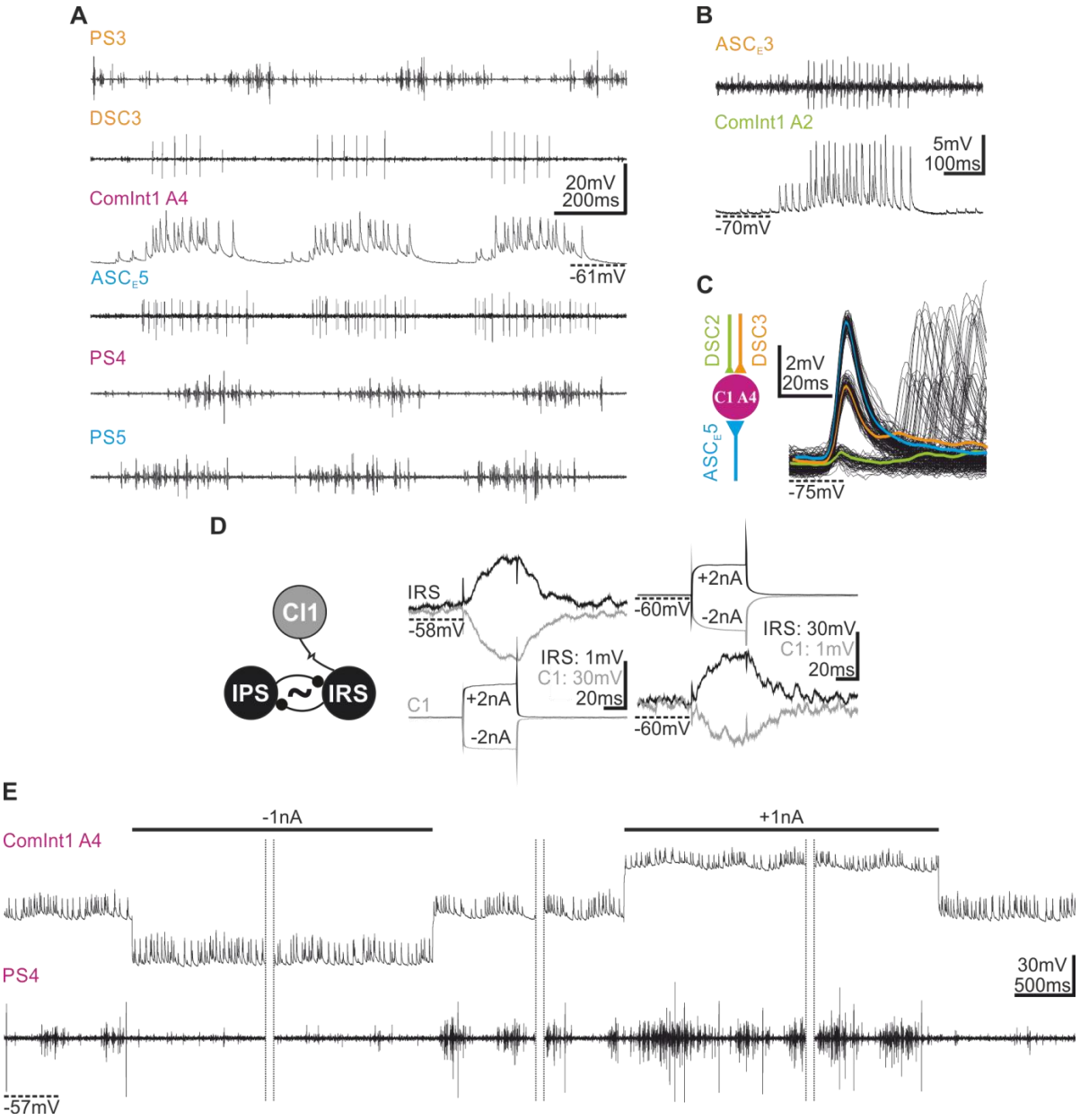

Figure 4: The physiology of ComInt1. **A:** Simultaneous extracellular recordings from coordinating axons (ASC_E5, DSC3), from PS3, PS4 and PS5, and simultaneous intracellular recording of ComInt1 in A4. ASC_E5 spikes occur simultaneously with PS5 bursts. DSC spikes occur antiphasic to PS3 bursts. Spikes of both, ASC_E and DSC arrive in ComInt1 concurrently. ComInt1's membrane oscillation starts shortly after the PS burst of its posterior neighbor ganglion (A5) but before the PS burst of its home ganglion (PS4) **B:** One cycle of an extracellular recording of ASC_E together with an intracellular recording of its target ComInt1 in the anterior neighbor ganglion. Each ASC_E spike elicits an EPSP in ComInt1 (modified from Smarandache et al., 2009). **C:** EPSPs that are elicited in ComInt1 in A4 by spikes of three different Coordinating Neurons (ASC_E5, DSC3, DSC2). The biggest EPSP is elicited by ASC_E5, the intermediate EPSP by DSC3 and the smallest EPSP by spikes from DSC2. Triangles symbolize excitatory synapses. Their size represents the synaptic strength. **D:** Simultaneous intracellular recordings of the Inhibitor of Return-Stroke hook (IRSh) and ComInt1, while the system was inactive. Depolarizing and hyperpolarizing current injections into ComInt1 caused immediate changes in IRSh and vice versa, indicating an electrical synapse between the two (resistor symbol). Filled circles symbolize inhibitory synapses. (Modified from Smarandache-Wellmann et al. 2014). **E:** Simultaneous intracellular ComInt1 recording and extracellular PS recording from its home ganglion. Hyperpolarization inhibits PS acitivity. Depolarization excites PS motor output.

1.2. Adaptation to different excitation levels

Rhythmic activity of the swimmeret system can be elicited in silent preparations and ongoing rhythmic activity can be modulated by the bath application of neuromodulators. Pilocarpine, a muscarinic agonist, activates a stable motor output of the swimmeret system (Braun and Mulloney 1993; Mulloney et al. 1987). Moreover, Braun and Mulloney (1993) found that application of nicotine did not elicit rhythmic motor output, but modulated ongoing swimmeret activity by dose-dependent increases of the output's frequency. Finally, they detected that Carbachol (CCh), a cholinergic agonist binding to muscarinic and nicotinic ACh-receptors, was able to elicit rhythmic motor output from silent preparations and furthermore to dose-dependently increase the excitation of ongoing rhythmic activity by shortening PS cycle periods and strengthening PS bursts, while phase lags between segments are maintained.

Braun and Mulloney (1995) performed split bath experiments in which they established gradients of excitation within the swimmeret system by applying CCh to different numbers of ganglia. They found that local excitation level increases affected the intrinsic periods of the CPGs. Correspondingly they observed a system wide decrease of cycle periods, whereby the period was dependent on the number of ganglia that were directly excited. The more ganglia were locally excited the shorter was the system wide cycle period. These observations led to the statement that the system's period emerges from different intrinsic periods (Skinner et al. 1997). When the boundary in the split bath experiments was between ganglia A4 and A3, Braun and Mulloney (1995) where able to expose each half of the swimmeret system to different excitation levels. They demonstrated that the period was constant, no matter if the anterior or the posterior part of the chain of ganglia were set to high or low excitation levels. However, they detected that the phase lags between ganglia at the boundary were affected.

The excitation level to which a module is set to did not only determine intrinsic cycle periods and PS burst strengths, but rather adapted the encoding of PS burst strength by ASC_E neurons (Mulloney and Hall 2007b). When excitation levels were not forced by bath application of CCh, PS bursts variations occurred spontaneously. In this case ASC_E tracked the timing, duration and PS burst strength in its home module, whereby the strength was encoded by the number of spikes in its burst. A 10% increase

in the strength of PS bursts, was encoded by one additional spike in ASC_E (Mulloney et al. 2006). This correlation was not ensured when the level of excitation was set by CCh application. Still, ASC_E tracked the timing and duration of PS bursts, but the mean number of spikes per burst did not change although the PS burst strength increased (Mulloney and Hall 2007b). These observations revealed that the Coordinating Neurons adapt to the changed excitation level to allow efficient coding of relative PS burst strengths in their home module by rescaling their gain (Schneider 2017; Schneider et al. in preparation). The excitation level determines the range of burst strengths in the whole system and rescales the encoding properties of the Coordinating Neurons. This describes a balancing mechanism for ASC_E and DSC to normalize their response range to the range of PS burst strengths, which are correlated to the excitation level. As a result, the same number of spikes can code for different burst strengths at different excitation levels (Schneider 2017; Schneider et al. in preparation).

These results can be explained by the Adaptive Encoding Hypothesis. The Coordinating Neurons and ComInt1 form a system of matched encoders and a decoder, which is tuned by the system's excitation level. If this change is uniform across the whole system, the en- and decoders operate in the same context, while non-uniform excitation level alterations create mismatches between the en- and decoders. Schneider and colleagues (in preparation) showed that the Coordinating Neurons adapted to the system's excitation level by tuning their encoding properties, so that large differences in burst strength are encoded by a narrow range of spikes. This finding leads to the hypothesis that ComInt1 also adapts to the level of excitation by similarly tuning its decoding abilities, to match its activity to different bursts strengths that correlate with the excitation level.

1.3. Aim of Study

One aim of this study is to test the above mentioned hypothesis. Therefore, I characterized the cellular properties of the decoder at different excitation levels. With this, I investigated if ComInt1 also adapts to given excitation levels to match its decoding abilities to the encoding properties of the Coordinating Neurons.

In order to uniformly set the system to different excitation levels, I used different chemicals. Aside from CCh, I used crustacean cardioactive peptide (CCAP) and edrophonium chloride (EdCl). CCAP is a muscarinic agonist, which activates silent preparations and modulates motor activity expressed by the swimmeret system (Gammie and Truman 1997; Mulloney et al. 1997; Weimann et al. 1997). Braun and Mulloney (1993) showed that the bath application of eserine, an ACh-esterase inhibitor, accelerated the burst frequency of the PS motor output similar to CCh. Additionally, Schneider (2018) could show that Coordinating Neurons contain ACh which is presumably used by Coordinating Neurons as neurotransmitter to excite ComInt1 via excitatory synapses. Therefore, I additionally used EdCl, also an ACh-esterase inhibitor, to modulate the excitation level of the swimmeret system. While changing the system's excitation level, I intracellularly recorded ComInt1 to investigate its cellular properties.

The second aim of my thesis was to unravel the gradient of synaptic strength that the Coordinating Neurons have onto ComInt1. I hypothesize that the gradient of synaptic strength has its origin in the number or in the size of synapses Coordinating Neurons form onto ComInt1. I choose a morphological approach to test this hypothesis by intracellularly dye-filling ComInt1 and Coordinating Neurons and by using immunohistochemically techniques to label synapses in the swimmeret system.

2. Materials and Methods

2.1. Animals

In my thesis I worked on adult signal crayfish, *Pacifastacus leniusculus* (DANA, 1852), of both sexes. Crayfish were fished in North Rhine-Westphalia from the Wupper at the Müngstener Brückenpark near Solingen, or from a private pond in Gummersbach by local fisher or from the Puhlheimer Bach near Cologne by the workgroup of Dr. Carmen Wellmann from the University of Cologne. They were kept in freshwater tanks at 14 to 16°C until sacrificing them in experiments. Once a week they were fed with carrots and monthly with shrimp pellets (Wardley, The Hartz Mountain Corporation, Secaucus, New Jersey, USA) additionally.

2.2. Dissection

All experiments were performed on the isolated abdominal nerve cord. For a detailed description of the preparation see Seichter et al. (2014). Briefly, the animals were anesthetized on ice for 30 min and exsanguinated by transfusion with 50ml cold normal saline (NR; concentrations in mM: 5.4 KCl, 2.6 $MgCl_2$, 13.5 $CaCl_2$ and 195 NaCl, buffered with 10 Tris base and 4.7 maleic acid at pH 7.4, and aerated for 2 h). Afterwards the crayfish were decapitated and the whole abdominal nerve cord together with the last two thoracic ganglia was isolated and pinned out straight with the dorsal side up in a dish lined with transparent Sylgard (Dow-Corning, Midland, MI, USA). Before starting the experiments the ganglia sheaths were removed on the dorsal side using fine scissors.

2.3. Electrophysiological setup

In this thesis I performed different electrophysiological protocols to characterize the cellular properties of ComInt1 and to intracellular dye-fill ComInt1 and Coordinating Neurons for later morphological experiments. Nonetheless, the general experimental electrophysiological setup was similar.

In every experiment I extracellularly recorded the bursting activity of PS motor neurons from ganglia A2 to A5 (Fig. 5, colored circles) by using stainless steel pin electrodes placed on the posterior branch of N1. I insulated the electrodes together with the target nerves from the bathing saline using petroleum jelly and placed the reference electrodes nearby to the associated recording electrode (Seichter et al., 2014). The electrodes were connected to a custom-made 12-channel 'switchbox' (Electronics Lab, University of Cologne, Germany) which was connected to two 4-channel differential amplifiers (Model 102, Electronics Lab, University of Cologne, Germany) allowing up to eight simultaneous extracellular recordings. The extracellular recordings were 1000fold amplified and filtered (low-cut 300 Hz; high-cut 2 kHz). The recordings were digitized by a Digidata 1440A (Molecular Devices, Sunnydale, CA, USA) and pClamp software (Molecular Devices) with a sampling frequency of 10 kHz to record and save the data on a computer (Dell, Round Rock, TX, USA) for later analysis.

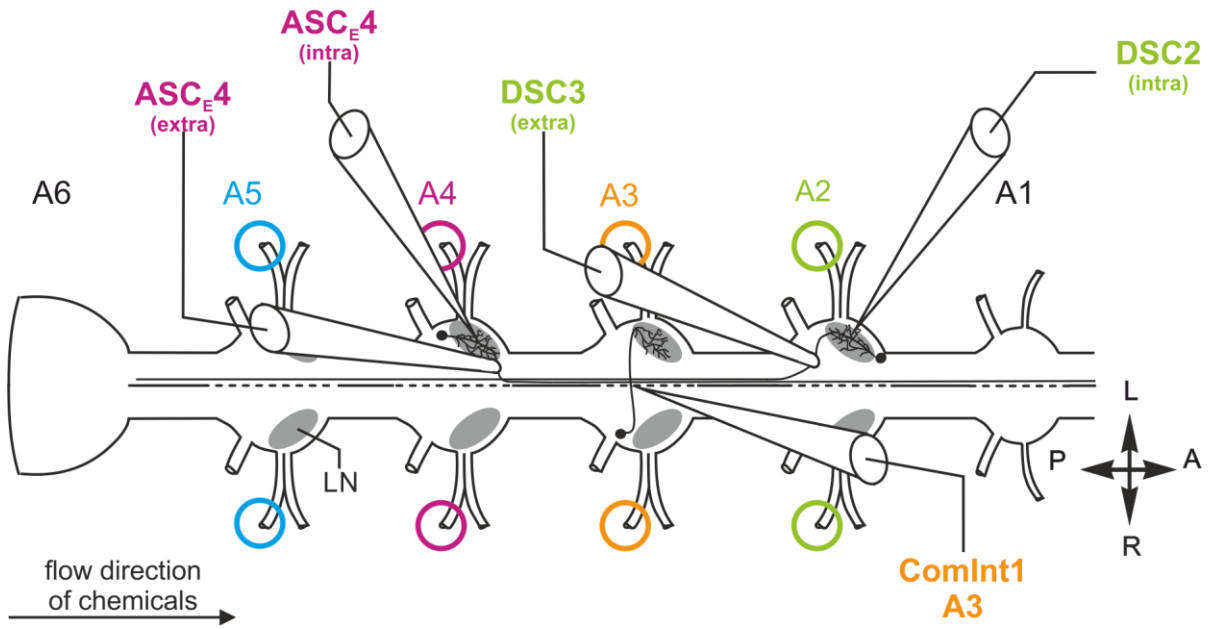

Figure 5: Experimental setup to intracellular record ComInt1, ASC$_E$ or DSC while recording extracellularly the PS activity from the posterior branch of N1 and ASC$_E$ or DSC with a suction electrode. The scheme shows the location of intracellular electrodes (intra) to record from ComInt1 and to record from ASC$_E$ or DSC. Additionally it displays the location of extracellular suction electrodes (extra) to record extracellularly the ASC$_E$ or DSC activity.

Additionally, I extracellularly recorded from one of the Coordinating Neurons with a suction electrode (MWE-F15B, Warner Instruments, Hamden, CT, USA) attached to a micromanipulator (M-3333, Narashige, Tokyo, Japan, USA). Pipetts were pulled on a P-87 micropipette puller (Sutter Instruments, Novato, CA, USA) from borosilicate capillaries (O.D. 1.5 mm; I.D. 0.86 mm, Sutter). The tip was broken down to a diameter slightly larger than the diameter of the lateral giant (LG) axon. For ASC_E recordings, I placed the suction electrode on the LG around the anterior margin of the ganglion where the anterior miniscule tract (MnT), containing the neurite of ASC_E, crosses the LG dorsally (Fig. 5; ASC_E (extra)). For DSC recordings, I placed the suction electrode on the LG posterior to the basis of N1 where the posterior MnT, containing the neurite of DSC, crosses the LG dorsally (Fig. 5; DSC (extra)). Extracellular signals from the suction electrode were preamplified 50fold (MA103, Electronics Lab) and sent to the differential amplifier. The settings were the same as for the extracellular recordings with pin electrodes

Simultaneously to extracellular recordings, I performed intracellular recordings of ComInt1 with sharp microelectrodes. I aimed for ComInt1 at the midline of the ganglion, beginning at the level of the anterior basis of the segmental nerve 2 and moving posteriorly where its neurite crosses the midline and sends its small branches anterior and posterior along the midline (Fig. 5; ComInt1). The electrode was attached to a micromanipulator (MM-3, Narishige) connected to a fine micromanipulator (Huxley Wall type MP-85, Sutter). In order to intracellularly record from ComInt1, I oriented the micromanipulator in an ankle of approximately 10 to 25° towards the abdominal nerve cord. Microelectrodes were pulled from borosilicate glass capillaries (O.D. 1 mm; I.D. 0.5 mm) with filament (Sutter Instruments) using a micropipette puller (P-1000, Sutter Instruments). The electrodes were filled with either 1% dextran Texas Red (dTR; Molecular Probes, Eugene, OR, USA) or 5% Neurobiotin Tracer (Nb; Vector Laboratories, Burlingame, CA, USA) + 1% Fluorescein (FITC; Life Technologies, Carlsbad, CA, USA) in 1 M KAc + 0.1 M KCl. The tip resistance of microelectrodes was between 20 and 60 MΩ. The intracellular signals were amplified 10fold using a SEC 05X amplifier (npi Electronic Instruments, Tamm, Germany). Recordings were made in discontinuous current clamp mode (1/4 duty cycle, 5 kHz current filter) with switching frequencies around 32 kHz.

Additionally, I intracellularly recorded from Coordinating Neurons to dye-fill them with dTR for later morphological experiments. Therefore, I used the same setting than for intracellular recordings of ComInt1, but the ankle of the micromanipulator towards the nerve cord and the region within the ganglion where I aimed for Coordinating Neurons differed. No matter if I impaled the primary neurite of Coordinating Neurons in the ipsi- or contralateral LN and independent of aiming for ASC_E or DSC (Fig. 5; ASC_E (intra), DSC (intra)), the ankle between the micromanipulator and the nerve cord was approximately 45°. I used two landmarks to intracellular record from Coordinating Neurons. Within each LN there is a region where the axons entering the LN through N1 and the margin of the connectives, passing each ganglion, run together in a 90° ankle. Anterior to this landmark I aimed for ASC_E and posterior to it for DSC.

Since none of these neurons is visible within the ganglion there need to be fulfilled criteria to confirm the identification of these neurons. ComInt1 needs to have membrane potential oscillations in phase with ASC_E activity from the posterior neighbor or in phase with the DSC activity from the direct anterior ganglion, respectively. Additionally, there should be at least one size of EPSPs that should correspond to spikes extracellularly recorded from coordinating axons in anterior or posterior ganglia. The last criteria are the effects of current injections into the neuron. Depolarizing currents into ComInt1 enhance, whereas hyperpolarizing currents decrease the bursting activity of PS in the home ganglion. The membrane potential of ASC_E and DSC should oscillate in phase or in antiphase with PS bursts in the home ganglion, respectively. The intracellular recorded spikes should correspond one to one to the spikes extracellularly recorded with the suction electrode. Depolarizations of ASC_E and DSC should enhance, and hyperpolarizations should decrease PS bursts in the target ganglion, respectively.

During the recordings the abdominal nerve cords were continuously perfused with saline and chemicals, which were delivered and removed via a perfusion pump (Alitea VS2-10R Midi, Watson-Marlow Alitea, Stockholm, Sweden). Flow rate was approximately 0.5 ml/min when searching for neurons and 1.5 to 2 ml/min during experiments. Wash-in and wash-out was considered complete after 30 to 40 ml (20-25 min) or when V_m changes reached a steady state.

2.4. Electrophysiological protocols

When I successfully impaled and identified a Coordinating Neuron, I iontophoretically stained the neuron with 1% dTR by giving short depolarizing current pulses (+1 nA; 250 ms) in 500 ms intervals into the neuron for at least 1 h. I used the same protocol to iontophoretically stain ComInt1 with 5% Nb + 1% FITC or with 1% dTR for 10 to 15 min.

After staining, I started the experiments to characterize the cellular properties of ComInt1. I conducted the experiments either with the network intact or with an isolated ComInt1. In intact network preparations, I recorded ComInt1 in NR and with chemicals changing the excitation level of the network. Therefore, I perfused 3 µM carbachol (CCh; Sigma-Aldrich, St. Louis; MO, USA) in normal saline (NR), 50 nM crustacean cardioactive peptide (CCAP; Bachem, Bubendorf, Switzerland) in NR and 75 µM edrophonium chloride (EdCl; Santa Cruz Biotechnology, Dallas, TX, USA) diluted in CCAP saline over the isolated abdominal nerve cord. If the bath application of a chemical decreased PS cycle periods and concurrently increased the PS burst strength it is considered to increase the excitation level of the swimmeret system. Prolonged PS cycle periods accompanied by weakened PS burst strength as a result of the application of a chemical describes a decrease of the excitation level of the swimmeret system.

CCh is a cholinergic agonist, acting on muscarinic and nicotinic receptors. Muscarinic agonists of ACh activate quiet swimmeret preparations but do not modulate ongoing rhythms, whereas nicotinic agonists do not activate silent preparations but modulate ongoing rhythmic activity (Braun and Mulloney 1993; 1995). CCAP is a neuropeptide which elicits and modulates motor activity in the swimmeret system (Gammie and Truman 1997; Mulloney et al. 1997; Weimann et al. 1997). EdCl is an acetylcholine esterase inhibitor, which does not activate the swimmeret system, therefore was used in combination with CCAP. To chemically isolate ComInt1 I used low Calcium – high Magnesium saline (LowCa^{2+}; concentrations in mM: 118 NaCl, 5.4 KCl, 52 $MgCl_2$, 2.4 $CaCl_2$) to block transmitter release at all chemical synapses (Tschuluun et al. 2009). I used 3 µM CCh in Low Ca^{2+} saline to increase the excitation level of isolated ComInt1's. When all drugs were washed in sufficiently and therefore the system's and ComInt1's excitation level was modulated in the intact network or in an isolated

condition, I measured the input resistance (R_{in}) of ComInt1. R_{in} was measured by giving brief hyperpolarizing current pulses (-1 nA, 150 ms) into ComInt1 (Fig. 3 C). I gave these pulses with an interval of 5 s for at least 100 repetitions. During these recordings I kept the through potential of ComInt1 constant between -55 and -70 mV, depending on the initial resting potential.

2.5. Analysis

The recorded files were imported into Spike2 (Cambridge Electronics Design, Cambridge, England) and were analyzed semi-automatically using Spike2 scripts or MATLAB (version R2014b, MathWorks, Natick, MA, USA).

First I analyzed the rhythmic motor output by analyzing the period, burst durations, duty cycles, on-sets and burst strengths for each PS (PS5 to PS2) under different excitation levels. Results are only shown for PS5 to PS3, since rhythmic activity was mostly absent in A2. The period is the time from the beginning of the first PS burst to the beginning of the next PS burst, no matter in which abdominal ganglion (Fig. 6 A). When I changed excitation levels, I analyzed the PS cycle period in A3, because I intracellularly recorded ComInt1 mostly in A3. The burst duration is the time from the beginning to the end of each burst (Fig. 6 A). The duty-cycle, which reflects how much percent of a period is captured by the activity of a PS burst, was calculated by dividing the burst duration by the PS period. The phase on-set was measured from segment to segment, always with the more posterior ganglion as reference. The calculation of the phase is exemplified for PS4 (Fig. 6 A). The phase on-set of PS4 is measured by dividing the latency L4a by the period. The phases of PS3 and PS2 (not shown) are calculated in the same way by using the appropriate latencies. The burst strength was analyzed by calculating the integral under rectified and smoothed PS recordings for each burst (Fig. 6 B). The measured integrals were divided by the respective burst duration and normalized to the median burst strength within one experiment (modified after Mulloney 2005).

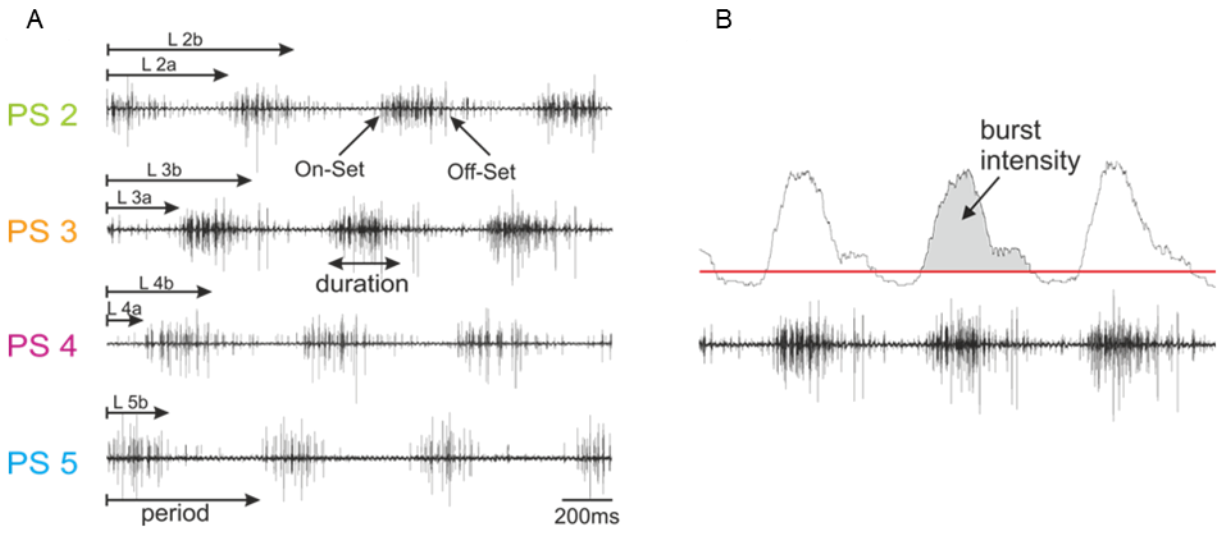

Figure 6: Demonstration of analyzed parameters of the coordinated rhythm. **A:** Analysis of the cycle period, duration, duty cycles, and the on-sets. **B:** Analysis of the PS burst strength. The burst intensity is the integral between a threshold and a rectified and smoothed extracellular PS burst trace. Dividing the burst intensity by the corresponding PS burst duration results the PS burst strength.

For intracellular recordings of ComInt1, I analyzed the same parameters (except on-sets) for bursts of EPSPs as described above for the PS motor output. Moreover, I analyzed V_m oscillations and EPSP shapes, resulting in the C1 intensity, ComInt1's V_m changes and R_{in} (Fig. 7). V_m oscillations were calculated by smoothing ComInt1 recordings to remove EPSPs. The maximum amplitude of the smoothed oscillation with reference to the trough potential was considered as membrane potential oscillation (Fig. 7 Ai). I analyzed the amplitude, the rise time, and the half-width of EPSPs in ComInt1 (Fig. 7 Aii). However, I analyzed these parameters only for the large EPSPs elicited by ASC_E from the posterior neighboring module. Therefore, I identified a threshold which was defined as the maximum value of the second derivative of the EPSP voltage trace. EPSPs were then detected by detecting peaks above this threshold. EPSP amplitude is the maximum amplitude of the EPSP voltage traces with reference to the threshold. The rise time of an EPSP is the latency from the threshold to the peak of an EPSP. The EPSP half-width is the width of an EPSP at half amplitude (Fig. 7 Aii).

I defined the term C1 intensity, in which the V_m oscillation amplitude and width as well as the shapes and numbers of EPSPs in ComInt1 are integrated. The C1 intensity is the area between a threshold at the trough potential of the cell and the intracellular voltage trace of ComInt1 (Fig. 7 Ai). The on- and off-set of ComInt1's V_m oscillations

were defined by the crossing of ComInt1's voltage trace through the threshold. I also measured the area of EPSPs by offsetting the DC to zero and calculating the integral between EPSPs and a manually set threshold. Subtracting the EPSP area from the C1 intensity resulted in the oscillation area (Fig. 7 B).

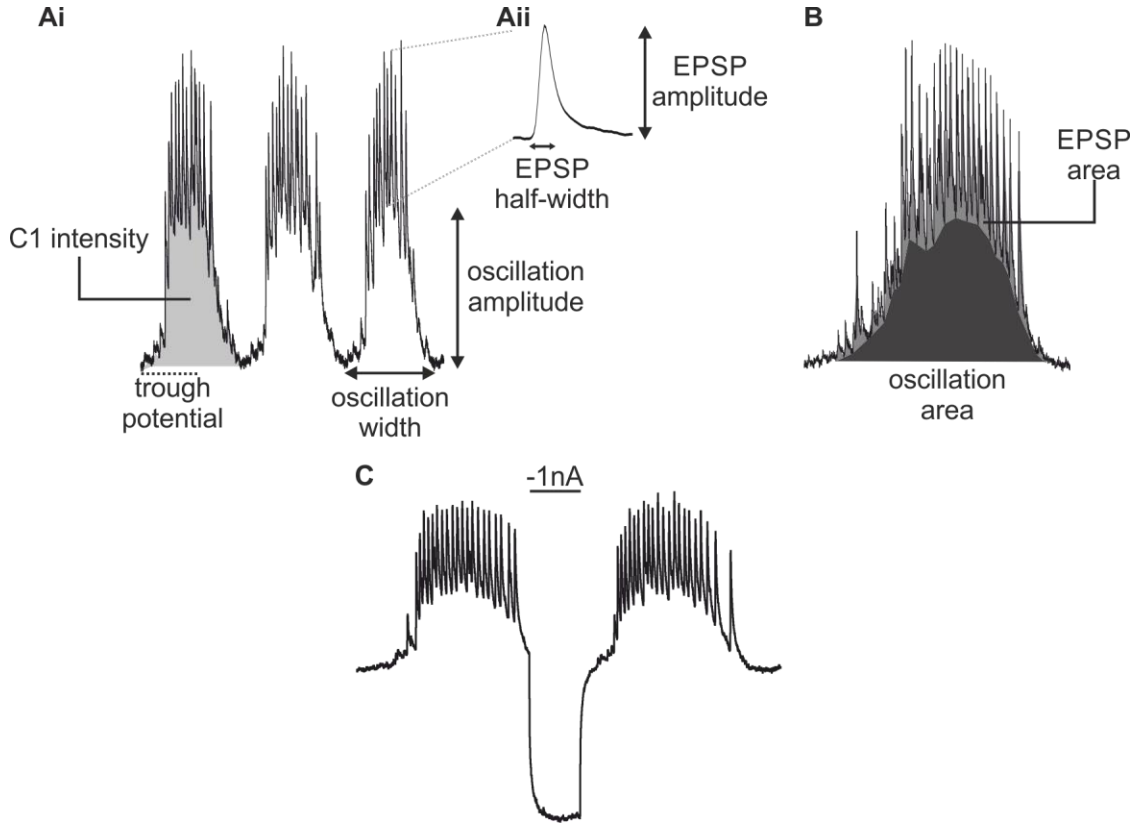

Figure 7: Demonstration of analyzed parameters of the activity of an intracellular ComInt1 recording. **Ai, Aii:** Analysis of ComInt1's V_m (trough potential), oscillation amplitude, oscillation width, EPSP amplitude, EPSP half-width, and its intensity (C1 intensity, grey), which combines all previously mentioned parameters. **B:** The C1 intensity can be divided into an EPSP area and an oscillation area. **C:** R_{in} measurement during an intracellular recording of ComInt1. R_{in} = injected current (I) / measured defelction of the V_m (U).

I calculated R_{in}s of ComInt1 by dividing the measured V_m deflection by the injected current, using Ohm's law (Fig. 7 C). V_m changes were calculated by measuring the trough potential before and after the wash-in of a chemical. The trough potential of ComInt1 in control condition was subtracted from the potential when a chemical was applied. The trough potential of ComIn1 in the control situation was the reference.

Therefore, positive values described a depolarization and negative values described hyperpolarizations of ComIn1s V_m.

2.6. Statistics

I processed the analyzed parameters in Excel (Microsoft, Redmond, WA, USA) and did statistics in SigmaPlot 12 (Systat Software Inc, San Jose, CA, USA) or MATLAB. I used nonparametric tests for statistical analysis. Two data sets were compared using a Wilcoxon rank-sum test (Mann-Whitney U) if unpaired or a Wilcoxon signed rank test if paired. The level of significance was P = 0.05. For the correlation of two parameters, I used the Spearman Rank Order Correlation test. The level of significance was P = 0.05. Pairs of variables with positive or negative correlation coefficients increase or decrease together, respectively. Additionally, linear regressions and their regression coefficients (R^2) were calculated. I created three-dimensional surface plots using MATLAB.

2.7. Morphology

After performing a successful experiment, where a ComInt1 was filled with either Nb + FITC or dTR, or a Coordinating Neuron was stained with dTR, I performed immunohistochemical experiments with the ganglia of interest. After staining the neurons, I kept the preparation in the refrigerator (4°C) for 24 h (ComInt1) or for at least 48 h (Coordinating Neurons) to allow dye diffusion. This was important especially for Coordinating Neurons, where the dye should be visible in the next anterior (ASC_E) or posterior (DSC) ganglion, respectively. When diffusion was sufficient, I started an immunohistochemical protocol to stain presynaptic boutons within the ganglia, using Anti-SYNORF1 antibodies (Erich Buchner, Institute for Genetics und Neurobiology, Universität Würzburg, Würzburg, Germany), which were then marked with a second antibody coupled with a fluorescence dye. Anti-SYNORF1 is an antibody against the protein synapsin1. Synapsin1 is a vesicle-associated protein, which regulates transmitter release into the synaptic cleft (Klagges et al. 1996). Since I worked with fluorescence dyes all following steps were performed in the absence of light.

The following step by step explanation is the protocol for experiments, where both dyes Nb + FITC and dTR, were used. All steps were carried out at room temperature if not mentioned otherwise:

1. Fix pinned ganglia for 90 min in selfmade 4% paraformaldehyde (Serva, Heidelberg, Germany) + 0.5% glacial acetic acid in 0.1 M phosphate buffered saline (PBS).
2. Wash ganglia 3 x 15 min in PBS + 0.1 M Glycine
3. Dehydrate the ganglia in 50 and 70% EtOH for 10 min and directly rehydrate them in 50% EtOH and 2 x in PBS for 10 min.
4. Preincubate ganglia in PBST (PBS + 1% Triton-X-100 (Fluka Chemie AG, Buchs, Switzerland)) for at least 2 h. I mostly left the ganglia in PBST over night (approximately 16 h) at 15°C. Before preincubation, I transferred the ganglia from a small sylgard lined dish into a small glass vial.
5. Incubate for at least 24 h but maximum 48 h in Streptavidin DyLight 488 (1 mg/ml; Thermo Fisher Scientific Inc.; Waltham, Massachusetts, USA) diluted 1:33 (9 µl in 300 µl per ganglion) in PBST-NGS (PBS with 1% Triton-X-100, 5% normal goat serum (Vector Laboratories, Burlingame, CA, USA), 0.1% sodium azide (NaN_3, Sigma-Aldrich; St. Louis, Missouri, USA) at 15°C on a rotator table. Streptavidin coupled with a fluorescent dye marks neurobiotin molecules and makes neurobiotin visible under a fluorescence microscope.
6. Rinse ganglia 3 x 15 min in PBS.
7. Preincubation in PBST-NGS for at least 2 h. I mostly preincubated over night (approximately 16 h) at 15°C.
8. Incubation in primary antibody anti-SYNORF1, raised in mouse, for 24 to 48 h diluted 1:75 (4 µl in 300 µl per ganglion) in PBST-NGS at 15°C on a rotator table.
9. Wash ganglia 6 x 1 h in PBST-NGS
10. Incubation in secondary antibody, Goat Anti-Mouse IgG (H + L) conjugated with DyLight633 (Thermo Fisher Scientific Inc) 1:75 (4 µl in 300 µl per ganglion) in PBST-NGS for 24 to 48 h at 15°C on a rotator table.
11. Rinse ganglia 3 x 1 h in PBS.

12. Dehydrate all ganglia in an ascending ethanol series (50, 70, 90, and 96% EtOH) 10 min each, and 2 x 100% EtOH for 5 min.
13. Clear and mount in methyl salicylate (Carl-Roth, Karlsruhe, Germany) on microscope slides.

If I did not dye-fill neurons with Nb + FITC, but rather just dTR, I skipped step 2 to 5 and continued at step 6.

I used the same protocol to immunohistochemically label postsynaptic terminals. Differences are shortly mentioned. To label postsynaptic terminals, I either used PSD-95 (Cell Signaling Technology, Cambridge, United Kingdom) or Homer-1 (Cell Signaling Technology) antibodies. PSD-95 is an antibody against the postsynaptic density protein 95, which is a scaffolding protein involved in the clustering of receptors, ion channels, and associated signaling proteins at the postsynaptic terminal (Hunt et al. 1996). Since the antibody was raised in mouse I only had to replace anti-SYNORF1 as primary antibody by PSD-95 antibodies in step 8 of the protocol above. I tried different dilution concentrations: 1:100 (3 µl in 300 µl PBST-NGS), 1:75 (4 µl in 300 µl PBST-NGS) and 1:50 (6 µl in 300 µl PBST-NGS) per ganglion. Homer-1 assembles signaling proteins, which are enriched in postsynaptic membranes of excitatory synapses and binds group 1 metabotropic glutamate receptors (Kato et al. 1998; Xiao et al. 1998). In step 8 of the protocol anti-SYNORF1 needs to be replaced by Homer-1 as primary antibody. I used the same dilution concentrations as explained for PSD-95 plus an additional 1:300 dilution. However, since Homer-1 antibodies were raised in rabbit, I had to change the secondary antibody used in step 10. Instead of using Goat Anti-Mouse IgG (H + L) conjugated with DyLight633, I used Donkey Anti-Rabbit IgG (H + L) conjugated with Alexa488 (Thermo Fisher Scientific Inc).

Another approach to label postsynaptic terminals was to apply tetramethylrhodamin-labeled α-bungarotoxin (Life Technologies, Eugene, Oregon, USA) diluted in NR to the isolated nerve cord. α-bungarotoxin binds with high affinity to the α-subunit of nicotinic ACh-receptors of neuromuscular junctions and within the CNS (Borodinsky and Spitzer 2007; Marshall 1981; Popova and Panchin Yu 1999). I dissolved 18 µg of powdery tetramethylrhodamin-labeled α-bungarotoxin per ml NR.

Afterwards, I diluted the α-bungarotoxin saline by adding 3.6 µl of it per ml NR. I applied 30 ml of the final α-bungarotoxin saline to the isolated nerve cord, kept it for approximately 12 h at 4°C in the refrigerator and directly proceeded to step 11 of the protocol.

2.8. Microscopy and Analysis

I scanned the ganglia possessing two different fluorescence dyes with confocal laser microscopes either using a Zeiss (LSM 510Meta, Zeiss, Oberkochen, Germany) or a Leica (SP-8, Leica Microsystems, Wetzlar, Germany) system. On both systems, I used a 10x magnification for overviews, but with a 1.75x zoom at the Leica system. At 10x magnification, scans were done in 5 to 10 µm z-stacks. For detailed scans I used a 40x (oil) or 100x (oil) magnification (Zeiss LSM 510Meta), or a 63x (water) magnification (Leica SP-8). The magnification was further increased with a 1.75x zoom on the Leica system. Here, the z-stack size varied between 1 µm (40x) and 0.56 µm (100x) for the Zeiss system and 0.36 µm for both magnifications on the Leica system. FITC and Streptavidin488 were excited at a wavelength of 488 nm on both systems. The emission wavelength was filtered by a 498 – 530 nm band pass filter at the SP-8 system, and by a 505 – 530 nm band pass filter at the Zeiss system. The excitation wavelength of dTR was 543 nm at the Zeiss LSM and 561 nm at the SP-8 and emission wavelength was filtered by a 560 – 615 nm band pass filter at the LSM system and by a 571 – 620 nm band pass filter at the SP-8 system. DyLight633 was excited at 633 nm independent of which system I used and the emission wavelength was filterd using a 643 – 680 nm band pass filter at the SP-8 system and a 650 nm long pass filter at the LSM system.

I had several regions of interest, depending on which neuron was stained. When ComInt1 was stained, I examined in detail the dorsal midline region of the ganglia, where ComInt1 sends small branches posteriorly and anteriorly along the midline, when its neurite crosses the midline. Moreover, I had a detailed look on its dendritic aborizations in the LN, where ComInt1 interacts with its home module. When I stained Coordinating Neurons, I confirmed their morphology in their home ganglia. After that, I examined the area along the midline of their target ganglia, where the axons of Coordinating Neurons pass through the ganglia and form en passant synapses onto the

small branches of ComInt1. I confirmed synapses of Coordinating Neurons, when I detected colocalizations of dTR in the axons of Coordinating Neurons and DyLight633 in presynaptic boutons.

In order to investigate if the gradient of synaptic strength that converges in ComInt1 has its origin in the size or number of excitatory synapses of the individual Coordinating Neurons onto ComInt1, I calculated the area of colocalization of the two signals using the LSM examiner (Zeiss) or the colocalization plug-in in Fiji (Wayne Rasband (NIH)). Here, I could adjust the detected signals of two different channels, in this case of dTR in the axons of Coordinating Neurons and DyLight633 marking presynaptic boutons, to frequencies where they overlap. The overlap of frequencies was converted into pixels and with this I calculated the area of colocalization per image. Knowing the step-size of each image, I was able to calculate the volume of colocalization in μm^3 per image. Afterwards, I stacked all images of one scan and calculated the area for this scan.

For ASC_E, I additionally carried out detailed scans of the region where its primary neurite leaves the ganglion anteriorly into the connective. In this region, ASC_E has a small projection posteriorly, dorsally along the midline into its home ganglion. Here, I investigated qualitatively if the signal of the intracellularly dye-filled ASC_E (dTR) colocalized with the signal of immunohistochemically marked presynaptic boutons (DyLight633).

To generally quantify if the antibodies, which label postsynaptic components (Homer-1 and PSD-95), and the labeling of postsynaptic ACh-receptors with tetramethylrhodamin-conjugated α-bungarotoxin work in the swimmeret system, I produced overviews of ganglia that were treated with those.

Scans and images were further processed in the LSM image browser (Zeiss) or Fiji and figures were produced with Corel Draw X (Corel Corporation).

3.Results

Coordinating Neurons projecting in posterior (DSC) and anterior (ASC_E) direction encode information about the timing, duration and relative burst strength of the motor output of their home modules (Namba and Mulloney 1999; Schneider 2017; Schneider et al. in preparation; Smarandache-Wellmann and Grätsch 2014; Tschuluun et al. 2001) and conduct this information via excitatory chemical synapses to ComInt1. This information converges simultaneously with a gradient of synaptic strength in each ComInt1 which decodes the coded information about the status of the other ganglia and integrates it via an electrical synapse to its own CPG (Mulloney et al. 2006; Smarandache-Wellmann et al. 2014; Smarandache et al. 2009; Tschuluun et al. 2001)..

There is still lack of knowledge about the mechanisms that allow ComInt1 to decode the encoded information about the other three ipsilateral microcircuits. The aim of the first part of my thesis was to investigate these mechanisms. Therefore, I applied different chemicals that changed the excitation level of the swimmeret system and investigated how these chemicals altered the system's motor output as well as the cellular properties of ComInt1.

In the second part of my thesis, I tried to reveal by using morphological methods how the principle for the gradient of synaptic strength of inputs onto ComInt1 is achieved. I studied that by analyzing the synaptic connections of single Coordinating Neurons onto ComInt1. Therefore, I iontophoretically stained ComInt1 and/or the Coordinating Neurons and additionally used immunohistochemical techniques to mark presynaptic boutons. With this approach, I wanted to answer the question if the gradient of synaptic strength is determined by differences in the number or in the size of synapses Coordinating Neurons form onto ComInt1.

Part I: Electrophysiology

3.1. Effects of excitation level changes on the swimmeret system

I modulated the excitation level of the swimmeret system by applying carbachol (CCh), a cholinergic agonist, crustacean cardioactive peptide (CCAP), a muscarinic agonist, and edrophonium chloride (EdCl), an ACh-esterase inhibitor on the isolated abdominal nerve cord. I applied CCh and CCAP diluted in normal crayfish ringer solution (NR), while EdCl was diluted in CCAP saline. Therefore, measurements serving as control condition were carried out in NR or CCAP respectively and I compared changes of analyzed parameters only in those combinations. I analyzed how excitation level changes affected the PS motor output of the swimmeret system before I investigated cellular properties of ComInt1 in greater detail.

3.1.1. Changes of PS cycle period, burst duration, duty cycle, and PS burst strength

CCh application accelerated the rhythmic activity (Fig. 8 B) by decreasing the PS cycle periods in 10 out of 11 experiments (NR: Mdn = 0.578 s, iqr = 0.448 – 0.638 s; CCh: Mdn = 0.405 s, iqr = 0.395 – 0.456 s; N = 11; $P < 0.05$; Fig. 9 Ai). Similarly, EdCl shortened PS periods compared to CCAP (CCAP: Mdn = 0.654 s, iqr = 0.596 – 0.816 s; EdCl: Mdn = 0.492 s, iqr = 0.412 – 0.586 s; N = 12; $P < 0.05$; Fig. 8 D & 9 Ci). Application of CCAP decelerated the rhythmic activity (Fig. 8 C) by prolonging PS cycle periods when it was applied to the isolated swimmeret system (NR: Mdn = 0.586 s, iqr = 0.560 – 0.691 s; CCAP: Mdn = 0.686 s, iqr = 0,610 – 0.793 s; N = 10; $P < 0.05$; Fig. 9 Bii).

PS3 burst durations decreased upon application of CCh in 7 out of 11 experiments (NR: Mdn = 0.196 s, iqr = 0.141 – 0.258 s; CCh: Mdn = 0.126 s, iqr = 0.103 – 0.161 s; N = 11; $P < 0.05$; Fig. 9 Aii). Shortened burst durations due to CCh application were also visible in PS4 ($P < 0.05$) and PS5, although not statistically significant different for PS5 (Suppl. Fig. 1). I detected similar results when I added EdCl to CCAP saline. PS3 burst durations decreased in 10 of 12 experiments (CCAP: Mdn = 0.259 s,

iqr = 0.160 – 0.307 s; EdCl: Mdn = 0.178 s, iqr = 0,113 – 0.196 s; N = 12; P < 0.05; Fig. 9 Cii). Burst duration also declined in PS4 (P < 0.05) and PS5, even though the change was not significant in PS5 (Suppl. Fig. 1). In 6 out of 10 experiments in which I applied CCAP to the swimmeret system, I observed longer PS bursts in A3. The median of all bursts durations measured in NR was significantly smaller than in CCAP condition, since I detected increased PS burst durations in 60% of my experiments when I applied CCAP. (NR: Mdn = 0.212 s, iqr = 0.172 – 0.233 s; CCAP: Mdn = 0.266 s, iqr = 0.202 – 0.314 s; N = 10; P < 0.05; Fig. 9 Bii). That result also pertained for PS5 and PS4 burst durations (P < 0.05; Suppl. Fig. 1).

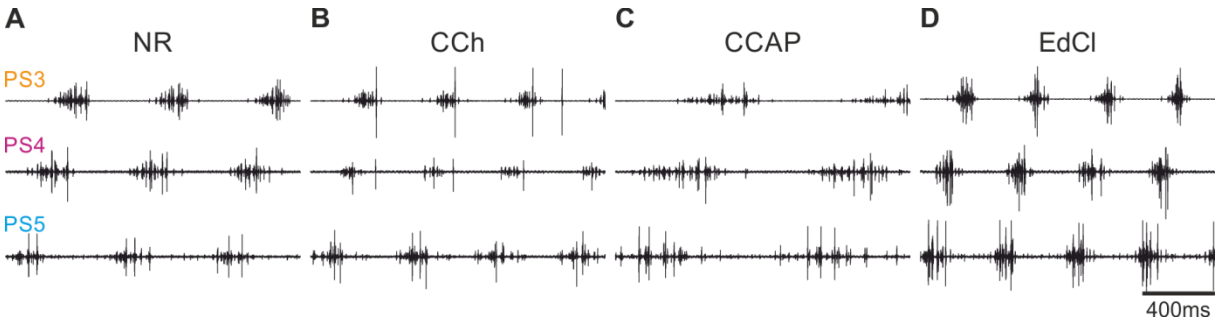

Figure 8: Simultaneous extracellular PS recordings from ganglia A5 to A3 (PS5 to PS3), while NR (**A**), CCh (**B**), CCAP (**C**) or EdCl in CCAP (**D**) is applied to the isolated nerve cord. Each cycle begins with a burst in A5. CCh and EdCl accelerate the rhythmic PS activity. CCAP decelerates the frequency of PS bursts. The coordinated posterior to anterior progression with its characteristic phase lags of ~ 23% is maintained.

PS3 duty cycles were maintained in 5, reduced in 4, and increased in 2 out of 11 experiments after replacing NR by CCh saline (Fig. 9 Aiii). Comparing the medians for PS3 duty cycles across all preparations in NR or NR containing CCh did not show any statistically different results (NR: Mdn = 34.8%, iqr = 29.7 – 39.2%; CCh: Mdn = 30.4%, iqr = 27.7 – 43.5%; P > 0.05, N = 11; Fig. 9 Aiii). This finding also applied for PS5 and PS4 (P > 0.05; Suppl. Fig. 2). Similarly, there were no statistically significant changes in PS3 duty cycles due to EdCl application (CCAP: Mdn = 34.2%, iqr = 25.8 – 43.1%; EdCl: Mdn = 36.1%, iqr = 0,246 – 38.7%; N = 12; P > 0.05; Fig. 9 Ciii). Similarly, I observed unchanged duty cycles in PS5 and in PS4 (P > 0.05; Suppl. Fig. 2). PS3 duty cycles during CCAP application in comparison to those in NR, were not significantly different (NR: Mdn = 33.1%, iqr = 25.6 – 40%; CCAP:

Mdn = 38.8%, iqr = 30.9 – 43.4%; N = 10; P > 0.05; Fig. 9 Biii). However, there was a slight increase of duty cycles. This trend to longer duty cycles in CCAP saline was statistically significant in PS5 and PS4 (P < 0.05; Suppl. Fig. 2).

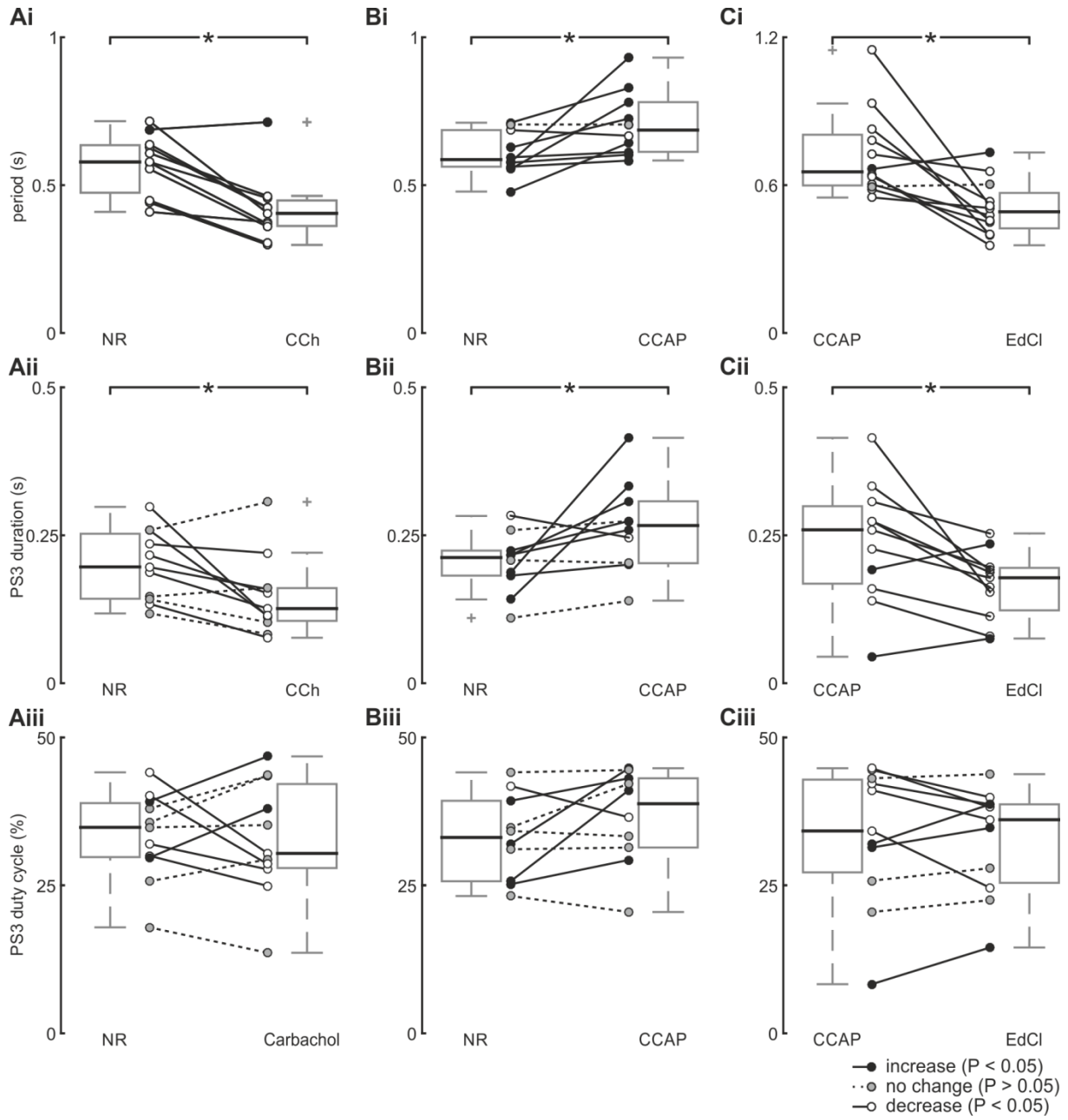

Figure 9: Modulations of the PS motor output upon bath application of CCh (**A**), CCAP (**B**), and EdCl (**C**). **Ai – Aiii:** Bath application of CCh decrease PS cycle periods (Ai) and burst durations (Aii), while PS duty cycles are unaffected (Aiii). **Bi – Biii:** Application of CCAP prolongs PS cycle periods (Bi) and burst durations (Bii). PS duty cycles remain unaffected (Biii). **Ci – Ciii:** EdCl diluted in CCAP shortens PS cycle periods (Ci) and its durations (Cii), keeping the duty cycles stable (Ciii). * P < 0.05 (Supplementary Figures 1 – 11).

PS burst strengths are, besides cycle periods, the most crucial criteria to determine if a perfused substance has an intensifying or a weakening effect on the excitation level of the swimmeret system. For evaluation, I calculated the PS burst strength by dividing the burst intensity by the burst duration (modified after Mulloney 2005). Application of CCAP decreased PS burst strengths in 7 out of 10 experiments (CCAP: Mdn = 0.722 normalized to NR, iqr = 0.346 – 0.974, N = 10, P < 0.05; Fig 10 B). In CCAP saline, I also detected a reduction of strengths for PS bursts in ganglion A4 (P < 0.05), but not for bursts measured in A5 (P > 0.05; Suppl. Fig. 3). Adding EdCl to CCAP saline strengthened PS3 bursts in median two- to sixfold (EdCl: Mdn = 1.824 normalized to NR, iqr = 1.569 – 3.916; P < 0.05, N = 11; Fig. 10 C). The same increase of burst strength was also present in PS of ganglia A5 and A4 (P < 0.05; Suppl. Fig. 3). CCh saline increased PS3 burst strengths in 7, but reduced strengths in 4 other experiments (CCh: Mdn = 1.438 normalized to NR, iqr = 0.658 – 1.795; P > 0.05, N = 11; Fig. 10 A). I did not observe a statistically significant difference between burst strengths in A5 and A4 when NR or CCh was bath applied to the isolated nerve cord, respectively (P > 0.05; Suppl. Fig. 3). These results are surprising, since previous publications (Braun and Mulloney 1993; 1995) showed that CCh application increased burst strength.

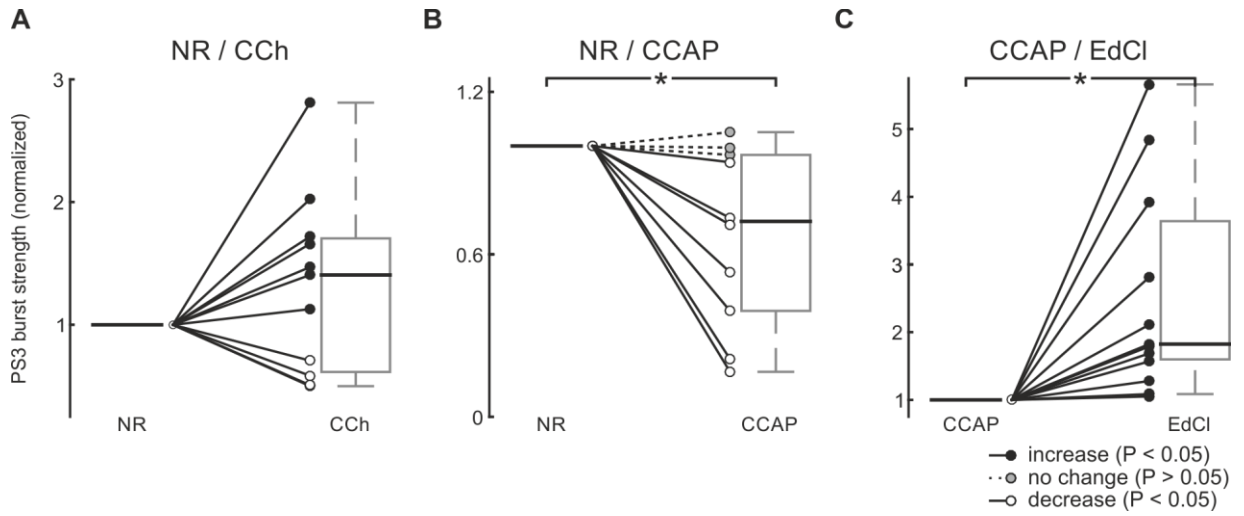

Figure 10: Normalized PS3 burst strength. **A:** PS3 burst strength measured in CCh normalized to burst strengths measured in NR, tend to increase. **B:** CCAP decreases PS3 burst strengths normalized to NR. **C:** Strengthened PS3 bursts are detected when EdCl is added to CCAP. * P <0.05 (Supplementary Figures 12 – 15).

All applied substances had in common that they modulated the PS motor output of each individual microcircuit within the swimmeret system. CCAP saline prolonged PS cycle period, burst duration and tended to increase duty cycles, but decreased the strength of PS bursts. EdCl diluted in CCAP saline affected the PS activity in the opposite way. It accelerated the rhythmic activity, by shortening PS cycle periods and durations equally, thereby duty cycles were maintained. Moreover, EdCl strengthened PS bursts. Similarly, CCh saline decreased PS period and duration, while duty cycles remained constant. PS burst strength tended to be increased due to CCh application. Taken together, these results show that EdCl and CCh application increased and CCAP application decreased the excitation level of the swimmeret system.

3.1.2. Influence on segmental PS coordination

Next I investigated if the swimmeret system is capable to maintain the coordination of the four ipsilateral distributed microcircuits, although I detected major changes of the PS motor output. I did this by analyzing segment to segment phase on-sets of PS bursts of one side of the abdominal nerve cord. The grey boxes in figure 11 ranging from 16 to 30%, describe the interval in which the phase on-sets could vary to be considered as maintained (Blumenthal and Smarandache-Wellmann in preparation). The inserted polar plots are explained exemplified for figure 11 Ai. I measured phase on-sets of PS3 with reference to PS4 in 11 preparations while either NR or CCh saline was applied. Each vector in the polar plot represents the mean on-sets for one animal, independent of either NR or CCh application. In the representative figure, the orange vector indicates the mean vector of all vectors. I also did this evaluation for PS4 (with PS5 as reference, Fig. 11 Aii – Cii) and for experiments, in which I replaced NR by CCAP saline (Fig. 11 B) or added EdCl to CCAP saline (Fig. 11 C).

As a result of CCh application, PS3 bursts advanced in 5, delayed in 2 experiments, and were maintained in 4 experiments. There was no change in the phase on-sets of PS3 across all experiments (NR: Mdn = 22.4%, iqr = 20.3 – 31.2%; CCh: Mdn = 20.8%, iqr = 17.6 – 28.3%, $P > 0.05$, N = 11; Fig. 11 Ai). This result was also valid for PS4 bursts normalized to the on-set of PS5 bursts (NR: Mdn = 18.6%, iqr = 14.3 – 20.2%; CCh: Mdn = 23%, iqr = 18.8 – 23.8%, $P > 0.05$, N = 11; Fig. 11 Aii).

I detected similar results when adding CCAP to NR saline. PS3 on-sets were unvaried in 5, advanced in 4 out of 10 experiments and delayed once (NR: Mdn = 21.7%, iqr = 19.6 – 27.8%; CCh: Mdn = 19.8%, iqr = 17.9 – 24.3%, P > 0.05, N = 10; Fig. 11 Bi). The same applied for PS4 bursts with reference to PS5 on-sets (NR: Mdn = 18.6%, iqr = 15 – 25.3%; CCh: Mdn = 21.7%, iqr = 18.5 – 24.8%, P > 0.05, N = 10; Fig. 11 Bii).

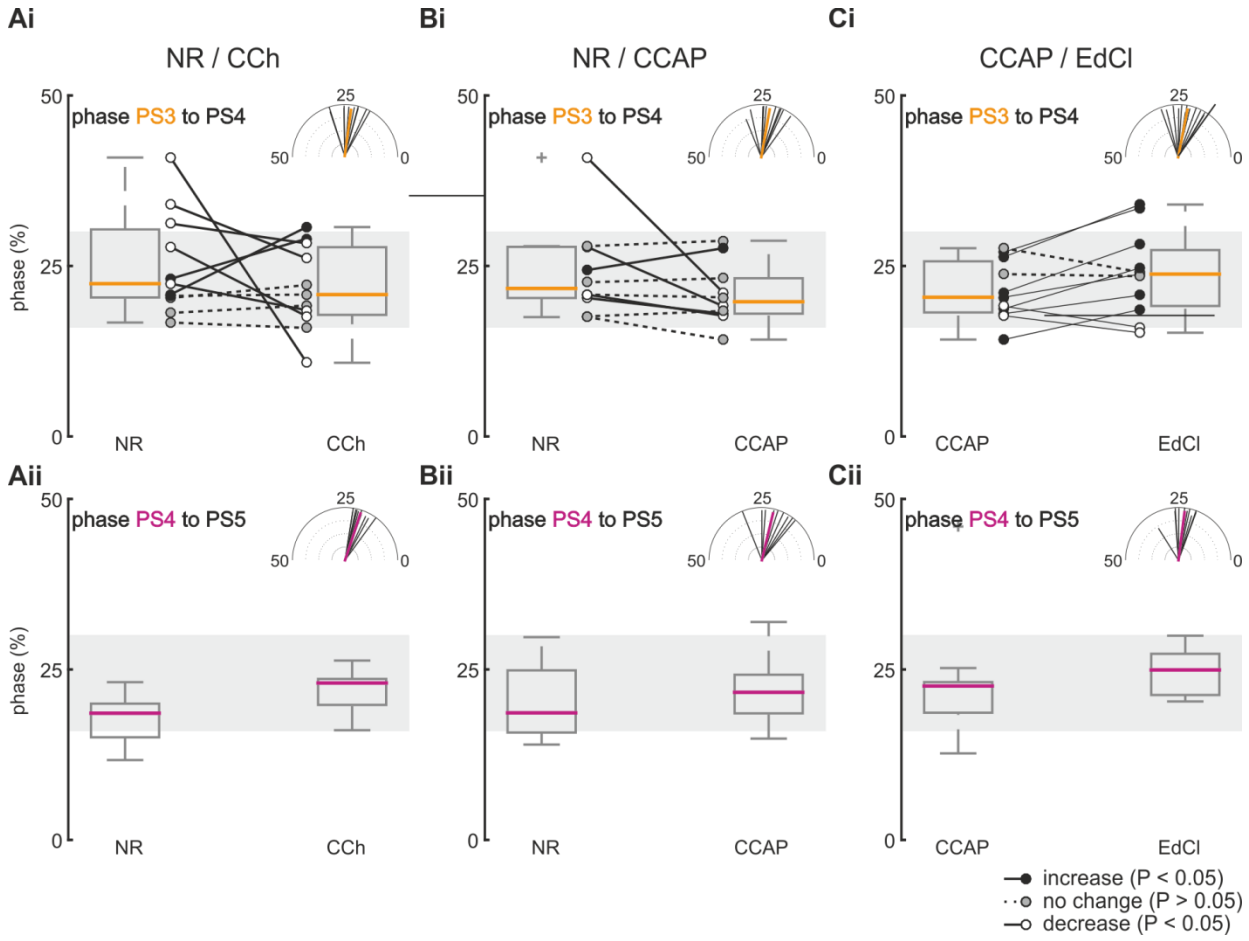

Figure 11: Segment to segment phase on-sets. **Ai + Aii:** Phase on-sets of PS3 with PS4 as reference (Ai) and phase on-sets of PS4 with PS5 as reference (Aii) measured during bath application of NR and CCh. Polar plots show the mean PS3 respectively PS4 on-set vector of all data across animals and across applied substance (NR and CCh) **Bi + Bii:** Phase on-sets of PS3 with PS4 as reference (Bi) and phase on-sets of PS4 with PS5 as reference (Bii) measured during bath application of NR and CCAP. Polar plots show the mean PS3 respectively PS4 on-set vector of all data across animals and across applied substance (NR and CCAP) **Ci + Cii:** Phase-on sets of PS3 with PS4 as reference (Ci) and phase on-sets of PS4 with PS5 as reference (Cii) measured during bath application of CCAP and EdCl. Polar plots show the mean PS3 respectively PS4 on-set vector of all data across animals and across applied substance (CCAP and EdCl). Grey boxes denote the range in which the coordination is considered as maintained. Despite variations in single animals the boxplots reflect that phase on-sets are maintained no matter in which segment and no matter which substance is applied (Supplementary Figures 16 – 21).

EdCl modulated PS3 on-sets in individual experiments. I detected delayed on-sets in six, advanced on-sets in two experiments and unchanged on-sets in two experiments. Despite changes in single experiments, across all experiments the median PS on-sets did not differ significantly when EdCl was applied (PS3: CCAP: Mdn = 20.4%, iqr = 18 – 26.3%; EdCl: Mdn = 23.8%, iqr = 18.6 – 28.2%, $P > 0.05$, N = 11; PS4: CCAP: Mdn = 22.6%, iqr = 18.6 – 23.7%; EdCl: Mdn = 24.9%, iqr = 21.1 – 27.3%, $P > 0.05$, N = 11; Fig. 11 Ci & ii).

Although, increase (CCh, EdCl) or decrease (CCAP) of the excitation level induced major changes in the PS motor output, the coordinating network was able to maintain PS phase on-sets. Medians and interquartile ranges of PS on-sets remained within the 16 to 30% interval. Therefore coordination was considered as maintained. This finding was emphasized by the polar plots, demonstrating that phase on-sets of mean vectors varied between phases of 20 and 25% independent of the applied substance.

3.2. Cellular properties of ComInt1

There are three neurons within each microcircuit that are responsible for the coordinated rhythmic posterior to anterior progression of the motor output. One of those neurons is ComInt1, whose cellular properties I explain in detail in the following chapter.

ComInt1 receives simultaneous inputs from three different Coordinating Neurons, which arrive with a gradient of synaptic strength (Mulloney and Hall 2003; Smarandache et al. 2009). ComInt1 decodes these inputs and integrates it into its own microcircuit via an electrical synapse onto one neuron of the CPG (Smarandache-Wellmann et al. 2014; Smarandache et al. 2009). However, knowledge of the mechanisms how ComInt1 decodes the encoded information transmitted by coordinating axons when excitation levels in the system changes and how it integrates the decoded information into its own microcircuit is sparse. The focus of this chapter is on the electrophysiological properties of ComInt1. I examined its cellular properties in an intact network while applying substances that either increase (CCh, EdCl) or decrease (CCAP) the excitation level of the swimmeret system. Additionally, I investigated ComInt1's electrophysiological properties when it was synaptically isolated from the network and then excited by

applying CCh. First, I investigated alterations of the timing and duration of ComInt1's activity.

3.2.1. Changes of ComInt1's period, duration and duty cycle

Figure 12 shows intracellular ComInt1 recordings with simultaneous extracellular recordings of the PS activity of its home ganglion, while I applied different substances. These recordings show that increases of the system's excitation level by CCh (Fig. 12 A) or EdCl application (Fig 12 C) accelerated ComInt1's oscillation frequency equally to PS burst frequencies. I detected opposite effects when the excitation level was decreased by CCAP application (Fig. 12 B). Here, ComInt1's oscillation frequency was decelerated equally to PS burst frequencies. Since Coordinating Neurons receive the same input from the CPG as motor neurons (Smarandache-Wellmann and Grätsch 2014), their cycle periods and burst durations increases or decreases accordingly to modulations of the motor output caused by excitation level alterations. Moreover, Coordinating Neurons are necessary and sufficient to maintain the posterior to anterior progression with its characteristic phase lags of 23 ± 7% between segments (Blumenthal and Smarandache-Wellmann in preparation; Namba and Mulloney 1999; Tschuluun et al. 2001). As a consequence, modulations of ComInt1's timing and duration should be determined by the input of the Coordinating Neurons. I investigated that by measuring the cycle period, duration and duty cycle of ComInt1. Therefore, I introduced the term EPSP burst. A burst of EPSPs is elicited by simultaneously arriving spikes from three different Coordinating Neurons. The beginning of an EPSP burst in ComInt1 is defined by its first EPSP elicited by the first spike that is received. The end of an EPSP burst is defined by the last EPSP elicited by the last spike that arrives in ComInt1.

Bath application of CCh saline accelerated the rhythmic PS motor output. I observed similar effects by analyzing ComInt1's bursts of EPSPs. The cycle period and duration of EPSP bursts decreased with an increase of the system's excitation level. ($Period_{NR}$: Mdn = 0.596 s, iqr = 0.467 – 0.651 s; $Period_{CCh}$: Mdn = 0.383 s, iqr = 0.348 – 0.431 s; N = 11; $P < 0.05$, Fig. 13 Ai; $Duration_{NR}$: 0.351 s, iqr = 0.305 – 0.391 s; $Duration_{CCh}$: Mdn = 0.223 s, iqr = 0.205 – 0.293 s; N = 11; $P < 0.05$; Fig. 13 Aii). Therefore, EPSP burst duty cycles did not change across all

experiments, although duty cycles increased in 5, decreased in 4 and did not change in 2 experiments (NR: Mdn = 58.3%, iqr = 54.9 – 68.6%; CCh: Mdn = 61.2 %, iqr = 54.7 – 63.6%; N = 11; P > 0.05, Fig. 13 Aiii).

ComInt1's EPSP burst activity also accelerated when I increased the system's excitation level by applying EdCl diluted in CCAP saline. Shorter periods were accompanied by shortened EPSP burst durations resulting in constant duty cycles ($Period_{CCAP}$:
Mdn = 0.636 s, iqr = 0.603 – 0.782 s; $Period_{EdCl}$:Mdn = 0.507 s, iqr = 0.451 – 0.606 s; N = 10; P < 0.05, Fig. 13 Ci; $Duration_{CCAP}$: 0.413 s, iqr = 0.384 – 0.442 s; $Duration_{EdCl}$: Mdn = 0.305 s, iqr = 0.288 – 0.386 s; N = 10; P < 0.05; Fig. 13 Cii; duty $cycle_{CCAP}$: Mdn: 64%, iqr = 60.6 – 70.5%; $Duration_{EdCl}$: Mdn = 64.4%, iqr = 59.9 – 75.4%; N = 10; P > 0.05; Fig. 13 Ciii).

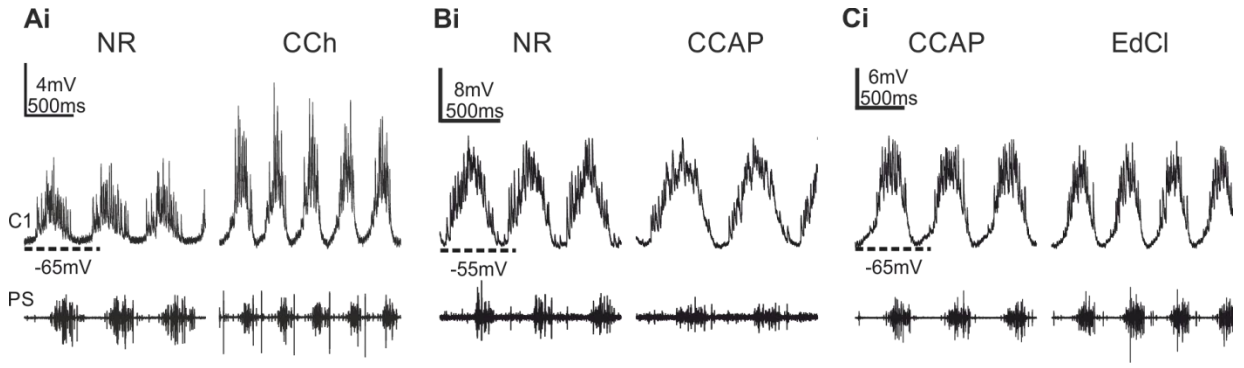

Figure 12: Intracellular recordings of ComInt1 (C1) whose membrane potential was clamped to the same values with simultaneous extracellular PS recording from its home ganglion (PS). **A:** Recordings performed while NR (left) or CCh (right) is applied to the isolated nerve cord. ComInt1's oscillation and PS burst cycle periods are shortened concurrently upon CCh application. **B:** Recordings performed while NR (left) or CCAP (right) is perfused. ComInt1's oscillation and PS burst frequencies are slowed down equally upon CCAP application. **C:** Recordings performed while CCAP (left) or EdCl (right) is presented to the isolated nerve cord. ComInt1's oscillation and PS burst frequencies accelerated concurrently as a result of adding EdCl to CCAP.

PS burst cycle periods and durations where prolonged when I replaced NR with CCAP saline. Similarly, cycle periods of bursts of EPSPs in ComInt1 increased significantly (NR:Mdn = 0.592 s, iqr = 0.546 – 0.688 s; CCAP: Mdn = 0.667 s, iqr = 0.606 – 0.752 s, N = 9, P < 0.05; Fig. 13 Bi). EPSP burst durations were unchanged in 2 experiments, decreased in other 2, and increased 4 experiments. Taken

together, these findings show a tendency of increased EPSP burst durations while CCAP was applied to the isolated nerve cord (NR: Mdn = 0.384 s, iqr = 0.36 – 0.399 s; CCAP: Mdn = 0.442 s, iqr = 0.399 – 0.486 s) (Fig. 13 Bii). This result was underpinned by an unchanged duty cycle (NR: Mdn = 68.2%, iqr = 65.3 – 75.1%; CCAP: Mdn = 67.7%, iqr = 62.1 – 74.7%; Fig. 13 Biii).

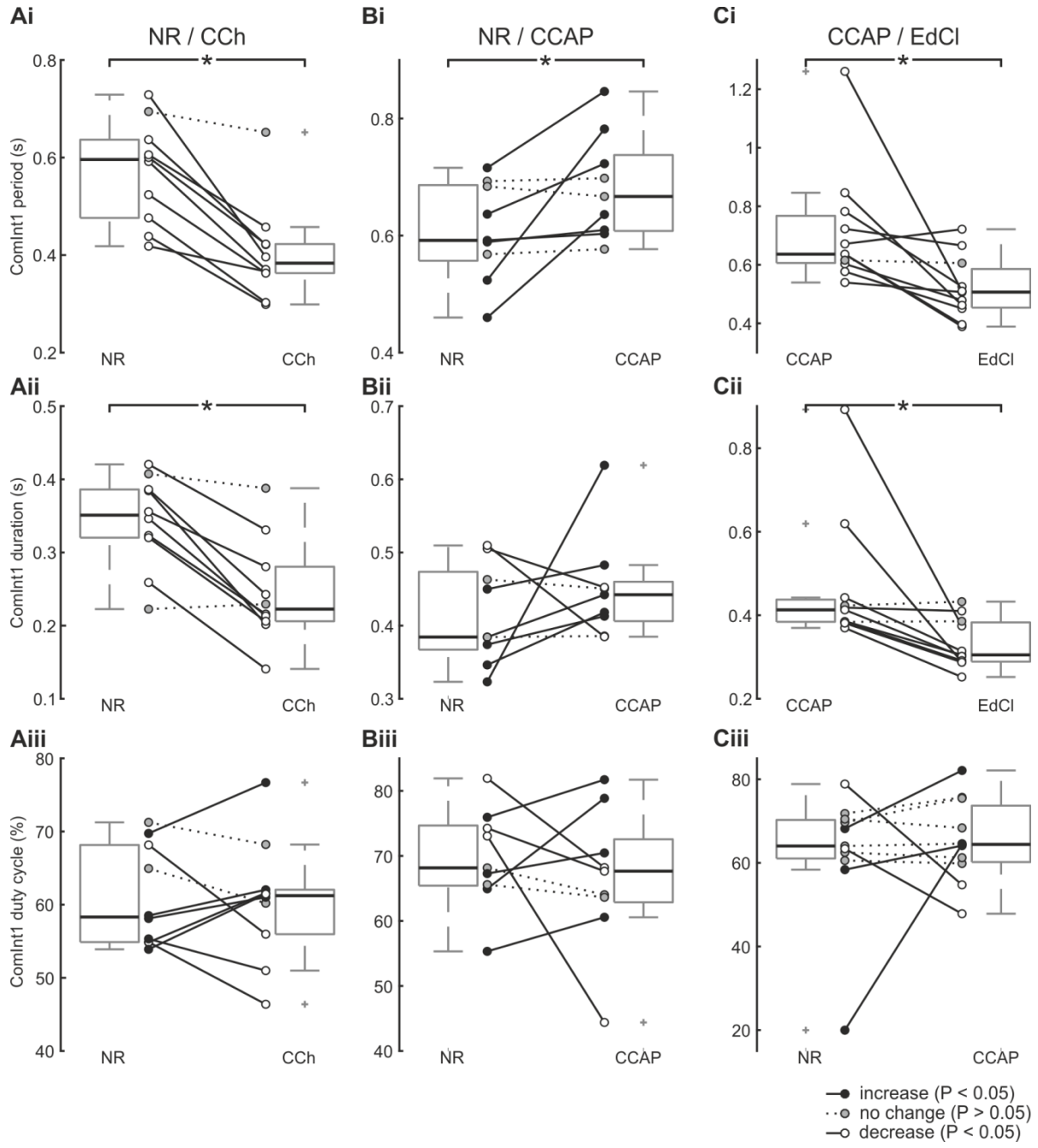

These results indicate that ComInt1's timing and duration is determined by the timing and duration of simultaneously arriving bursts of spikes from Coordinating Neurons. Their timing and duration in turn is determined by the CPGs from their home module (Smarandache-Wellmann and Grätsch 2014). However, the arriving input of Coordinating Neurons into ComInt1 not only encodes information about the timing and duration of their home ganglion's motor output. Moreover, they encode information about the relative strength of the motor output (Mulloney et al. 2006; Schneider 2017; Schneider et al. in preparation; Smarandache-Wellmann and Grätsch 2014), which is not reflected by analyzing periods and durations of EPSP bursts in ComInt1. Strengthened motor output is coded by a higher number of spikes in bursts of Coordinating Neurons (Mulloney et al. 2006), whereby the same number of spikes could code for several burst strengths when the excitation level changes (Schneider 2017; Schneider et al. in preparation). Nevertheless, if changes in the number of spikes and therefore changes in the strength of the motor output of the neighboring ganglia occur, these changes need to be decoded by ComInt1 to adjust the strength of its home module's motor output. Figure 14 shows that hyperpolarizing currents injected into ComInt1 decreased the strength of the PS activity in its home module. In contrast, depolarizing currents strengthened PS bursts. Both, hyperpolarizations and depolarizations of ComInt1's V_m only affected the strength of the motor output without modulating its timing and duration. Since modulations of the swimmeret system's excitation level are accompanied by modulations of the strength of the motor output which is relatively encoded by Coordinating Neurons, ComInt1 has to decode and integrate the coded information into its own CPG.

Figure 13: Changes in the timing and duration of ComInt1's bursts of EPSPs caused by spikes of Coordinating Neurons upon bath application of CCh (**A**), CCAP (**B**) and EdCl (**C**). **Ai - Aiii:** CCh application decreases periods significantly (Ai) and durations (Aii) of ComInt1's bursts of EPSPs, while their duty cycles increase or decrease equally so that it remains unchanged when analyzing across all experiments (Aiii). **Bi – Biii:** Application of CCAP induces significantly longer periods (Bi) and durations (Bii) of EPSP bursts in ComInt1. Its duty cycles remain unaffected (Biii). **Ci – Ciii:** Addition of EdCl to CCAP shortens periods (Ci) and durations significantly (Cii), resulting in stable duty cycles of the bursts of EPSPs measured in ComInt1 (Ciii). * $P < 0.05$ (Supplementary Figures 22 – 30).

How ComInt1 decodes the coded information about the strength of the motor output of the neighboring ganglia is unknown when excitation level changes. The following sections of my thesis address this question by investigating the cellular properties of ComInt1 in more detail. If not mentioned explicitly, changes in ComInt1's V_m were not considered in my analyses. Changes upon modulations of the system's excitation level were examined while I clamped the trough potential of ComInt1 to the same value within one experiment. I clamped ComInt1's V_m to prevent that direct effects of the applied chemicals on its cellular properties are masked by intrinsic modulations in ComInt1's activity, i.e. by changes of its V_m.

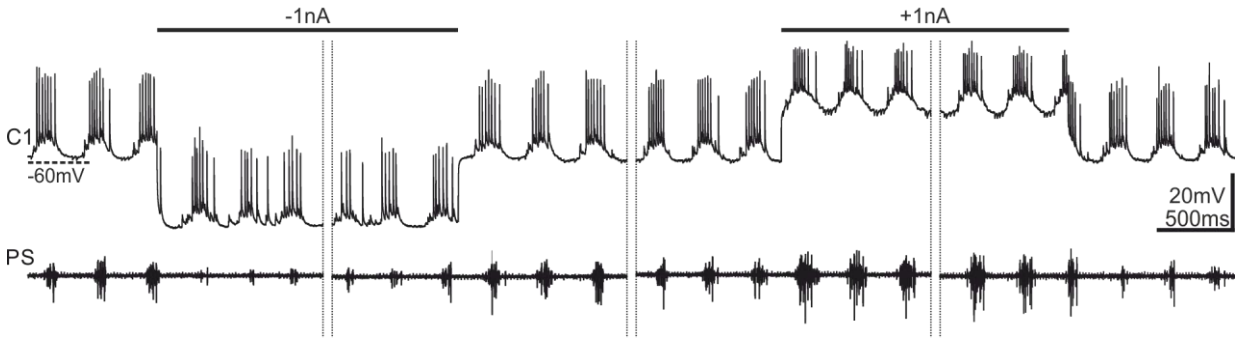

Figure 14: Simultaneous intracellular recording of ComInt1 with the extracellular recorded PS motor output of its home module. Hyperpolarizing currents decrease the PS burst strength, while depolarizing currents into ComInt1 increase the PS burst strength Both, de- and hyperpolarizing stimulations only modulate the PS burst strength but not the timing and duration of the PS motor output.

3.2.2. Effects of different excitation levels on the amplitude of membrane potential oscillations

Mulloney and colleagues (1997) showed that all motor neurons increase their membrane potential (V_m) oscillation amplitude during CCAP application. Similar effects were observed for ASC_E neurons intracellularly recorded while the system's excitation level was increased with CCh application (Namba and Mulloney 1999). Since CCAP decreased and CCh increased the excitation level of the swimmeret system, these results lead to the assumption that neurons receiving the same inhibitory input from the CPG seem to be affected similarly by apparently opposing modulations. So far it is unknown how changes of the excitation level in the swimmeret system modulate V_m oscillation amplitudes of ComInt1.

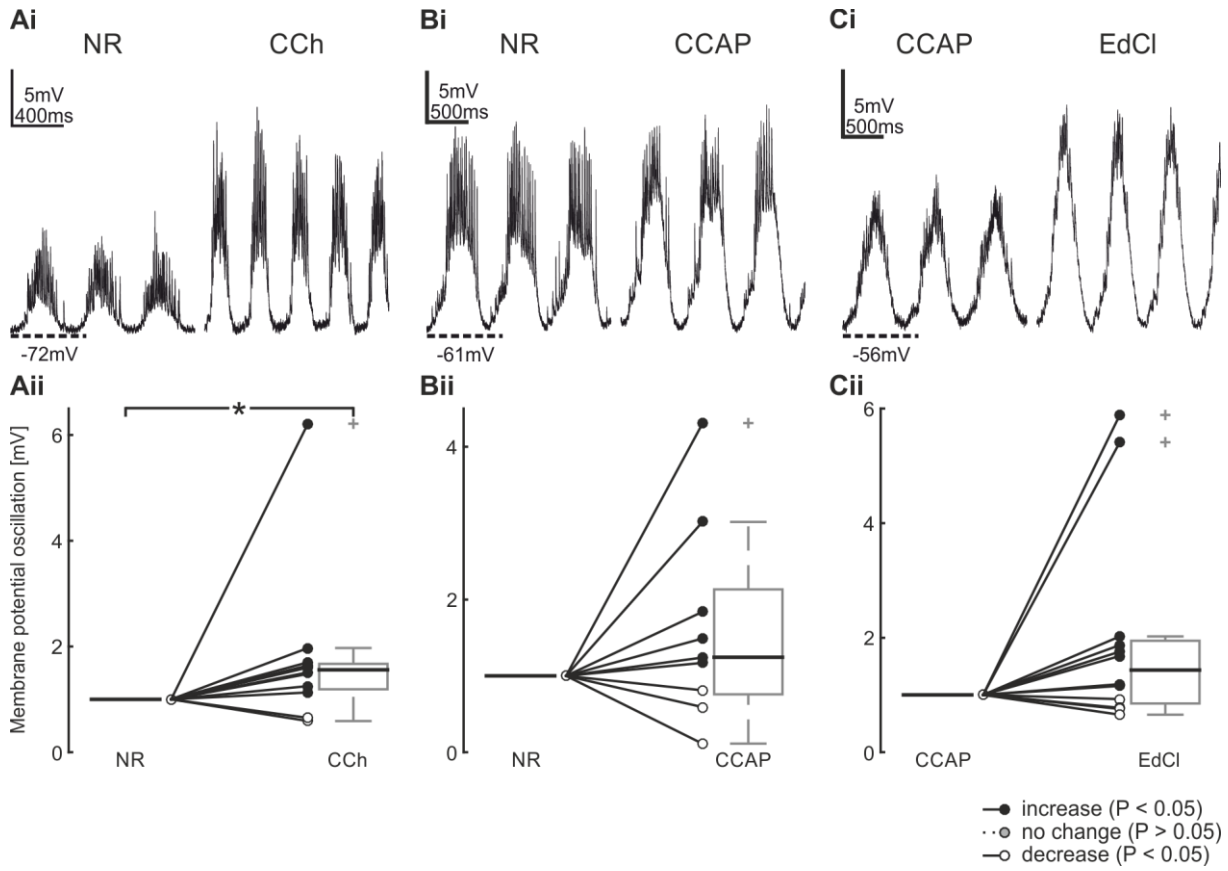

Figure 15: Changes of ComInt1's membrane potential (V_m) oscillation amplitude during modulations of the excitation level. **Ai:** Intracellular recording of a clamped ComInt1 during NR or CCh application. ComInt1's Vm oscillation amplitudes increase. **Aii:** Alterations of ComInt1's Vm oscillation amplitudes as a result of an increased excitation level due to CCh application. Results are shown for single experiments and as median across all experiments in boxplots. ComInt1's V_m oscillation amplitudes increased significantly. **Bi:** Intracellular recording of a clamped ComInt1 during NR or CCAP application. ComInt1's Vm oscillation amplitudes increase. **Bii:** Changes of ComInt1's Vm oscillation amplitudes as a result of a decreased excitation level due to CCAP application. Results are shown for single experiments and as median across all experiments in boxplots. ComInt1's V_m oscillations tend to increase in amplitude **Ci:** Intracellular recording of a clamped ComInt1 during CCAP or EdCl application. ComInt1's V_m oscillation amplitudes increased. **Cii:** Modulations of ComInt1's V_m oscillation amplitudes as a result of an increased excitation level due to EdCl diluted in CCAP saline. Results are shown for single experiments and as median across all experiments in boxplots. ComInt1's V_m oscillation amplitudes tend to increase. * P <0.05 (Supplementary Figure 31 – 33).

Exemplary intracellular recordings of ComInt1 whose V_m is clamped, show that its V_m oscillations increased in amplitude when I perfused CCh (Fig. 15 Ai), CCAP (Fig. 15 Bii), or EdCl diluted in CCAP saline (Fig. 15 Ci), although these substances had opposing effects on the system's excitation level. CCh application increased ComInt1's V_m oscillation amplitudes in 10 out of 12 experiments. (CCh: Mdn = 1.558 mV normalized to NR, iqr = 1.159 – 1.684 mV; P < 0.05; N = 12; Fig. 15 Aii). CCAP application increased oscillation amplitudes in 6 out of 9 experiments in which the

amplitude increased up to 4fold. However, there were 3 experiments in which oscillation amplitudes were reduced, resulting in a not statistically significant difference between medians measured while NR and CCAP was applied (CCAP: Mdn = 1.244 mV normalized to NR, iqr = 0.702 – 2.427 mV; P > 0.05; N = 9; Fig.15 Bii). The addition of EdCl to CCAP saline caused increased V_m oscillation amplitudes in 8 out of 12 experiments, but a drecreased in the other 4 experiments (EdCl: Mdn = 1.433 mV normalized to NR, iqr = 0.812 – 1.983 mV; P > 0.05; N = 12; Fig. 15 Cii).

These results show that a higher excitation level is accompanied by larger V_m oscillation amplitudes. Paradoxically, I observed the same tendency, when I decreased the excitation level in the system. In order to further understand how ComInt1 is coping with modulations of the system's excitation level, to robustly decode and integrate information about the other ganglia, I investigated if EPSPs in ComInt1, elicited by spikes in coordinating axons, were altered.

3.2.3. Influence of altered excitation levels on EPSP shapes

I examined if the input from the Coordinating Neurons is enhanced or diminished by modulations of the excitation level. Therefore, I analyzed changes in EPSP amplitude, rise time and half-width of the largest EPSPs in ComInt1, recorded intracellularly in A3 or A4 at the midline. This means I analyzed the EPSPs that were elicited by ASC_E spikes originating from the immediate posterior ganglia (A4 or A5, respectively). Also here, ComInt1's V_m was clamped to the same value as in the control.

EPSP averages show a slight modulation in EPSP shapes when excitation levels were changed (Fig. 16 Ai – Aiii). EPSP amplitudes tended to increase with increased excitation level during application of CCh saline (CCh: Mdn = 1.12 normalized to NR, iqr = 0.946 – 1.225; P > 0.05; N = 12; Fig. 16 Ai + ii). This finding was observed in 8 out of 12 experiments in which EPSPs increased in amplitude. The medians across all experiments of EPSP amplitudes measured during bath application of CCAP indicated that amplitudes tended to decrease when the system's excitation was reduced (CCAP: Mdn = 0.782 normalized to NR, iqr = 0.673 – 1.045; P > 0.05; N = 9; Fig. 16 Bi + ii). After

addition of EdCl to CCAP saline, EPSP amplitudes remained unaffected (EdCl: Mdn = 0.987 normalized to CCAP, iqr = 0.797 – 1.132; P > 0.05; N = 12; Fig. 16 Ci + ii).

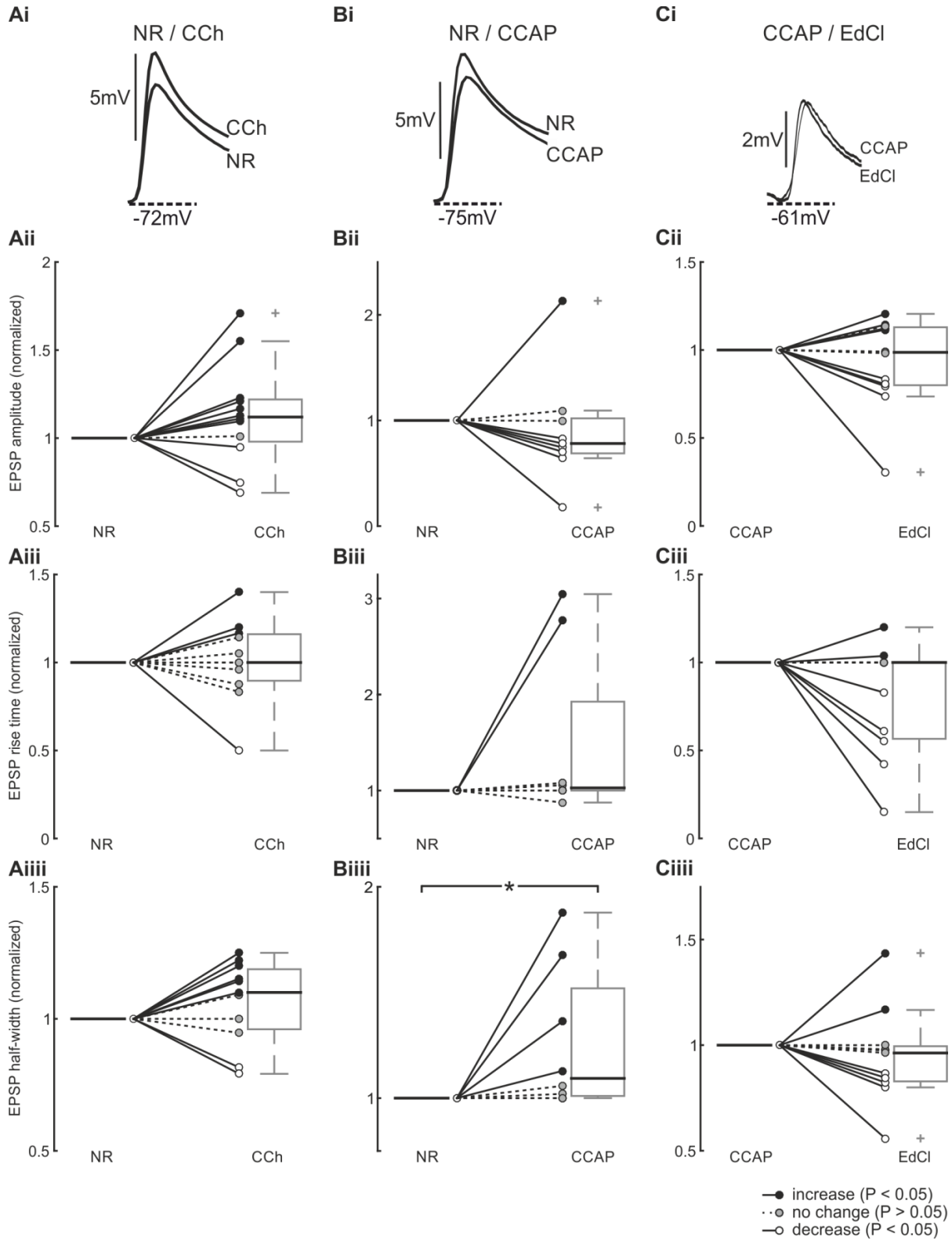

Figures 16 Aiii to Ciii show EPSP rise times of single experiments and their medians across all experiments. EPSP rise time was unaltered by CCh (CCh: Mdn = 1 normalized to NR, iqr = 0.875 – 1.167; P > 0.05; N = 11; Fig 16 Aiii) and CCAP application (CCAP: Mdn = 1.028 normalized to NR, iqr = 1 – 2.349; P > 0.05; N = 8; Fig. 16 Biii). Application of EdCl tended to decrease EPSP rise times, in 5 out of 9 experiments (EdCl: Mdn = 1 normalized to CCAP, iqr = 0.552 – 1; P > 0.05; N = 9, Fig. 16 Ciii).

Bath application of CCh (higher excitation level) broadened ComInt1's EPSP half-width in 6 and narrowed it in 2 experiments, while it remained constant in the other 3 experiments. This data suggests that EPSP half-width tended to increase during CCh application (CCh: Mdn = 1.1 normalized to NR, iqr = 0.947 – 1.2; P > 0.05; N = 11; Fig. 16 Aiiii). In contrast, higher excitation level evoked by EdCl did not affect EPSP half-width (EdCl: Mdn = 0.963 normalized to CCAP, iqr = 0.823 – 1; P > 0.05; N = 9; Fig. 16 Ciiii). The half-width of the largest EPSPs increased significantly by decreasing the system's excitation during CCAP application. In the individual experiments, the half-width broadened in 4 further experiments while it stayed unchanged in the other 4 experiments (CCAP: Mdn = 1.093 normalized to NR, iqr = 1.005 – 1.598; P > 0.05; N = 8; Fig. 16 Biiii).

Figure 16: EPSP shape modulation with excitation level alteration. **A:** Averaged EPSPs measured in one ComInt1 while NR or CCh is bath applied. Changes of EPSP amplitude (Aii), EPSP rise time (Aiii), and EPSP half-width (Aiiii) measured in ComInt1 during NR and CCh application. Medians of the values measured in independent experiments, are normalized to NR and their medians across all experiments are shown in boxplots. EPSP amplitudes tend to increase (Aii). EPSP rise time is unaltered (Aiii). EPSP half-widths tend to increase (Aiiii). **B:** Averaged EPSPs measured in one ComInt1 while NR or CCAP is bath applied (Bi). Medians of the values measured in independent experiments, are normalized to NR and their medians across all experiments are shown in boxplots. As a result of CCAP application EPSP amplitudes tend to decrease (Bii). EPSP rise time is unaltered (Biii). EPSP half-widths is increased (Biiii). **C:** Averaged EPSPs measured in one ComInt1 while CCAP or EdCl is bath applied (Ci). Medians of the values measured in independent experiments, are normalized to NR and their medians across all experiments are shown in boxplots. EPSP amplitude (Cii), rise time (Ciii), and half-width were unaffected (C iii). * P <0.05 (Supplementary Figures 34 – 42).

Together these findings suggest that excitation level modulations had minor effects on large EPSPs amplitude and shape. On the assumption that intermediate and small EPSPs in ComInt1 would change in relation to large EPSPs these minor effects would have considerable effects on ComInt1's decoding and integrating properties. Nevertheless, I was not able to prove that assumption, because the analysis of particularly small EPSPs was difficult and sometimes not possible.

Because I examined only ComInt1's V_m oscillation amplitudes I did not consider changes in the width of these oscillations. In order to additionally incorporate all sizes of EPSPs and the width of V_m oscillations into this analysis, I introduced the term "ComInt1 intensity", short C1 intensity.

3.2.4. ComInt1 (C1) intensity modulation due to increased and decreased excitation levels

The C1 intensity is the area between an intracellularly recorded voltage trace of ComInt1 and a threshold at its trough potential (Fig. 17 Ai – Ci). This area takes into account not only the amplitude, but also the width of V_m oscillations. Moreover, C1 intensity included the number and shapes of all sizes of EPSPs. Therefore, the C1 intensity is a measure for the degree of inputs from the Coordinating Neurons via excitatory synapses and from IRSh via an electrical synapse into ComInt1. That means that it displays the level of excitation of ComInt1 within the network, when the system is producing rhythmic motor output. C1 intensity was analyzed from ComInt1s whose V_m was clamped to the same value as in the control.

I described the effect of CCh on the swimmeret system as excitatory. ComInt1's V_m oscillation amplitudes and the amplitudes of the large EPSPs, and its half-width increased during CCh application. C1 intensity also increased when the system's excitation increased to a higher level by applying CCh (CCh: Mdn = 1.17 normalized to NR, iqr = 1.051 – 1.369; $P > 0.05$; N = 11; Fig. 17 Aii). This was demonstrated by the exemplary experiment shown in figure 17 Ai and by 8 additional experiments in which C1 intensities increased (Fig. 17 Aii). Without the outlying data point ComInt1's intensity would have been significantly increased during CCh application.

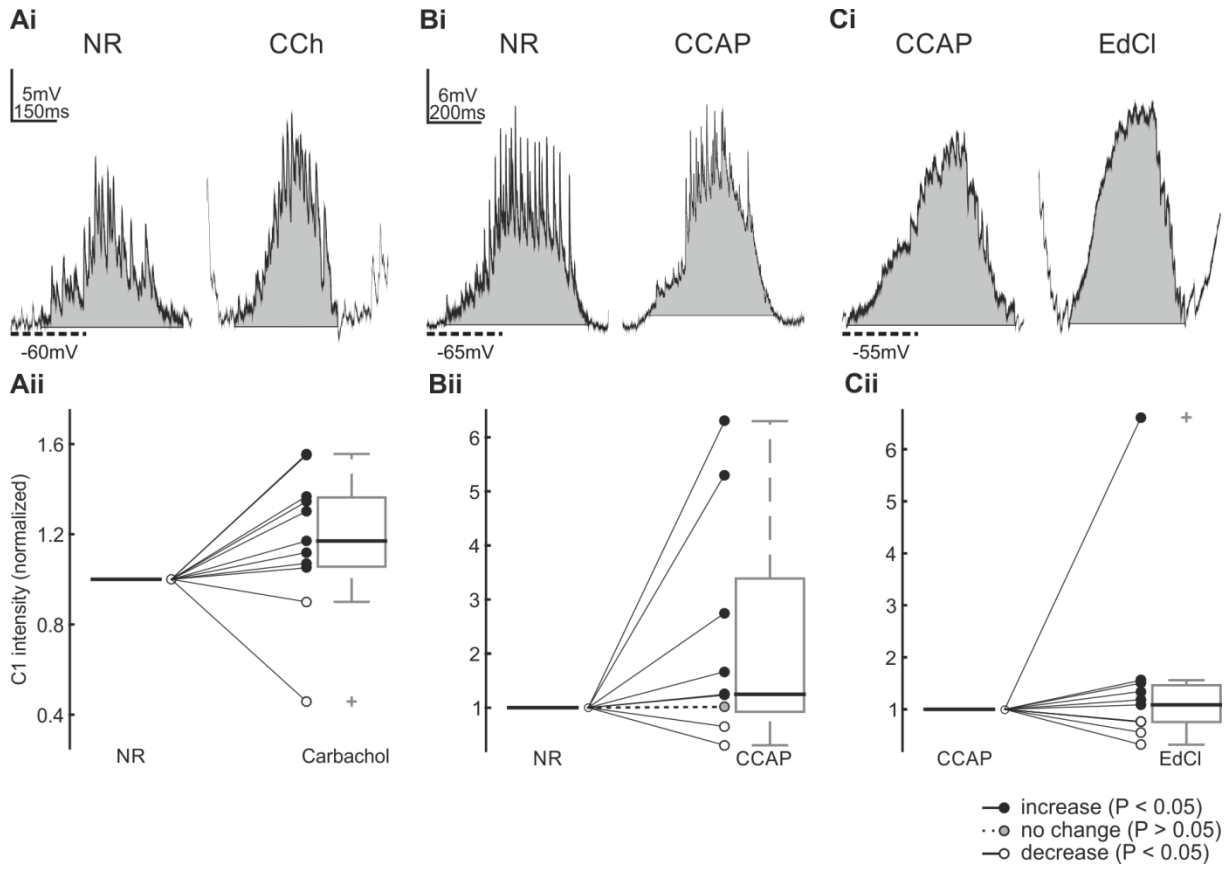

Figure 17: C1 intensity modulations as a result of excitation level alterations. C1 intensity is the area between intracellularly recorded voltage traces of ComInt1 and a threshold at its trough potential. This area integrates V_m oscillation amplitudes, V_m oscillation widths and the number, amplitude, and shapes of all EPSPs. For all excitation levels, the data is shown as the median of each individual experiment normalized to the control condition, and as boxplots across all experiments. The V_m of ComInt1 of each individual experiment is clapmed to the value of the control **A:** Changes of C1 intensity during NR and CCh application. C1 intensity increased. **B:** Changes of C1 intensity during NR and CCAP application. C1 intensity tends to increase. **C:** Changes of C1 intensity during CCAP and EdCl in CCAP application. C1 intensity does not change (Supplementary Figures 43 – 45).

I observed dichotomic results when I added EdCl to CCAP saline. In these experiments I observed 6 increases and 5 decreases of C1 intensity. These results implied that excitation level increases did not alter C1 intensities reliably during bath application of EdCl. Therefore, I considered the C1 intensity to be unaffected by bath application of EdCl in CCAP saline (EdCl: Mdn = 1.086 normalized to CCAP, iqr = 0.755 – 1.503; P > 0.05; N = 11; Fig. 17 Ciii).

Amplitude and width of ComInt1's V_m oscillations have the most distinct effect on C1 intensity when CCAP was perfused on the whole isolated nerve cord. Therefore, C1 intensities tended to increase, although the system's level of excitation decreased during

CCAP application. The medians across all experiments revealed differences between measurements performed while NR or CCAP was applied. C1 intensity increased up to 6fold in CCAP condition. Nevertheless, changes due to CCAP application were not reliable and therefore not significantly different from the NR condition (CCAP: Mdn = 1.247 normalized to NR, iqr = 0.833 – 4.027; P > 0.05; N = 9; Fig. 17 Bii).

In summary I showed, that C1 intensities tended to increase during CCh or CCAP application on the isolated nerve cord, although these substances had opposing effects on the level of excitation. Moreover, adding EdCl to CCAP saline did not further affect C1 intensities.

3.2.5. Input resistance (R_{in}) changes due to excitation level alterations

Another parameter determining the level of a neuron's excitation level is the input resistance (R_{in}). The R_{in} of a neuron depends on the number of open or closed ion channels. The more channels are open the lower the R_{in} and the higher the conductance for specific ions. Less opened channels results in an increased R_{in} and reduced conductance of ions across the membrane. R_{in} measurements of PSE, RSE and Coordinating Neurons during ongoing rhythmic activity showed that the R_{in} of these neurons was highest during spiking and lowest in the interburst (Schneider 2017; Schneider et al. in preparation; Smarandache-Wellmann and Grätsch 2014; Tschuluun et al. 2009). In other words, R_{in} was highest when the V_m was depolarized and lowest when hyperpolarized. This means, in theory, if a neurons V_m depolarized due to an increase of its excitation level its R_{in} should also increase. Since I clamped ComInt1's V_m to the same values within one experiment, I was not able to determine if changes in its R_{in} were attributable to its V_m changes. Similarly, during ongoing rhythmic motor output ComInt1's V_m oscillated and its R_{in} was highest at the maximal depolarization and lowest at the most hyperpolarized point of its oscillation (Fig. 18 D). Altering the system's excitation level while measuring ComInt1's R_{in} allowed me to investigate if ComInt1's level of excitation was modulated.

Figure 18 Ai - Ci depict three example experiments illustrating how ComInt1's R_{in} could change during bath application of CCh (Ai), CCAP (Bi), and EdCl (Ci).

Experiments that were chosen in these examples exhibit R_{in} alterations which were similar to the medians of the normalized data of all experiments. The larger the voltage deflection, the bigger was the measured resistance. This indicated that in these examples application of CCh and CCAP increased, but application of EdCl in CCAP saline did not further affect ComInt1's R_{in} (Fig. 18 Ai – Ci).

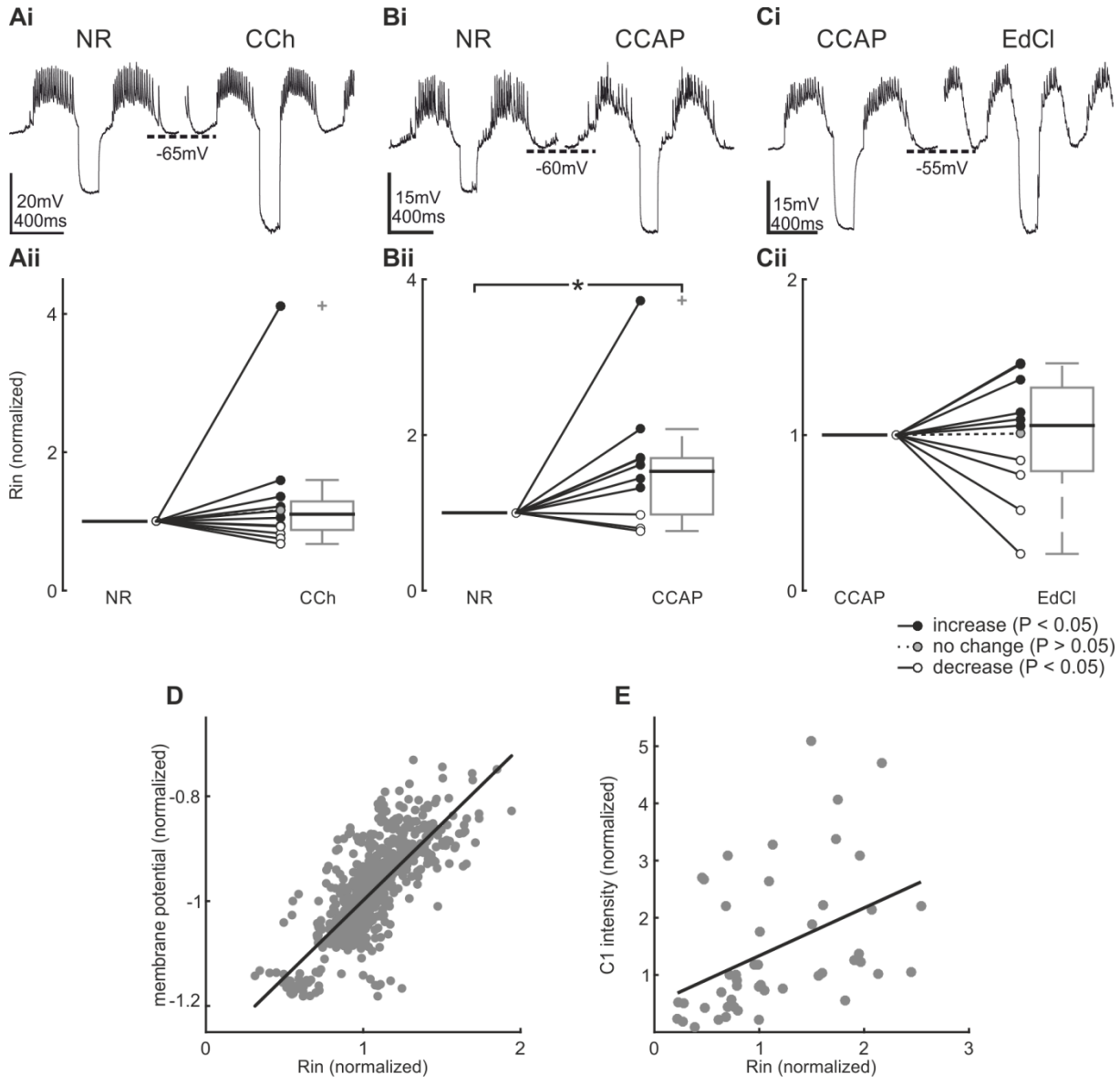

When each experiment was considered individually, I observed an increase of R_{in} in 7 experiments, a R_{in} decrease in 4, and no change in 1 experiment, when CCh was used to increase the excitation level. However, this resulted in an unchanged R_{in}, across all experiments although the system was excited with CCh (CCh: Mdn = 1.103 normalized to NR, iqr = 0.851 – 1.324; $P > 0.05$; Fig. 18 Aii). After EdCl application R_{in} ranged between 0.235 and 1.46 demonstrating a huge variation. This variation led to a not statistically significant difference in R_{in} (EdCl: Mdn = 1.061 normalized to CCAP, iqr = 0.744 – 1.358; $P > 0.05$; N = 11; Fig. 18 Cii). CCAP application increased R_{in} in 7 out of 10 experiments. As a result of this, R_{in} increased significantly (CCAP: Mdn = 1.533 normalized to NR, iqr = 0.934 – 1.769; $P < 0.05$; N = 10; Fig. 18 Bii).

The positive correlation between ComInt1's R_{in} and its intensity proved that both parameters, in combination, were sufficient to describe the excitation level of ComInt1. A high R_{in} was accompanied by high C1 intensities, indicating that ComInt1 was excited. A low R_{in} was accompanied by low C1 intensities, indicating that ComInt1 was unexcited. Moreover, these findings proved that the C1 intensity is the most usefull criterion to reveal how the information transfer across different segments is decoded and integrated into the CPGs of each microcircuit by ComInt1.

Figure 18: Changes of ComInt1's input resistance (R_{in}) due to modulations of the excitation level **Ai - Ci:** Intracellular recording of ComInt1 whose V_m is clamped, with hyperpolarizing current pulse to measure the input resistance in NR and CCh (Ai), NR and CCAP (Bi), CCAP and EdCl (Ci). **Aii – Cii:** Analyzed R_{in} across all experiments normalized to its own control condition, single experiments are connected. The median of ComInt1's Rin does not change statistically across all experiments when CCh increases the excitation level (Aii). The median of ComInt1's Rin does not change statistically across all experiments when CCAP decreases the excitation level (Bii). The median of ComInt1's Rin does not change statistically across all experiments when EdCl diluted in CCAP increases the excitation level (Cii). **D:** Correlation of all medians across experiments and excitation level of ComInt1's R_{in} with its normalized V_m. R_{in} is highest at the maximal depolarization and lowest at the most hyperpolarized point of ComInt1's V_m oscillations. These two parameters increase together, depicted by a positive correlation coefficient (cc = 0.75; $P < 0.05$) in a Spearman's rank order correlation (Spearman's rho) and by a positive slope of the regression line (RL: $y = -1.291 + (0.293 * x)$, $R^2 = 0.59$, $P < 0.05$). **E:** Correlation of C1 intensities with ComInt1's R_{in}. Spearman's rho correlation coefficient results in a positive correlation (cc = 0.554; $P < 0.05$). C1 intensity and R_{in} increase together (RL: $y = 0.499 + (0.837 * x)$, $R^2 = 0.19$; $P < 0.05$). * $P < 0.05$ (Supplementary Figures 46 – 48).

3.3. C1 intensity vs. PS burst strength

In this chapter of the thesis I investigated the correlation of C1 intensities with the PS motor output. The change in PS burst strength is encoded by Coordinating Neurons from neighboring segments, which transmit the coded information to the target ComInt1. ComInt1 in turn decodes this information and sends it directly to the CPG of its home module via an electrical synapse. Normally, a 10% increase in the strength of PS bursts is encoded by an additional ASC_E spike (Mulloney et al. 2006). Thus, I decided to analyze spontaneously occurring rhythmic activity first. Spontaneous rhythms include on-off activity of PS motor outputs. That means, that PS burst strength vary considerably, which has do be encoded by Coordinating Neurons and decoded and integrated by ComInt1.

I hypothesized that the burst strength of spontaneously occurring motor outputs correlates with the C1 intensities of spontaneously occurring ComInt1 activity. Therefore, I correlated the PS burst strengths of spontaneously emerging rhythms with the corresponding C1 intensities, to test if stronger PS motor outputs can be coded with a higher activity of ComInt1. Each plotted data point represents the C1 intensity at a given PS burst strength. Medians of the parameters of interest were calculated, pooled and normalized to the median across experiments. I analyzed spontaneously elicited swimmeret rhythms in 8 different animals. I included experiments in which Comint1's oscillations almost vanish or came to a halt and no PS bursts were present (Fig. 19 Ai + Aii), or C1 intensities changed and at differently appearing PS bursts are present (Fig. 19 Aiii + Aiiii).

During these intrinsic varying excitation levels, I detected a positively correlated dependence between C1 intensities and PS burst strength. Strong bursts were thereby associated with high C1 intensities and weak bursts were accompanied by low C1 intensities (Spearman's rho: cc = 0.591, $P < 0.05$, n = 219; RL: y = 0.677 + (0.292 * x), $R^2 = 0.3$, $P < 0.05$; Fig. 19 B).

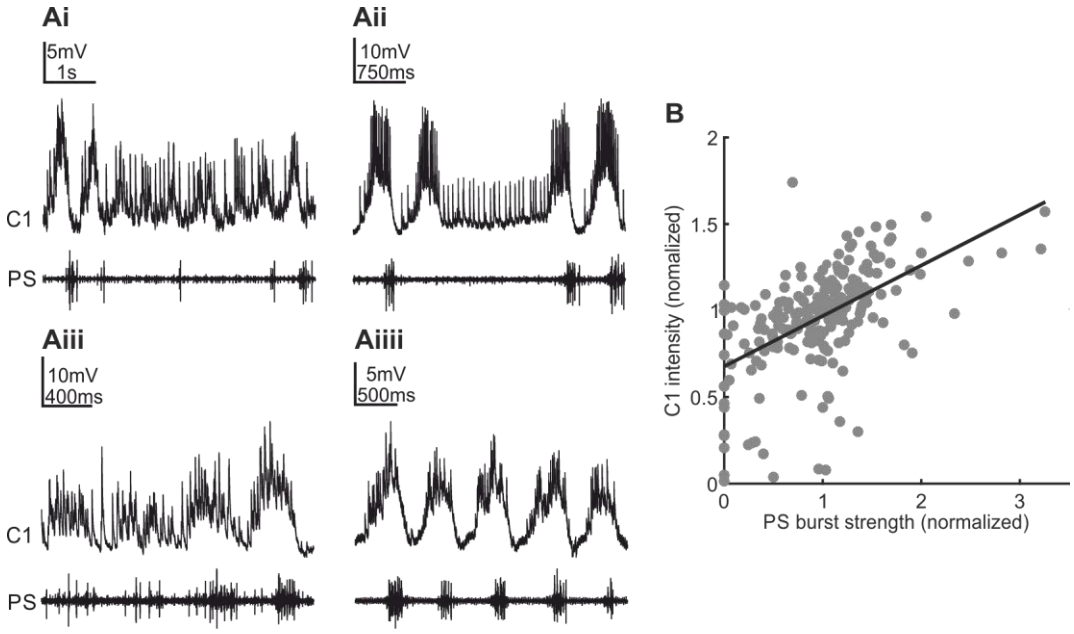

Figure 19: C1 intensity modulations correlated to the PS burst strength measured in the same microcircuit during spontaneous rhythms. **Ai - iiii:** Exemplary simultaneous intracellular ComInt1 recordings with their corresponding extracellularly recorded PS motor output during spontaneously occurring rhythms. Different sized oscillations are accompanied by differently appearing PS burst strength. A loss of V_m oscillations is correlated with silent PS recordings. **B:** Correlation of C1 intensities with PS burst strength. The two parameters increase together (Spearman's rho: cc = 0.591; $P < 0.05$, n = 219), emphasized by a linear regression with positive slope (RL: y = 0.677 + (0.292 * x), $R^2 = 0.3$; $P < 0.05$, n = 219).

This result indicates that spontaneously arising rhythms showed a broad variation of PS burst strengths. These variations were coded by different numbers of spikes in Coordinating Neurons. Few spikes in Coordinating Neurons coded weak bursts whereas many spikes coded for strong bursts. The more spikes arrived in ComInt1 simultaneously the more excited was ComInt1. Stronger excitation levels of ComInt1 were reflected by higher C1 intensities. Higher C1 intensities modulated the activity of its own CPG, which in turn could modulate the strength of the motor output.

In the next step I investigated if C1 intensities and PS burst strength also correlate when the excitation level and therefore PS burst strength were forced by the application of chemicals/neurotransmitters. Therefore, I correlated the previously calculated medians for PS burst strength measured during NR, CCh, CCAP, or EdCl application with the corresponding calculated medians of the C1 intensity. Figure 20 shows the results of the correlation analyses individually for each substance across animals (A – D) and pooled across animals and excitation levels (E). Each data point represents the C1 intensity at a given PS burst strength.

The results of these correlation analyses were in contrast to previous findings where rhythmic activity occurred spontaneously. Independent of the applied substances, I did not detect a correlation between C1 intensities and PS burst strengths (Spearman's rho: P > .0.05; Fig. 20 A – D). Pooling the data emphasized the independence of these two parameters (Speraman's rho: cc = 0.105, P > 0.05; N = 47; RL: y = 1.359 + (0.0435 * x); R^2 = 0.01, P > 0.05; Fig. 20 E).

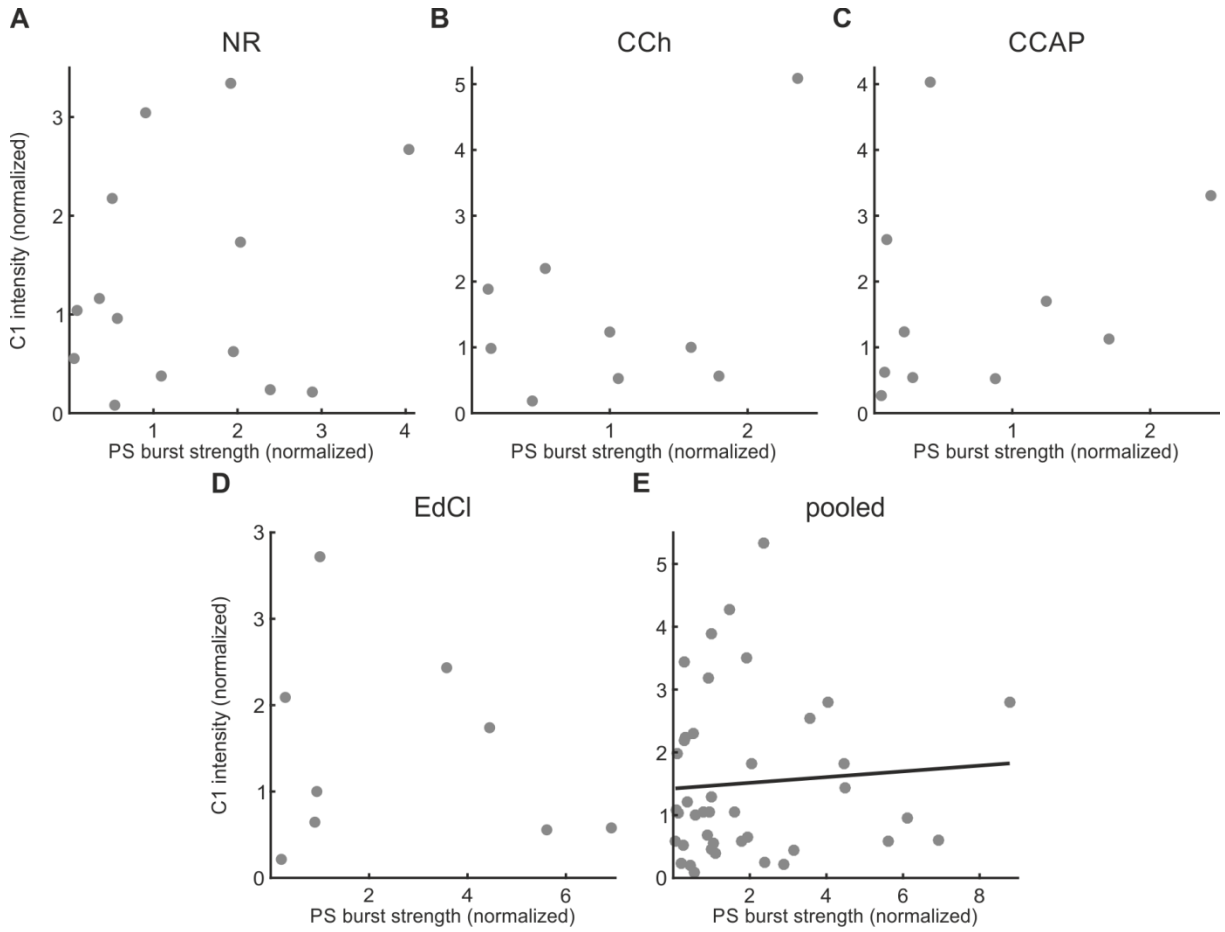

Figure 20: C1 intensity does not correlate with extrinsically forced PS burst strength. C1 intensity modulations plotted over PS burst strength measured during NR (**A**), CCh (**B**), CCAP (**C**), or EdCl (**D**) application. **E:** Correlation of C1 intensities with pooled median PS burst strengths across animals and excitation level. No correlation could be found across all individual experiments (Spearman's rho: cc = 0.105, P > 0.05; N = 47), emphasized by the linear regression (RL: y = 1.359 + (0.0435 * x), R^2 = 0.01; P > 0.05, N = 47).

Together these results indicated that spontaneously occurring rhythmic activity seems to be a more natural condition to analyze the correlation between C1 intensity and PS burst strength, than elicited rhythms which showed minor modulations of PS burst strength. Additionally, Schneider and colleagues (in preparation) showed that the Coordinating Neurons adapt to the excitation level which was set by chemicals. This means that the same number of spikes could code for different burst strengths, depending on the excitation level of the swimmeret system. Therefore, changes of burst strengths are encoded relatively to the set excitation level by Coordinating Neurons. With this additional information in mind my findings could be explained. As a result of only analyzing forced motor outputs, changes in PS burst strengths were too small to cause changes in the spike count in Coordinating Neurons. Therefore, C1 intensities did not correlate with the PS burst strength.

There are still puzzling questions why different induced excitation levels did not change C1 intensity according to normal variations of intrinsic excitation levels. CCh application raised the swimmeret system's excitation level, which became apparent by strengthened PS bursts accompanied by increased C1 intensities. Whereas, EdCl application also increased the excitation level of the swimmeret system and therefore increased PS burst strengths, but it did not affect C1 intensities. And interestingly, CCAP increased C1 intensities, but weakened PS burst strength indicating that it decreased the system's excitation level.

Together with findings from Mulloney and Hall (2003) where each burst of spikes in ASC_E and DSC causes EPSPs in ComInt1 that sum to depolarize its V_m, my results suggest that there has to be a second mechanism, in addition to modulations of C1 intensity, that contribute to cope with excitation level modulations. In all experiments and analyses I carried out so far I clamped the voltage of ComInt1 to the trough potential observed in control condition. This means, I disregarded changes in ComInt1's V_m and therefore I now hypothesize that the combination of changes in its V_m and its intensities unravels how ComInt1 manages to cope with extrinsically applied excitation levels, in order to decode this information in a more natural manner.

3.4. C1 intensity and the membrane potential (V_m) as decoding integrators

Next to the statement of Mulloney and Hall (2003) that EPSPs elicited by spikes from Coordinating Neurons sum to depolarize ComInt1, Smarandache-Wellmann and colleagues (2014) proposed that modulations of ComInt1's V_m would continuously affect its target. ComInt1's target, IRSh, in turn modulates the motor output of its local microcircuit. First, I asked how modulations of the system's excitation level would affect ComInt1's V_m. Second, I was interested in how V_m changes in turn affect C1 intensities. Third, I address how V_m and C1 intensity modulations together determine the impact onto the CPG which then modulates the strength of the PS motor output of ComInt1's home ganglion.

3.4.1. V_m changes due to excitation level modulations

Mulloney and Hall (2007b) hypothesized that an increase of local excitation would depolarize the V_m of ComInt1. I examined changes in ComInt1's V_m during uniform increases (CCh, EdCl) or decreases (CCAP) of the excitation level of the swimmeret system. Since ComInt1 oscillates when active, I analyzed changes of its trough potential. Measured V_ms were normalized to the control (NR, CCAP). Positive values mean depolarizations and negative values hyperpolarizations of ComIn1's V_m.

Although both, carbachol (CCh) and edrophonium chloride (EdCl) application increased the excitation level of the swimmeret system, they did not affect ComInt1's V_m similarly. Bath application of CCh depolarized ComInt1's V_m. This is shown as an example by an intracellular recording over a period of 10 min where CCh replaced NR (Fig. 21 Ai). I observed this depolarization of ComInt1's V_m in 8 out of 10 experiments. (CCh: Mdn = +1.395 mV normalized to NR, iqr = 0.369 – 2.092 mV; $P < 0.05$; N = 10; Fig. 21 Aii). ComInt1's V_m changes on the other hand were ambivalent as a result of an increased excitation level caused by adding EdCl to CCAP saline. The V_m hyperpolarized in 4 and depolarized in 5 of 9 experiments. This resulted across all preparations in a not significant difference of V_m measured while CCAP or CCAP containing EdCl were applied to the isolated nerve cord (EdCl: Mdn = +0.475 mV normalized to CCAP; iqr = -1.805 – 1.795 mV; $P > 0.05$; N = 9; Fig. 21 Cii). The

intracellular recording in figure 21 Ci shows no or rather an ambivalent effect of EdCl on ComInt1's V_m. Here, an initial depolarization was followed by a slight hyperpolarization. I observed similar results during application of only CCAP, which represents a lower excitation level to the system. In 3 experiments I observed a hyperpolarization, in other 3 a depolarization of ComInt1's V_m. Additionally, in 2 experiments the V_m did not change (CCAP: Mdn = 0.115 mV normalized to NR; iqr = -2.805 – 1.61 mV; P > 0.05; N = 8, Fig. 21 Bi + Bii).

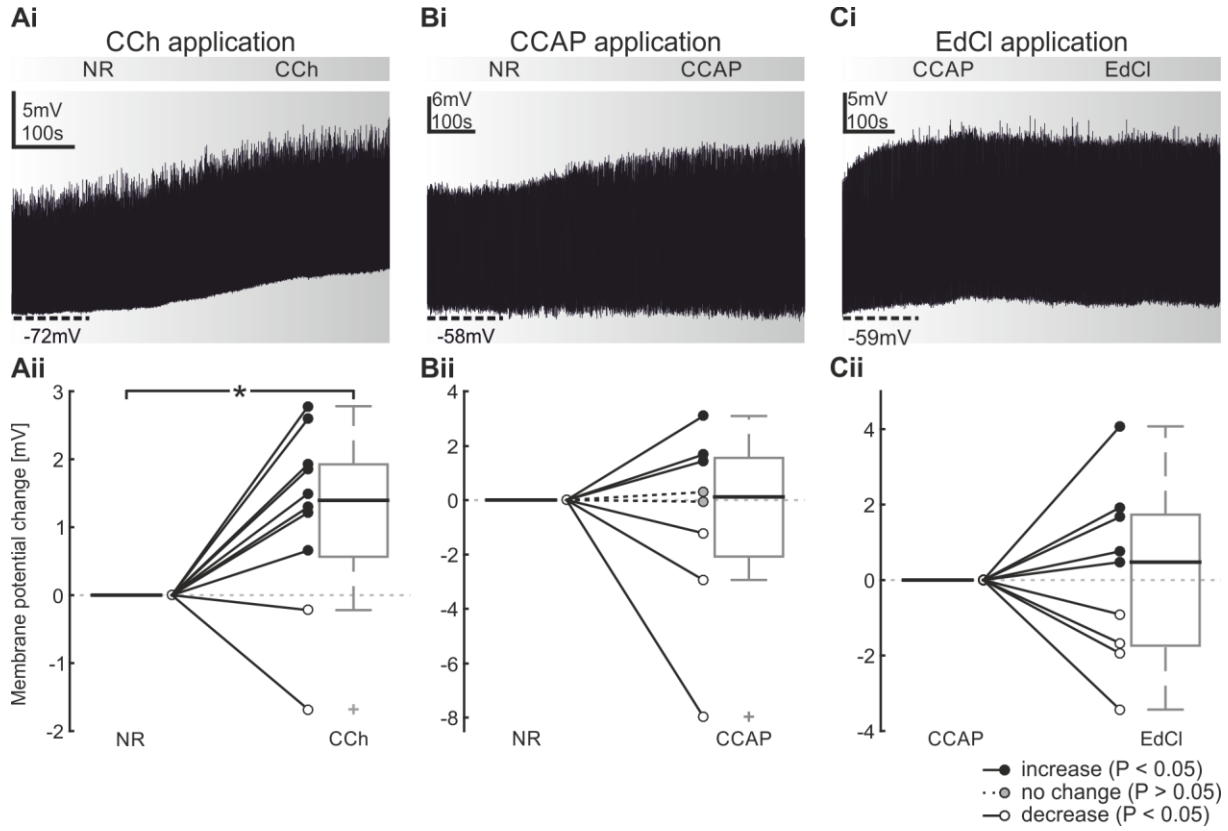

Figure 21: Changes of ComInt1's membrane potential (V_m) due to modulations of the excitation level of the swimmeret system. **Ai:** Intracellular ComInt1 recording during CCh is added to NR. ComInt1's Vm depolarizes. **Aii:** Changes of ComInt1's V_m during NR and CCh application in individual experiments and across all experiments shown in boxplots. ComInt1's V_m depolarizes significantly. **Bi:** Intracellular ComInt1 recording during CCAP is added to NR. ComInt1's Vm stays unchanged. **Bii:** Changes of ComInt1's V_m during NR and CCAP application in individual experiments and across all experiments shown in boxplots.ComInt1's V_m does not change. **Ci:** Intracellular ComInt1 recording during EdCl was added to CCAP. ComInt1's Vm stays unchanged. **Cii:** Changes of ComInt1's V_m during CCAP and EdCl application in individual experiments and across all experiments shown in boxplots. ComInt1's V_m remains unchanged. * P <0.05

In summary, these results show a significant depolarizing effect during CCh application that substantiated its ability to increase the networks excitation level. Moreover, these findings indicated that CCAP as well as the addition of EdCl had across all preparations minor effects on ComInt1's V_m. But when these experiments were analyzed independently, they showed significant hyper- or depolarizations of ComInt1's V_m. That raised the question of how and if C1 intensities change in consequence of ComInt1's V_m changes

3.4.2. Effects of ComInt1's V_m modulations on its intensity

I investigated the effect of ComInt1's V_m changes on the C1 intensity by analyzing both parameters during application of NR or CCh, NR or CCAP, and CCAP or EdCl diluted in CCAP saline. I calculated C1 intensities at the beginning and at the end of a recording when ComInt1's V_m reached a steady state and the wash-in process was considered as sufficient. C1 intensities were normalized to the median within one experiment. V_m changes were normalized to the V_m in the control condition. I plotted the data in a dot density plot and performed a correlation analysis. Each data point represents C1 intensities of a single ComInt1 oscillation at a given V_m and a certain excitation level. Three experiments are illustrated in figure 22 Ai – Ci. The change of normalized C1 intensities while V_m changes due to the presented excitation level, are summarized in figure 22 Aii – Cii.

Replacing NR by CCh mostly caused ComInt1's V_m to depolarize. Albeit in 2 experiments the V_m hyperpolarized. C1 intensities increased in these two experiments. Depolarizations of V_m in contrast were accompanied by decreased C1 intensities. To sum up, I observed that depolarizations were associated with decreasing C1 intensities resulting in a significant negative correlation between these two parameters (Spearman's rho: cc = -0.354, $P < 0.05$, n = 307; RL: y = 0.998 - (0.039 + x), $R^2 = 0.06$, $P < 0.05$; Fig. 22 Aii). This finding led to the assumption that hyperpolarized V_ms were compensated by increased C1 intensities and that depolarizations were sufficient enough to ensure a higher excitation as a result of CCh application.

The linear regression fitted through the data measured before and after replacing NR by CCAP exhibited a positive slope (RL: y = 1.044 + (0.0087 * x), R^2 = 0.02, P > 0.05; Fig. 22 Bii). However, I detected no significant correlation between ComInt1's V_m and C1 intensities (Spearman's rho: cc = 0.073, P > 0.05, n = 173). This means that C1 intensities were unaffected by ComInt1's V_m changes when CCAP induced lower excitation levels in the isolated nerve cord (Fig. 22 Bi + Bii).

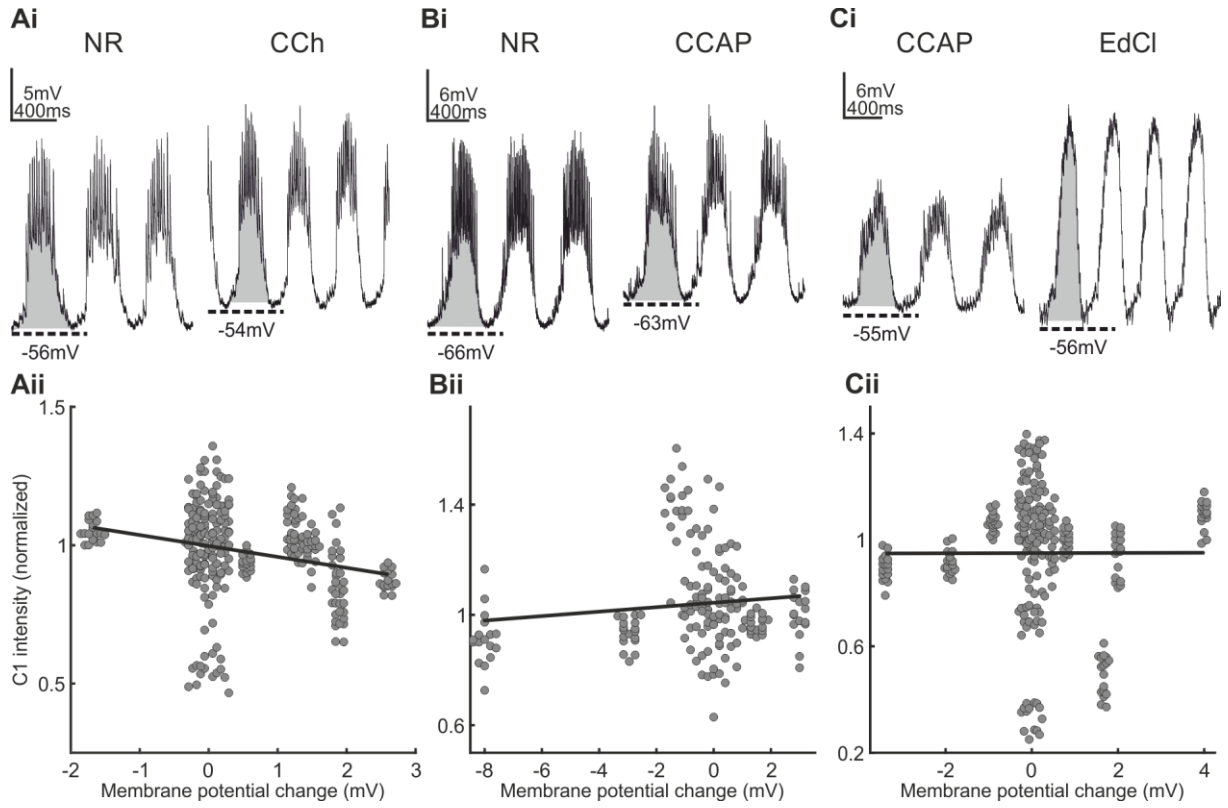

Figure 22: C1 intensity and V_m changes during a change of excitation levels. **Ai:** One example of an intracellular recording of ComInt1 in NR or in CCh saline. ComInt1 depolarizes as a results of CCh application while its intensity is reduced. **Aii**: C1 intensities at de- or hyperpolarized V_ms during CCh application normalized to NR (zero) across all experiments. C1 intensities tend to decrease with depolarizing V_ms (Spearman's rho: cc = -0.354, P < 0.05, n = 307; RL: y = 0.998 - (0.039 + x), R^2 = 0.06, P < 0.05). **Bi:** One example of an intracellular recording of ComInt1 in NR or in CCAP saline. ComInt1 depolarizes as a result of CCAP application but its intensity remains stable. **Bii:** C1 intensities at de- or hyperpolarized V_ms during CCAP application normalized to NR (zero) across all experiments. C1 intensities do not change when ComInt1's V_m de- or hyperpolarizes (Spearman's rho: cc = 0.073, P > 0.05, n = 173; RL: y = 1.044 + (0.0087 * x), R^2 = 0.02, P > 0.05). **Ci**: One example of an intracellular recording of ComInt1 in CCAP or in EdCl diluted in CCAP saline. ComInt1 hyperpolarizes slightly. **Cii:** C1 intensities at de- or hyperpolarized V_ms during EdCl application normalized to CCAP (zero) across all experiments. C1 intensities does not change when ComInt1's V_m de- or hyperpolarizes (Spearman's rho: cc = 0.018, P > 0.05, n = 271; RL: y = 0.950 + (0.0003 * x), R^2 = 0.000004, P > 0.05).

Adding EdCl to CCAP yielded similar results to CCAP application. No matter if ComInt1's V_m de- or hyperpolarized, its C1 intensities remained unchanged (Spearman's rho: cc = 0.018, P > 0.05, n = 271; RL: y = 0.950 + (0.0003 * x), R^2 = 0.000004, P > 0.05 Fig. 22 Cii).

These results demonstrated that V_m changes had significant effects on C1 intensities when excitation changed with CCh. In contrast, when the excitation level was set with CCAP or with EdCl in CCAP V_m changes had minor effects on the C1 intensities. Still, these findings admitted the assumption that minor modulations of C1 intensities together with de- or hyperpolarizations of ComInt1's V_m could decode the information transmitted from neighboring ganglia. Furthermore, the results indicated that the combination of V_m and C1 intensity modulations could affect ComInt1's home module. In the next step of my investigation, I examined how C1 intensities together with V_m changes affect the strength of the PS motor output.

3.4.3. Combined effects of ComInt1's V_m and its intensity on the PS burst strength

In order to investigate the combined effects of V_m and C1 intensity modulations on the corresponding PS burst strength, I analyzed at least 15 ComInt1 oscillations and PS bursts at control (beginning of recording) and when the excitation level was set by neuromodulators (end of recording). Thereby, I measured changes in C1 intensity, in the V_m of ComInt1, and in the strength of the corresponding PS bursts. I normalized C1 intensities and PS burst strengths to the median within one experiment. V_m changes were normalized to the control condition. I plotted the data in a three dimensional plot. The x-axis always shows V_m changes, the y-axis C1 intensity, and the z-axis depicts the PS burst strengths. With this method I could match the overall activity of ComInt1 to the strengths of PS bursts that correlate with ComInt1 activity. Each data point represents one cycle of activity. Red dots represent measurements performed in control conditions. Blue dots denote data gathered while modulating substances changed the system's excitation level.

Figure 23 represents the raw data of three single experiments each that show how V_m and C1 intensity change during the application of CCh (Ai – Aiii), CCAP (Bi – Biii) or EdCl (Ci – Ciii). Moreover, the figure shows how V_m and C1 intensities together affected the PS burst strength indirectly.

During CCh application ComInt1's V_m could either hyperpolarize (Fig. 23 Ai), or depolarize (Fig. 23 Aii + Aiii). Interestingly, its intensity adapted to the changes of V_m to reliably produce stronger bursts. A hyperpolarized V_m (-1.68 mV) resulted in C1 intensities that were almost doubled (Mdn_{NR} = 8008 ms*t; Mdn_{CCH} = 15043 ms*t). That means, that the hyperpolarized V_m was compensated by higher C1 intensities which was accompanied with PS burst strength that increased almost 3fold (Mdn_{NR} = 0.00006; Mdn_{CCH} = 0.00016, Fig. 23 Ai). Figure 23 Aii shows an example in which ComInt1's V_m depolarized during CCh application (+1.49 mV), but its intensity did not change (Mdn_{NR} = 7070 ms*t; Mdn_{CCH} = 6829 ms*t). Nevertheless, the corresponding PS burst strength was doubled (Mdn_{NR} = 0.00018; Mdn_{CCH} = 0.00036). This means that a depolarized membrane potential alone was sufficient to correlate with increased burst strengths due to a higher level of excitation. I observed a 6fold increase of the PS burst strength (Mdn_{NR} = 0.00024; Mdn_{CCH} = 0.00148) when both, V_m (+1.2 mV) and C1 intensity (Mdn_{NR} = 8498 ms*t; Mdn_{CCH} = 9672 ms*t) increased (Fig. 23 Aiii).

Although CCAP decreased the system's excitation level the application of it revealed similar ComInt1 mechanisms to cope with such changes. Bath application of CCAP entailed that ComInt1's V_m either hyperpolarized (Fig. 23 Bi) or depolarized (Fig. 23 Bii + Biii). A hyperpolarization of ComInt1's V_m (-1.3 mV) was accompanied by an increase in its intensity (Mdn_{NR} = 35209 ms*t; Mdn_{CCAP} = 54436ms*t) to counteract a greater decrease of the PS burst strength (Mdn_{NR} = 0.00071; MdN_{CCAP} = 0.00068; Fig. 23 Bi). Figure 23 Biii shows an example where ComInt1's V_m depolarized (+1.5 mV) as a result of CCAP application, but its intensity decreased slightly (Mdn_{NR} = 43731 ms*t; Mdn_{CCAP} = 41290 ms*t). Together these changes correlated with PS bursts that were weakened (Mdn_{NR} = 0.00118; Mdn_{CCAP} = 0.00099). Even if a depolarization (+3 mV) was accompanied by an unchanged C1 intensity (Mdn_{NR} = 37801 ms*t; Mdn_{CCAP} = 38216 ms*t), PS burst strength was not larger than the strengths measured in NR (Mdn_{NR} = 0.00405; MdN_{CCAP} = 0.00383; Fig. 23 Bii).

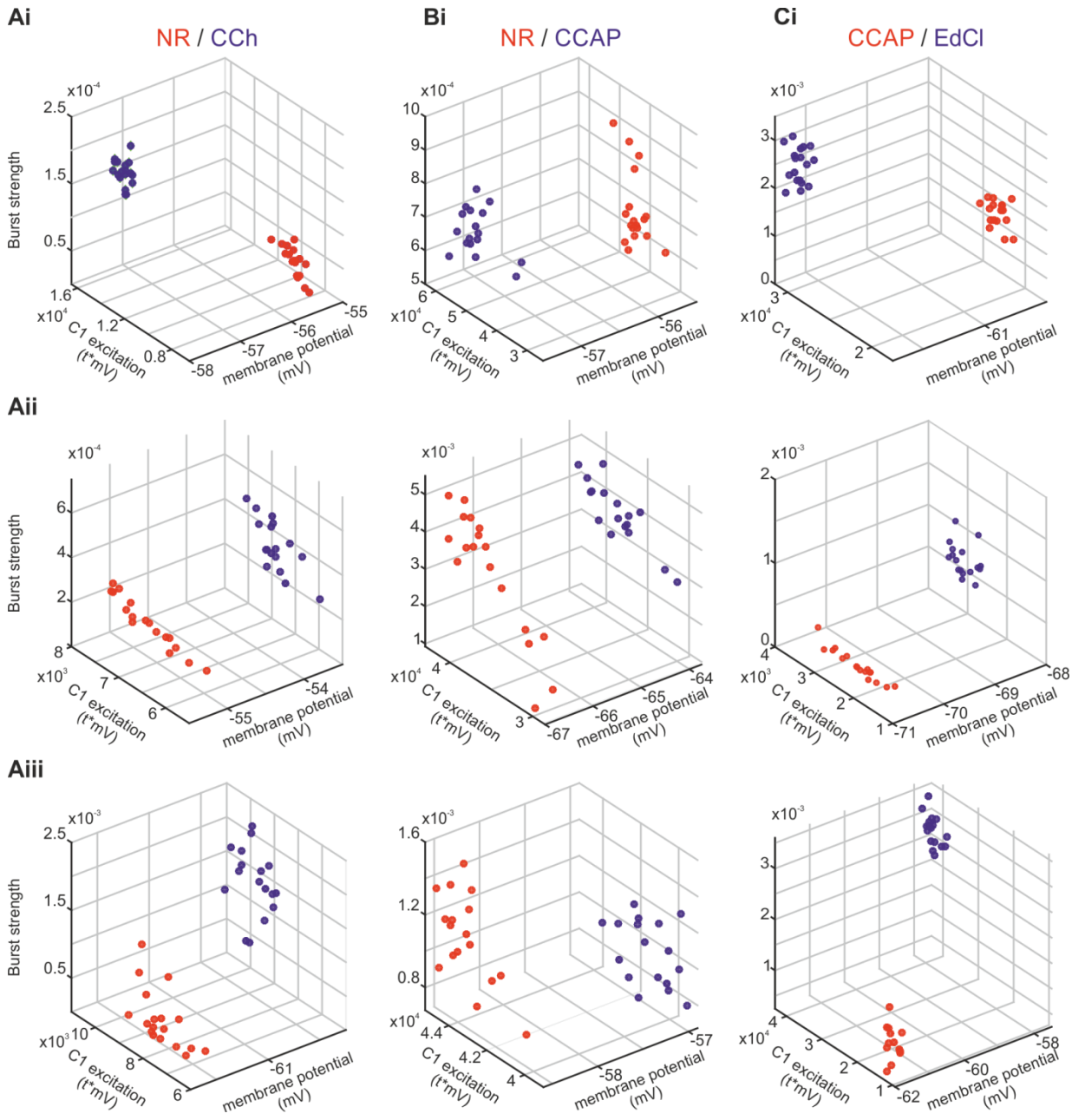

I observed similar effects when I added EdCl to CCAP. An increase in the system's excitation level, caused by EdCl, prompted hyper- (Fig. 23 Ci) or depolarizations (Fig. 23 Cii + Ciii) of ComInt1's V_m. The hyperpolarization (-0.9 mV) in this example was accompanied by an increased C1 intensity (Mdn_{CCAP} = 19778 ms*t; Mdn_{EdCl} = 29267 ms*t) and a PS burst strength increase (Mdn_{CCAP} = 0.00185; MdN_{EdCl} = 0.0028; Fig. 23 Ci). Figure 23 Cii represents an experiment in which ComInt1's V_m depolarized (+2 mV) during the application of EdCl diluted in CCAP saline

accompanied by a slightly decreasing C1 intensity (Mdn_{CCAP} = 4461 ms*t; Mdn_{EdCl} = 4026 ms*t). This depolarization was sufficient to increase IRSh's activity, which in turn increased the strength of the PS motor output almost 6fold (Mdn_{CCAP} = 0.00026; MdN_{EdCl} = 0.00144). A depolarized V_m (+4 mV) combined with an almost 4fold increase in C1 intensity (Mdn_{CCAP} = 12953 ms*t; Mdn_{EdCl} = 40379 ms*t) excited IRSh leading to PS bursts that were strengthened more than 3fold (Mdn_{CCAP} = 0.00088; MdN_{EdCl} = 0.0029; Fig. 23 Ciii).

Figure 24 shows the normalized and pooled data for experiments in which I added CCh (A), CCAP (B) or EdCl diluted in CCAP (C) to the isolated nerve cord. The surfaces within the figures are polynomial linear regression fits, representing how ComInt1's V_m and its intensity changed with certain PS burst strengths. For the better visualization of the data the polynomial regression surfaces are colorcoded from blue to yellow. Blue represents weak PS burst strengths whereas yellow represents strong PS bursts. Control experiments, which were experiments performed in NR or CCAP saline, were not included into the surfaces. However, normalized and pooled control experiments showed that higher C1 intensities were correlated with stronger PS bursts, when ComInt1's V_m did not change (Fig. 24 A – C, red dots).

Figure 23: Examples of how ComInt1's V_m and intensity could change in response to application of CCh (**A**), CCAP (**B**) and EdCl diluted in CCAP (**C**) which correlate with PS burst strengths. **Ai**: A hyperpolarization of ComInt1's V_m as a result of CCh application is accompanied by an increased C1 intensity and a stronger PS burst compared to NR. **Aii**: A depolarization of ComInt1's V_m as a result of CCh application is accompanied by an unchanged C1 intensity and a stronger PS burst compared to NR. **Aiii**: A depolarization of ComInt1's V_m as a result of CCh application is accompanied by an increased C1 intensity and a stronger PS burst compared to NR. **Bi**: A hyperpolarization of ComInt1's V_m as a result of CCAP application is accompanied by an increased C1 intensity and an almost equal PS burst strength compared to NR. **Bii**: A depolarization of ComInt1's V_m as a result of CCAP application is accompanied by an unchanged C1 intensity and a weaker PS burst strength compared to NR. **Biii**: : A depolarization of ComInt1's V_m as a result of CCAP application is accompanied by a decreased C1 intensity and a weaker PS burst strength compared to NR. **Ci**: A hyperpolarization of ComInt1's V_m as a result of EdCl application is accompanied by an increased C1 intensity and an increased PS burst strength compared to CCAP. **Cii:** A depolarization of ComInt1's V_m as a result of EdCl application is accompanied by an unchanged C1 intensity and an increased PS burst strength compared to CCAP. **Ciii:** A depolarization of ComInt1's V_m as a result of EdCl application is accompanied by an increased C1 intensity and an increased PS burst strength compared to CCAP.

In general CCh application depolarized ComInt1's V_m, but occasionally hyperpolarized its V_m. Hyperpolarizations were compensated by increased C1 intensities so that the indirectly generated PS bursts were still stronger in NR. The surface (R^2 = 0.08; P < 0.05) substantiated this finding. Moreover, it confirmed results already shown in single experiments in which depolarized V_ms were sufficient to correlate with stronger PS bursts. Corresponding PS bursts were further strengthened when C1 intensity increased additionally (Fig. 24 A). Hyperpolarizations and a decreased C1 intensity were accompanied by the weakest PS bursts. However, the difference in burst strengths between CCh and NR application (Mdn_{NR} = 0.89; Mdn_{CCh} = 1.111) was reduced compared to the experiments in which I clamped ComInt1's V_m. PS bursts strength was 40% stronger during CCh than in NR application when ComInt1's V_m was clapmed and 12% stronger when V_m changes were included in the analysis

The surface plot (R^2 = 0.01, P > 0.05; Fig. 24 B) of normalized and pooled data acquired while I applied CCAP revealed that changes in ComInt1's V_m and its intensity had minor effects on the PS burst strengths. No matter if depolarizations or hyperpolarizations were combined with increases or decreases of C1 intensity, PS burst strength remained unchanged. However, PS bursts strength was slightly weaker in CCAP than in NR (Mdn_{NR} = 1.029; Mdn_{CCAP} = 0.974; Fig. 24 B). Moreover, this analysis supports the idea that the combination of V_m and C1 intensity modulations mitigated the decrease of PS burst strength. When ComInt1's V_m is clamped, PS burst strength in CCAP was three-quarters of the strength than during NR application. Admitting ComInt1 to de- or hyperpolarize reduced the difference between PS burst strength during NR and CCAP application by 20%.

An attenuating effect of ComInt1's V_m on PS bursts strength was visible when I added EdCl to CCAP saline. Clamping ComInt1's V_m during EdCl application increased PS bursts strengths by 70%. Admitting ComInt1 to change its V_m reduced the difference of PS burst strength during EdCl compared to CCAP application by 20% (Mdn_{CCAP} = 0.732; Mdn_{EdCl} = 1.369) This result was supported by the fact that all data points acquired during CCAP application were underneath the polynomial regression surface, that describes the changes upon EdCl application (Fig. 24 C). Moreover, the surface (R^2 = 0.04; P < 0.05) shows also that stronger PS bursts were correlated with depolarized

V_ms, whereas weak PS bursts were accompanied by hyperpolarized V_ms. Furthermore, increased C1 intensities facilitated the generation of stronger PS bursts (Fig. 24 C).

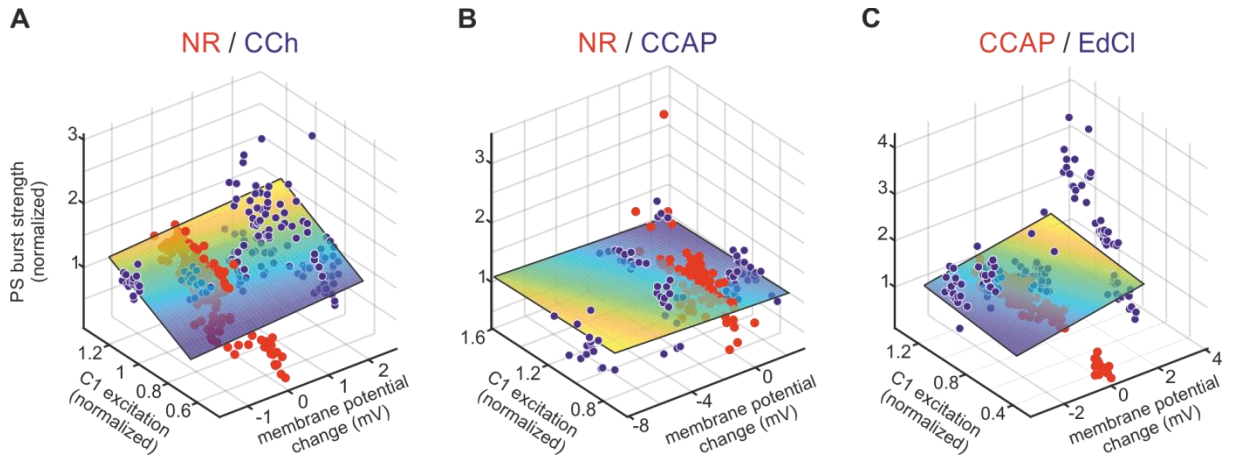

Figure 24: Pooled data illustrating how ComInt1's V_m together with its intensity changed in relation to the strength of PS bursts in its home module when the networks excitation level was either increased by bath application of CCh (**A**) or EdCl (**C**) or decreased by applying CCAP (**B**). **A:** Compared to bath application of NR, PS burst strength is generally stronger when CCh is applied to the isolated nerve cord. The fitted polynomial surface depicts V_m, C1 intensity and PS burst strength changes when CCh is applied (R^2 = 0.08; P < 0.05). PS bursts are strongest when ComInt1's V_m is depolarized and its intensity is high. Weakest PS burst are accompanied by low C1 intensities and hyperpolarized V_ms. Hyperpolarized V_ms are compensated by increased C1 intensities and depolarizations are sufficient to correlate with stronger bursts. **B:** PS burst strength is not changed during NR or CCAP application. The fitted polynomial surface (R^2 = 0.01, P > 0.05) shows that regardless of whether ComInt1's V_m and C1 intensity changed PS burst strength was not affected with a tendency to increased when ComInt1's V_m hyperpolarizes and its intensity is low. **C**: PS burst strength is higher when EdCl is added to CCAP. The surface (R^2 = 0.04; P < 0.05) highlights that PS bursts measured while EdCl was applied are strongest when ComInt1's V_m depolarizes and its intensity increases. Weaker PS bursts are accompanied by low C1 intensities and hyperpolarized V_ms. Depolarized V_ms together with low C1 intensities are associated with stronger PS bursts than hyperpolarized V_ms that are accompanied by high C1 intensities. Red dots denote measurements performed in control condition (NR or CCAP), blue dots represent measurements performed when the excitation level of the swimmeret system is either increased or decreased. The color range of the surfaces ranged from blue to yellow. Blue represents weak PS bursts whereas yellow illustrates strong bursts.

I summarized all results in figure 25. Here, I pooled the data across animals and excitation levels and normalized it to the median of the respective parameter within one experiment. The weakest PS bursts always occured when hyperpolarizations were accompanied by low C1 intensities. This finding was in agreement to a decreased excitation level of the swimmeret system. A strong increased excitation level was revealed by a strong motor output, which in turn was accompanied by a depolarized V_m and enlarged C1 intensities in ComInt1. Moreover, depolarizations were sufficient to excite the CPG to generate stronger PS bursts, while hyperpolarizations needed to be

compensated by increased C1 intensities to support the generation of stronger bursts. Together, these results indicated that this double-tracked mechanism enables ComInt1 to match its own excitation adequately to the excitation level of the swimmeret system.

Higher excitation levels caused stronger PS bursts in all ganglia. Stronger PS bursts are encoded by a higher number of spikes of the Coordinating Neurons, which converge simultaneously in ComInt1 eliciting more EPSPs. My results indicate that ComInt1 decodes this information by modulations of its intensity and its V_m, which are in turn integrated into its own CPG via an electrical synapse. Since the electrical synapse between ComInt1 and IRSh is bidirectional, ComInt1 consequently also receives information about the status of its own CPG. This raises the question how much of ComInt1's intensity and V_m modulations are driven by the excitatory inputs from the Coordinating Neurons and to what extent its own CPG contributes to these modulations.

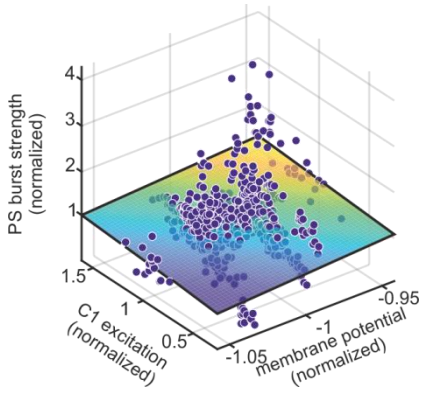

Figure 25: Relationship between changes in ComInt1's V_m, C1 intensity, and PS burst strength in one module. The data was pooled across animals and excitation level. Strong PS bursts are accompanied by depolarized V_ms and high C1 intensities. Hyperpolarizations together with low C1 intensities are associated with weak PS bursts. Depolarizations in ComInt1 are sufficient to support the generation of stronger PS bursts whereas hyperpolarizations have to be compensated by increased C1 intensities (R^2 = 0.02, $P < 0.05$).

3.5. Contribution of the Coordinating Neurons and of its own CPG to changes in ComInt1's activity

Changes of ComInt1's cellular properties could be described by changes in its intensity and its V_m. It is unlikely that the modulation of ComInt1's cellular properties was solely sustained by the inputs from the Coordinating Neurons. Clearly, I attributed the EPSPs to the input received from the Coordinating Neurons. Albeit, I hypothesized that

the bulk of changes of ComInt1's V_m and of its oscillations could be attributed to the inputs of its own CPG and to a certain extend to intrinsic properties of ComInt1. Therefore, I divided the calculated C1 intensities into two parts. In one part, the EPSPs describe the proportion of the input from the Coordinating Neurons. In the second part, the oscillations of ComInt1 describe the proportion of C1 intensities which I attributed to the input from the CPG in its home module and to intrinsic changes in ComInt1. Hence, I calculated the area under all sizes of EPSPs and subtracted this area from the previously calculated C1 intensity (Fig. 26 A). With this subtraction I was able to divide the C1 intensity into an EPSP area and an oscillation area. This allowed me to distinguish between inputs that arose from Coordinating Neurons and inputs that arose from the CPG of ComInt1's home module and its intrinsic changes respectively. Afterwards, I calculated the percentage of the EPSP area and of the oscillation area in C1 intensities (Fig. 26 B) and correlated the percentages with pooled V_ms normalized to the median V_m to investigate if and how V_m changes affect EPSP and oscillation areas (Fig. 26 C). I also pooled the PS burst strength across animals and excitation levels and normalized it to the median PS burst strength and correlated those to EPSP and oscillation areas (Fig. 26 D) In the following figures, grey dots represent EPSP areas and black dots represent oscillation areas, whereby each single dot represents the EPSP area respectively oscillation area of one single cycle at a given V_m or PS burst strength.

Figure 26 B illustrates the contribution of EPSP and oscillation areas in C1 intensities across excitation levels (N = 21; n = 752). EPSP areas covered between 2 to 45% of C1 intensities, whereby 55 to 98% were covered by oscillation areas. Increases in C1 intensities were accompanied by decreasing EPSP areas (Spearman's rho: cc = -0.185; $P < 0.05$, n = 752; RL: $y = 30.388 – (11.188 * x)$, $R^2 = 0.05$, $P < 0.05$). Consequently oscillation areas increased to the same extent (Spearman's rho: cc = 0.185, $P < 0.05$, n = 752; RL: $y = 69.612 + (11.188 * x)$, $R^2 = 0.05$, $P < 0.05$). This result was emphasized by identical regression line slopes and identical correlation coefficients that differ in signs.

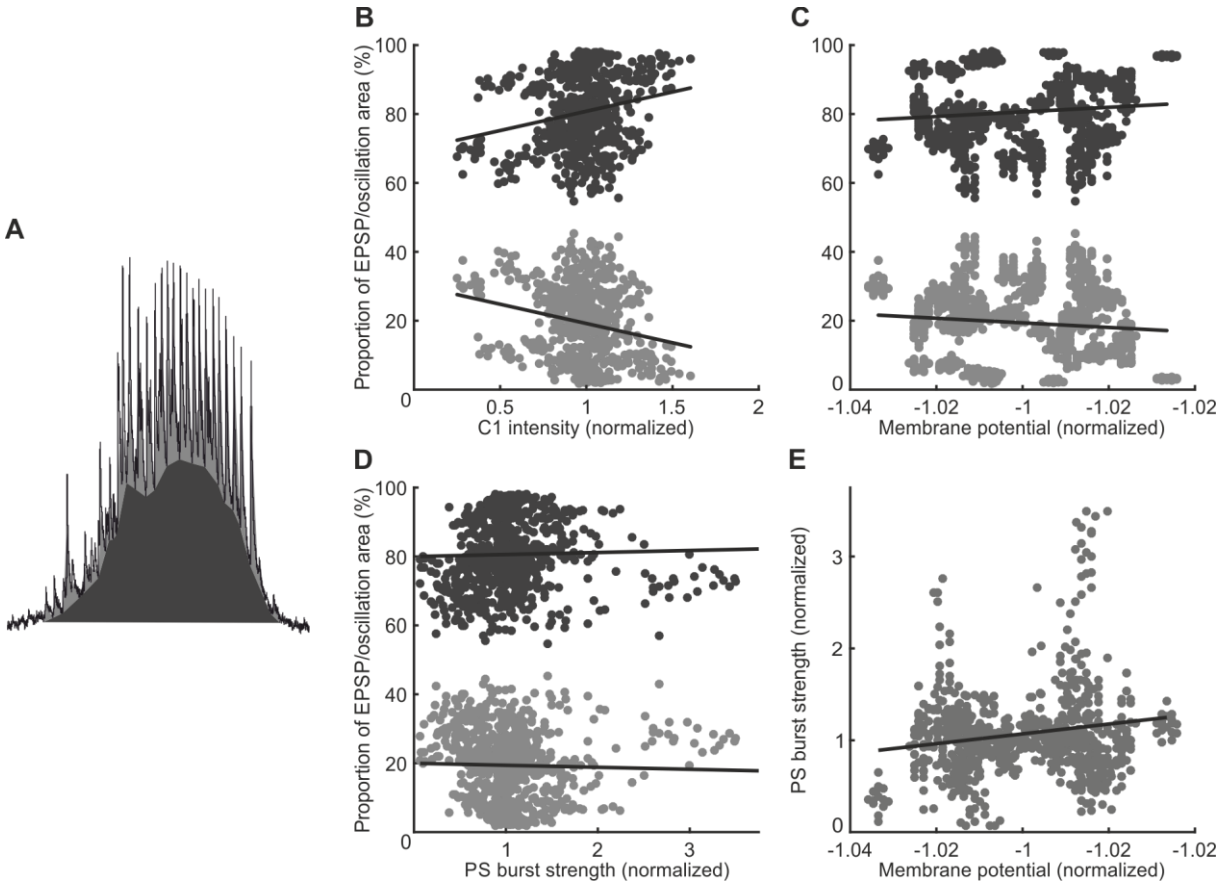

Figure 26: EPSP and oscillation areas and their contribution to PS burst strength. **A:** The EPSP area is depicted in light grey. The oscillation area yields from subtracting the EPSP area from the C1 intensity and is depicted in dark grey. **B**: The contribution of the EPSP area to C1 intensities is smaller than the contribution of oscillation areas. Increased C1 intensities reduce EPSP areas, but enlarge oscillation areas to the same extend (EPSP area: Spearman's rho: cc = -0.185; $P < 0.05$, N = 21, n = 752; RL: y = 30.388 – (11.188 * x), $R^2 = 0.05$, $P < 0.05$; oscillation area: Spearman's rho: cc = 0.185, $P < 0.05$, N = 21, n = 752; RL: y = 69.612 + (11.188 * x), $R^2 = 0.05$, $P < 0.05$) **C:** EPSP and oscillation areas are not correlated to V_m changes in ComInt1. (EPSP area: Spearman's rho: cc = -0.087; $P < 0.05$, N = 21, n = 752; RL: y = -47.380 – (66.765 * x), $R^2 = 0.05$, $P < 0.05$; oscillation area: Spearman's rho: cc = 0.087, $P < 0.05$, N = 21, n = 752; RL: y = 147.38 + (66.75 * x), $R^2 = 0.01$, $P < 0.05$) **D:** Changes in the percentage of EPSP and oscillation areas in C1 intensities are not correlated with PS burst strength (EPSP area: Spearman's rho: cc = -0.146; $P < 0.05$, N = 21, n = 752; RL: y = 20.088 – (0.584 * x), $R^2 = 0.0001$, $P > 0.05$; oscillation area: Spearman's rho: cc = 0.146, $P < 0.05$, N = 21, n = 752; RL: y = 79.992 + (0.584 * x), $R^2 = 0.0001$, $P > 0.05$) **E:** PS burst strength is positively correlated to depolarizations of ComInt1's V_m (Spearman's rho: cc = 0.0823, $P < 0.05$, N = 21, n = 752; RL: y = 6.411 + (5.341 * x), $R^2 = 0.03$, $P < 0.05$).

I plotted EPSP areas and oscillation areas against changes in ComInt1's V_m. This revealed that both were unaffected by de- or hyperpolarizations (Fig. 26 C). When I plotted ComInt1's EPSP areas and oscillation areas against the PS bursts strength I did not detect correlations between none of the parameters (26 D). However, depolarizations of ComInt1's V_m were positively correlated with increased strengths of the PS motor output of its home module (Spearman's rho: cc = 0.0823, $P < 0.05$, n =

752; RL: y = 6.411 + (5.341 * x), R^2 = 0.03, P < 0.05; Fig. 26 E). This result indicated that PS burst strengths were predominantly accompanied by depolarized ComInt1's.

Together, these results indicate that ComInt1's activity pattern is not only shaped by arriving inputs from the Coordinating Neurons but also by inputs from its own microcircuit, that together needs to be decoded and matched.

3.6. Cellular properties of synaptically isolated ComInt1's

To chemically isolate neurons, by suppressing transmitter release, is a useful technique to investigate if observed changes in neuronal activity due to bath application of chemicals are direct effects or mediated by the network. Bath application of low Calcium – high Magnesium saline (Low Ca^{2+}) was shown to depolarize the V_m of intracellularly recorded PSE and RSE motor neurons (Tschuluun et al. 2009). In these two types of neurons V_ms were further depolarized when carbachol (CCh) was added to Low Ca^{2+} (Tschuluun et al. 2009). The same depolarization was also observed in isolated ASC_E and DSC neurons (Schneider 2017). Synaptic isolation of ComInt1 suppressed the excitatory input from the Coordinating Neurons via chemical synapses. However, the electrical synapse between ComInt1 and IRSh was not affected by Low Ca^{2+} application. Therefore, I am not able to decipher whether changes in ComInt1 upon synaptic isolation were either caused by changes of intrinsic properties of ComInt1 or if changes were mediated by IRSh or both.

Figure 27 A and B illustrate the difference of spontaneously stopping rhythmic activity (A) and rhythmic activity that came to a halt upon application of Low Ca^{2+} (B). When rhythmic activity stopped spontaneously ComInt1's V_m oscillations came to a halt locked in the hyperpolarized phase, while EPSPs occurred tonically (Fig. 27 A). Bath application of Low Ca^{2+} entailed that ComInt1's oscillations disappeared. The rhythmic PS activity disappeared as well (Fig. 27 Bii). I only observed cessation of PS activity in 2 out of 7 experiments. In the other five experiments PS activity became tonic. Low Ca^{2+} never isolated ComInt1 completely from the coordinating network. In all small inputs in form of EPSP from ASC_E and DSC were persistent when Low Ca^{2+} was applied to the swimmeret system (Fig 27 Bii). When I added CCh to Low Ca^{2+} to increase the

excitation level of the almost synaptically isolated ComInt1 I observed that the persistent inputs were enhanced in form of tonically occurring EPSPs (Fig. 27 Biii; N = 5). CCh application also elicited tonic PS activity or enhanced tonic PS activity present in Low Ca^{2+} conditions (Fig. 27 Biii).

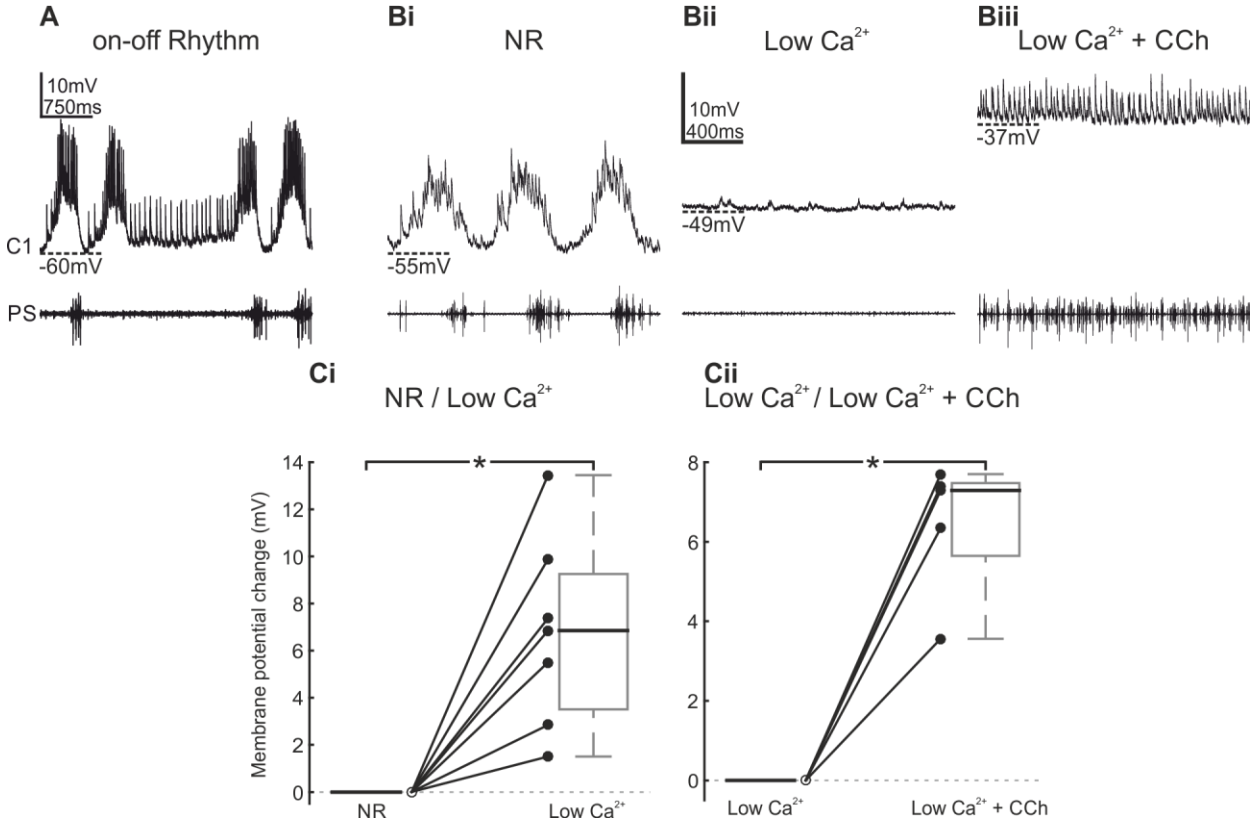

Fig 27: Effect on membrane potential (V_m) during isolation of ComInt1 with low Calcium – high Magnesium saline (Low Ca^{2+}). **A:** Simultaneous intracellular ComInt1 recording with the corresponding extracellular recorded PS motor output during spontaneous expressed rhythmic activity. ComInt1 hyperpolarizes and its oscillations come to a halt when rhythmic activity stops. **B:** Simultaneous intracellular recording of ComInt1 and extracellular PS recordings from ComInt1's home ganglion when NR (**i**), Low Ca^{2+} (**ii**) and Low Ca^{2+} / CCh (**iii**) was applied to the isolated nerve cord. **Bii**: Application of Low Ca^{2+} stops ComInt1's oscillations and depolarizes its V_m. Small EPSPs are still visible in ComInt1. PS motor output is inhibited. **Biii:** Adding CCh causes further depolarizations in ComInt1 and tonic EPSP activity occurs. Tonic PS activity increases by adding CCh to Low Ca^{2+} saline . **Ci:** Quantification of ComInt1's V_m depolarizations as a result of Low Ca^{2+} application. **Cii:** Bath application of CCh diluted in Low Ca^{2+} further depolarizes ComInt1's Vm. * P <0.05

The most significant effect of chemically isolating ComInt1 from the network was the change in its membrane potential (V_m; Fig. 27 Bi – Biii). Bath application of Low Ca^{2+} depolarized ComInt1's V_m in 7 out of 7 experiments (Low Ca^{2+}: Mdn = +6.85mV normalized to NR, iqr = 2.84 – 9.88mV; P < 0.05; N = 7; Fig. 27 Ci). Adding CCh to Low

Ca^{2+} depolarized the V_m of isolated ComInt1's even more (Low Ca^{2+} / CCh: Mdn = +7.29mV normalized to NR, iqr = 4.95 – 7.55mV; $P < 0.05$; N = 5; Fig. 27 Cii).

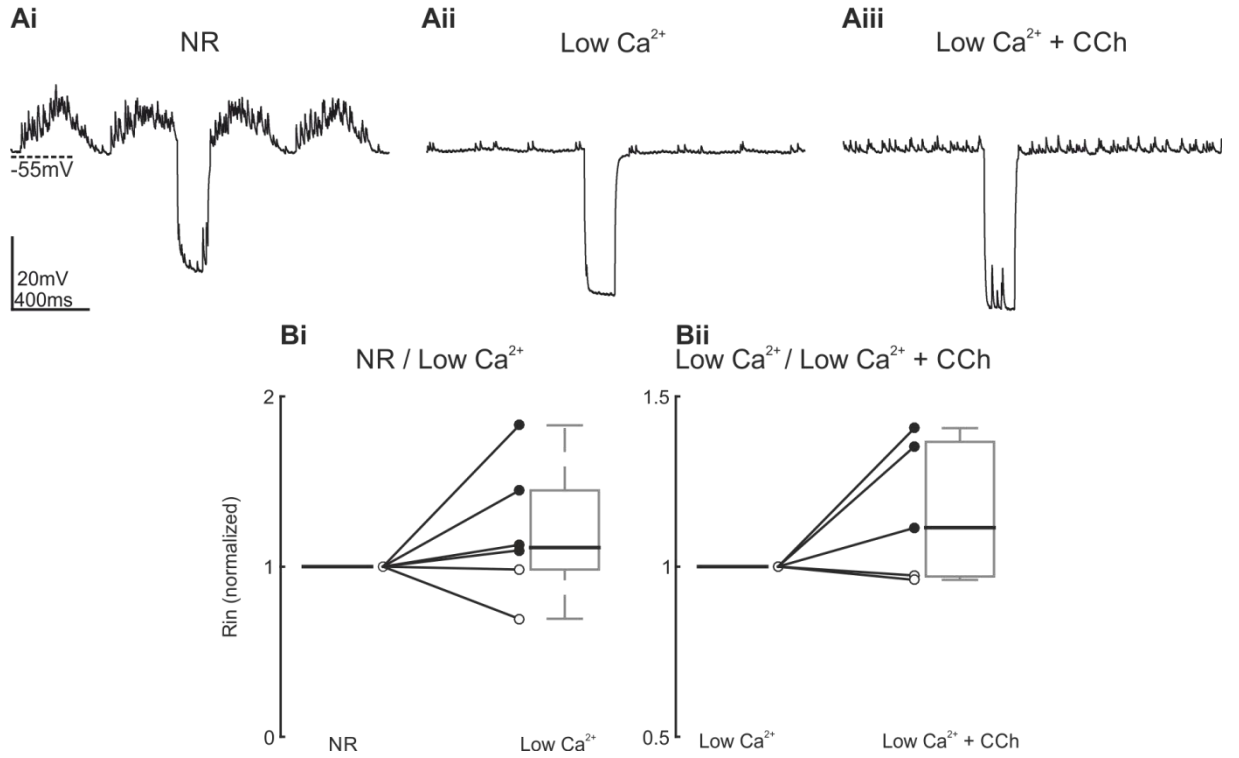

Figure 28: R_{in} changes due to isolating ComInt1 from the network. **A:** Exemplary R_{in} measurement while NR (**Ai**), Low Ca^{2+} (**Aii**) or Low Ca^{2+} containing CCh (**Aiii**) is applied. R_{in} does not change. **B:** R_{in} remains unchanged when Low Ca^{2+} is added to NR (**Bi**) and when CCh is added to Low Ca^{2+} (Supplementary Figures 49 + 50).

I also measured ComInt1's input resistance (R_{in}) while it was synaptically isolated. An example of a R_{in} measurement in one ComInt1 is shown in figure 28. Compared to the control condition (NR, Fig. 28 Ai), isolating ComInt1 with Low Ca^{2+} caused an increased R_{in}. This became apparent at a slightly larger deflection of its V_m as a response to a short hyperpolarizing current pulse (Fig. 28 Aii). The deflection was minimally increased when ComInt1 was then excited by adding CCh to the chemically isolated neuron (Fig. 28 Aiii). These weak tendencies were revealed by plotting the medians of normalized R_{in}s against the applied chemical (Fig. 28 B). As a result of Low Ca^{2+} application R_{in}s increased significantly in 4 out of 6 experiments and decreased in two experiments. The tendency of ComInt1's R_{in} to increase was undersized and therefore not significant across all animals (Mdn = 1.112 normalized to NR, iqr = 1.011 –

1.368, P > 0.05, N = 7; Fig. 28 Bi). There was no significant difference between R_{in}s measured when the isolated nerve cord was either bathed with Low Ca^{2+} or Low Ca^{2+} saline containing 3 µM CCh (Mdn = 1.114 normalized to Low Ca^{2+}, iqr = 0.974 – 1.353, P > 0.05, N = 5; Fig. 28 Bii).

These findings revealed that similarly to the V_m of PSE and RSE neurons, ComInt1's V_m depolarized when it was synaptically isolated from the network. ComInt1's V_m depolarized about 3 to 10 mV in Low Ca^{2+} saline and additionally about 5 to almost 8 mV when 3 µM CCh was added. Nevertheless, its R_{in} was nearly unchanged. These findings indicated that depolarizations were either intrinsically driven or mediated by IRSh via the electrical synapse or both.

3.7. Summary

I used carbachol (CCh) and edrophonium chloride (EdCl) to increase the excitation level of the swimmeret system. An increased excitation level always accelerated and strengthened rhythmic PS motor output. I achieved a decreased excitation level of the swimmeret system by application of crustacean cardioactive peptide (CCAP) to the isolated nerve cord. A decrease of the excitation level was manifested by a slow rhythm with weak PS bursts. Despite these modulations of the motor output, the phase lags from segment to segment were unchanged and the characteristic metachronal wave from posterior to anterior was maintained. The timing and duration of ComInt1's activity changed similarly to the PS activity in its home module. Current injections into intracellular recorded ComInt1's showed that ComInt1 was able to modulate indirectly the strength of PS bursts recorded in its home module. Therefore, I chose the PS burst strength as the most prominent parameter for the evaluation of the excitation level. Strong bursts are tantamount to high excitation levels, whereas weak bursts are tantamount to low excitation levels.

Increases and decreases of the network's excitation level were also manifested in cellular properties of ComInt1. I introduced the term C1 intensity to describe changes in ComInt1's activity. The C1 intensity is the calculated area between ComInt1's voltage trace and a threshold set at its trough potential. It depicts changes in the amplitude and

width of ComInt1's membrane potential (V_m) oscillations as well as alterations in the number and shapes of EPSPs. Excitation levels that were set by applied chemicals had minor effects on C1 intensities. However, CCh application tended to increase C1 intensities when ComInt1's membrane potential (V_m) was clamped. Nevertheless, I observed correlations between C1 intensities and PS burst strengths when the system was spontaneously active. A division of C1 intensities into an EPSP and an oscillation area revealed that neither EPSPs nor ComInt1's V_m oscillations correlated with the strength of PS bursts that were set by application of chemicals. This finding led to the assumption that ComInt1 did not only continuously decode the encoded information transmitted by the Coordinating Neurons but rather matched these inputs with inputs it additionally received from its own CPG. Moreover, my results emphasize the importance of V_m changes in ComInt1, since I found that V_m changes in ComInt1 did not affect C1 intensities, but that ComInt1's V_m correlated with the PS burst strength measured in its own module.

Part II: Morphology

3.8. The gradient of synaptic strength: A matter of synapses?

In the second part of my thesis I want to reveal the morphological basis of the gradient of EPSP amplitudes (gradient of synaptic strength) into ComInt1. Coordinating Neurons from anterior (DSC) and posterior (ASC_E) ganglia transmit information about the status of their home modules to ComInt1 (Mulloney and Hall 2003; Mulloney et al. 2006; Namba and Mulloney 1999; Schneider 2017; Schneider et al. in preparation; Smarandache-Wellmann and Grätsch 2014; Tschuluun et al. 2001). This information is encoded by bursts of spikes that converge simultaneously in ComInt1 with a gradient of synaptic strength (Smarandache et al. 2009). ComInt1 in A3 receives excitatory synaptic input from ASC_E originating from A5 and A4, additionally from DSC arising from ganglion A2. Spikes generated by ASC_E from the direct posterior neighboring ganglion, A4, elicits

the biggest EPSP in ComInt1. Spikes transmitted by DSC originating from the direct anterior neighboring ganglion, A2, elicits intermediate sized EPSPs in ComInt1. The smallest EPSP is therefore elicited by spikes of the Coordinating Neuron that travels the longest way through the abdominal nerve cord, in this case by ASC_E arising in ganglion A5. Hence, ComInt1 in A4 receives the strongest input from ASC_E in A5, the intermediate input from DSC in A4 and the weakest input from DSC in A2. ComInt1 in A5 only receives input from DSCs and ComInt1 in A2 on the contrary only receives inputs from ASC_Es. Here, the strengths of the inputs decreases with distance to the ganglion ComInt1 is located in (Smarandache et al. 2009).

I hypothesized that the gradient of synaptic strength has its origin in the composition of synaptic connections between Coordinating Neurons and ComInt1. This means that the Coordinating Neurons, which have the biggest impact onto ComInt1, form more or bigger synapses onto ComInt1 than the Coordinating Neurons, whose inputs are weaker. I investigated this by focusing on the morphology of synaptic connections between single Coordinating Neurons onto ComInt1. Therefore, I iontophoretically stained ComInt1 together with Coordinating Neurons and used immunohistochemical techniques to mark presynaptic boutons. In each figure I present in the following sections, a scheme illustrates the neurons and synaptic regions of interest ipsilaterally of one side of the swimmeret system. Furthermore colors highlight the neurons and synaptic regions that are stained in the images, whereby the colors correspond to the appearance as seen in the confocal images.

3.8.1. Morphology of ComInt1, Coordinating Neurons and the distribution of synapses

ComInt1 is located in each hemiganglion from A2 to A5 (Mulloney and Hall 2003). The scheme as well as the intracellular staining of ComInt1 illustrates its morphology (Fig. 29). Their cell bodies are located posterio-laterally on the contralateral side of their home module. From the cell body they process a small primary neurite dorsally to cross the midline in the posterior Minuscule Tract (MnT). From the midline the thin process continues anterio-laterally to enter the LN of its home module where it interacts with its

CPG. As ComInt1 crosses the midline, it projects small branches anterior and posterior parallel along the midline (Fig. 29).

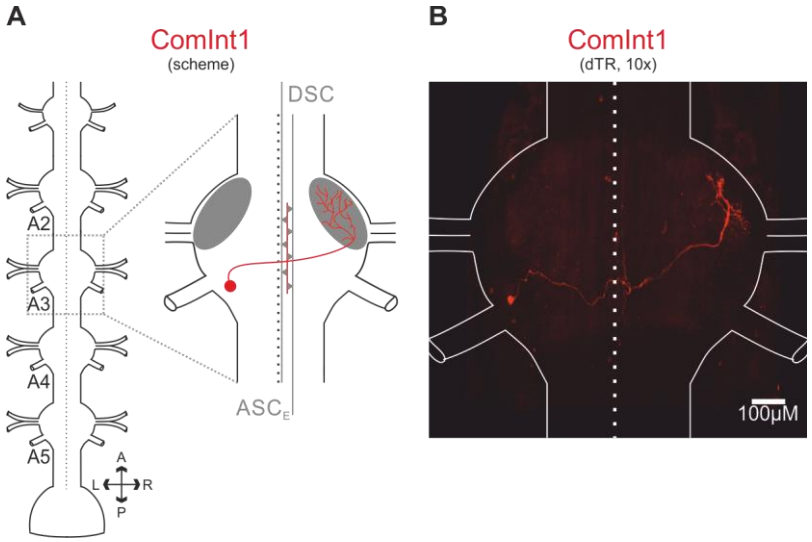

Figure 29: Morphology of ComInt1. **A:** Scheme showing ganglia A1 to A6 of the abdominal nerve cord and the morphology of ComInt1, highlighted in red, schematically in one ganglion. The same neurons of the contralateral side are not indicated. Coordinating Neurons and its synapses as well as the LN are shown in grey and are not discussed in B. **B:** Whole mount of ComInt1 (confocal z-stack). Overview of an abdominal ganglion, viewed from the dorsal side, illustrating a ComInt1 neuron that is dye-filled with dTR. The soma is located in the left hemiganglion posterior to the base of N1 from where a thin process extends to the midline. Here, it sends small branches posterior and anterior along the midline and then continues into the LN of the right hemiganglion, where it branches intensively.

ASC_E is one of the two Coordinating Neurons located in all hemiganglia from A5 to A2 (Mulloney et al. 2006). The morphology is explained by its appearance in its home module and its anterior neighbor (Fig. 30). ASC_E's soma is located posterior to the basis of N1 and sends its primary neurite into the LN where it branches intensively. From there ASC_E projects dorsally through the anterior MnT towards the midline. Before its axon reaches the midline it turns anteriorly and leaves the ganglion through the Area 78 of the connective along the midline (Skinner 1985a; Wiersma and Hughes 1961), towards anterior ganglia. The axon enters the anterior ganglia dorsally and passes the ganglion running parallel along the midline, where ComInt1 sends its small branches anteriorly and posteriorly. Here, the axon of ASC_E forms en passant synapses.

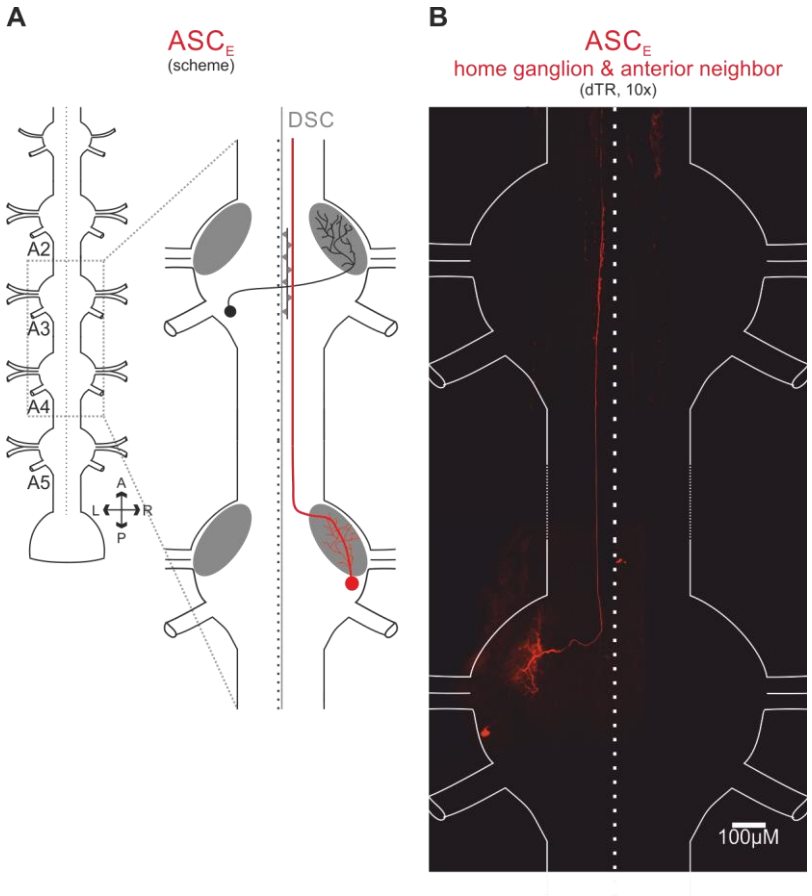

Figure 30: Morphology of an ASC_E neuron. **A:** Scheme showing ganglia A1 to A6 of the abdominal nerve cord (left) and an enlargement of two ganglia, highlighting in red the morphology of an ASC_E neuron within its home ganglion and in the anterior neighbor ganglion. The synapses of ASC_E in its target ganglion, DSC, ComInt1 and the LN are shown greyed out and are not discussed in B. The same neurons of the contralateral side are not indicated. **B:** Whole mount of ASC_E (confocal z-stack). Overview of two abdominal ganglia viewed from the dorsal side, illustrating an ASC_E neuron, dye-filled with dTR, in its home ganglion and in the anterior neighbor ganglion. The soma is located posterior to the basis of N1 and sends a primary neurite into the LN where it branches intensively. From there it extends an axon anteriorly to the midline where it leaves the ganglion into the connective (Area 78) projecting to anterior ganglia. The axon projects dorsally along the midline through the target ganglion aligned with the small branches of ComInt1.

DSC is located in each module from ganglion A4 to A2 (Mulloney et al. 2006). The morphology of DSC is explained by its appearance in its home module and its posterior neighbor (Fig. 31). DSC's soma is located anterior to the LN where it sends its primary neurite to. Within the LN it branches intensively to interact with its CPG. From there, DSC projects an axon posteriorly through the posterior MnT towards the midline. Before its axon reaches the midline, it turns posteriorly and leaves the ganglion through the Area 78 of the connective along the midline towards posterior ganglia. The axon enters the anterior ganglion dorsally and passes it running parallel along the midline, where it

also forms en passant synapses. This means that also DSC passes through each ganglion in the region where each ComInt1 sends small branches anteriorly and posteriorly parallel to the midline.

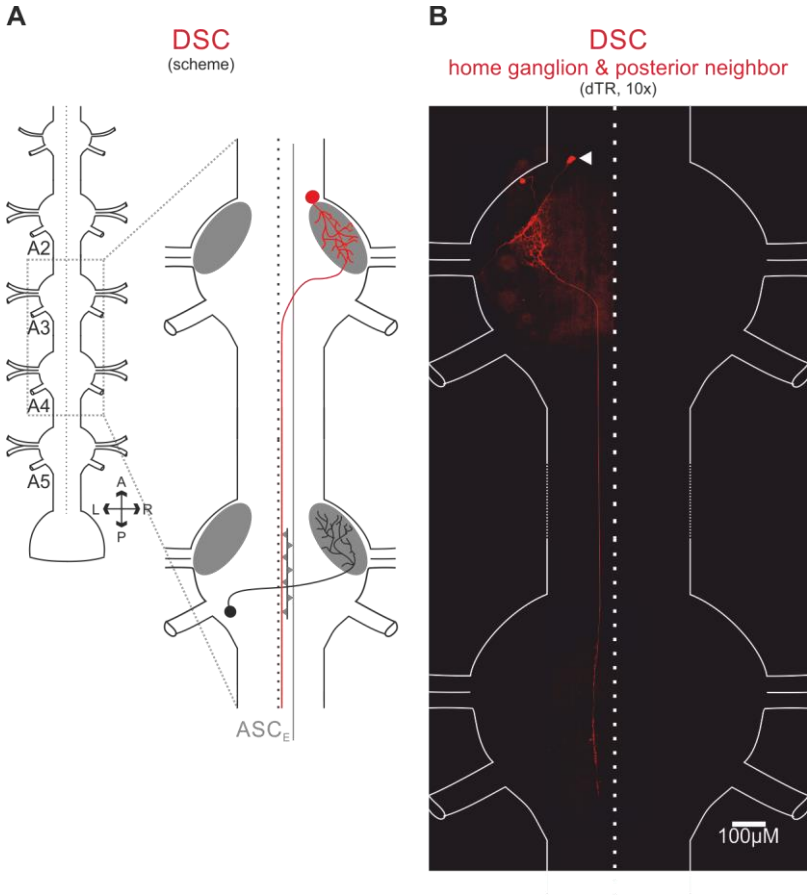

Figure 31: Morphology of a DSC neuron. **A:** A scheme showing the abdominal nerve cord with its ganglia A1 to A6 (left) and an enlargement of two ganglia highlighting the morphology of a DSC neuron in red within its home ganglion and in the posterior neighbor ganglion. The synapses of DSC in its target ganglion, ASC_E, ComInt1 and the LN are shown greyed out and are not discussed in B. The same neurons of the contralateral side are not indicated. **B:** Whole mount of DSC (confocal z-stack). Overview of two abdominal ganglia, viewed from the dorsal side, illustrating a DSC neuron, dye-filled with dTR, in its home ganglion and in the posterior ganglion. The soma is located anterior to the LN (arrow) and sends a primary neurite into the LN, where it branches intensively. From there, it extends an axon posteriorly to the midline, where it leaves the ganglion into the connective (Area 78) projecting to posterior ganglia. The axon projects dorsally along the midline through the target ganglion aligned with the small branches of ComInt1.

The morphology of ComInt1, ASC_E and DSC, revealed that these neurons run close to each other in the dorsal midline region. Therefore it is highly likely that the Coordinating Neurons synapse onto ComInt1 in this region. In order to to investigate if

synapses exist in the dorsal midline region of abdominal ganglia, I immunohistochemically marked presynaptic boutons

Presynaptic boutons were marked using the antibody “Anti-SYNORF1” (Ant-Synapsin), raised in mouse. Anti-Synapsin marks the presynaptic protein synapsin1 in chemical synapses and was visualized by a second antibody, raised in rabbit against mouse that was conjugated with a fluorescent dye. Figure 32 illustrates the distribution of synapsin1 and therefore of synapses that appeared green in my images, exemplarily shown within one abdominal ganglion. The distribution was identical in each of the 48 ganglia I investigated. An overview of a ganglion shows that presynaptic boutons were distributed all over the core of a ganglion, but most prominently in the LN, where most of the synaptic connections between neurons of the swimmeret system take place (Fig. 32 Bi). A higher magnification with the focus on the dorsal midline region revealed a thin band parallel along the midline, manifesting a higher density of presynaptic boutons. This finding proved that in the region where I assume that Coordinating Neurons form synapses onto ComInt1, exhibited a higher density of synapses (Fig. 32 Bii).

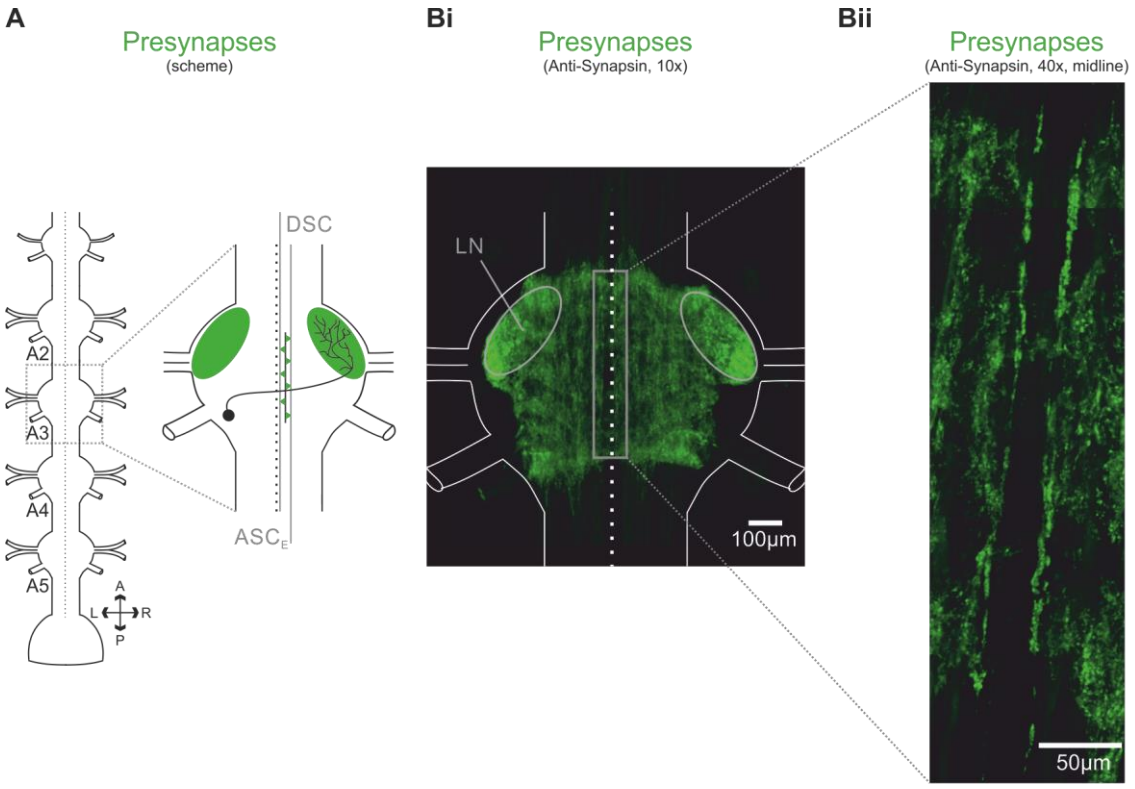

In the next step of my investigation, I immunohistochemically marked presynaptic boutons in ganglia, in which I previously intracellularly dye-filled ComInt1 neurons or Coordinating Neurons to verify that the small processes of ComInt1, the axons of Coordinating Neurons and the detected presynaptic boutons run close together along the midline.

3.8.2. Presynaptic boutons at the midline connect Coordinating Neurons with ComInt1

Figure 33 illustrates a scheme and exemplary images of one ganglion, in which I intracellularly dye-filled a ComInt1 neuron with dTR (red) and immunohistochemically marked the protein synapsin1 with a fluorescence dye (green). An overview displays the previously explained morphology of ComInt1 and the distribution of presynaptic boutons within the ganglion (Fig. 33 Bi). A merged stack of confocal images scanned with a 100x magnification with the focus on the dorsal midline region revealed that the small branches of ComInt1 and the presynaptic boutons run close to one another, parallel along the midline. I rather observed that presynaptic boutons clustered around the posterior and the anterior branch of ComInt1. This clustering of presynaptic boutons around ComInt1's aborizations was present in each of the 19 ganglia in which I stained ComInt1 and marked synapsin1 in. Since ComInt1 is the postsynaptic neuron and Anti-Synapsin solely marks presynaptic components, I never detected colocalizations of the two dyes (Fig. 33 Biii). The close approximation of presynaptic boutons around ComInt1's branches indicated that ComInt1 receives its synaptic inputs at this juncture, but it remained unknown if all presynaptic boutons represented en passsant synapses of Coordinating Neurons.

Figure 32: Distribution of synapses within abdominal ganglia of the swimmeret system **A:** Scheme of the abdominal nerve cord with its ganglia A1 to A6 (left) and an enlargement of one ganglion highlighting, in green, the LN and the putative excitatory chemical synapses, which Coordinating Neurons form onto ComInt1. ComInt1 and the Coordinating Neurons are greyed out and are not discussed in B. The same neurons of the contralateral side are not indicated. **B**: Whole mount of the distribution of presynaptic boutons (confocal z-stack). Overview of an abdominal ganglion, viewed from the dorsal side up, illustrating the distribution of immunohistochemically labeled presynaptic boutons. Synapses are expressed everywhere in the ganglion but most prominently in the LN (**Bi**). A higher magnification with focus on the dorsal midline region, where small branches of ComInt1 aligned with the axons of the Coordinating Neurons reveals a higher density of presynaptic boutons.

Moreover, by intracellularly dye-filling ComInt1, marking presynaptic terminals, and focusing on the LN of ComInt1's home module with a higher magnification, I never detected colocalizations of the fluorescence dyes (N = 11; Fig. 33 Bii). This fact proved that ComInt1 did not exhibit connections via chemical synapses within the LN and furthermore proved previous findings that ComInt1 is solely connected to IRSh and the lateral descending neuron via electrical synapses (Smarandache-Wellmann et al. 2014)

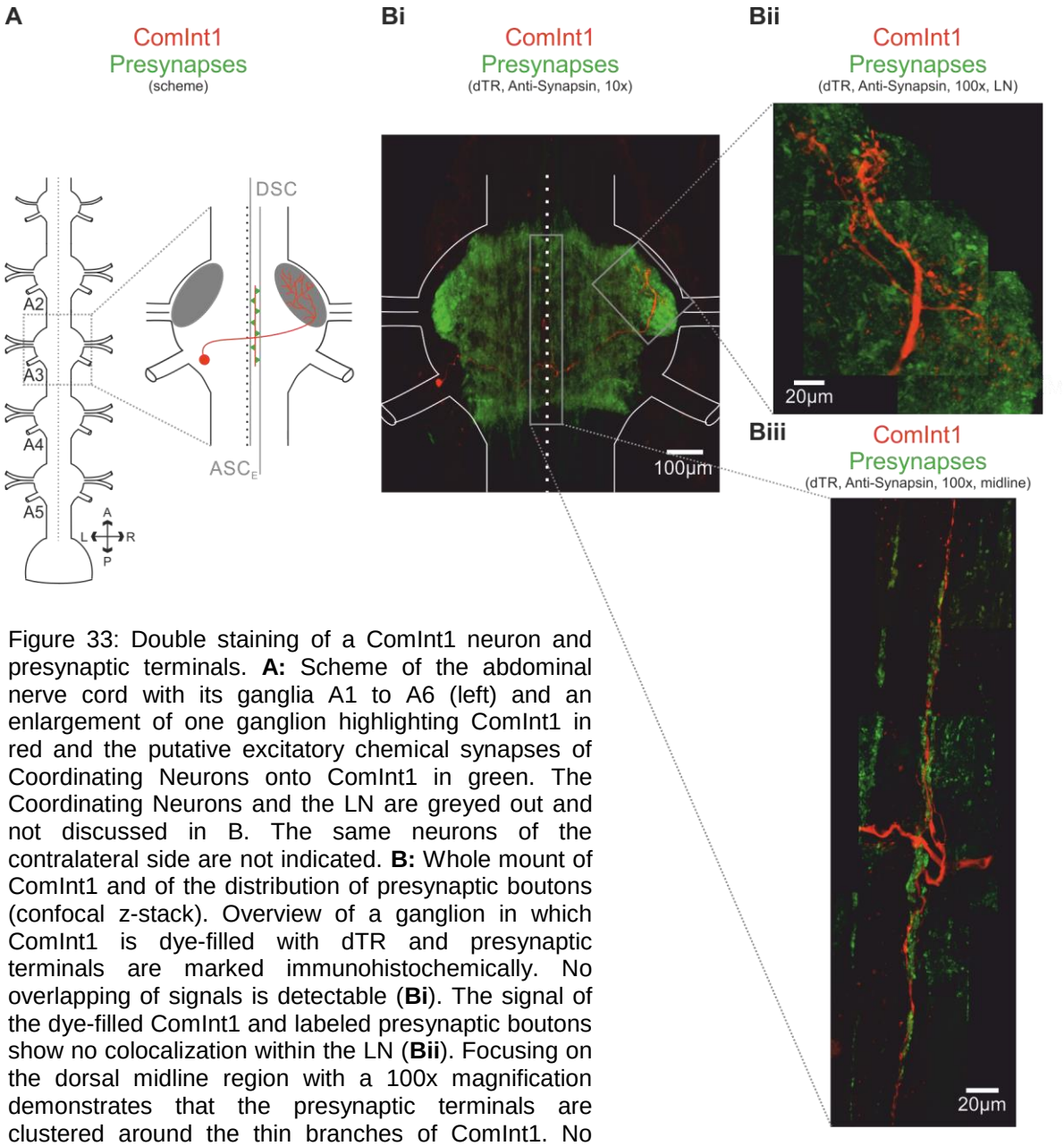

Figure 33: Double staining of a ComInt1 neuron and presynaptic terminals. **A:** Scheme of the abdominal nerve cord with its ganglia A1 to A6 (left) and an enlargement of one ganglion highlighting ComInt1 in red and the putative excitatory chemical synapses of Coordinating Neurons onto ComInt1 in green. The Coordinating Neurons and the LN are greyed out and not discussed in B. The same neurons of the contralateral side are not indicated. **B:** Whole mount of ComInt1 and of the distribution of presynaptic boutons (confocal z-stack). Overview of a ganglion in which ComInt1 is dye-filled with dTR and presynaptic terminals are marked immunohistochemically. No overlapping of signals is detectable (**Bi**). The signal of the dye-filled ComInt1 and labeled presynaptic boutons show no colocalization within the LN (**Bii**). Focusing on the dorsal midline region with a 100x magnification demonstrates that the presynaptic terminals are clustered around the thin branches of ComInt1. No overlapping of the two signals is detectable (**Biii**).

Figure 34 A shows schematically the previously explained morphology of an ASC_E neuron (red) that arises in its home ganglion and projects its axon anteriorly into the neighboring ganglion. ASC_E's axon traverses the ganglion dorsally parallel to the midline, where it forms en passant synapses (green triangles). A detailed investigation of this region revealed that marked presynaptic boutons and the axon of ASC_E were in close approximation to each other (Fig. 34 Bi). By means of a 100x magnification I was able to detect small ramifications that branch off the axons of ASC_E, whose fluorescence signals overlapped with the fluorescence signals of immunohistochemically marked presynaptic terminals (Fig. 34 Bii). I reconstructed the areas in which the overlapping appeared. Figure 34 Biii shows an exemplary z-stack of images in which areas, that exhibited overlapped signals of the two dyes, were reconstructed. The colocalization of signals of the two dyes was the first indication that the axons of ASC_E neurons form en passant synapses in the dorsal midline region of an anterior neighbor ganglion. Moreover, I calculated areas of colocalization for 3 out of 21 intracellular dye-filled ASC_E neurons, in which the staining was detected in the next anterior ganglion. The areas of colocalization were 212.28 μm^3 and 129.78 μm^3 for two ASC_E neurons stained in A3 and scanned in A2 and 250 μm^3 for an ASC_E neuron originating in A4 whose axon was scanned in A3.

Figure 35 A illustrates schematically the previously explained morphology of a DSC neuron (red) that arises in its home ganglion and projects its axon posteriorly into the neighboring ganglion. DSC's axon traverses the ganglion dorsally parallel to the midline where it forms en passant synapses (green triangles). A detailed investigation of this region revealed that marked presynaptic boutons and the axon of DSC were in close proximity to each other (Fig. 35 Bi). By means of a 100x magnification I was able to detect small ramifications that branch off the DSC axons. The signal of the fluorescence dye that was present in the small branches overlapped with the fluorescence signal of immunohistochemically marked presynaptic terminals (Fig. 35 Bii) and could be reconstructed. Figure 34 Biii shows an exemplary z-stack of confocal images in which areas, that exhibited overlapped signals of the two dyes, were reconstructed. Also here, the colocalization of signals of the two dyes described the first indication that axons of DSC neurons form en passant synapses in the dorsal midline region of a posterior neighbor ganglion. Furthermore, I calculated areas of colocalization for 2 out of 9

intracellular dye-filled DSC neurons. Once I detected the staining of a DSC axon in the next posterior ganglion. In a second staining the dye traveled even one ganglion further but was not detectable in the direct neighboring ganglion. The areas of colocalization were 111.62 µm^3 for a DSC neuron originating in A3 and scanned in A4 and 54.45 µm^3 for a DSC neuron originating in A2, whose axon was scanned in A4.

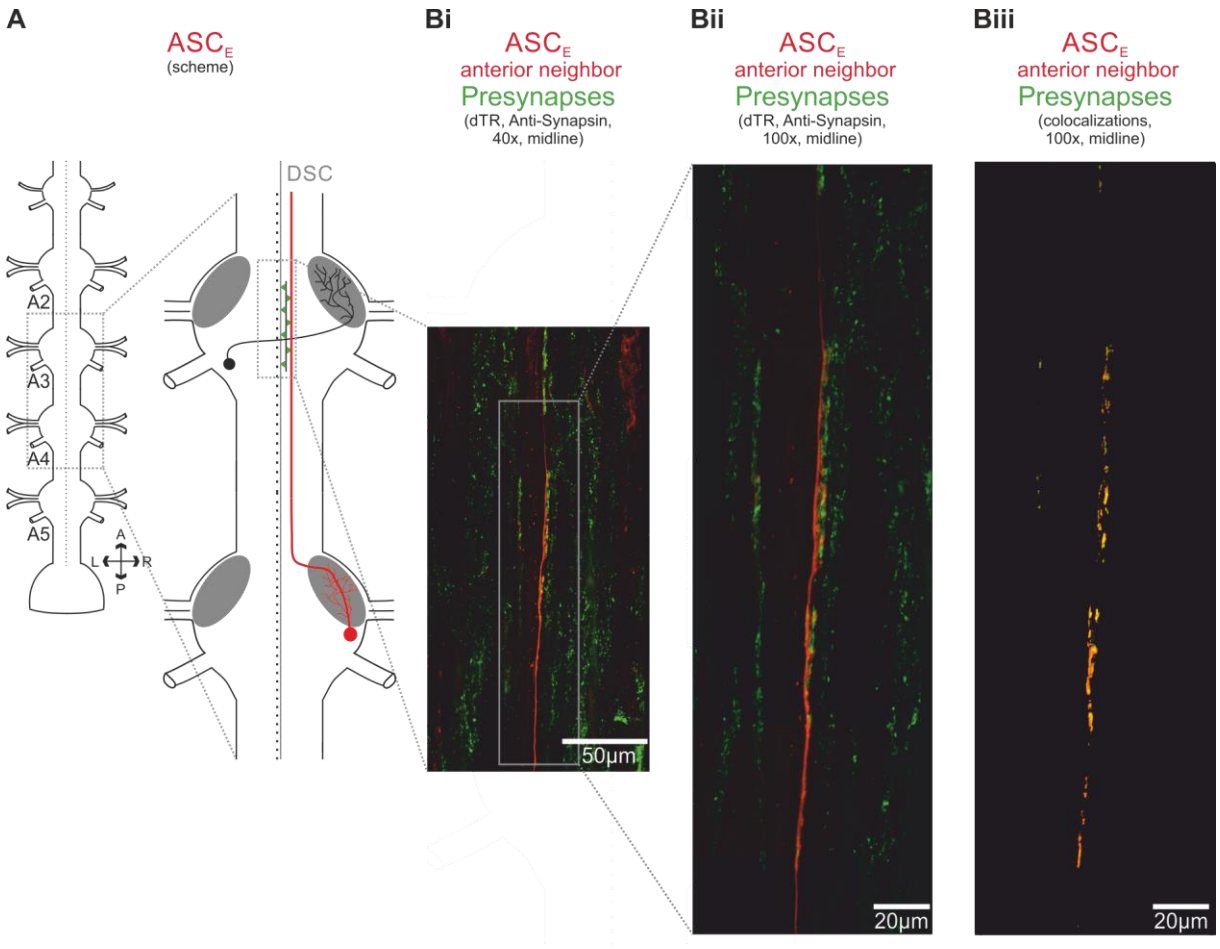

Figure 34: Double staining of an axon of an ASC$_E$ neuron and presynaptic terminals. **A:** Scheme of the abdominal nerve cord with its ganglia A1 to A6 (left) and an enlargement of two ganglia highlighting, in red, the morphology of an ASC$_E$ neuron within its home ganglion and in the anterior neighbor ganglion. The putative excitatory chemical en passant synapses of the axon of ASC$_E$ onto ComInt1 are highlighted in green. ComInt1, DSC and the LN are greyed out and are not discussed in B. The same neurons of the contralateral side are not indicated. **B:** Enlargement of the dorsal midline region in which the axon of ASC$_E$ traverses the anterior ganglion and is in close proximity to the presynaptic boutons along the midline (**Bi**). A higher magnification of this region reveals small ramifications that branch off the axon of ASC$_E$ and overlap with presynaptic boutons (**Bii**). The area of colocalization between the signals of the two fluorescence dyes is calculated in each confocal image and reconstructed in a stack (**Biii).**

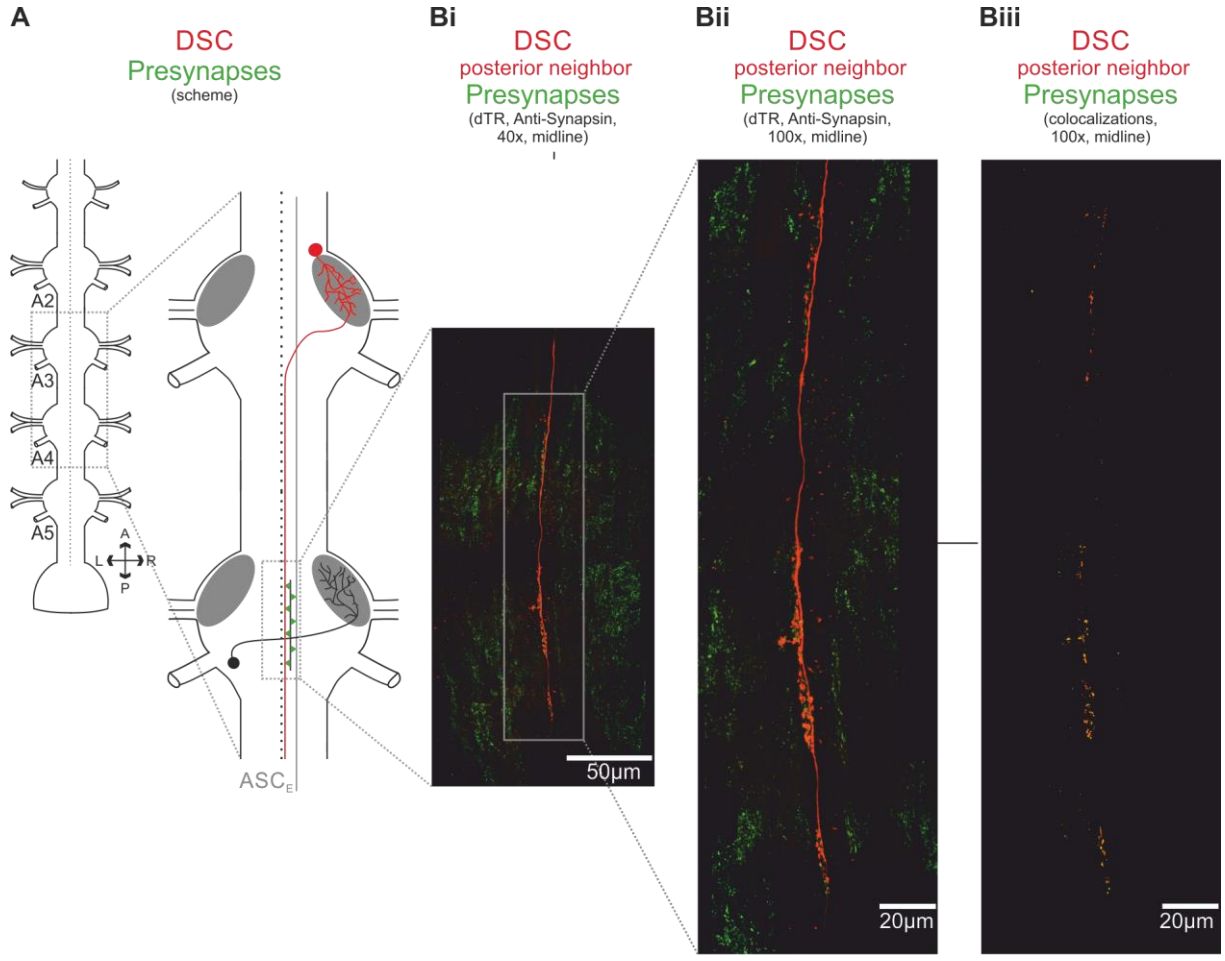

Figure 35: Double staining of an axon of a DSC neuron and presynaptic terminals. **A:** Scheme of the abdominal nerve cord with its ganglia A1 to A6 (left) and an enlargement of two ganglia highlighting the morphology of a DSC neuron within its home ganglion and in the anterior neighbor ganglion in red. Putative excitatory chemical en passant synapses of the axon of DSC onto ComInt1 are highlighted in green. ComInt1, ASC_E and the LN are greyed out and are not discussed in B. The same neurons of the contralateral side are not indicated. **B:** Enlargement of the dorsal midline region, in which the axon of DSC traverses the posterior ganglion and is in close proximity to the presynaptic boutons along the midline (**Bi**). A higher magnification of this region reveals small ramifications that branch off the axon of DSC and overlap with presynaptic boutons (**Bii**). The areas of colocalizations between the signals of the two fluorescence dyes are calculated in each confocal image and reconstructed in a stack (**Biii).**

To sum up, by using iontophoretical and immunohistochemical techniques, I detected presynaptic boutons at the dorsal midline region, which clustered in close proximity around ComInt1's small branches along the midline. Moreover, I detected colocalizations of the fluorescence dyes between marked presynaptic boutons and small ramifications of axons of intracellularly dye-filled Coordinating Neurons that traverse the anterior (ASC_E) respectively posterior (DSC) ganglion dorsally parallel to the midline.

These colocalizations were the first evidence that Coordinating Neurons exhibit en passant synapses in this region. However, the calculated areas of colocalization between the axons of intracellular dye-filled Coordinating Neurons and labeled presynapses, were the first approach to explain the three distinct sizes of EPSPs in ComInt1. The mean area of colocalization between ASC_E neurons (N = 3) and labeled presynaptic boutons in its anterior neighbor ganglion was 197.38 ± 61.52 μm^3. The areas of colocalization calculated for DSC (N = 1) was 111.62 μm^3 in the next posterior ganglion and 54.45 μm^3 in the ganglion after next (N = 1). This indicates that the strength of inputs from Coordinating Neurons would be determined by the size of areas of synapses onto ComInt1.

By all means, these results did not uncover if the different sizes of calculated areas were caused by different numbers of synapses or by synapses that differ in size. Moreover, I was not able to state if all detected presynapses were indeed synapses between Coordinating Neurons and ComInt1, because the fluorescence dyes were not stable and none of the triple labeled probes, in which ComInt1, ASC_E or DSC and presynapses were labeled within one ganglion (N = 7) could be analyzed.

3.8.3. Different approaches to visualize postsynaptic components within the swimmeret system

As a consequence that no staining of ComInt1, a Coordinating Neuron and presynaptic boutons worked in the same preparation, I had to choose different approaches to reveal if the presynaptic boutons of coordinating axons interconnect with the branches of ComInt1. Therefore, I tried to establish a protocol for two different antibodies, PSD-95 and Homer-1 that mark postsynaptic components. PSD-95 is an antibody against the postsynaptic density protein 95, which is a scaffolding protein, involved in the clustering of receptors, ion channels, and associated signaling proteins at the postsynaptic terminal. Its direct and indirect partners include neuroligin, NMDA receptors, AMPA receptors, and potassium channels (Hunt et al. 1996). Homer-1 also assembles signaling proteins, which are enriched in postsynaptic membranes of excitatory synapses and binds group 1 metabotropic glutamate receptors (Kato et al. 1998; Xiao et al. 1998). I used the same protocol as explained for

immunohistochemically labeling synapsin1 proteins in presynaptic boutons. I varied the concentration of the antibodies ranging from 1:300 up to 1:50 dilutions. Howbeit, both antibodies never labelled postsynaptic components within each 6 abdominal ganglia that were used for these immunohistochemical studies.

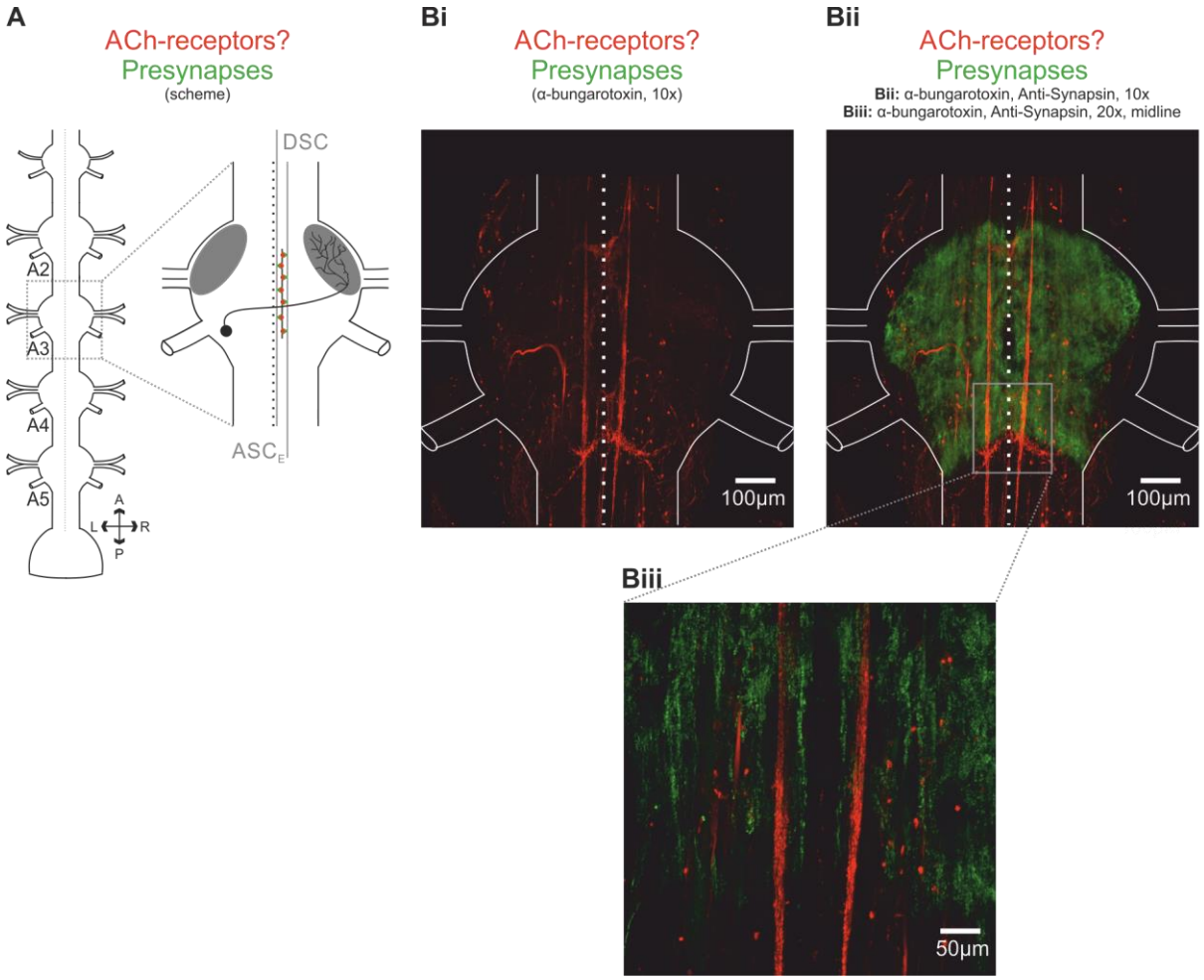

Figure 36: The attempt to label postsynaptic nicotinic ACh-receptors. **A:** Scheme of the abdominal nerve cord with its ganglia A1 to A6 (left) and an enlargement of one ganglion highlighting, in red, putative nicotinic ACh-receptors and excitatory chemical en passant synapses of the axon of Coordinating Neurons onto ComInt1 in green. ComInt1, ASC_E, DSC and the LN are greyed out and are not discussed in B. The same neurons of the contralateral side are not indicated. **B:** Whole mount of postsynaptic nicotinic ACh-receptors (Bi) and with immunohistochemically marked presynaptic boutons (confocal z-stack). Overview of an abdominal ganglion, viewed from the dorsal side up, illustrating unidentified neuronal structures that were stained by bath application of saline containing tetramethylrhodamin-labeled α-bungarotoxin. The unidentified structure crosses the midline at the posterior margin of the ganglion and projects axon like extensions bilaterally posterior and anterior along the midline (**Bi**). An additional labeling of presynaptic boutons highlights that these axon like structures are not in close proximity to the region of interest in which Coordinating Neurons synapse onto ComInt1 (**Bii + Biii**).

Since Schneider and colleagues (Schneider 2017; Schneider et al. 2018) demonstrated that the Coordinating Neurons ASC_E and DSC contain ACh, which these neurons might release at the synapse to ComInt1, I attempted to mark postsynaptic components of ComInt1. If ACh constitute the neurotransmitter used by Coordinating Neurons, there should be ACh-receptors expressed on the postsynaptic membrane of ComInt1. Therefore, I tried to label ACh-receptors using tetramethylrhodamin-labeled α-bungarotoxin. α-bungarotoxin binds with high affinity to the α-subunit of nicotinic ACh-receptors of neuromuscular junctions and within the CNS (Borodinsky and Spitzer 2007; Marshall 1981; Popova and Panchin Yu 1999).

Bath application of NR containing 18µg/ml tetramethylrhodamin-labeled α-bungarotoxin stained unidentified neuronal structures ventral at the posterior margin of abdominal ganglia, which crossed the midline in this region, in 7 out of 7 preparations (Fig. 36 Bi + ii). Moreover, application of α-bungarotoxin revealed promising structures within abdominal ganglia that appeared dorsally as axon-like branches bilaterally parallel along the midline (Fig. 36 Bi + ii). By means of a higher magnification with focus on the dorsal midline region, I was able to show that these axon-like structures did not occupy the same location as immunohistochemically labeled presynaptic terminals. Therefore, they could not be accounted to the thin branches of ComInt1, which were extended posterior and anterior where ComInt1 crosses the midline (Fig. 29 Biii). This finding led to the assumption that ComInt1 as the postsynaptic neuron does not exhibit nicotinic ACh-receptors.

3.9. ASC_E and its home ganglion

Mulloney and Hall (2007b) showed that ASC_E did not only affect the motor output of its target ganglion, but did also affect the motor output of its home module. In almost 50% of 15 experiments, in which I intracellularly recorded ASC_E in its home module, I saw that currents injected into ASC_E affected the PS motor output of its home module. Figure 37 A illustrates an exemplary experiment in which I simultaneously recorded intra- and extracellularly from an ASC_E neuron and extracellularly the PS motor output of its home module. ASC_E oscillated subthreshold in phase with PS bursts. A positive current injection into ASC_E elicited spiking activity in this neuron also demonstrated by

the extracellular ASC_E recording with a suction electrode. Concurrently, the depolarization that elicited spiking activity in ASC_E was accompanied by strengthened PS bursts in the home ganglion. Hyperpolarizing current impulses into ASC_E on the other hand prevent spiking activity of this neuron and additionally inhibited the PS motor output of its home module.

While scanning ASC_E neurons in its home module to confirm its morphology, I detected in the region where its axon leaves the ganglion anteriorly along the midline it also extended a small branch posteriorly into its home ganglion (Fig. 37 C). Additionally, labeling presynaptic terminals revealed, already with a 10x magnification, that the signals of the intracellular dye-filled ASC_E and of marked presynaptic boutons overlapped in this region. No overlapping of signals on the contrary was detectable within the LN (Fig. 37 Di). Increasing the magnification and focusing on the dorsal midline region at the anterior margin of the ganglion revealed that ASC_E exhibited small ramifications, which branch off its posteriorly directed extension. The signals of these ramifications overlapped with labeled presynaptic terminals (Fig. 37 Dii). This fact was manifested by 12 out of 15 preparations in which I successfully iontophoretically stained ASC_E neurons in its home ganglion.

This finding was the first morphological evidence that indicated that ASC_E interacts with its home module by projecting its primary neurite towards the dorsal midline region where they form chemical synapses at the anterior margin of the ganglion. Moreover, the presynaptic boutons that overlapped with ramifications of ASC_E's posteriorly projecting branch were part of the previously detected thin band of higher synaptic density along the midline (see Fig. 32). The same band describes the location in which presynaptic boutons clustered around the small branches of ComInt1 and in which I detected colocalizations between presynaptic terminals and coordinating axons. However, these presynaptic boutons cannot be accounted to connections between ASC_E and ComInt1 in its home ganglion. Firstly, the small branch ComInt1 sends anteriorly along the midline did not project far enough to interact with the posteriorly directed extension of ASC_E. Secondly, when recording intracellularly from ComInt1 stimulating ASC_E in its home module did not affect ComInt1's activity (personal communication Dr. Carmen Wellmann).

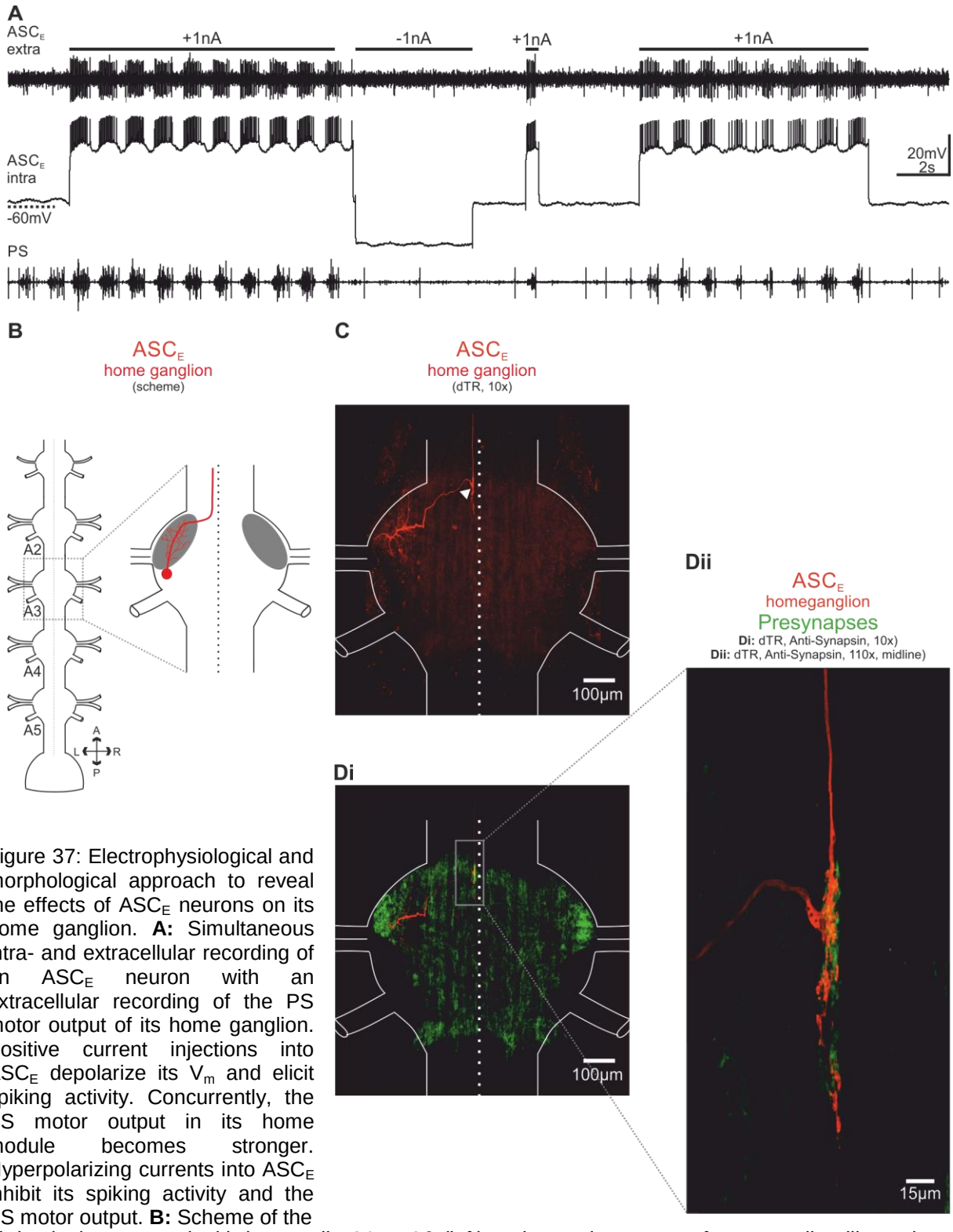

Figure 37: Electrophysiological and morphological approach to reveal the effects of ASC_E neurons on its home ganglion. **A:** Simultaneous intra- and extracellular recording of an ASC_E neuron with an extracellular recording of the PS motor output of its home ganglion. Positive current injections into ASC_E depolarize its V_m and elicit spiking activity. Concurrently, the PS motor output in its home module becomes stronger. Hyperpolarizing currents into ASC_E inhibit its spiking activity and the PS motor output. **B:** Scheme of the abdominal nerve cord with its ganglia A1 to A6 (left) and an enlargement of one ganglion illustrating, in red, the morphology of an ASC_E neuron within its home ganglion. ASC_E of the contralateral side is not indicated. **C:** Whole mount of ASC_E (confocal z-stack). Overview of an abdominal ganglion, viewed from the dorsal side up, highlighting that the axon of ASC_E branch off a small extension posteriorly into its home ganglion where it leaves the ganglion anteriorly (arrow) (**C**). An additional labeling of presynaptic terminals reveals that ASC_E forms chemically synapses in the anterior dorsal midline region of its home ganglion (**Di + ii**).

4. Discussion

In this study I used the crayfish swimmeret system to test the adaptive encoding hypothesis. It states, that matched encoders and a decoder are tuned to the system's excitation level. Here, I investigated the decoder in detail.

One side of the swimmeret system consists of four distributed oscillators that drive alternating PS and RS motor outputs, and are coordinated in a metachronal wave propagating from posterior to anterior (Hughes and Wiersma 1960; Wiersma and Ikeda 1964). Information about the timing, duration and relative burst strengths of the motor output is transmitted by Coordinating Neurons as corollary discharge to anterior and posterior ipsilateral microcircuits (Schneider et al. in preparation). The number of spikes in bursts of Coordinating Neurons encodes the strength of the respective motor outputs (Mulloney et al. 2006). However, following the adaptive encoding hypothesis, Coordinating Neurons adapt to the excitation level so that the same number of spikes could code for a weak burst at low excitation and a strong burst at high excitation levels (Schneider 2017; Schneider et al. in preparation). The information transmitted by these Coordinating Neurons converges simultaneously on ComInt1, the decoder. ComInt1 decodes this information and integrates it into its CPG. I found that ComInt1, in addition, continuously receives information about the status of its own CPG via a bidirectional electrical synapse (Smarandache-Wellmann et al. 2014). This allows its adaptation to the excitation level of its home module. As a result, ComInt1 samples and compares the activity of its own microcircuit with the periodic arriving inputs of all other CPGs, serving as a hub neuron (Gutierrez et al. 2013) that is able to detect mismatches between these inputs and capable to change its activity to synchronize all four ipsilateral oscillators.

4.1. Electrophysiology

I applied carbachol (CCh), crustacean cardioactive peptide (CCAP), or edrophonium chloride (EdCl) diluted in CCAP to modulate the excitation level of the swimmeret system. Concurrently, I intracellularly recorded from ComInt1 to characterize its decoding properties in order to investigate if ComInt1 adapts to the different excitation levels to match its decoding properties to the encoding properties of the Coordinating Neurons.

I will discuss my electrophysiological results that characterize ComInt1's cellular properties upon changing excitation levels in detail for the application of CCh. Afterwards, I shortly discuss ComInt1's cellular property modulations during CCAP and EdCl application, by highlighting findings that differ from modulations caused by CCh application.

4.1.1. Bath application of carbachol (CCh)

I uniformly increased the excitation level of the swimmeret system by applying CCh to the isolated nerve cord. CCh is a cholinergic agonist that activates all muscarinic and nicotinic ACh-receptors, and therefore elicits and modulates the motor output (Braun and Mulloney 1993). Mulloney and Hall (2007) stated that uniform changes of excitation levels of the swimmeret system alter PS burst strength and PS cycle period in all microcircuits in the same manner. Similarly, in my extracellular recordings from the posterior branch of N1, which contains the axons of approximately 35 PS motor neurons (Davis 1970; Mulloney and Hall 2000), CCh tended to increase burst strength and decreased PS cycle period of the PS motor output equally in all four ganglia (Braun and Mulloney 1993; Mulloney 1997).

The activity of PS motor neurons is shaped by inhibitory inputs of IPS, which is a part of the CPG (Mulloney et al. 2003; Smarandache-Wellmann et al. 2013). IPS also shapes ASC_E's activity through an inhibitory synapse. As this Coordinating Neuron receives the same input as PS motor neurons, its activity reflects the PS activity in its home module (Smarandache-Wellmann and Grätsch 2014). ASC_E sends the information about timing, duration, and relative strength of the PS motor output of its home ganglion

as a corollary discharge to anterior ganglia. DSC, whose activity is shaped trough an inhibitory synapse from IRS, the other CPG neuron, sends information about the status of the RS activity of its home ganglion as corollary discharge to posterior ganglia (Mulloney and Hall 2003; Mulloney et al. 2006; Namba and Mulloney 1999; Schneider 2017; Schneider et al. in preparation; Tschuluun et al. 2001). The timing and duration of motor neuron bursts are encoded by the on-set and off-set of bursts of spikes in Coordinating Neurons. The PS and RS burst strength is encoded by the number of spikes in an ASC_E and DSC bursts, respectively. For example, a 10% increase in PS burst strength is encoded with one more spike in an ASC_E burst (Mulloney et al. 2006). The capability of Coordinating Neurons to generate spikes is limited. ASC_E fires between 10 to 20 spikes and DSC 3 to 10 spikes per bursts (Mulloney and Hall 2007b; Mulloney et al. 2006; Namba and Mulloney 1999). That means that ASC_E and DSC have finite capacities to encode different burst strength and therefore have to adapt their output to different excitation levels (Schneider 2017; Schneider et al. in preparation). For example, if the isolated nerve cord is bathed in NR, weak PS burst strengths are encoded by 11 spikes in an ASC_E burst. A strong burst in turn is encoded by 17 spikes. As a result of CCh application the strength of PS bursts increased. Also under these conditions, PS burst strength could vary when CCh is applied. Therefore here, a weak PS burst strengths could be still encoded by 11 spikes and strong bursts by 17 spikes in an ASC_E burst, although burst strength is generally increased upon CCh application. In summary, Coordinating Neurons adapt to the range of expressed activity and therefore encode relative burst strength, meaning that the same number of spikes can code for different burst strengths (Schneider 2017; Schneider et al. in preparation).

ComInt1 is the decoder of the encoded information transmitted by Coordinating Neurons. How does ComInt1 decode the information about timing, duration and relative burst strength of the motor output of the other ganglia? Does ComInt1 also adapt to the level of excitation?

4.1.1.1. ComInt1's cellular properties

In order to answer these questions, I intracellularly recorded from ComInt1 while I modulated the excitation level of the swimmeret system. Afterwards, I analyzed ComInt1's cellular properties in response to changes of the excitation level.

For example, ComInt1 in A3 receives simultaneous input from ASC_E in A5, ASC_E in A4, and DSC in A2 (Mulloney and Hall 2003; Smarandache et al. 2009). These inputs arrive with a gradient of synaptic strength, whereby each spike in coordinating axons elicits one EPSP in ComInt1. The timing of motor outputs of the other ganglia is coded by the first EPSP that is elicited in ComInt1 by the first arriving spike. The duration of motor outputs is coded by the duration of bursts of EPSPs that is elicited by spikes of respective Coordinating Neurons. The distinct sizes of elicited EPSPs allow ComInt1 to distinguish between timing and duration of the respective motor outputs. This information is directly transmitted to the local CPG via an electrical synapse to IRSh (Smarandache-Wellmann et al. 2014). ComInt1 oscillates with the same period as the motor output of its home ganglion, due to this electrical synapse, and continuously receives information about the status of its own CPG. Therefore, the bi-directionality of the electrical synapse allows ComInt1 to sample the oscillations of its own CPG and to align these to the input transmitted by the Coordinating Neurons. That means that the Coordinating Neurons are necessary and sufficient to maintain the segment to segment phase lags of the rhythmic motor pattern (Namba and Mulloney 1999; Tschuluun et al. 2001), while ComInt1 is able to synchronize the activity of its own microcircuit with the activity of the other ganglia

The EPSPs elicited by individual Coordinating Neurons show no facilitation (Smarandache et al. 2009). Yet, as a consequence of arriving simultaneously in ComInt1, I hold to the opinion of Mulloney and Hall (2003) that EPSPs sum to depolarize ComInt1. This summation of EPSPs results in small membrane potential ($V_{m)}$ oscillations of ComInt1, which are directly transmitted to IRSh via the electrical synapse. Therefore, the summed EPSPs can contribute to enhance the PS motor output. The more spikes arrive in ComInt1 the more pronounced is the summation of EPSPs. Following the adaptive encoding hypothesis, the number of spikes in ASC_E and DSC bursts encode the relative burst strengths and adapt to the excitation level of the swimmeret system

(Schneider 2017; Schneider et al. in preparation). The number of EPSPs in ComInt1 together with the small depolarizing V_m deflection could be sufficient to decode the burst strength, however, relatively. The question remains of how ComInt1 perceives the system's excitation level?

4.1.1.2. ComInt1 (C1) intensity

I chose the C1 intensity as a measurement to investigate if ComInt1 adapts to the excitation level and how its cellular properties are modulated. The C1 intensity is a measurement for changes in the amplitude and width of V_m oscillations and EPSPs. It reflects the whole oscillation and inputs in ComInt1 and provides information about modulations due to the level of excitation. When I clamped ComInt1's V_m to the same value within one experiment, bath applications of CCh increased C1 intensities, predominantly borne by increased oscillation amplitudes. Since ComInt1's oscillations were shortened correspondingly to shortened cycle periods of the PS motor output, increases in oscillation and EPSP amplitude prevailed the shortening of oscillation widths, leading to an increased C1 intensity. If EPSP summations only cause small periodic occurring depolarizing deflections in ComInt1's membrane, where do the huge oscillations in ComInt1 emerge from?

Since it is highly likely that ACh is the neurotransmitter used by Coordinating Neurons (Schneider et al. 2018), it is likewise highly presumable that ComInt1's postsynaptic membrane exhibits nicotinic and muscarinic ACh-receptors. Bath application of CCh increases its concentration in the extracellular space within the whole isolated nerve cord, also surrounding ComInt1. CCh binds to muscarinic and nicotinic ACh-receptors, causing the excitation level of ComInt1 to increase by opening ion channels that allow positive charged ions to enter ComInt1. However, I measured that ComInt1's R_{in} tended to increase when CCh is applied. This finding revealed that fewer channels are open, which does not conciliate with the assumption that CCh opens more ion channels to excite ComInt1 more. Additionally, I found that ComInt1's R_{in} was highest when its membrane was depolarized, meaning it was highest at the maximum amplitude of ComInt1's oscillations, which describes the point in which the majority of its EPSPs are generated. An increased R_{in} during depolarized and low R_{in}s during

hyperpolarized phases were also found in ASC_E, DSC (Schneider 2017; Smarandache-Wellmann and Grätsch 2014), PSE, and RSE (Tschuluun et al. 2009). In ASC_E, DSC, PSE, and RSE neurons a low R_{in} during the hyperpolarized phase is explainable by an increased inhibition of the CPG. This cannot be applied to ComInt1, since its received inputs are on the one hand mediated from the CPG via an electrical synapse and on the other hand from Coordinating Neurons via excitatory chemical synapses.

The presence of the M-type channel in the membrane of ComIn1 could support also my findings. The M-type channel is a metabotropic voltage-gated ion channel, which is already open at hyperpolarized V_ms ensuring K^+ outward currents to stabilize the resting membrane potential of a cell. ACh or muscarinic agonists bind to the receptor, causing the M-channel to close (Adams et al. 1982; Alaburda et al. 2002; Brown and Adams 1980; Halliwell and Adams 1982), preventing K^+ ions to leave the cell. This accumulation of K^+ ions leads to a slow depolarization of the membrane, accompanied by a higher R_{in}. The kinetics of this metabotropic ion channel requiring second messenger cascades are to slow to describe EPSPs in ComInt1, but could contribute to enlarge ComInt1's oscillations. The generation of EPSPs requires the presence of ionotropic nicotinic ACh-receptors responsible for fast depolarizations of a cell (Kandel et al. 2000). Still, as measured by ComInt1's R_{in}, the closing M-type channels could counteract the channel openings needed for the EPSP generation in ComInt1.

The M-type channel is also proven to exist in the membrane of the cockroach giant interneurons and in crayfish walking leg motor neurons. In the giant interneuron of the cockroach, the application of muscarinic agonists depolarizes its V_m while the conductance of K^+ ions decreases (Corronc and Hue 1993). In motor neurons of crayfish legs, the inactivation of voltage-gated K^+ currents underlies long lasting exclusively muscarinic induced depolarizations (Cattaert et al. 1994). However, these slow depolarizations caused by M-type channel closings together with the small summation of EPSPs alone are not capable to explain ComInt1's huge oscillations.

Another possibility to explain that R_{in} is higher at depolarized and low at hyperpolarized V_m could be the HCN channel. The HCN is a cation channel that activates at hyperpolarized membrane potentials and closes during depolarization,

resulting in an increased R_{in} and in a reduction of the EPSP response to excitatory inputs (Mayford et al. 1996). However, a reduced EPSP response to excitatory inputs would be counterproductive for ComInt1 function to decode coordinating information. Therefore it is unlikely that HCN channels exist in ComInt1's membrane.

The electrical synapse between ComInt1 and IRSh, one neuron of the local CPG, is very important for the activity of ComInt1. The main function of electrical synapses is the effective fast transmission of i.e. currents between two neurons (Korn et al. 1977; Slesinger and Bell 1985; Zipser and Bennett 1976). That means that ComInt1 is able to transmit the information conveyed by Coordinating Neurons to its own CPG within 2 – 2.5ms (Smarandache-Wellmann et al. 2014), measured at the ganglion's midline (ComInt1) and in the LN (IRSh). In contrast, the transmission via chemical synapses takes 2 – 3.5ms (Nakagawa and Mulloney 2001; Namba et al. 1997; Sherff and Mulloney 1996). Additionally, the electrical synapse between ComInt1 and IRSh is bidirectional. Currents injected into ComInt1 directly evoke voltage deflections in the same direction in the membrane of IRSh. Consequently, depolarizing or hyperpolarizing currents injected into IRSh causes depolarization or hyperpolarization, respectively, in ComInt1 (Smarandache-Wellmann et al. 2014). Since electrical synapses can promote synchrony of coupled neurons (Bennett and Zukin 2004; Kopell and Ermentrout 2004), the electrical synapse between ComInt1 and IRSh manifests to perfectly synchronize the oscillations of these two neurons. Characteristics of bidirectional electrical synapses and the findings that the oscillation amplitudes in ComInt1 are not explainable with its cellular properties admit the assumption that a bulk of oscillations in ComInt1 is caused by oscillations of IRSh.

4.1.1.3. ComInt1's membrane potential (V_m)

Correlation analysis showed that the PS bursts strength is not correlated with C1 intensity. This finding emphasized that there has to be an additional mechanism to cope with varying inputs from Coordinating Neurons and the CPG of ComInt1's home module. A suitable candidate is ComInt1's V_m that correlated to measured PS burst strength. Bath application of CCh led to a median depolarization of ComInt1's V_m by 1.4 mV. Depolarizations in ComInt1 are caused by an increased CCh concentration in the

extracellular space, which opens ligand controlled ion channels enabling positive charged ions to enter the cell (Tschuluun et al. 2009). In addition the closing of M-type channels could contribute to this depolarization. When I did not clamp ComInt1's V_m during CCh application to the V_m in control condition, therefore admitted depolarizations, C1 intensities showed tendencies to decrease with depolarized V_m. That means that, most prominently ComInt1's oscillation amplitude could decrease abetted by M-type channels that might be closed due to muscarinic agonists (Adams et al. 1982; Alaburda et al. 2002; Brown and Adams 1980; Halliwell and Adams 1982). Additionally, the driving force for EPSP generation is reduced, resulting in decreased EPSP amplitudes which promote decreasing C1 intensities.

Correlation analysis between PS burst strength and ComInt1's V_m modulations revealed that these two parameters are positively correlated. Concurrently to ComInt1's V_m depolarization, the membrane of IRSh also depolarizes during CCh saline application (personal communication Dr. Carmen Wellmann). Due to the electrical synapse between ComInt1 and IRSh, it is intricate to state whether ComInt1 causes depolarizations in IRSh or whether depolarizations in IRSh are intrinsic and persuade ComInt1's membrane to depolarize. Both scenarios would explain a positive correlation between PS burst strength and ComInt1's depolarized membrane. However, it is most likely that the V_m of both cells, ComInt1 and IRSh, depolarize upon CCh application boosted and balanced by the electrical synapse. Regardless of the mechanism that depolarizes ComInt1 and IRSh, depolarizations in IRSh have strong effects on its transmitter release, which then enhances the inhibition of IPS. Stronger inhibition of IPS prompts that its graded transmitter release is reduced (Mulloney et al. 2003), which weakens its inhibitory influence on PS motor neurons, resulting in stronger PS bursts. Strong effects of small V_m modulations on the transmitter release have been shown in local premotor interneurons in thoracic ganglia of locust (Burrows 1979; Burrows and Siegler 1978), for stretch receptors in crab (Blight and Llinas 1980), and also in the swimmeret system for Coordinating Neurons by graded inhibition from CPG interneurons (Smarandache-Wellmann and Grätsch 2014). Additionally, in the stomatogastric nervous system of crab, the V_m of lateral gastric neurons hyperpolarizes by 2 to 3mV upon temperature increases. This allegedly small hyperpolarization results in increased leak currents,

which prevents rhythmic bursting of these neurons affecting the output of the whole system (Städele et al. 2015).

Taking everything together, ComInt1 adapts to the excitation level of its own microcircuit via an electrical synapse to IRSh by changing its V_m adequately. However, in case of the uniform excitement of the swimmeret system by CCh application, PS burst strength changes were similar across all four segments. Therefore, burst strength changes were insufficiently to cause detectable changes in spike number of Coordinating Neurons which then would cause detectable changes in ComInt1. Nevertheless, my experiments performed during spontaneous occurring rhythmic activity emphasized that C1 intensity alterations are important for ComInt1's decoding properties by continuously varying the intensity and by accurately representing the strength of the PS motor outputs of its home module.

4.1.2. Bath application of CCAP

CCAP is a nonapeptide in the CNS and in neurohemal organs. In crab, like pilocarpine and other muscarinic agonists, CCAP is a ligand for single voltage-gated inward currents of positive charged ions (Swensen and Marder 2000). Neurons containing CCAP were found in each segmental ganglion of crustaceans and insects (Ewer and Truman 1996; Stangier et al. 1988), in which it was able to elicit and modulate motor output (Gammie and Truman 1997; Weimann et al. 1997). Trube and colleagues (1994) detected two pairs of three neurons in each abdominal ganglion of crayfish that showed CCAP immunoreactivity. Axons of these neurons traverse through the whole abdominal nerve cord. Moreover, Mulloney (1997) found that CCAP immunoreactive neurons send projections into the LN of each hemisegment where they might interact with neurons of the CPG. He stated that bath application of CCAP elicited the swimmeret rhythm and also modulated the motor output by increasing the force of the PS, manifested by prolonged burst durations and increased burst intensities while the cycle period was unaffected. My results were partly congruent to Mulloneys (1997) findings. In my experiments, I also detected that CCAP biased the motor output towards PS by prolonging PS burst durations. However, disparate from Mulloney (1997) I detected that CCAP also increased the cycle period. Moreover, I calculated that CCAP

weakened PS bursts strength, although their intensity, the integral between a rectified and smoothed PS burst and a threshold, increased. Taking my results together, CCAP had state dependent effects on the swimmeret system. In silent preparations CCAP application increased the system's excitation level, manifested by its ability to excite rhythmic motor output. However, CCAP application decreased the excitation level of already active preparations by decreasing the cycle period and burst strength of the PS motor output.

The uniform decrease of the system's excitation level causes that the motor outputs of all micro circuits change equally (Mulloney and Hall 2007b). Following the adaptive encoding hypothesis, ASC_E and DSC also adapt to the set excitation level by tuning their encoding properties (Schneider 2017; Schneider et al. in preparation). Thus, ComInt1 did not detect mismatches between the timing and duration of IRSh oscillations and simultaneous arriving coordinating information and its oscillations followed the frequencies of the motor output of its own microcircuit.

Nevertheless, CCAP application compared to NR application prompted a tendency to increase C1 intensities. These increases were borne by enlarged amplitudes and prolonged widths of ComInt1's V_m oscillations, not by EPSPs. Those tended to decrease in amplitude as a result of a reduced driving force. In his paper, Mulloney (1997) performed intracellular recordings of PSE motor neurons. V_m oscillations of PSE motor neurons increased in amplitude over time after CCAP application. He assumed that these enlargements were not intrinsic to motor neurons itself, but rather driven by larger oscillations, and therefore by larger graded transmitter release, as shown in other systems (Burrows 1979; Burrows and Siegler 1978; Golowasch and Marder 1992; Nagayama et al. 1984; 1983; Paul and Mulloney 1985; Siegler 1985). This assumption supports my hypothesis that the bulk of ComInt1's oscillations are driven by IRSh via the electrical synapse. Increases in IRSh oscillation amplitude would then explain the enlarged amplitudes in ComInt1. Since CCAP is a ligand for muscarinic receptors (Swensen and Marder 2000), enlarged oscillation amplitudes could be additionally explained by the presence of M-type channels in the membrane of ComInt1 and IRSh. Bath application of CCAP increased the concentration of the nonapeptide in the extracellular space. CCAP binding to muscarinic receptors might have caused the

M-channels to close. This resulted in an accumulation of K^+ ions, and therefore in larger slow depolarizations of the membrane of ComInt1 and IRSh in terms of larger V_m oscillations (Adams et al. 1982; Alaburda et al. 2002; Brown and Adams 1980; Halliwell and Adams 1982). This hypothesis is supported by the finding that ComInt1's R_{in} increased due to CCAP application.

Li and colleagues (2018) detected recently that CCAP provides an enhancing effect on electrical synapses in the stomatogastric ganglion (STG) of crab. In the STG, pyloric dilator (PD) neurons are connected via an electrical synapse to a pacemaker neuron called anterior burster (AB), which then inhibits the lateral pyloric (LP) neuron. They measured synaptic currents in the LP neuron in response to voltage step stimulations in PD neurons and revealed that CCAP enhanced measured synaptic currents in LP. The currents injected into PD transmitted to LP via the AB neuron involving an electrical synapse. Therefore, they stated that CCAP enhances this electrical synapse. Related to the electrical synapse between ComInt1 and IRSh these findings would suggest that inputs transmitted by the Coordinating Neurons would be amplified by the electrical transmission through the gap junction. Moreover, the enhancing effect of CCAP on the electrical synapse between ComInt1 and IRSh could also be manifested in goading each other oscillations, hence prolonging IRSh oscillations and therefore the PS motor output.

Also here I did not detect correlating changes between C1 intensities and PS burst strength measured in ComInt1's home ganglion. This finding yielded an additional piece of evidence that uniform excitation level modulations are insufficient to examine ComInt1's decoding properties as measured by its intensities due to a lack of motor output changes.

4.1.3. Comodulation of CCAP and EdCl

Braun and Mulloney (1993) ascertained that bath applications of eserine, an inhibitor of the ACh-esterase, accelerated the frequency of the PS motor output. In my experiments, I used EdCl to investigate the action of an ACh-esterase inhibitor on the PS motor output and on the cellular properties of ComInt1. Since it is highly likely that

Coordinating Neurons use ACh as neurotransmitter to convey information about the status of their home modules to ComInt1 (Schneider et al. 2018), the use of EdCl seems to be a more natural method to modulate ComInt1's cellular properties. Bath application of EdCl delays the depletion of ACh in the synaptic cleft and therefore prolongs the activity of ACh at the postsynaptic membrane. Since EdCl is able to modulate ongoing rhythmic activity but cannot elicit rhythmic activity from silent preparations, I applied EdCl diluted in CCAP saline. Thus, this experimental approach describes not only the effect of EdCl, but rather the comodulating effect of CCAP and EdCl.

While CCAP alone decreased the system's excitation level, the addition of EdCl in turn increased its level of excitation predominantly manifested by decreased cycle periods and strengthened PS bursts. Here, the modulation of the excitation level was uniformly, causing coherent changes in all hemi segments and the coordinated rhythm was maintained. Therefore, the timing and duration of ComInt1's oscillations were again determined by synchronous V_m oscillations of IRSh and enhanced by simultaneously arriving inputs from Coordinating Neurons. The addition of EdCl did not change C1 intensities, although the width of ComInt1's oscillations decreased with the burst duration of the PS motor output in its home module. The C1 intensity area gained due to enlarged oscillation amplitudes weighted equally to the loss of C1 intensity area due to narrowed oscillations. In terms of the comodulation that means that ComInt1's huge oscillations upon CCAP application were further increased but shortened by adding EdCl.

This could be explained by the following hypothesis. Since CCAP is a muscarinic agonist, it ligates to muscarinic ACh-receptors in the membrane of ComInt1 (Swensen and Marder 2000) closing M-type channels (Adams et al. 1982; Alaburda et al. 2002; Brown and Adams 1980; Halliwell and Adams 1982). The closing prompts an enhancement of the slower component of ComInt1's voltage changes. Additionally, EdCl affects the EPSPs in ComInt1, representing the fast component of its voltage changes. ACh is released from presynaptic boutons of the Coordinating Neurons in response to arriving action potentials. These ACh molecules bind to nicotinic ACh-receptors causing ionotropic ion channels to open and positively charged ions to enter the cell. The presence of EdCl might prolong the opening of these ion channels resulting in a longer

inward current into ComInt1. Thus, EPSPs in ComInt1 could sum to further enlarge ComInt1's oscillation amplitude. This enhancing effect might be directly transmitted via the electrical synapse to IRSh, enlarging its oscillations, causing an increased transmitter release and therefore a stronger inhibition of IPS, resulting in strengthened PS motor output. Moreover, the presence of CCAP could additionally enhance the electrical synapse between ComInt1 and IRSh, boosting the effect of EdCl. This boosting effect is supported by the finding of Li and colleagues (2018). They found that in the STG the comodulation of proctolin with CCAP enhances the effect of proctolin on the measured synaptic currents in LP due to stimulations in PD neurons.

My hypothesis, that oscillation amplitude enlargements are caused on the one hand by closed M-type channels and on the other hand by extended openings of ionotropic ion channels, is supported by an unchanged R_{in} when CCAP and EdCl are simultaneously applied. That might indicate that the number of closed M-type channels causing ComInt1's R_{in} to increase is counterbalanced by longer ion channel openings due to the inhibition of the ACh-esterase.

Also here I did not detect any correlation between C1 intensities and PS burst strength measured in ComInt1's home ganglion. This finding yielded additional evidence that uniform excitation level modulations are insufficient to examine ComInt1's decoding properties as measured by its intensities due to a lack of motor output changes. However, ComInt1's V_m depolarized, in median, by 0.48 mV might cause minimal depolarizations of the V_m of IRSh. As discussed previously even small depolarizations in IRSh could have strong effects on the transmitter release on IPS and therefore on the PS burst strength (Blight and Llinas 1980; Burrows and Siegler 1978), which is supported by my finding that PS bursts strength correlated with V_m alterations in ComInt1.

4.1.4. ComInt1 as a hub neuron

My experiments revealed that each applied substance modulated the excitation level of the swimmeret system and therefore altered the motor output of each single hemi segment. However, these changes were alike in all modules and therefore

changes in burst strength and, according to that in spike number of bursts of Coordinating Neurons were insufficient to reveal in detail how ComInt1 decodes this information. Neither did I detect correlations between EPSP changes and PS burst strengths nor between oscillation changes and PS burst strength. Yet, I detected a tendency that PS burst strengths increased together with depolarizations of ComInt1's V_m. Through the presence of the electrical synapse between ComInt1 and IRSh I was not able to discriminate if the depolarization in ComInt1 is borne by depolarization of IRSh or vice versa. However, I assume that both neurons depolarize to establish a common V_m. Moreover, I previously discussed that a bulk of ComInt1's oscillations is driven by simultaneous oscillations of IRSh transmitted via the electrical synapse. Therefore, I conclude that ComInt1's adaptations to the excitation level of its local microcircuit, is ensured via the bidirectional electrical synapse to IRSh.

Moreover, my results together with results from previous investigations on ComInt1 (Mulloney and Hall 2003; Smarandache-Wellmann et al. 2014; Smarandache et al. 2009) reveal that ComInt1 is part of the coordinating circuit as well as of the local microcircuit. It rather describes the point of intersection between both circuits. That means that ComInt1 decodes information sent by Coordinating Neurons and simultaneously samples continuously the activity of its home ganglion to synchronize these inputs with each other. In my experimental approach there was no need for ComInt1 to act to synchronize these inputs since the excitation level changes ensued uniformly. Nevertheless, I assume that if ComInt1 detects a mismatch between the received information of Coordinating Neurons and the activity of its home CPG, ComInt1 would have the ability to act to synchronize the four ipsilateral distributed oscillators.

The ability of ComInt1 to process and integrate chemical inputs from three microcircuits and electrical input from one microcircuit and to synchronize these inputs via an electrical synapse describes a typical hub neuron (Gutierrez et al. 2013; Smarandache-Wellmann et al. 2014). Two circuits are synchronous if they oscillate with the same period and a constant phase (Izhikevich 2007; Rosenblum and Pikovsky 2007). Synchronizing means to adjust time and strength of one CPG to the others, to maintain phase delays for effective thrust (Zhang et al. 2014), which can already be achieved by weak coupling (Kopell and Ermentrout 2004; Kopell and Ermentrout 1988).

ComInt1 achieves the synchrony of its own micro circuit with the other oscillators by enhancing its input onto IRSh to recruit indirectly more PS motor neurons or by reducing its input to IRSh to indirectly weaken PS motor neurons as also shown i.e. in neocortical networks (Roopun et al. 2008). This modulation happens very fast via the electrical synapse which supports synchrony more than chemical synapses. Moreover, the presence of the electrical synapse connotes that although inputs into ComInt1 could vary, the synchronization via a gap junction could result in similar network outputs (Marder 2011; Prinz et al. 2004).

My analysis of spontaneously occurring rhythmic activity, including on-off rhythms, which exhibit huge PS burst strength variations, revealed that then C1 intensities varied accordingly resulting in a positive correlation of these two parameters. I will explain the importance of C1 intensities for the synchronization of coupled oscillators by means of a switch from a silent to an active state of the swimmeret system. Elicited rhythmic activity always starts in the most posterior ganglion A5. While the first PS burst is generated in A5, the anterior ganglia remain silent. However, the information about timing, duration and strength of the occurring burst in A5 is transmitted to anterior ganglia by ASC_E. This information arrives first in ComInt1 located in A4, which is silent for the moment. The arriving bursts of ASC_E spikes in ComInt1 in ganglion A4 describe a mismatch between the activities of ganglion A5 with its own ganglion. This mismatch is perceived as EPSPs in ComInt1 and is directly reported to IRSh via the electrical synapse. The excitation of IRSh might be enough to inhibit IPS and therefore to generate PS bursts. That means that ComInt1 synchronizes the activity of its own CPG to the activity of the CPG located in A5. Moreover, the excitement of IRSh not only excited indirectly PS motor neurons but also ASC_E in its home module which in turn sends the information about the PS motor output to anterior ganglia initiating the same cascades.

Taking everything together, ComInt1 oscillates perfectly in phase with IRSh, which is part of the CPG of its local microcircuit. Simultaneously bursts of spikes that arrive in ComInt1 cause periodic perturbations in ComInt1 in the form of EPSPs. Through the elicited EPSPs, ComInt1 is able to decode the received perturbations and is rather able to compare their timing, duration, and strength with the timing, duration, and strengths of its own microcircuit. If ComInt1 perceives a mismatch between the inputs, it can

compensate for these mismatches by modulating its activity to entrain the outputs to the same period and therefore to synchronize the distributed oscillators (Kopell and Ermentrout 1988; Schwemmer and Lewis 2014; Skinner et al. 1994; Zhang and Lewis 2013). This multilevel integration of ComInt1 improves the signal-to-noise ratio of received and conveyed inputs enabling a more complex input and output relationship (Rigotti et al. 2013; Stein et al. 1993; van Atteveldt et al. 2014).

4.1.5. Isolating ComInt1

In the intact network ComInt1 oscillates in phase with IRSh. If rhythmic activity stops, ComInt1's oscillations come to a halt and its V_m is locked in the hyperpolarized phase. Application of Low Ca^{2+} stops synaptic transmission at all chemical synapses within the swimmeret system, resulting in a disruption of the rhythmic motor output. Synaptically isolating ComInt1 with Low Ca^{2+} dispersed ComInt1's oscillations and paradoxically most prominently depolarized ComInt1's V_m. The same effect of Low Ca^{2+} was also observed when synaptically isolating PSE, RSE (Tschuluun et al. 2009). Since ComInt1 is connected to IRSh via a bidirectional transmitting electrical synapse, I am not able to state if this depolarization is intrinsic to ComInt1, driven by IRSh or both. Moreover, I occasionally observed EPSPs in ComInt1 whose amplitude was reduced by 50% compared to EPSPs in the intact network (Schneider et al. 2018), indicating that the Ca^{2+} concentration was not low enough to block chemical synaptic transmission completely.

An excitation level increase of the isolated ComInt1 by adding CCh to Low Ca^{2+} saline further depolarized its V_m. The same effect was detected for PSE, RSE and also for ASC_E and DSC (Schneider 2017; Schneider et al. in preparation; Tschuluun et al. 2009). Unfortunately, I am not able to state if this depolarization is intrinsic to ComInt1, assisted by depolarizations in IRSh, or only driven by IRSh. However, the application of CCh diluted in Low Ca^{2+} enabled me to assume that ComInt1's V_m depolarizations are not driven by Ca^{2+} influx. Due to the lack of Ca^{2+} in the extracellular space it appeared highly likely that depolarizations in ComInt1 are driven by Na^{2+} influx.

4.2. Morphology

In the second part of my thesis I wanted to unravel the gradient of synaptic strength that the Coordinating Neurons have onto ComInt1. I hypothesized that the gradient of synaptic strength has its origin in the number or in the size of synapses Coordinating Neurons form onto ComInt1. I choose a morphological approach to test this hypothesis by intracellularly dye-filling ComInt1 and Coordinating Neurons and by using immunohistochemically techniques to label synapses in the swimmeret system.

4.2.1. The gradient of synaptic strength

The colocalization area of dye-filled Coordinating Neurons and immunohistochemically labeled presynaptic boutons was the first evidence that the gradient of synaptic strengths has its origin in the synaptic composition. I am not able to state if the calculated areas differed because the number of synapses or the size of synapses differed. In drosophila larvae the number of synapses between two cells determined the responsiveness of the postsynaptic cell to a stimulation of the presynaptic cell (Ohyama et al. 2015). Additionally, at the neuromuscular junction, the strength of the postsynaptic response is positively correlated with the number of synapses (McLean and Dougherty 2015; Ruiz-Canada and Budnik 2006). These findings among others leaded to the general statement that in the CNS of drosophila larvae the number of synapses is positively correlated with the strength of the synapse (Zwart et al. 2016). That means that a higher count of synapses results in a stronger input and a weak input is accompanied by a low count of synapses.

In addition to the gradient of synaptic strength, where the nearest ganglia always exhibit the strongest input and ASC_E's input is always stronger than the input of DSC (Smarandache et al. 2009), Mulloney (2006) detected a gradient of spike count for ASC_E. He described that ASC_E in A5 generated more spikes than ASC_E in more anterior ganglia. ASC_E in A2 thereby generated the fewest spikes per burst. Together these gradients, intrinsically in ASC_E neurons and shaped by the synaptic composition between ASC_E and ComInt1, promotes the characteristic metachronal wave of the motor output from posterior to anterior. According to this, the information transmitted from the

posterior ganglion via ASC_E is always the strongest input and therefore the most important input for the maintenance of the segmental phase delay. Hence, the weaker inputs about the status of the other ganglia might be redundant for the establishment and maintenance of the coordination or rather a failsafe mechanism of the swimmeret system (Tschuluun et al. 2001). That failsafe mechanism implies that the metachronal wave could be maintained even if the input of one ganglion is absent due to i.e. damages of this ganglion.

As discussed above, I assume that the gradient of synaptic strength is most likely established by the number of synapses the Coordinating Neurons make onto ComInt1. Nevertheless, I cannot rule out the possibility that the gradient of synaptic strength might be established by the amount of released transmitters of Coordinating Neurons onto ComInt1. However, I was not able to investigate this possibility with my experimental approach. Although, the areas of colocalization are the first evidence to uncover the gradient of synaptic strength, I am not able to verify if the detected synapses are actually synapses of Coordinating Neurons onto ComInt1 because I did neither successfully stain additionally a ComInt1 neuron nor label postsynaptic components within the same ganglion.

4.2.2. ACh-receptor labeling with α-bungarotoxin

It is most likely that ACh is the neurotransmitter used by Coordinating Neurons onto ComInt1. There are several findings supporting this hypothesis. CCh, a cholinergic agonist, directly influenced the action of ComInt1. EdCl, an ACh-esterase inhibitor, increased the summation of EPSPs in ComInt1. Schneider and colleagues (2018) found that the soma of Coordinating Neurons contained ACh using Matrix-Assisted Laser Desorption/Ionization – Time of Flight Mass Spectrometry (MALDI-TOF MS). Moreover, they were able to rule out glutamate, GABA, and serotonin as neurotransmitters of Coordinating Neurons. Nevertheless, the morphological identification of ACh in the swimmeret system remains difficult and problematic. The immunohistochemical labeling of ACh-transferase using polyclonal antibodies failed (Mulloney and Smarandache-Wellmann 2012). I used tetramethylrhodamin-labeled α-bungarotoxin to mark nicotinic

ACh-receptors (Borodinsky and Spitzer 2007; Marshall 1981; Popova and Panchin Yu 1999) in the membrane of ComInt1, the postsynaptic neuron of Coordinating Neurons.

With this morphological approach I did not detect colocalizations between structures that were stained by α-bungarotoxin application and dye-filled ComInt1 neurons. Moreover, the stained structures were not even in close proximity to the detected synapses of Coordinating Neurons. Therefore, I was not able to provide additional evidence for ACh being the neurotransmitter used by Coordinating Neurons. Since α-bungarotoxin is a ligand for the α-unit of nicotinic ACh-receptors (Borodinsky and Spitzer 2007; Marshall 1981; Popova and Panchin Yu 1999), no overlap of signals between labeled nicotinic receptors and ComInt1 could imply that ComInt1 only exhibits muscarinic ACh-receptors in its membrane. In my opinion, this possibility is disproved by the presence of EPSPs in ComInt1. EPSPs are fast current changes in ComInt1's membrane which are largely borne by ionotropic nicotinic ACh-receptors (Siegel 1999). Another possibility explaining my results could be that Coordinating Neurons do not use ACh as neurotransmitter onto ComInt1. I am not able to make a point about that assumption since I did neither perform extracellular recordings of the PS activity nor intracellularly recorded ComInt1 while applying α-bungarotoxin to the isolated abdominal nerve cord. If ComInt1 possess nicotinic ACh-receptors, the bath application of α-bungarotoxin should have a very strong impact on its activity and on the rhythmic motor output of the swimmeret system.

4.2.3. ASC_E and morphological structures in its home ganglion

In another project I detected colocalizations of dye-filled ASC_E neurons with presynaptic boutons in its home ganglion. Before ASC_E turns to leave its ganglion anterior into the connectives, it projects a small branch posterior into its home ganglion. Here, I detected small ramifications overlapped with presynaptic boutons. The detection of these synapses is the first morphological evidence that ASC_E forms synapses within its home ganglion which might be of high importance for ASC_E to affect the motor output of its home module.

These colocalizations occurred in the dorsal midline region at the anterior margin of the ganglion. It is not known and therefore highly speculative with which neuron or neurons ASC_E might interact in this region. There are some identified neurons in the swimmeret system that traverses this region. The axons of Coordinating Neurons enter and leave the ganglion at this region. If ASC_E would interact with axons of Coordinating Neurons originating from other ganglia it would be more likely that it interacts with DSC entering from anterior ganglia because enhancing or weakening inputs of DSC would then directly transmitted back to ComInt1 and therefore to its own CPG. Another identified neuron whose neurite crosses the midline in this region is a RSE neuron arising in the contralateral hemisegment that is coupled via an electrical synapse to IPS in ASC_E's microcircuit (Paul and Mulloney 1985; Smarandache-Wellmann et al. 2013). Modulating its activity would then be directly transmitted to IPS, causing fast modulations of the PS motor output of its home module. As third possibility, there is the Commissural Interneuron 2 (ComInt2) that also projects through this region (personal communication Prof. Dr. Brian Mulloney). Therefore it could also be a target of ASC_E. Anyhow, nothing is known about the projection and the activity of ComInt2, yet. However, I cannot rule out that ASC_E synapses onto neurons that are not yet identified.

4.3. Conclusion

ComInt1 is a hub neuron between circuits that synchronizes the oscillations of four ipsilateral distributed oscillators. Its activity is mainly shaped by the CPG activity of its home module via a bidirectional electrical synapse to IRSh. Thus, ComInt1 adapts to the excitation level of its own CPG. Moreover, it is capable to decode and to integrate information about the motor output status of the other three CPGs. Therefore, ComInt1 samples continuously the activity of its own microcircuit and receives perturbations transmitted via chemical synapses from the Coordinating Neurons. The timing, duration, and strengths of these simultaneously arriving inputs are processed in the form of EPSPs and compared with the activity of its own CPG. That means that if bursts of ASC_E and DSC arrive earlier or later or with more or less spikes than ComInt1 expects, it detects a mismatch between the states of activity of its own and the other CPGs. In this case ComInt1's cellular properties are modulated to synchronize the chain of coupled oscillators very fast via the electrical synapse to IRSh. The gradient of synaptic strength of inputs of Coordinating Neurons onto ComInt1 is most likely caused by different numbers of synapses. Moreover, this gradient is not only important for the synchronization but rather essential for the establishment and maintenance of the coordinated metachronal wave of the motor outputs from posterior to anterior.

4.4. Comparison to other systems

The crayfish swimmeret system exhibits the advantage that the isolated CNS generates motor outputs with cycle periods and intersegmental phases similar to motor outputs of the intact animal (Murchison et al. 1993). That means that sensory input plays only a minor role for rhythm generation in the swimmeret system. There are other systems in which sensory inputs are important for the coordination of muscles that drive i.e. walking or swimming movements.

Sensory input plays a crucial role for the coordination of legs for terrestrial locomotion. In stick insects, walking activity is driven by segmental CPGs that innervate segmented legs. Within the segmented legs, antagonistic muscles of each joint are driven each by its own CPG (Büschges 1995; 2005). Each stick insect leg has three joints. Therefore, each leg comprises three CPGs (Bässler and Büschges 1998; Büschges 1995). These three CPGs are independently active and the coordination of the CPGs requires sensory feedback, i.e. about the load or the position of the leg, to perform adequate leg movements (Büschges 2005). Sensory input is also required for interleg coordination to adopt walking gaits that are adequately for the terrain or the walking speed (Borgmann et al. 2011).

Sensory inputs are also important for the intersegmental phase lags for swimming in lamprey and leech. In lamprey, the intersegmental phase lags of isolated spinal cord recordings are approximate to the phase lags in the intact animal. However, the cycle periods are abnormally long (McClellan 1990; Wallen and Williams 1984). Phase lags generated by the isolated leech CNS are smaller, whereby cycle periods are prolonged in comparison to swimming in the intact animal (Pearce and Friesen 1984; Yu et al. 1999). Still, both systems are suitable to study intersegmental coordination of distributed oscillators. During swimming, both leech and lamprey produce movements that form a sinusoidal wave propagating from anterior to posterior (Gray 1968; Grillner et al. 1991; Kristan et al. 1974). The lamprey is constituted of 100 body segments exhibiting a phase lag of 1% from segment to segment. The phase lag is maintained by asymmetric intersegmental coupling. Excitatory neurons project in both directions along the neuraxis and inhibitory neurons project only anteriorly. The projections span up to 40 segments (Buchanan 2001; Miller and Sigvardt 2000) but coupling weakens with distance. That

means that short-distance coupling is strong and is therefore the main factor in generating intersegmental phase lags in posterior direction (Hagevik and McClellan 1999; McClellan and Hagevik 1999; Sigvardt and Williams 1996), which is also observable in the crayfish swimmeret system. In leech, 18 body segments are involved in swimming, whereby the phase lag from segment to segment is between 5 to 6% (Kristan et al. 1974). Also in the leech CNS, the intersegmental coupling is asymmetric and connections span approximately 6 segments in both directions (Friesen and Hocker 2001; Pearce and Friesen 1985; Poon et al. 1978), whereby the functional strength of both ascending and descending interactions are equal (Friesen and Hocker 2001). Yet here, coordination occurs via nearest neighbor interactions as well, since local coupling is not stable for long chains of oscillators (Pearce and Friesen 1988; Sigvardt and Williams 1996). However, if the CNS of an intact leech is cut into two halves the sinusoidal waveform during leech swimming is still persistent (Harley et al. 2015). This finding indicates that also in leech long distance coupling might serve as a failsafe mechanism to maintain coordination.

The leech possesses another network in which the functional strength of interactions plays an important role, namely the leech heartbeat network. The blood flow in leech is driven by constrictions of a bilateral pair of heart tubes. One side constricts from posterior to anterior in peristaltic activity, while the other side constricts synchronous (Kristan et al. 2005; Norris et al. 2006). The heart tubes receive excitatory inputs from HE motor neurons located in the segmental ganglia 3 to 18 (Maranto and Calabrese 1984). Motor neurons, i.e. in segmental ganglion 8 (HE (8)) and 12 (HE (12)), receive the identical compositions of premotor synaptic inputs. That means that during rhythmic activity, in the peristaltic mode, these motor neurons receive the identical temporal pattern of inputs but with different relative synaptic strength. Wright and Calabrese (2011) performed dynamic clamp experiments and showed that motor neurons that receive complement synaptic inputs could display different firing patterns when the synaptic strength gradients are altered. In case of the peristaltic activity of the heart tube, strengthening of the ensemble of synaptic inputs could reduce phase lags between HE (8) and HE (12) motor neurons. Deranging the hierarchy of synaptic strength profiles of premotor neurons onto motor neurons could even invert the peristaltic mode from rear-to-front to front-to-rear. In the crayfish swimmeret system, the

synaptic strength decreased with distance whereby ASC_E provides always a stronger input than DSC. This gradient of synaptic strength is fixed and stabilizes the coordinating rhythmic activity from posterior to anterior, whereby the temporal pattern of inputs can vary and therefore affect the timing of individual oscillators.

In the swimmeret system, ComInt1 receives the inputs with a gradient of synaptic strength. The inputs encode information about the status of the motor output of different ganglia and arrive simultaneously in ComInt1. ComInt1 continuously receives information about the CPG of its home ganglion via a bidirectional electrical synapse. Therefore, its function is to decode periodic inputs from other CPGs, compare these with the status of its own CPG, and to synchronize all oscillators with each other. According to the model of Gutierrez (2013) these features describe ComInt1 as a hub neuron.

The system that was at the basis of Gutierrez model is the stomatogastric ganglion (STG) of crab. The STG generates a fast pyloric rhythm and a slow gastric rhythm. The CPG of the pyloric rhythm consists of the endogenous burster, coupled with another neuron forming a pacemaker group. The CPG of the gastric mill rhythm consists of two cells which form a half-center. These two oscillators have very different periods, and need to be coordinated to allow ingestion (Bucher et al. 2006; Dickinson et al. 1990; Katz and Harris-Warrick 1991). The coordination is established by the inferior-cardiac motor neuron (IC), a gastro-pyloric neuron, which is connected to both, the gastric and the pyloric CPG via an electrical synapse serving as a hub neuron. Additionally, it receives inhibitory inputs from both oscillators allowing IC to switch between the frequencies of the oscillators (Weimann and Marder 1994; Weimann et al. 1991). Therefore the IC neuron is capable to affect and synchronize the output of both CPGs.

The swimming speed of Zebrafish determines the recruitment of premotor V2a interneurons in the spinal cord. V2a interneurons excite distinct topographically separated motor neuron pools (Ausborn et al. 2012), whose recruitment is also determined by swimming frequency (Ampatzis et al. 2013). At slow swimming speeds slow motor neurons are recruited that innervate the slow musculature. As the swimming speed increases intermediate motor neurons are additionally recruited which further excite the intermediate swimming musculature. Fast motor neurons are recruited at fast speeds driving fast muscles (Ampatzis et al. 2013). However, Song and colleagues

(2016) detected that these motor neurons manifest hub neuron-like properties. 70 to 100% of the motor neurons exhibit electrical synapses to feedback information about its status to the V2a interneurons to recruit more motor neurons for faster swimming or to release motor neurons from excitation for slower swimming. In crayfish swimmeret system, the bidirectional electrical synapse between ComInt1 and IRSh inherits also a feedback function. IRSh continuously feeds back the status of the CPG to enable ComInt1 to compare the CPGs state of activity with periodic perturbations and if necessary to modulate its activity to indirectly recruit or dismiss motor neurons.

Hub neurons exist manifold in vertebrate brains and are crucial to combine multisensory modalities. Peripheral hub neurons thereby are restricted to one brain areal orchestrating the output of this particular area. Connector hub neurons are located in one areal but are connected to surrounding areas to integrate their activity and to synchronize the outputs of these brain areas with each other. Kinless hub neurons do not affiliate to any areal but connect different areas with each other to synchronize their activities. The integration and synchronization enables the animal or human to adequately respond to external stimuli (Zamora-López et al. 2011). Simplified, the external stimuli could be that a mouse hears and smells a predator. These sensory inputs are processed in different cortices of the brain but need to be combined and synchronized to trigger the escape behavior of the mouse. In relation to the hub neuron in the swimmeret system, ComInt1 ranks in the category connector hub neuron. It is affiliated to a local microcircuit but integrates inputs of surrounding circuits and synchronizes all circuits with each other.

4.5. Future experiments

In my electrophysiological experiments I investigated the motor output and ComInt1's cellular properties upon CCh or CCAP diluted in NR. Moreover, I performed experiments in which I applied EdCl diluted in CCAP saline. That means that the modulations of the motor output and ComInt1 were affected by both, CCAP and EdCl. However, I showed that CCAP alone already modulated the input and output of ComInt1, probably by closing M-type channels but rather by enhancing the electrical synapse to IRSh (Li et al. 2018). To completely prove if CCAP has an enhancing effect

on the electrical synapse, experiments should be performed with EdCl diluted in NR, when the swimmeret system produces spontaneous rhythmic activity. This experimental approach would then provide results about the mode of action of EdCl alone. Additionally, this approach would provide additional information about CCAP's enhancing effect on the electrical synapse between ComInt1 and IRSh, by comparing EdCl's effects on ComInt1 with its effects diluted in CCAP.

With my experimental approach, I was not able to uncover the entire decoding capabilities of ComInt1. Uniform excitation level modulations of the swimmeret system caused that all CPGs oscillated with the same period and strengths, so that the periodic perturbations in ComInt1 were insufficient to cause mismatches between the distributed oscillators that would force ComInt1 to act to synchronize. Therefore, experiments should be performed in which ComInt1 is intracellularly recorded i.e. in A3, without clamping its V_m. Simultaneously, all Coordinating Neurons that synapse onto ComInt1 in A3, namely ASC_E in A5, ASC_E in A4, and DSC in A2 should be extracellularly recorded with suction electrodes. Concurrent extracellular recordings of the PS motor output of all or at least of all ipsilateral microcircuits are obligatory. While recording, NR should be continuously bath applied over a long period of time with the aim to measure the activity of ComInt1, Coordinating Neurons and PS motor outputs during spontaneous occurring rhythmic activity, including switches between active and silent states. With this approach, PS cycle periods and PS burst strengths would vary extensively without adapting to a forced excitation level, meaning that the motor outputs of different segments could also vary from each other. This would allow detailed investigations, under more natural conditions of how ComInt1's cellular properties are modulated due to spontaneously changing inputs and therefore to fastidiously examine ComInt1's decoding, integrating and synchronizing properties.

If the swimmeret system is not producing spontaneously rhythmic activity but is in a silent state, these properties could still be investigated by stimulating each axon of Coordinating Neurons individually or simultaneously, while measuring how these perturbations alter ComInt1's cellular properties as well as its capability to decode, integrate, and synchronize.

Another interesting experimental approach would be a split bath experiment. Mulloney and Hall (2007b) performed split bath experiments with the boundary between A4 and A3. They then exposed the posterior and anterior halves of the swimmeret system to different excitation levels and detected that the phase lag across the boundary changed. While performing this experiment, they did not intracellularly record ComInt1 to investigate how it copes with these diverse inputs. I would repeat these experiments, but would expose the two halves to more extreme excitation levels, by i.e. applying CCAP on one half and 3 µM CCh on the other. Another attempt to prevent uniform excitation of the swimmeret system is the focal application of ACh agonist or antagonists to the midline of one ganglion, which could reveal effects of the transmission of Coordinating Neurons on ComInt1 and therefore alter ComInt1's activity locally in one hemisegment.

The importance of the electrical synapse is omnipresent in my work. Therefore, it would be important to perform experiments in which the bidirectional transmission between ComInt1 and IRSh is prevented. This could be achieved by applying octanol, which blocks electrical coupling, to the intact network. Hormuzdi and colleagues (2004) showed that octanol attenuated synchronization of mouse hippocampal interneurons. Provided that octanol also works in invertebrates, application could affect the synchronization of the four ipsilateral distributed oscillators. Moreover, applying octanol diluted in Low Ca^{2+} could help to uncover if ComInt1's modulations are borne by IRSh via the electrical synapse or if these changes are intrinsic in ComInt1.

The supreme discipline in all electrophysiological future experiments would be to intracellularly record from IRSh, simultaneously. With that experimental approach it would be possible to investigate how ComInt1 and IRSh affect each other. Furthermore, an intracellular double recording of ComInt1 and IRSh would allow the detailed investigation of the electrical synapse to reveal its importance for the synchronization of ComInt1's own CPG to the activity transmitted from the other three CPGs.

Furthermore, it would also be interesting to choose a more theoretical approach to investigate ComInt1's decoding, integration, and synchronizing properties. Mathematical models would be valuable for that, since modeling complements and predicts outcomes from real experiments, and therefore becomes increasingly important in neuroscience. In case of ComInt1 it would be reasonable to develop a model similar to the hub neuron

model of Gutierrez and colleagues (2013). They modeled competing fast and slow oscillators that are connected to a hub neuron via an electrical synapse and inhibitory synapses. Using ComInt1 as a hub neuron between two or three oscillators, the question of how individual neurons or groups of neurons are recruited into different network oscillations and therefore become synchronized with each other could be answered. Small modifications of Gutierrez model need to be done. For the sake of simplicity the model could scale the swimmeret system down to two ipsilateral microcircuits or rather down to two CPGs (Fig. 38). IPS and IRS reciprocally inhibiting each other and oscillate in antiphase. In both oscillators, IRS is connected to ComInt1 via an electrical synapse. IPS of the posterior CPG directly excites ComInt1 of the anterior ganglion via an excitatory chemical synapse, while IRS of the anterior oscillator forms an excitatory chemical synapse on ComInt1 of the posterior ganglion. The excitatory synapse of IPS is stronger than the excitatory synapse of IRS onto ComInt1 (Fig. 38). Additionally, specific ionic currents could be added to single neurons to examine how these currents could influence the activity of ComInt1 and therefore alter the synchronization of these two oscillators. Moreover, the properties of the electrical synapse could be altered to investigate how changes in, i.e. the coupling strength of the electrical synapse, alters the synchronization of these two CPGs.

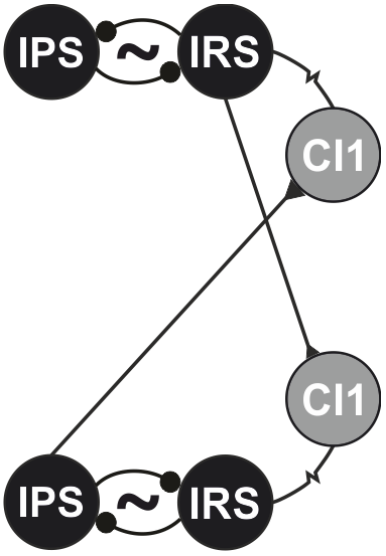

Morphologically it would be of high importance to accomplish the triple staining in which ComInt1 and an axon of one Coordinating Neuron are dye-filled and presynaptic boutons are labeled using anti-synapsin within one ganglion. Moreover, the morphological proof that Coordinating Neurons use ACh as neurotransmitter should be further forced morphologically and physiologically. To entirely prove that the gradient of synaptic strength is established by different numbers of synapses and not by different sized synapses or by a higher release of neurotransmitters, therefore electron microscopy is essential.

Figure 38: Model network of the swimmeret system, scaled down to two CPGs. The Inhibitors of PS (IPS) and the Inhibitors of RS (IRS) form the kernel of the CPG, which are connected via reciprocal inhibition. IPS of the posterior CPG directly excites ComInt1 (CI1) of the anterior module. IRS from the anterior CPG directly excites ComInt1 of the posterior module. Both excitatory synapses are chemical (triangles) and differ in strength (size of the triangles). In both modules ComInt1 is connected to IRS via an electrical synapse (resistor symbols).

References

Acevedo LD, Hall WM, and Mulloney B. Proctolin and excitation of the crayfish swimmeret system. *J Comp Neurol* 345: 612-627, 1994.

Adams PR, Brown DA, and Constanti A. M-currents and other potassium currents in bullfrog sympathetic neurones. *J Physiol* 330: 537-572, 1982.

Alaburda A, Perrier JF, and Hounsgaard J. An M-like outward current regulates the excitability of spinal motoneurones in the adult turtle. *J Physiol* 540: 875-881, 2002.

Ampatzis K, Song J, Ausborn J, and El Manira A. Pattern of innervation and recruitment of different classes of motoneurons in adult zebrafish. *J Neurosci* 33: 10875-10886, 2013.

Ausborn J, Mahmood R, and El Manira A. Decoding the rules of recruitment of excitatory interneurons in the adult zebrafish locomotor network. *Proc Natl Acad Sci U S A* 109: E3631-3639, 2012.

Bässler U, and Büschges A. Pattern generation for stick insect walking movements--multisensory control of a locomotor program. *Brain Res Brain Res Rev* 27: 65-88, 1998.

Bennett MV, and Zukin RS. Electrical coupling and neuronal synchronization in the Mammalian brain. *Neuron* 41: 495-511, 2004.

Blight AR, and Llinas R. The non-impulsive stretch-receptor complex of the crab: a study of depolarization-release coupling at a tonic sensorimotor synapse. *Proc Clin Dial Transplant Forum* 290: 219-276, 1980.

Blumenthal F, and Smarandache-Wellmann C. Robustness of coordination to temperature perturbation in a chain of microcircuits. in preparation.

Borgmann A, Toth TI, Gruhn M, Daun-Gruhn S, and Buschges A. Dominance of local sensory signals over inter-segmental effects in a motor system: experiments. *Biol Cybern* 105: 399-411, 2011.

Borodinsky LN, and Spitzer NC. Activity-dependent neurotransmitter-receptor matching at the neuromuscular junction. *Proc Natl Acad Sci U S A* 104: 335-340, 2007.

Braun G, and Mulloney B. Cholinergic modulation of the swimmeret motor system in crayfish. *J Neurophysiol* 70: 2391-2398, 1993.

Braun G, and Mulloney B. Coordination in the crayfish swimmeret system: differential excitation causes changes in intersegmental phase. *J Neurophysiol* 73: 880-885, 1995.

Brown DA, and Adams PR. Muscarinic suppression of a novel voltage-sensitive K+ current in a vertebrate neurone. *Nature* 283: 673-676, 1980.

Buchanan JT. Contributions of identifiable neurons and neuron classes to lamprey vertebrate neurobiology. *Progress in Neurobiology* 63: 441-466, 2001.

Bucher D, Taylor AL, and Marder E. Central pattern generating neurons simultaneously express fast and slow rhythmic activities in the stomatogastric ganglion. *J Neurophysiol* 95: 3617-3632, 2006.

Burrows M. Graded synaptic interactions between local premotor interneurons of the locust. *J Neurophysiol* 42: 1108-1123, 1979.

Burrows M, and Siegler MV. Graded synaptic transmission between local interneurones and motor neurones in the metathoracic ganglion of the locust. *J Physiol* 285: 231-255, 1978.

Büschges A. Role of local nonspiking interneurons in the generation of rhythmic motor activity in the stick insect. *J Neurobiol* 27: 488-512, 1995.

Büschges A. Sensory control and organization of neural networks mediating coordination of multisegmental organs for locomotion. *J Neurophysiol* 93: 1127-1135, 2005.

Cattaert D, Araque A, Buno W, and Clarac F. Nicotinic and muscarinic activation of motoneurons in the crayfish locomotor network. *J Neurophysiol* 72: 1622-1633, 1994.

Cohen AH, and Wallen P. The neuronal correlate of locomotion in fish. "Fictive swimming" induced in an in vitro preparation of the lamprey spinal cord. *Exp Brain Res* 41: 11-18, 1980.

Corronc HL, and Hue B. Pharmacological and Electrophysiological Characterization of a Postsynaptic Muscarinic Receptor in the Central Nervous System of the Cockroach. *The Journal of Experimental Biology* 181: 257-278, 1993.

Davis WJ. Lobster righting responses and their neural control. *Proceedings of the Royal Society of London Series B Biological Sciences* 170: 435, 1968.

Davis WJ. Motoneuron morphology and synaptic contacts: determination by intracellular dye injection. *Science* 168: 1358-1360, 1970.

Delcomyn F. Neural basis of rhythmic behavior in animals. *Science* 210: 492-498, 1980.

Dickinson PS, Mecsas C, and Marder E. Neuropeptide fusion of two motor-pattern generator circuits. *Nature* 344: 155-158, 1990.

Ewer J, and Truman JW. Increases in cyclic 3', 5'-guanosine monophosphate (cGMP) occur at ecdysis in an evolutionarily conserved crustacean cardioactive peptide-immunoreactive insect neuronal network. *J Comp Neurol* 370: 330-341, 1996.

Friesen WO, and Hocker CG. Functional analyses of the leech swim oscillator. *J Neurophysiol* 86: 824-835, 2001.

Gammie SC, and Truman JW. Neuropeptide hierarchies and the activation of sequential motor behaviors in the hawkmoth, Manduca sexta. *J Neurosci* 17: 4389-4397, 1997.

Golowasch J, and Marder E. Proctolin activates an inward current whose voltage dependence is modified by extracellular Ca^{2+}. *J Neurosci* 12: 810-817, 1992.

Gray J. *Animal Locomotion*. London: Weidenfeld and Nicolson, 1968.

Grillner S, Wallen P, Brodin L, and Lansner A. Neuronal network generating locomotor behavior in lamprey: circuitry, transmitters, membrane properties, and simulation. *Annu Rev Neurosci* 14: 169-199, 1991.

Gutierrez GJ, O'Leary T, and Marder E. Multiple mechanisms switch an electrically coupled, synaptically inhibited neuron between competing rhythmic oscillators. *Neuron* 77: 845-858, 2013.

Hagevik A, and McClellan AD. Coordination of locomotor activity in the lamprey: role of descending drive to oscillators along the spinal cord. *Exp Brain Res* 128: 481-490, 1999.

Halliwell JV, and Adams PR. Voltage-clamp analysis of muscarinic excitation in hippocampal neurons. *Brain Res* 250: 71-92, 1982.

Harley CM, Reilly MG, Stewart C, Schlegel C, Morley E, Puhl JG, Nagel C, Crisp KM, and Mesce KA. Compensatory plasticity restores locomotion after chronic removal of descending projections. *J Neurophysiol* 113: 3610-3622, 2015.

Harris-Warrick RM, Marder E, Selverston AI, and Moulins M. *Dynamic biological networks: The stomatogastric nervous system*. Cambridge, MA, US: The MIT Press, 1992, p. xvii, 328-xvii, 328.

Hormuzdi SG, Filippov MA, Mitropoulou G, Monyer H, and Bruzzone R. Electrical synapses: a dynamic signaling system that shapes the activity of neuronal networks. *Biochimica et Biophysica Acta (BBA) - Biomembranes* 1662: 113-137, 2004.

Hughes GM, and Wiersma CAG. The Co-ordination of Swimmeret Movements in the Crayfish, Procambarus Clarkii (Girard). *Journal of Experimental Biology* 37: 657-670, 1960.

Hunt CA, Schenker LJ, and Kennedy MB. PSD-95 is associated with the postsynaptic density and not with the presynaptic membrane at forebrain synapses. *J Neurosci* 16: 1380-1388, 1996.

Huxley THP. *The crayfish; an introduction to the study of zoology*. New York: D. Appleton and company, 1880.

Ikeda K, and Wiersma CA. Autogenic Rhythmicity in the Abdominal Ganglia of the Crayfish: The Control of Swimmeret Movements. *Comp Biochem Physiol* 12: 107-115, 1964.

Izhikevich EM. *Dynamical systems in neuroscience: the geometry of excitability and bursting*. 2007.

Kandel ER, Schwartz JH, and Jessell TM. Chapter 11. In: *Principles of neural science*. New York: McGraw-Hill, Health Professions Division, 2000.

Kato A, Ozawa F, Saitoh Y, Fukazawa Y, Sugiyama H, and Inokuchi K. Novel members of the Vesl/Homer family of PDZ proteins that bind metabotropic glutamate receptors. *J Biol Chem* 273: 23969-23975, 1998.

Katz PS, and Harris-Warrick RM. Recruitment of crab gastric mill neurons into the pyloric motor pattern by mechanosensory afferent stimulation. *J Neurophysiol* 65: 1442-1451, 1991.

Klagges BRE, Heimbeck G, Godenschwege TA, Hofbauer A, Pflugfelder GO, Reifegerste R, Reisch D, Schaupp M, Buchner S, and Buchner E. Invertebrate Synapsins: A Single Gene Codes for Several Isoforms in Drosophila. *The Journal of Neuroscience* 16: 3154-3165, 1996.

Kopell N, and Ermentrout B. Chemical and electrical synapses perform complementary roles in the synchronization of interneuronal networks. *Proc Natl Acad Sci U S A* 101: 15482-15487, 2004.

Kopell N, and Ermentrout GB. Coupled oscillators and the design of central pattern generators. *Mathematical Biosciences* 90: 87-109, 1988.

Korn LJ, Queen CL, and Wegman MN. Computer analysis of nucleic acid regulatory sequences. *Proc Natl Acad Sci U S A* 74: 4401-4405, 1977.

Kristan WB, Calabrese RL, and Friesen WO. Neuronal control of leech behavior. *Progress in Neurobiology* 76: 279-327, 2005.

Kristan WB, Jr., and Calabrese RL. Rhythmic swimming activity in neurones of the isolated nerve cord of the leech. *J Exp Biol* 65: 643-668, 1976.

Kristan WB, Stent GS, and Ort CA. Neuronal control of swimming in the medicinal leech. *Journal of comparative physiology* 94: 97-119, 1974.

Li X, Bucher DM, and Nadim F. Co-modulation of synapses and voltage-gated ionic currents by combined actions of multiple neuromodulators follow distinct rules. *bioRxiv* 2018.

Maranto AR, and Calabrese RL. Neural control of the hearts in the leech,Hirudo medicinalis. *Journal of Comparative Physiology A* 154: 367-380, 1984.

Marder E. Variability, compensation, and modulation in neurons and circuits. *Proc Natl Acad Sci U S A* 108 Suppl 3: 15542-15548, 2011.

Marder E, and Calabrese RL. Principles of rhythmic motor pattern generation. *Physiol Rev* 76: 687-717, 1996.

Marshall LM. Synaptic localization of alpha-bungarotoxin binding which blocks nicotinic transmission at frog sympathetic neurons. *Proc Natl Acad Sci U S A* 78: 1948-1952, 1981.

Mayford M, Bach ME, Huang YY, Wang L, Hawkins RD, and Kandel ER. Control of memory formation through regulated expression of a CaMKII transgene. *Science* 274: 1678-1683, 1996.

McClellan AD. Locomotor recovery in spinal-transected lamprey: regenerated spinal coordinating neurons and mechanosensory inputs couple locomotor activity across a spinal lesion. *Neuroscience* 35: 675-685, 1990.

McClellan AD, and Hagevik A. Coordination of spinal locomotor activity in the lamprey: long-distance coupling of spinal oscillators. *Exp Brain Res* 126: 93-108, 1999.

McLean DL, and Dougherty KJ. Peeling back the layers of locomotor control in the spinal cord. *Curr Opin Neurobiol* 33: 63-70, 2015.

Miller WL, and Sigvardt KA. Extent and Role of Multisegmental Coupling in the Lamprey Spinal Locomotor Pattern Generator. *Journal of Neurophysiology* 83: 465-476, 2000.

Mulloney B. *A method to measure the strength of multi-unit bursts of action potentials*. 2005, p. 98-105.

Mulloney B. A test of the excitability-gradient hypothesis in the swimmeret system of crayfish. *J Neurosci* 17: 1860-1868, 1997.

Mulloney B, Acevedo LD, and Bradbury AG. Modulation of the crayfish swimmeret rhythm by octopamine and the neuropeptide proctolin. *J Neurophysiol* 58: 584-597, 1987.

Mulloney B, and Hall WM. Functional organization of crayfish abdominal ganglia. III. Swimmeret motor neurons. *J Comp Neurol* 419: 233-243, 2000.

Mulloney B, and Hall WM. Local and intersegmental interactions of coordinating neurons and local circuits in the swimmeret system. *J Neurophysiol* 98: 405-413, 2007.

Mulloney B, and Hall WM. Local commissural interneurons integrate information from intersegmental coordinating interneurons. *J Comp Neurol* 466: 366-376, 2003.

Mulloney B, and Hall WM. Not by spikes alone: responses of coordinating neurons and the swimmeret system to local differences in excitation. *J Neurophysiol* 97: 436-450, 2007b.

Mulloney B, Harness PI, and Hall WM. Bursts of information: coordinating interneurons encode multiple parameters of a periodic motor pattern. *J Neurophysiol* 95: 850-861, 2006.

Mulloney B, Namba H, Agricola HJ, and Hall WM. Modulation of force during locomotion: differential action of crustacean cardioactive peptide on power-stroke and return- stroke motor neurons. *J Neurosci* 17: 6872-6883, 1997.

Mulloney B, and Smarandache-Wellmann C. Neurobiology of the crustacean swimmeret system. *Prog Neurobiol* 96: 242-267, 2012.

Mulloney B, and Smarandache C. Fifty Years of CPGs: Two Neuroethological Papers that Shaped the Course of Neuroscience. *Front Behav Neurosci* 4: 2010.

Mulloney B, Tschuluun N, and Hall WM. Architectonics of crayfish ganglia. *Microsc Res Tech* 60: 253-265, 2003.

Murchison D, Chrachri A, and Mulloney B. A separate local pattern-generating circuit controls the movements of each swimmeret in crayfish. *J Neurophysiol* 70: 2620-2631, 1993.

Nagayama T, Takahata M, and Hisada M. Functional characteristics of local non-spiking interneurons as the pre-motor elements in crayfish. *Journal of Comparative Physiology A* 154: 499-510, 1984.

Nagayama T, Takahata M, and Hisada M. Local spikeless interaction of motoneuron dendrites in the crayfishProcambarus clarkii girard. *Journal of comparative physiology* 152: 335-345, 1983.

Nakagawa H, and Mulloney B. Local specification of relative strengths of synapses between different abdominal stretch-receptor axons and their common target neurons. *J Neurosci* 21: 1645-1655, 2001.

Namba H, and Mulloney B. Coordination of limb movements: three types of intersegmental interneurons in the swimmeret system and their responses to changes in excitation. *J Neurophysiol* 81: 2437-2450, 1999.

Namba H, Nagayama T, and Takahata M. Non-spiking local interneurones mediate abdominal extension related descending control of uropod motor neurones in the crayfish terminal abdominal ganglion. *J Comp Physiol A Neuroethol Sens Neural Behav Physiol* 180: 463– 472, 1997.

Norris BJ, Weaver AL, Morris LG, Wenning A, García PA, and Calabrese RL. A Central Pattern Generator Producing Alternative Outputs: Temporal Pattern of Premotor Activity. *Journal of Neurophysiology* 96: 309-326, 2006.

Ohyama T, Schneider-Mizell CM, Fetter RD, Aleman JV, Franconville R, Rivera-Alba M, Mensh BD, Branson KM, Simpson JH, Truman JW, Cardona A, and Zlatic M. A multilevel multimodal circuit enhances action selection in Drosophila. *Nature* 520: 633-639, 2015.

Paul DH, and Mulloney B. Nonspiking local interneuron in the motor pattern generator for the crayfish swimmeret. *J Neurophysiol* 54: 28-39, 1985.

Pearce RA, and Friesen OW. Intersegmental coordination of leech swimming: comparison of in situ and isolated nerve cord activity with body wall movement. *Brain Research* 299: 363-366, 1984.

Pearce RA, and Friesen WO. Intersegmental coordination of the leech swimming rhythm. II. Comparison of long and short chains of ganglia. *J Neurophysiol* 54: 1460-1472, 1985.

Pearce RA, and Friesen WO. A model for intersegmental coordination in the leech nerve cord. *Biol Cybern* 58: 301-311, 1988.

Pearson K. Motor systems. *Curr Opin Neurobiol* 10: 649-654, 2000.

Pearson KG, and Iles JF. Discharge patterns of coxal levator and depressor motoneurones of the cockroach, Periplaneta americana. *J Exp Biol* 52: 139-165, 1970.

Poon M, Friesen WO, and Stent GS. Neuronal control of swimming in the medicinal leech. V. Connexions between the oscillatory interneurones and the motor neurones. *J Exp Biol* 75: 45-63, 1978.

Popova LB, and Panchin Yu V. Staining of central neurons of the pteropod mollusk Clione limacina with fluorescein-labeled alpha-bungarotoxin. *Neurosci Behav Physiol* 29: 317-320, 1999.

Prinz AA, Bucher D, and Marder E. Similar network activity from disparate circuit parameters. *Nat Neurosci* 7: 1345-1352, 2004.

Rigotti M, Barak O, Warden MR, Wang XJ, Daw ND, Miller EK, and Fusi S. The importance of mixed selectivity in complex cognitive tasks. *Nature* 497: 585-590, 2013.

Roopun AK, Kramer MA, Carracedo LM, Kaiser M, Davies CH, Traub RD, Kopell NJ, and Whittington MA. Temporal Interactions between Cortical Rhythms. *Front Neurosci* 2: 145-154, 2008.

Rosenblum M, and Pikovsky A. Self-organized quasiperiodicity in oscillator ensembles with global nonlinear coupling. *Phys Rev Lett* 98: 064101, 2007.

Ruiz-Canada C, and Budnik V. Introduction on the use of the Drosophila embryonic/larval neuromuscular junction as a model system to study synapse development and function, and a brief summary of pathfinding and target recognition. *Int Rev Neurobiol* 75: 1-31, 2006.

Schneider AC. Encoding of Coordinating Information in a Network of Coupled Oscillators. In: *Zoological Institute*. Cologne: University of Cologne, 2017.

Schneider AC, Blumenthal F, and Smarandache C. Adaptive Encoding of Coordinating Information in the Crayfish Central Nervous System. in preparation.

Schneider AC, Seichter HA, Neupert S, Hochhaus AM, and Smarandache-Wellmann CR. Profiling neurotransmitters in a crustacean neural circuit for locomotion. *PLoS One* 13: e0197781, 2018.

Schwemmer MA, and Lewis TJ. The robustness of phase-locking in neurons with dendro-dendritic electrical coupling. *J Math Biol* 68: 303-340, 2014.

Sherff CM, and Mulloney B. Tests of the motor neuron model of the local pattern-generating circuits in the swimmeret system. *J Neurosci* 16: 2839-2859, 1996.

Siegel GJ. *Basic neurochemistry : molecular, cellular, and medical aspects*. Philadelphia: Lippincott Williams & Wilkins, 1999.

Siegler MVS. Nonspiking Interneurons and Motor Control in Insects. In: *Advances in Insect Physiology*, edited by Berridge MJ, Treherne JE, and Wigglesworth VBAcademic Press, 1985, p. 249-304.

Sigvardt KA, and Williams TL. Effects of local oscillator frequency on intersegmental coordination in the lamprey locomotor CPG: theory and experiment. *J Neurophysiol* 76: 4094-4103, 1996.

Skinner FK. The structure of the fourth abdominal ganglion of the crayfish, Procambarus clarki (girard). I. Tracts in the ganglionic core. *Journal of Comparative Neurology* 234: 168-181, 1985a.

Skinner FK, Kopell N, and Marder E. Mechanisms for oscillation and frequency control in reciprocally inhibitory model neural networks. *J Comput Neurosci* 1: 69-87, 1994.

Skinner FK, Kopell N, and Mulloney B. How does the crayfish swimmeret system work? Insights from nearest-neighbor coupled oscillator models. *J Comput Neurosci* 4: 151-160, 1997.

Skinner FK, and Mulloney B. Intersegmental Coordination of Limb Movements during Locomotion: Mathematical Models Predict Circuits That Drive Swimmeret Beating. *The Journal of Neuroscience* 18: 3831-3842, 1998.

Slesinger P, and Bell CC. Primary afferent fibers conduct impulses in both directions under physiological stimulus conditions. *J Comp Physiol A* 157: 15-22, 1985.

Smarandache-Wellmann C, and Grätsch S. Mechanisms of coordination in distributed neural circuits: encoding coordinating information. *J Neurosci* 34: 5627-5639, 2014.

Smarandache-Wellmann C, Weller C, and Mulloney B. Mechanisms of coordination in distributed neural circuits: decoding and integration of coordinating information. *J Neurosci* 34: 793-803, 2014.

Smarandache-Wellmann C, Weller C, Wright TM, Jr., and Mulloney B. Five types of nonspiking interneurons in local pattern-generating circuits of the crayfish swimmeret system. *J Neurophysiol* 110: 344-357, 2013.

Smarandache C, Hall WM, and Mulloney B. Coordination of rhythmic motor activity by gradients of synaptic strength in a neural circuit that couples modular neural oscillators. *J Neurosci* 29: 9351-9360, 2009.

Smith JC, Ellenberger HH, Ballanyi K, Richter DW, and Feldman JL. Pre-Botzinger complex: a brainstem region that may generate respiratory rhythm in mammals. *Science* 254: 726-729, 1991.

Smith JC, and Feldman JL. In vitro brainstem-spinal cord preparations for study of motor systems for mammalian respiration and locomotion. *J Neurosci Methods* 21: 321-333, 1987.

Song J, Ampatzis K, Bjornfors ER, and El Manira A. Motor neurons control locomotor circuit function retrogradely via gap junctions. *Nature* 529: 399-402, 2016.

Städele C, Heigele S, and Stein W. Neuromodulation to the Rescue: Compensation of Temperature-Induced Breakdown of Rhythmic Motor Patterns via Extrinsic Neuromodulatory Input. *PLoS Biol* 13: e1002265, 2015.

Stangier J, Hilbich C, Dircksen H, and Keller R. Distribution of a novel cardioactive neuropeptide (CCAP) in the nervous system of the shore crab Carcinus maenas. *Peptides* 9: 795-800, 1988.

Stein BE, Meredith MA, and Wallace MT. The visually responsive neuron and beyond: multisensory integration in cat and monkey. *Prog Brain Res* 95: 79-90, 1993.

Swensen AM, and Marder E. Multiple peptides converge to activate the same voltage-dependent current in a central pattern-generating circuit. *J Neurosci* 20: 6752-6759, 2000.

Trube A, Audehm U, and Dircksen H. Crustacean cardioactive peptide-immunoreactive neurons in the ventral nervous system of crayfish. *J Comp Neurol* 348: 80-93, 1994.

Tschuluun N, Hall WM, and Mulloney B. Limb movements during locomotion: Tests of a model of an intersegmental coordinating circuit. *J Neurosci* 21: 7859-7869, 2001.

Tschuluun N, Hall WM, and Mulloney B. State-changes in the swimmeret system: a neural circuit that drives locomotion. *J Exp Biol* 212: 3605-3611, 2009.

van Atteveldt N, Murray MM, Thut G, and Schroeder CE. Multisensory integration: flexible use of general operations. *Neuron* 81: 1240-1253, 2014.

Wallen P, and Williams TL. Fictive locomotion in the lamprey spinal cord in vitro compared with swimming in the intact and spinal animal. *J Physiol* 347: 225-239, 1984.

Weimann JM, and Marder E. Switching neurons are integral members of multiple oscillatory networks. *Curr Biol* 4: 896-902, 1994.

Weimann JM, Meyrand P, and Marder E. Neurons that form multiple pattern generators: identification and multiple activity patterns of gastric/pyloric neurons in the crab stomatogastric system. *J Neurophysiol* 65: 111-122, 1991.

Weimann JM, Skiebe P, Heinzel HG, Soto C, Kopell N, Jorge-Rivera JC, and Marder E. Modulation of oscillator interactions in the crab stomatogastric ganglion by crustacean cardioactive peptide. *J Neurosci* 17: 1748-1760, 1997.

Wiersma CA, and Hughes GM. On the functional anatomy of neuronal units in the abdominal cord of the crayfish, Procambarus clarkii (Girard). *J Comp Neurol* 116: 209-228, 1961.

Wiersma CA, and Ikeda K. Interneurons Commanding Swimmeret Movements in the Crayfish, Procambarus Clarki (Girard). *Comp Biochem Physiol* 12: 509-525, 1964.

Wilson DM. The Central Nervous Control of Flight in a Locust. *Journal of Experimental Biology* 38: 471-490, 1961.

Wright TM, and Calabrese RL. Patterns of Presynaptic Activity and Synaptic Strength Interact to Produce Motor Output. *The Journal of Neuroscience* 31: 17555-17571, 2011.

Xiao B, Tu JC, Petralia RS, Yuan JP, Doan A, Breder CD, Ruggiero A, Lanahan AA, Wenthold RJ, and Worley PF. Homer regulates the association of group 1 metabotropic glutamate receptors with multivalent complexes of homer-related, synaptic proteins. *Neuron* 21: 707-716, 1998.

Yu X, Nguyen B, and Friesen WO. Sensory feedback can coordinate the swimming activity of the leech. *J Neurosci* 19: 4634-4643, 1999.

Zamora-López G, Zhou C, and Kurths J. Exploring Brain Function from Anatomical Connectivity. *Frontiers in Neuroscience* 5: 83, 2011.

Zhang C, Guy RD, Mulloney B, Zhang Q, and Lewis TJ. Neural mechanism of optimal limb coordination in crustacean swimming. *Proc Natl Acad Sci U S A* 111: 13840-13845, 2014.

Zhang C, and Lewis TJ. Phase response properties of half-center oscillators. *J Comput Neurosci* 35: 55-74, 2013.

Zipser B, and Bennett MV. Interaction of electrosensory and electromotor signals in lateral line lobe of a mormyrid fish. *J Neurophysiol* 39: 713-721, 1976.

Zwart MF, Pulver SR, Truman JW, Fushiki A, Fetter RD, Cardona A, and Landgraf M. Selective Inhibition Mediates the Sequential Recruitment of Motor Pools. *Neuron* 91: 944, 2016.

Appendix

In the results section of this thesis, I only showed the medians of analyzed motor outputs of ganglion A3 (PS3). Here, I show the raw data of each analyzed parameter for each single experiment and the period, duration, and burst strength (boxplots) for PS5 and PS4, respectively.

Period in normal saline (NR) and carbachol (CCh)

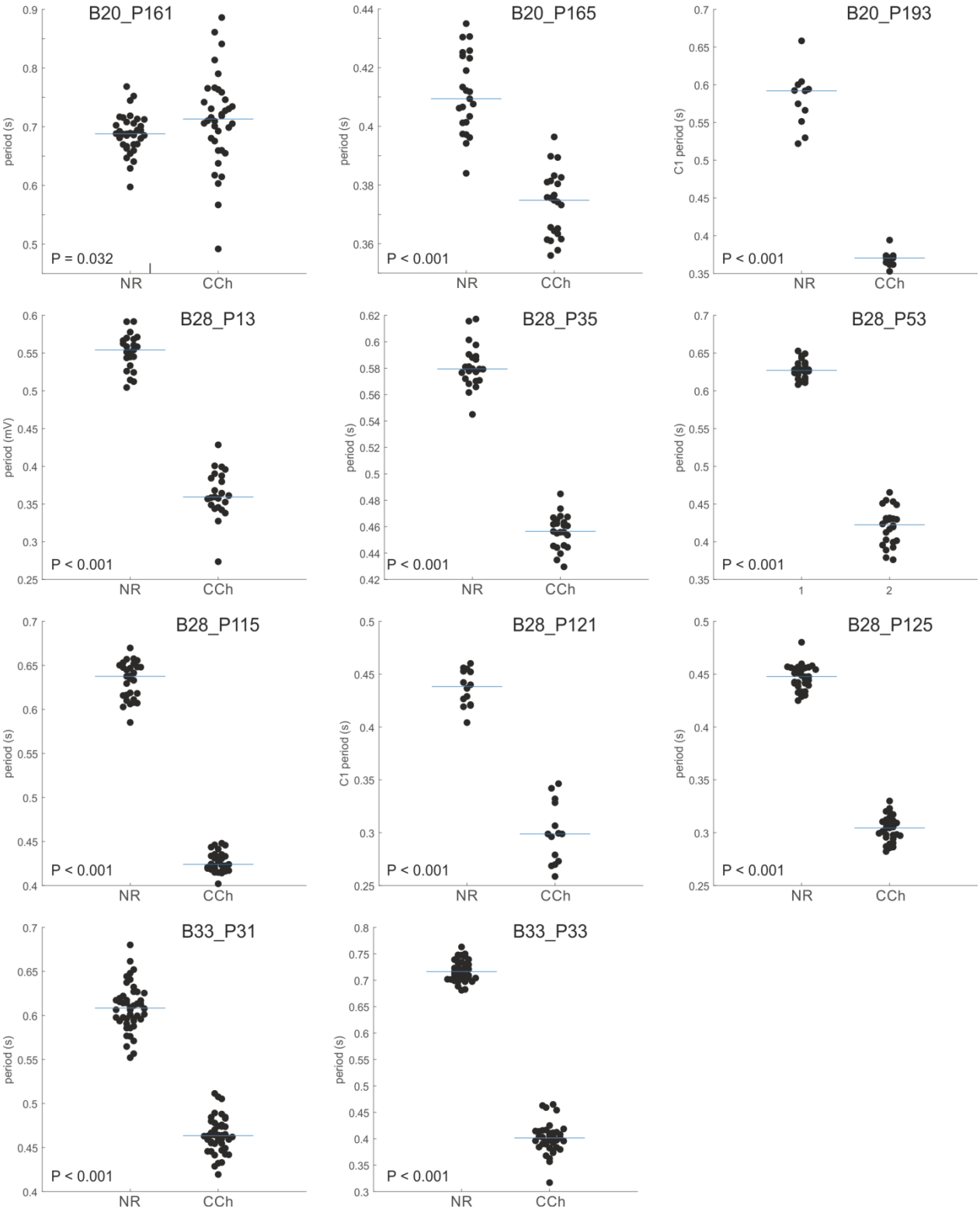

Supplementary Figure 1: PS cycle period in single experiments during NR and CCh application.

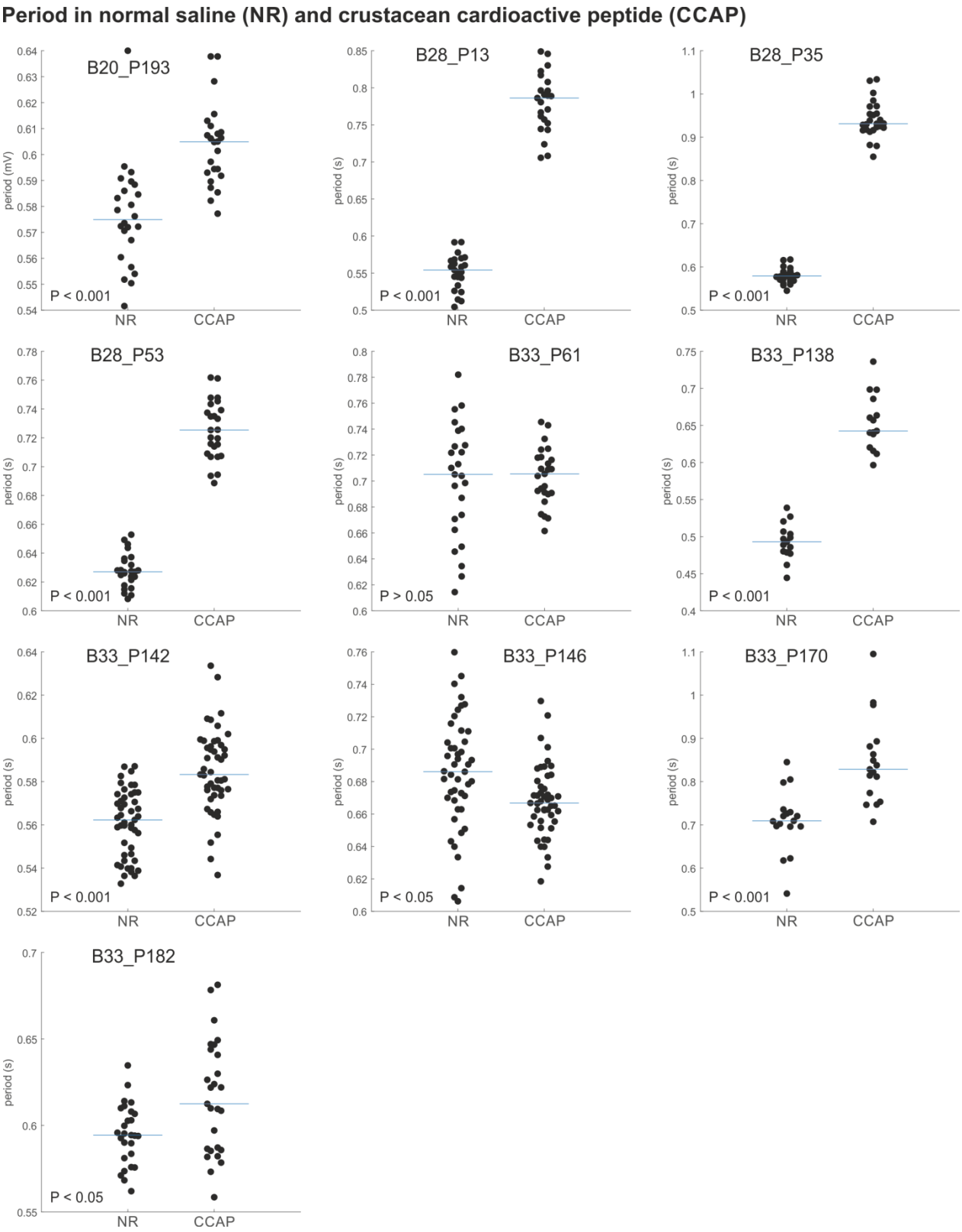

Supplementary Figure 2: PS cycle period in single experiments during NR and CCAP application.

Period in crustacean cardioactive peptide (CCAP) and edrophonium chloride (EdCl)

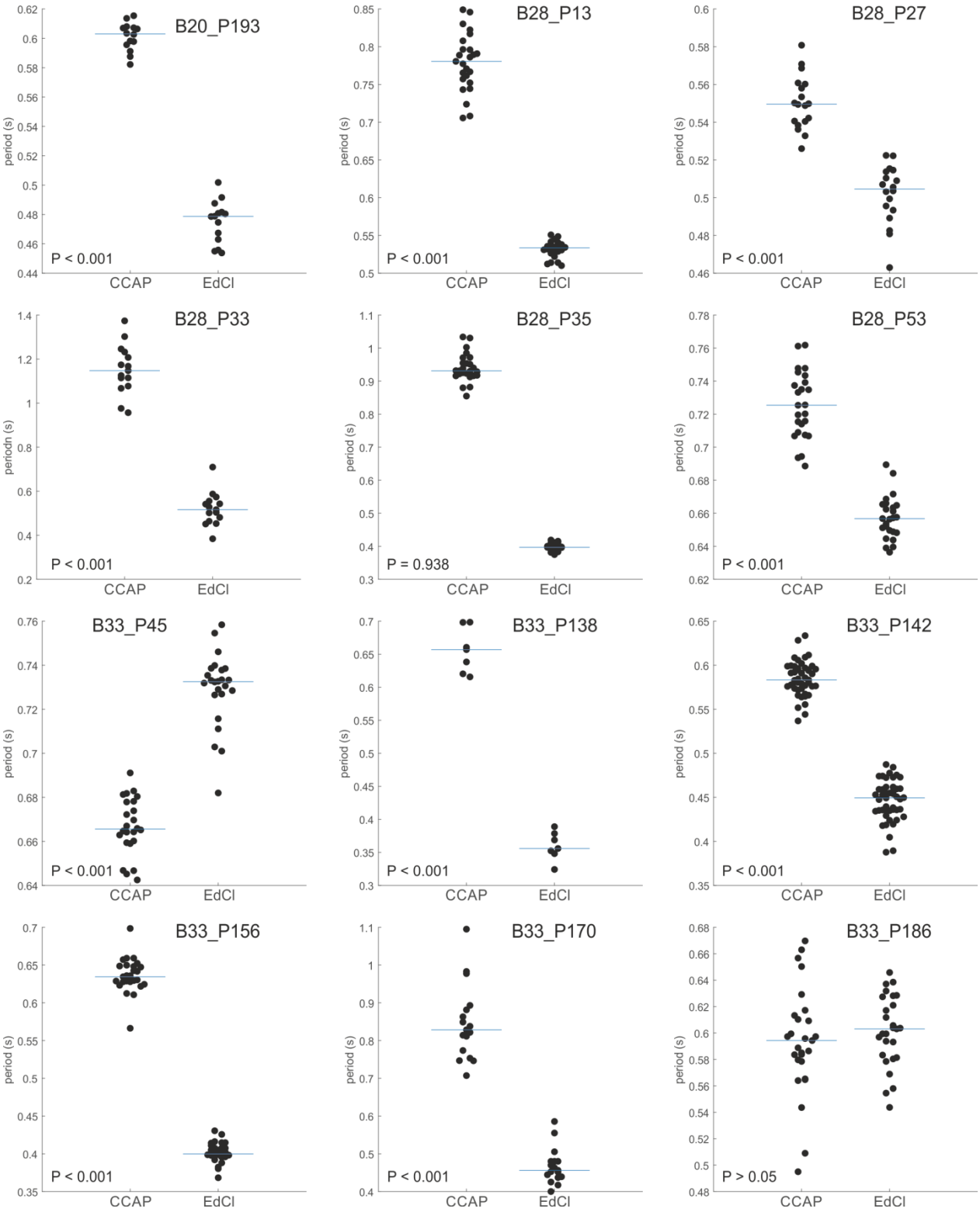

Supplementary Figure 3: PS cycle period in single experiments during CCAP and EdCl application.

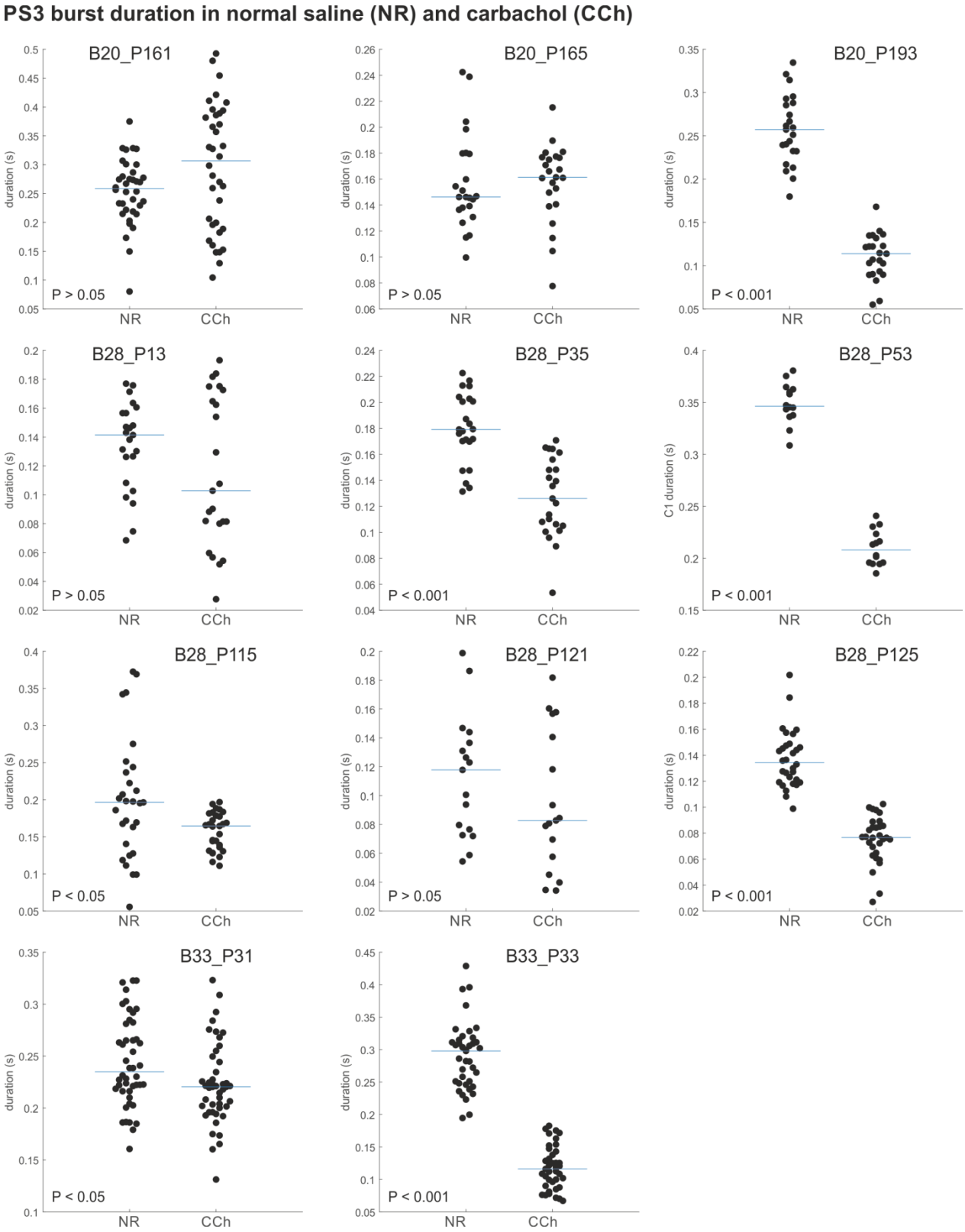

Supplementary Figure 4: PS3 burst duration in single experiments during NR and CCh application.

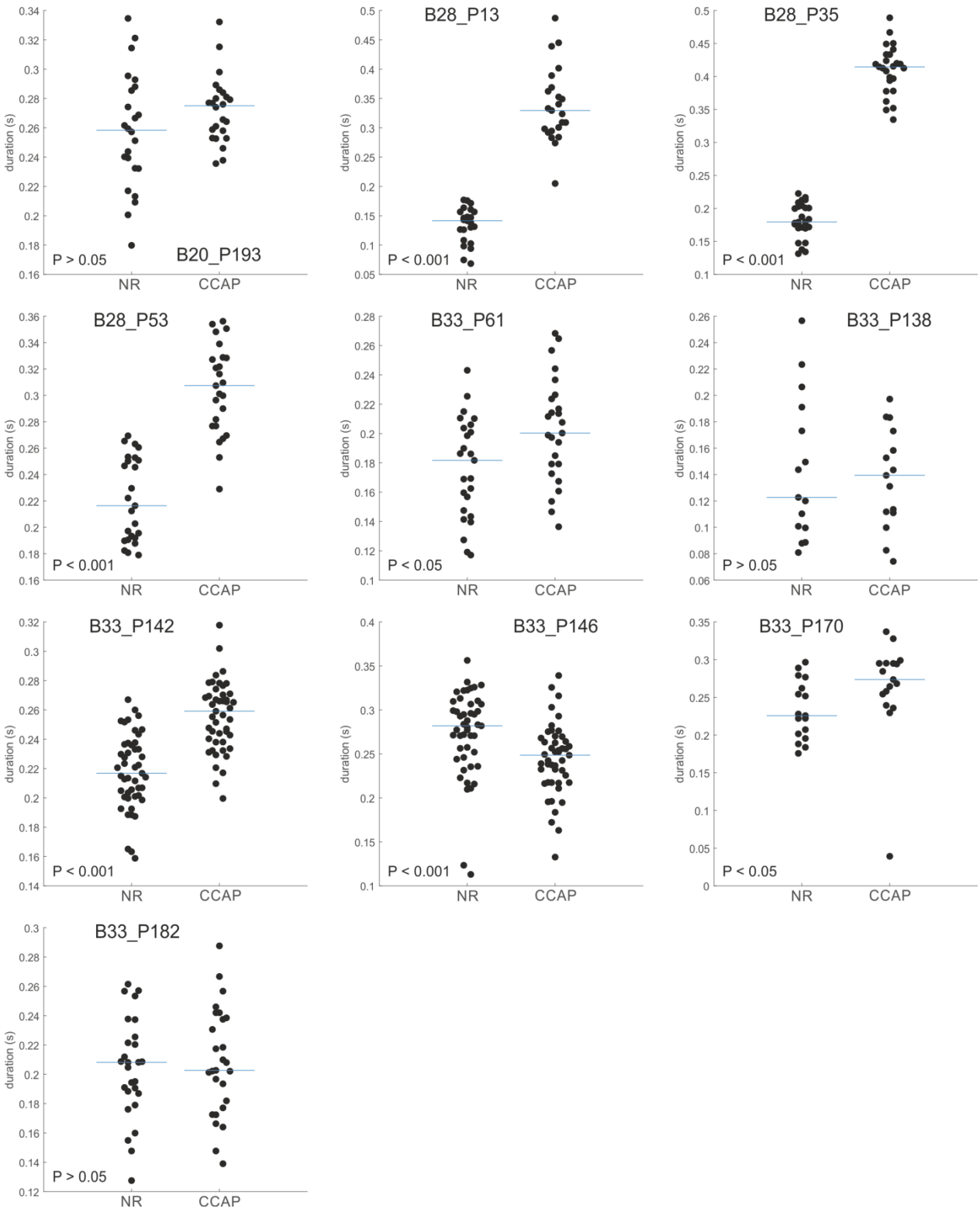

Supplementary Figure 5: PS3 burst duration in single experiments during NR and CCAP application.

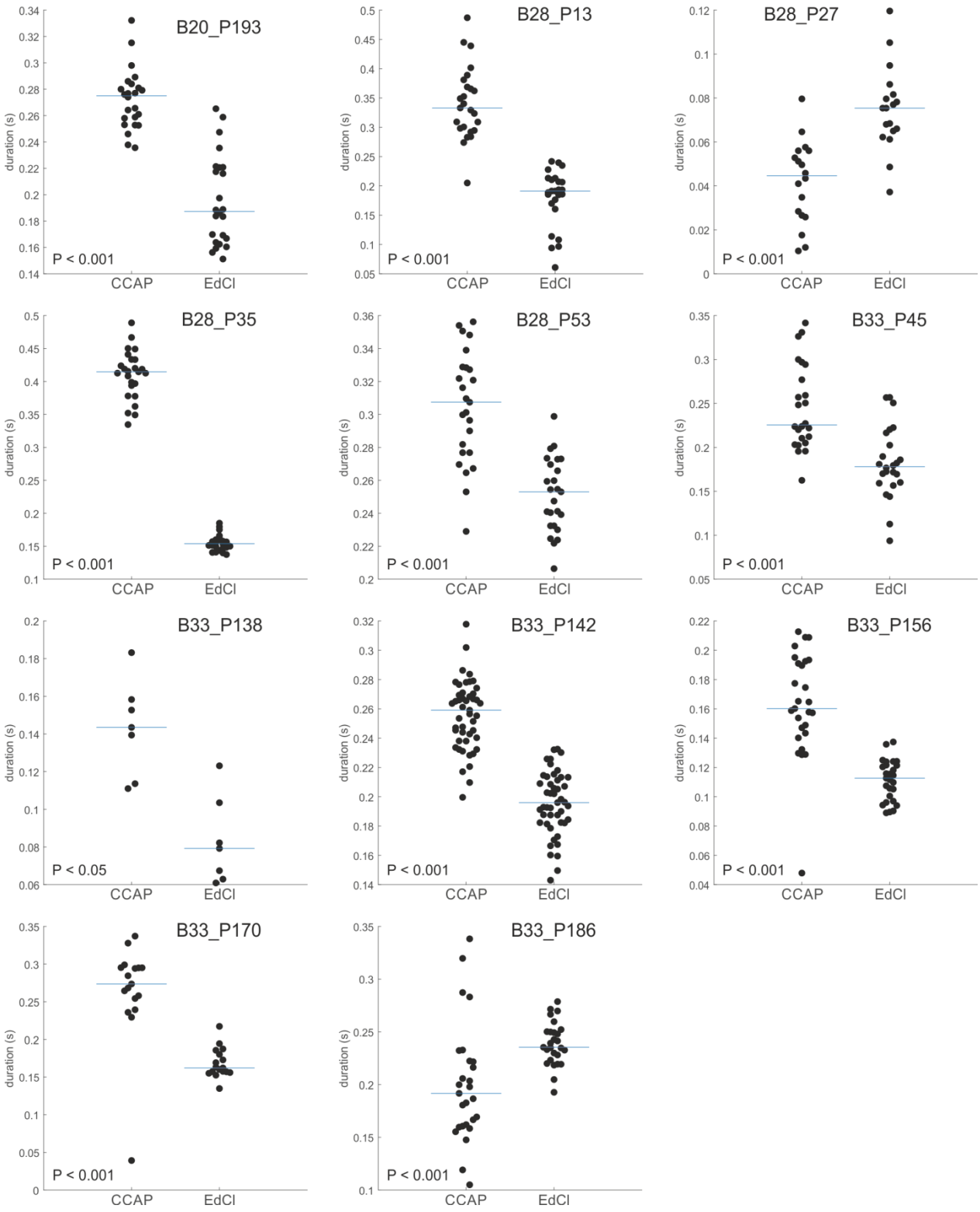

Supplementary Figure 6: PS3 burst duration in single experiments during CCAP and EdCl application.

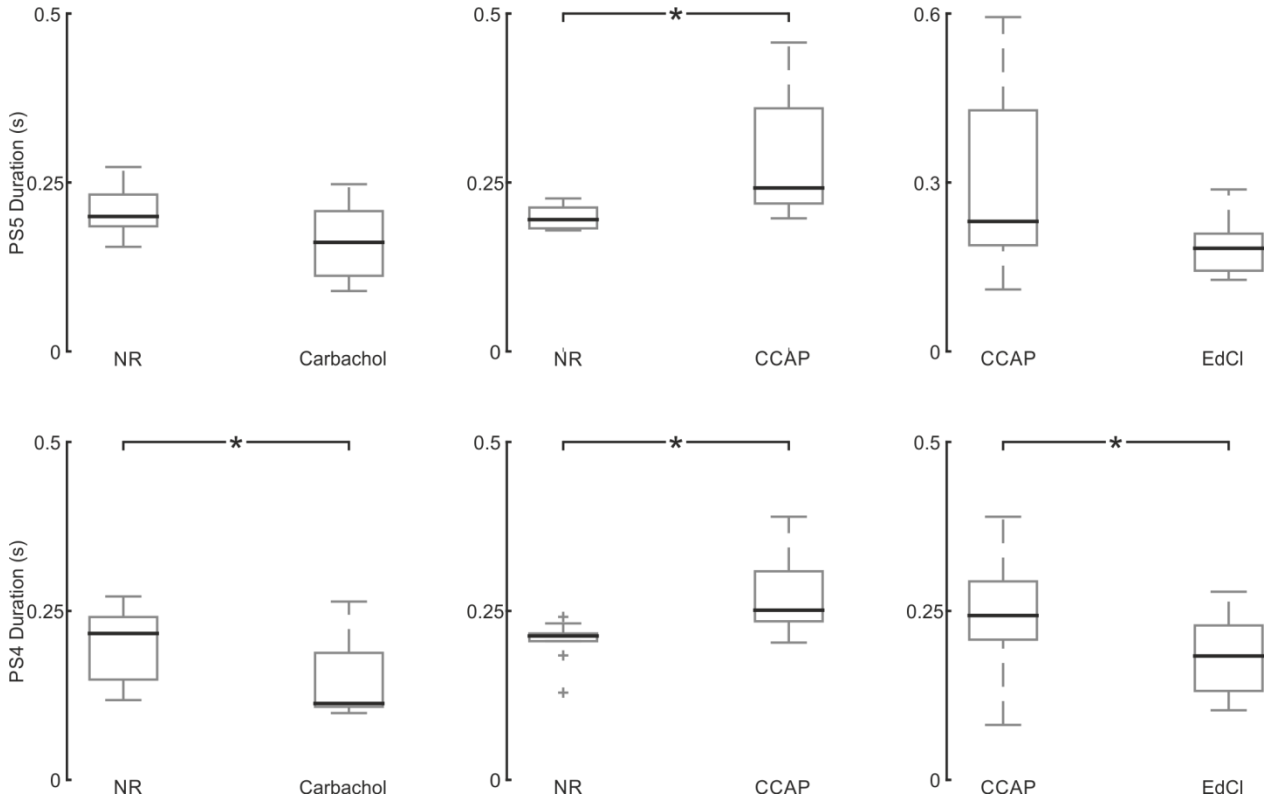

Supplementary Figure 7: PS5 (1st row) and PS4 (2nd row) burst duration during NR and CCh application (left), NR and CCAP application (middle), and during CCAP and EdCl application (right).

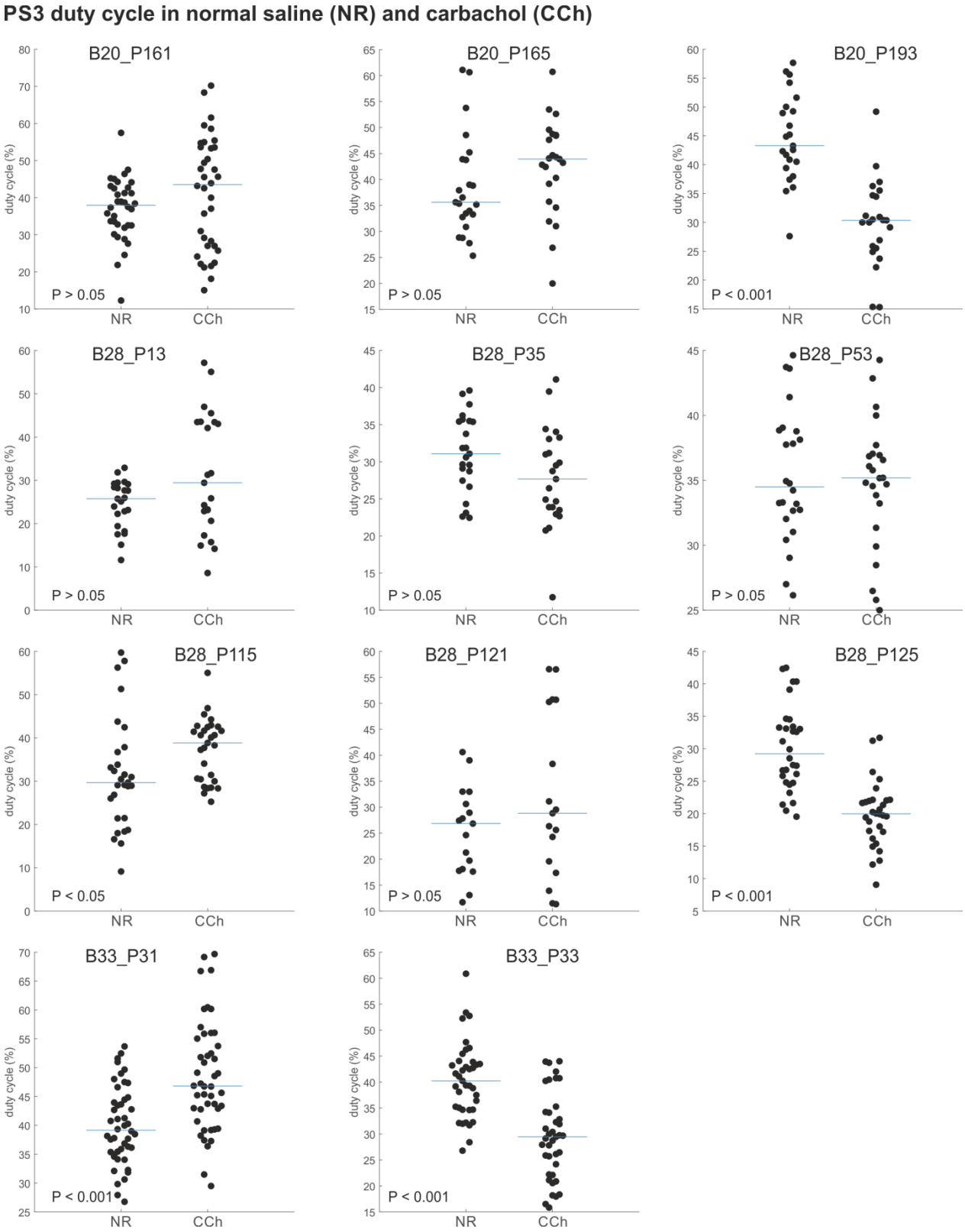

Supplementary Figure 8: PS3 duty cycle in single experiments during NR and CCh application.

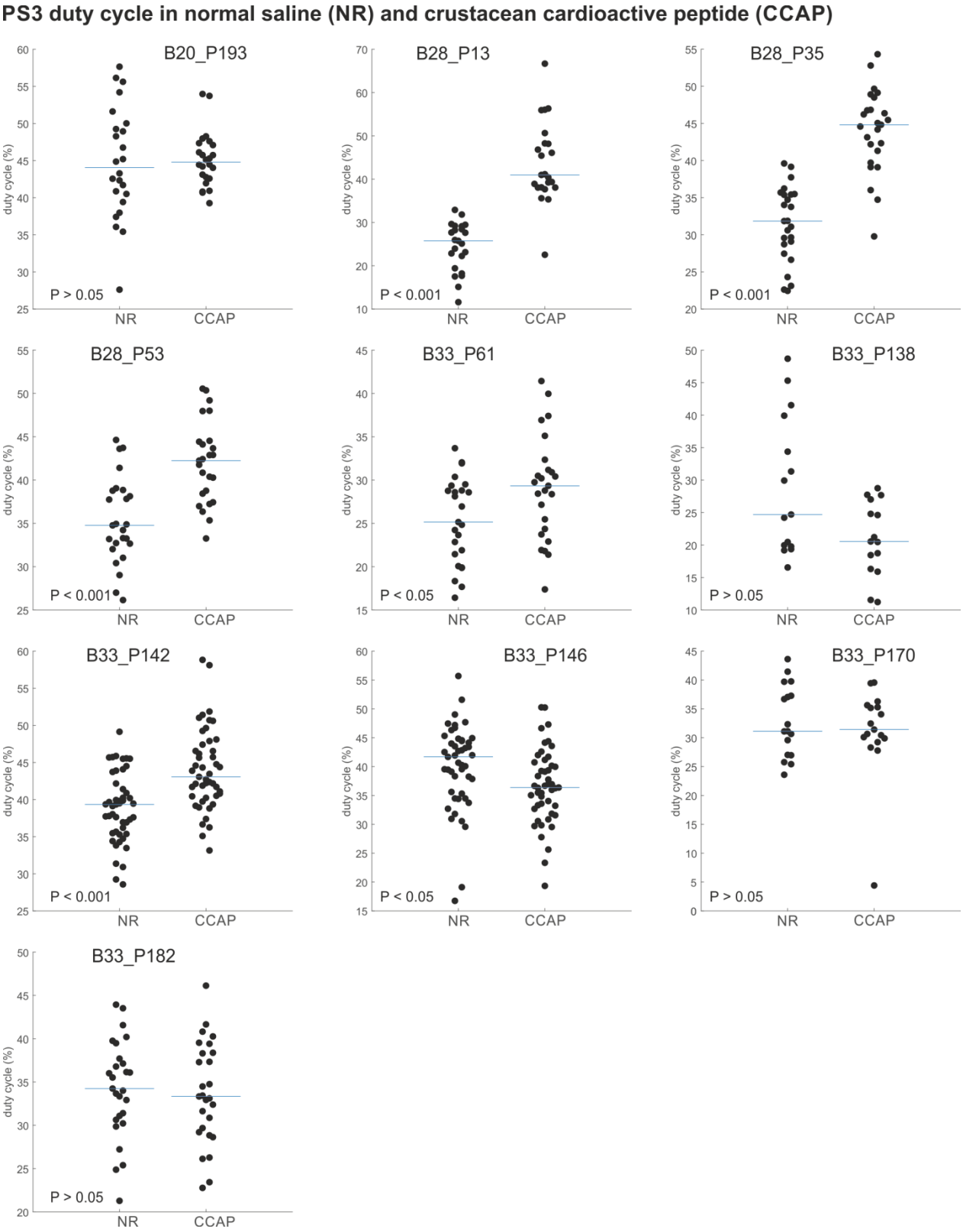

Supplementary Figure 9: PS3 duty cycle in single experiments during NR and CCAP application.

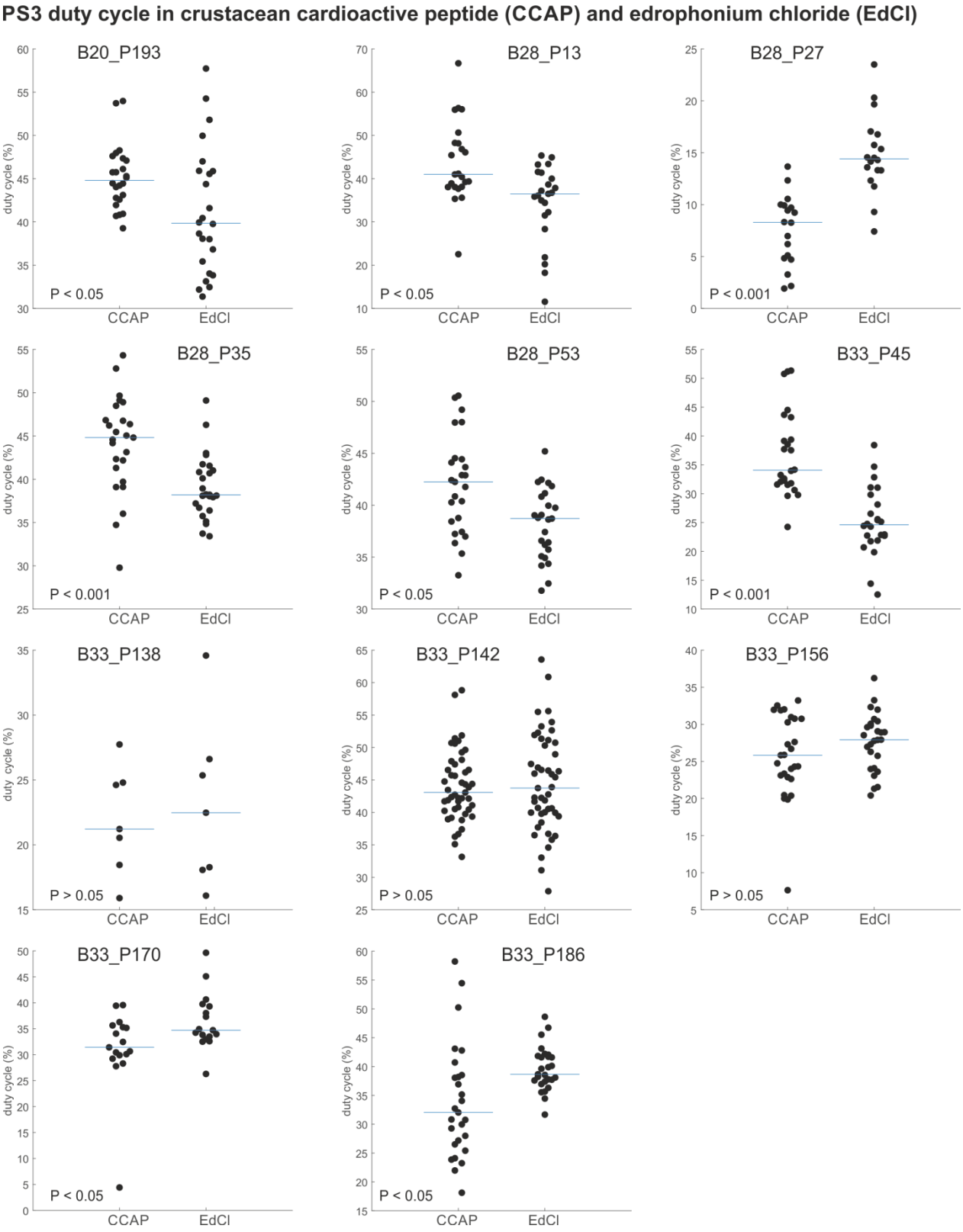

Supplementary Figure 10: PS3 duty cycle in single experiments during CCAP and EdCl application.

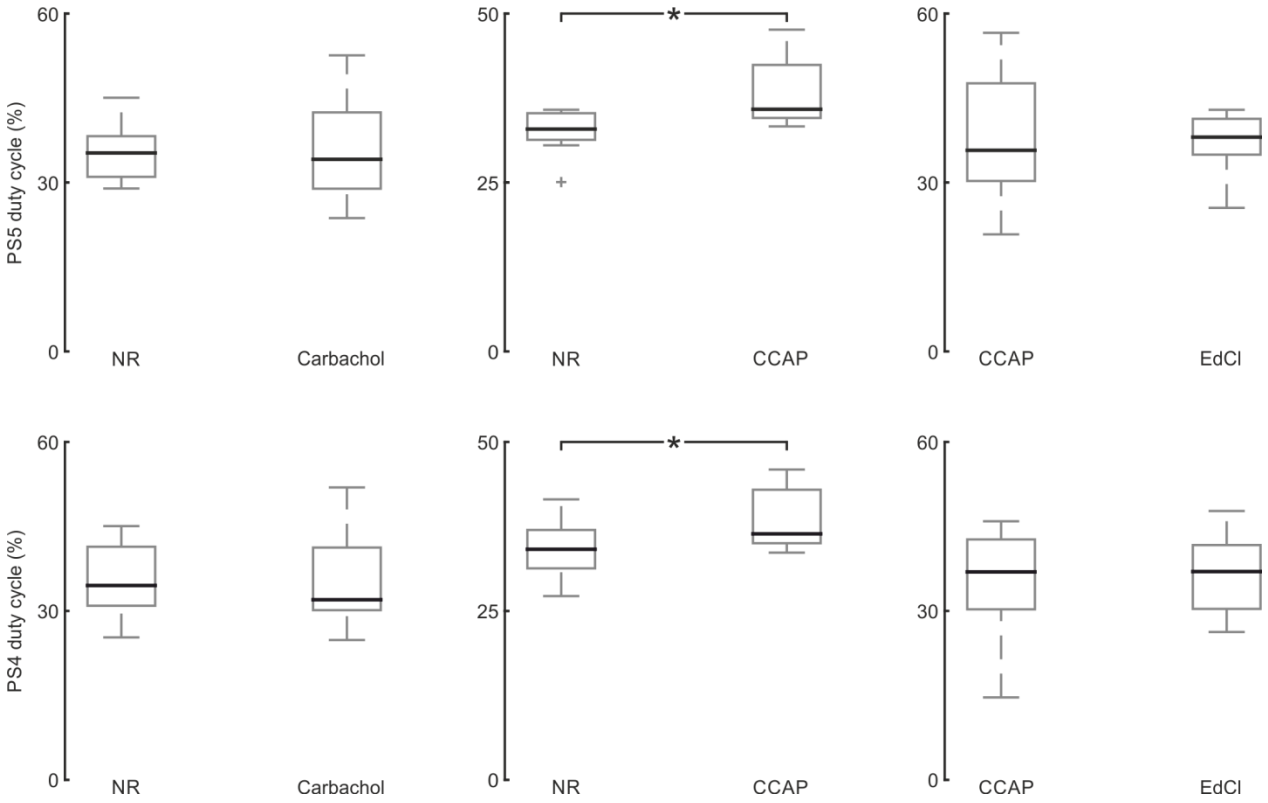

Supplementary Figure 11: PS5 (1st row) and PS4 (2nd row) duty cycle during NR and CCh application (left), NR and CCAP application (middle), and during CCAP and EdCl application (right).

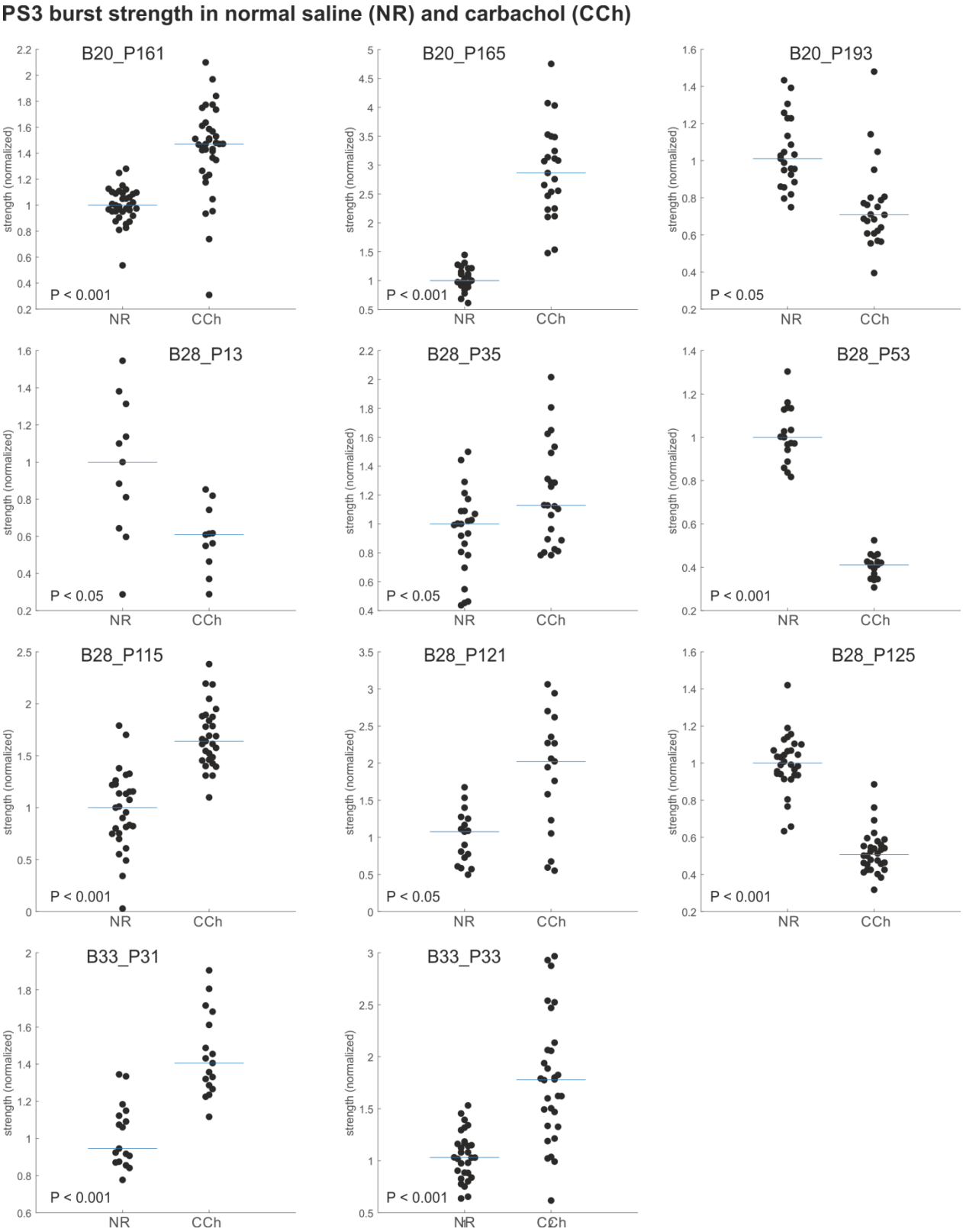

Supplementary Figure 12: PS3 burst strength in single experiments during NR and CCh application.

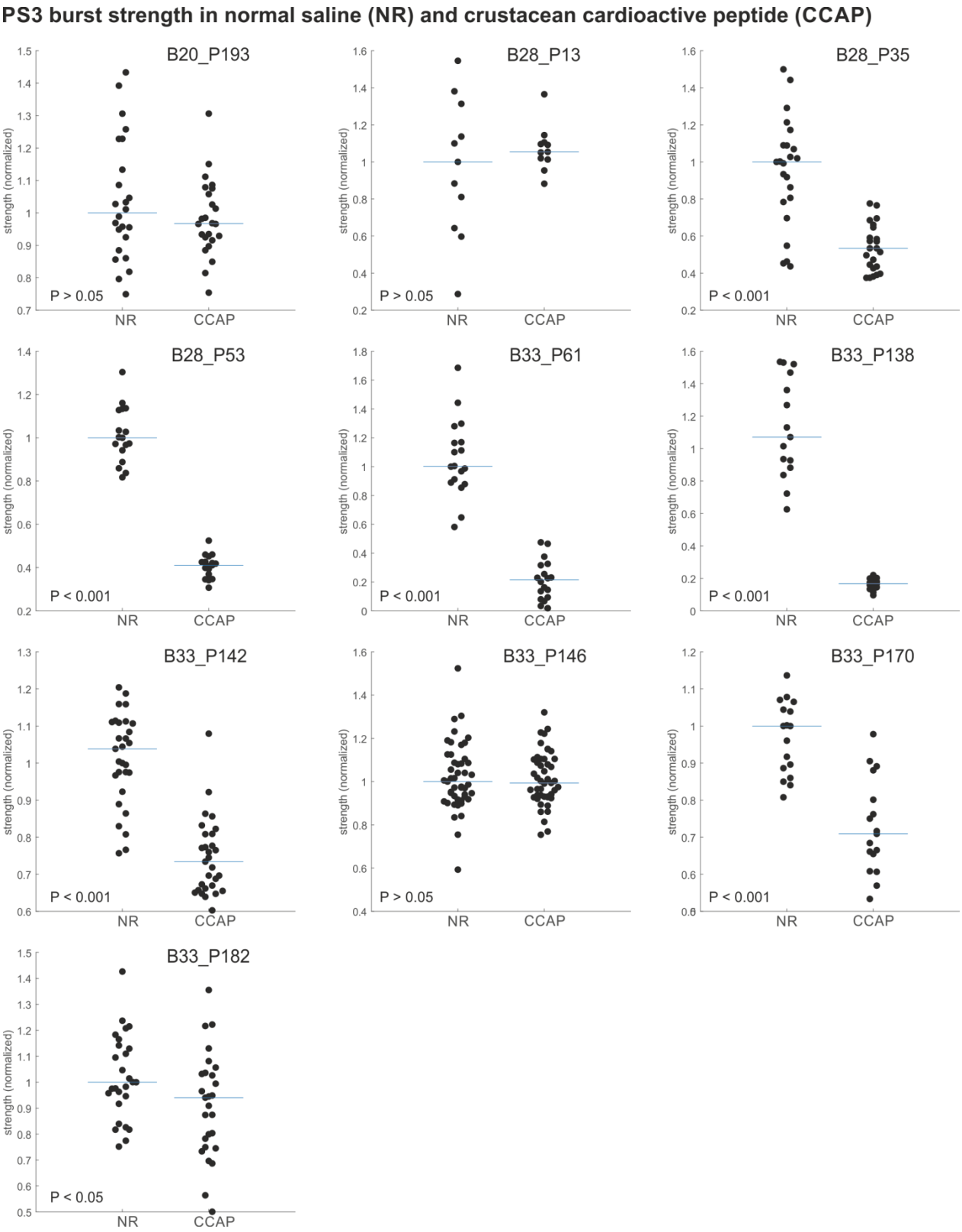

Supplementary Figure 13: PS3 burst strength in single experiments during NR and CCAP application.

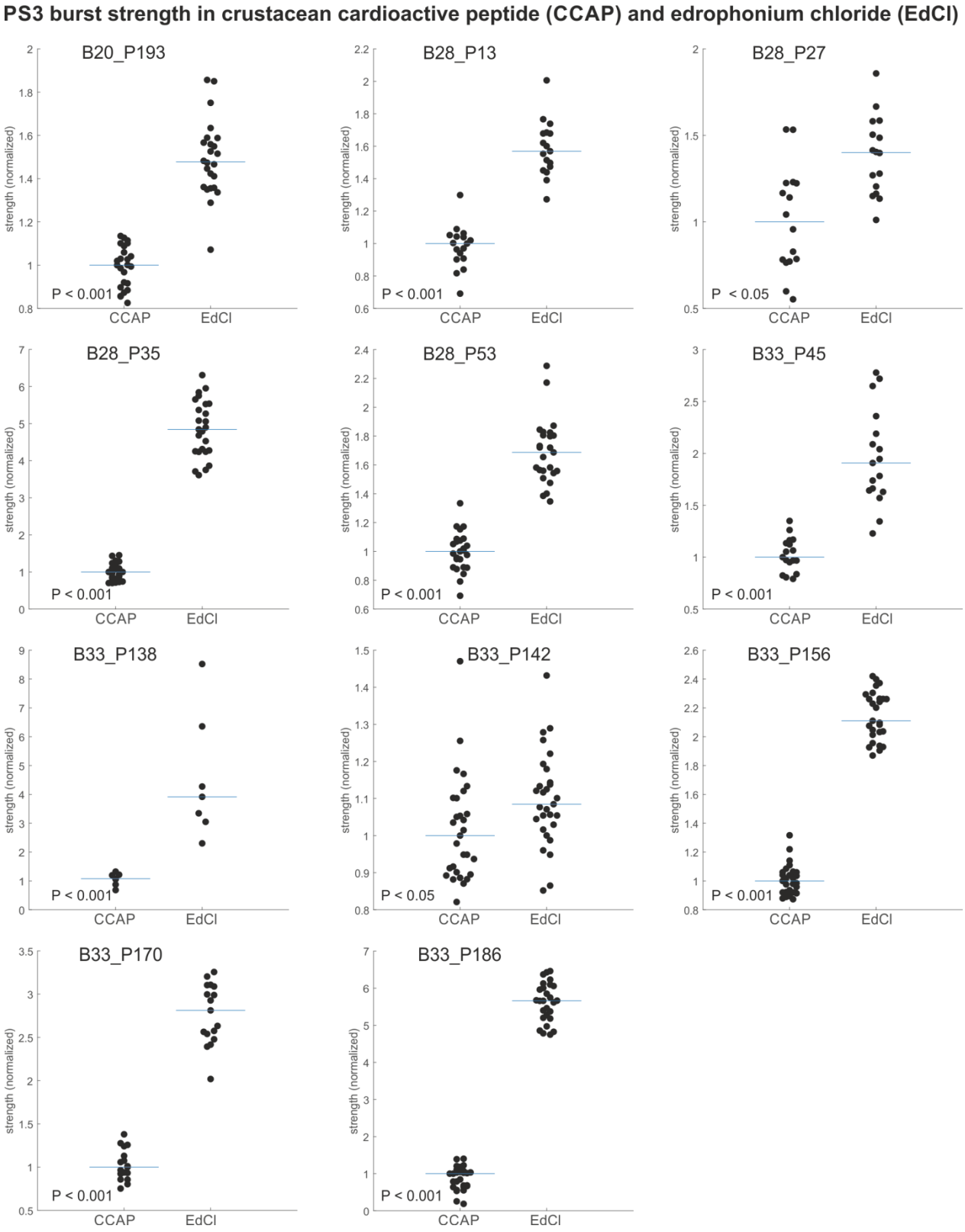

Supplementary Figure 14: PS3 burst strength in single experiments during CCAP and EdCl application.

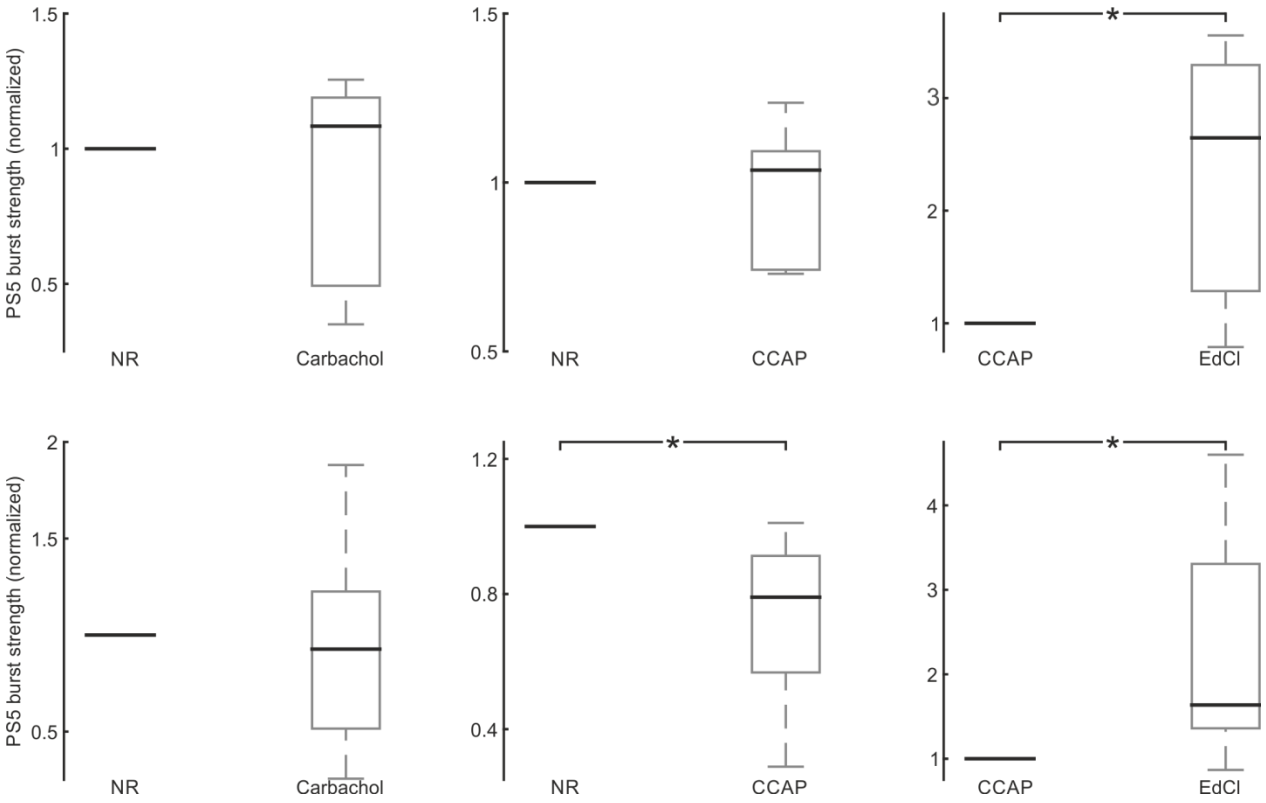

Supplementary Figure 15: PS5 (1st row) and PS4 (2nd row) duty cycle during NR and CCh application (left), NR and CCAP application (middle), and during CCAP and EdCl application (right).

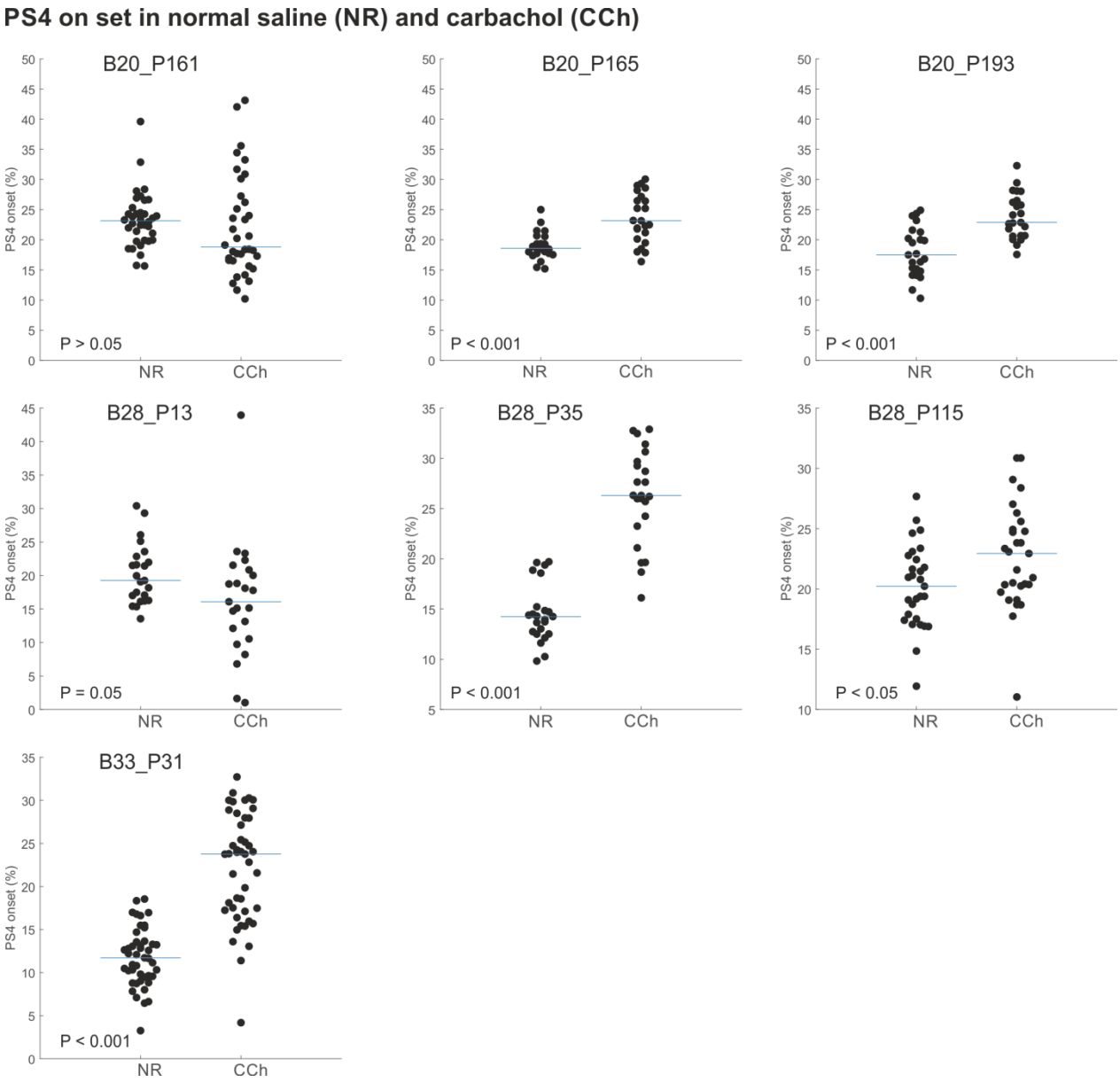

Supplementary Figure 16: PS4 onset in single experiments during NR and CCh application.

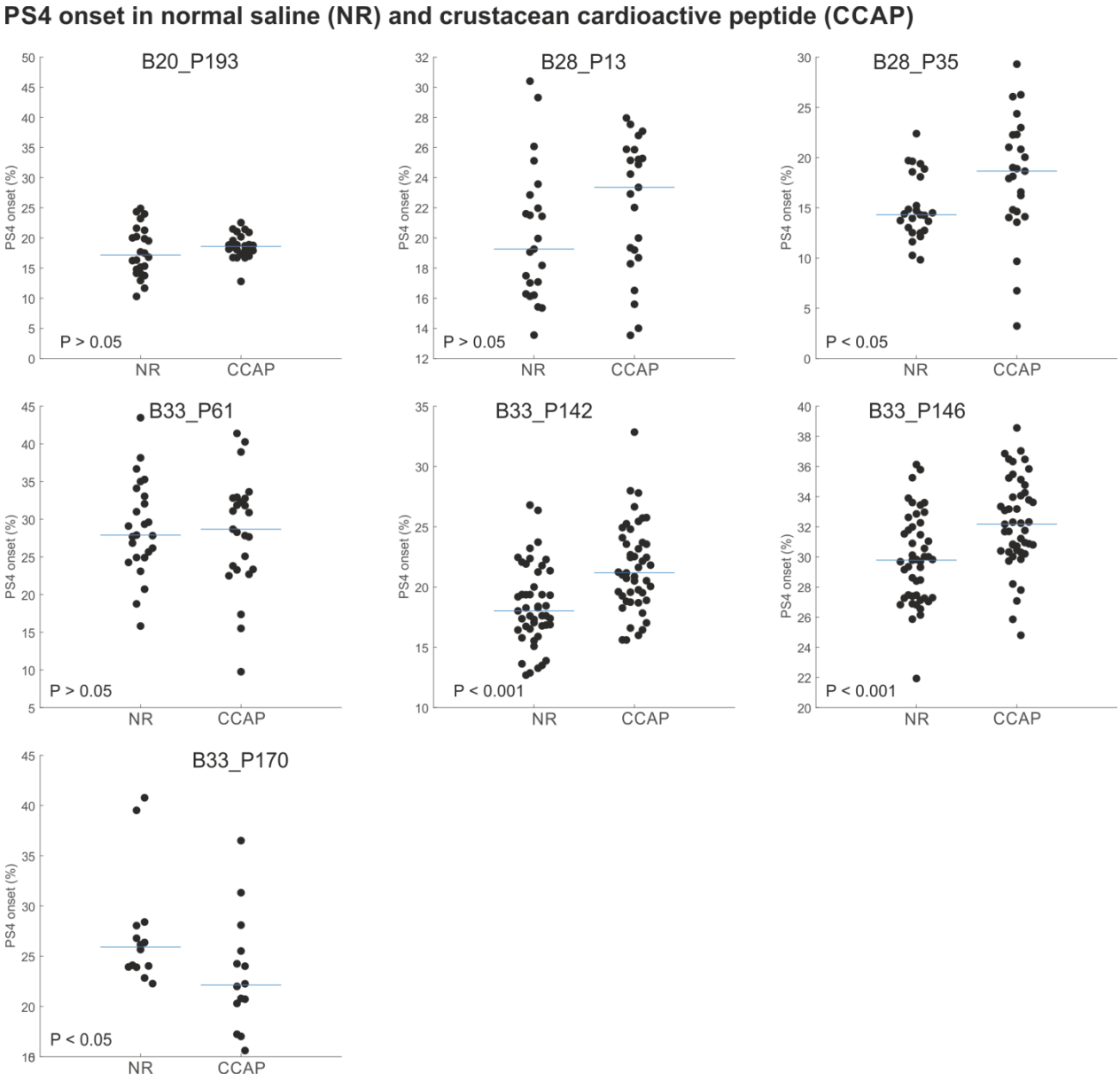

Supplementary Figure 17: PS4 onset in single experiments during NR and CCAP application.

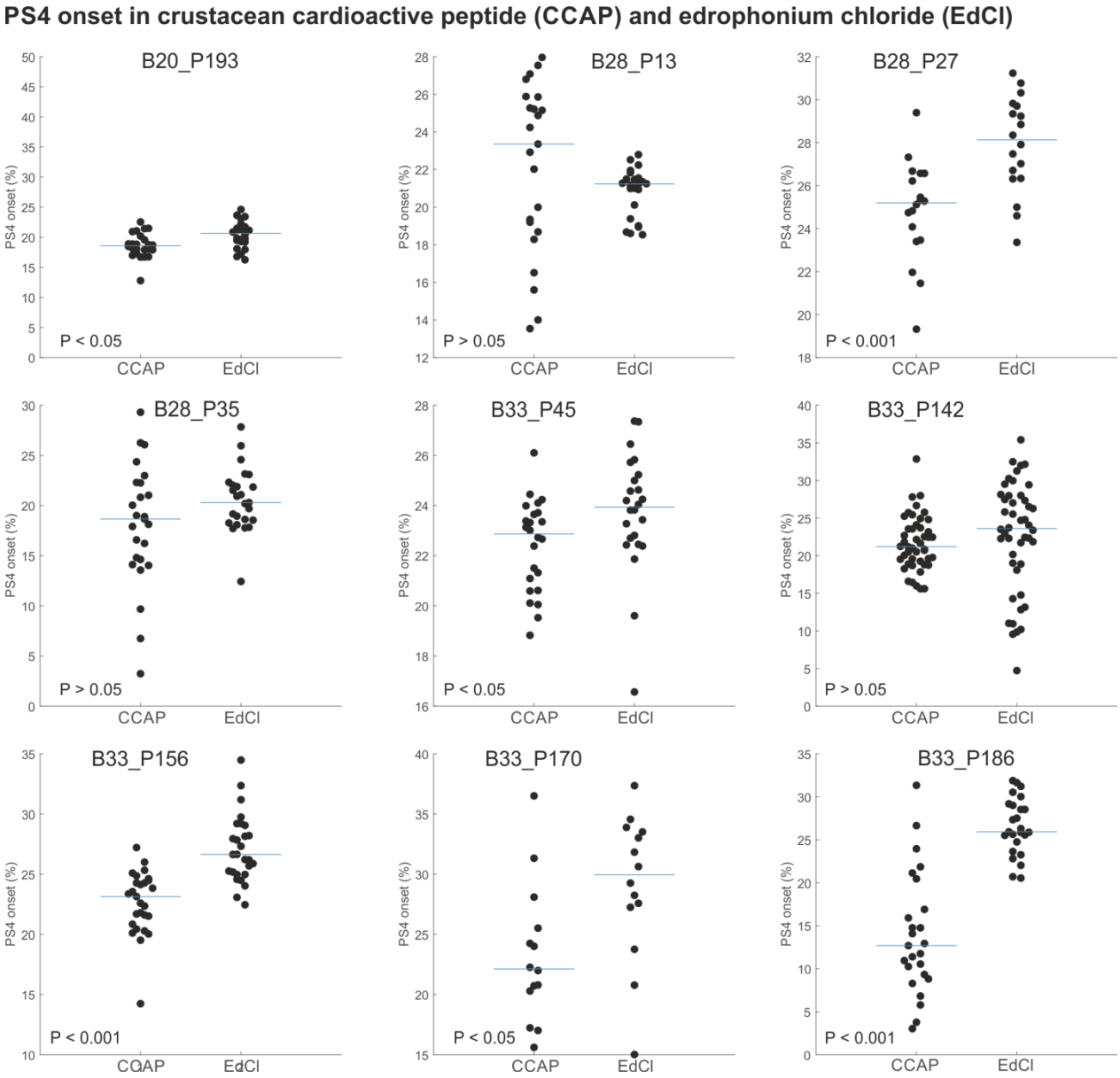

Supplementary Figure 18: PS4 onset in single experiments during CCAP and EdCl application.

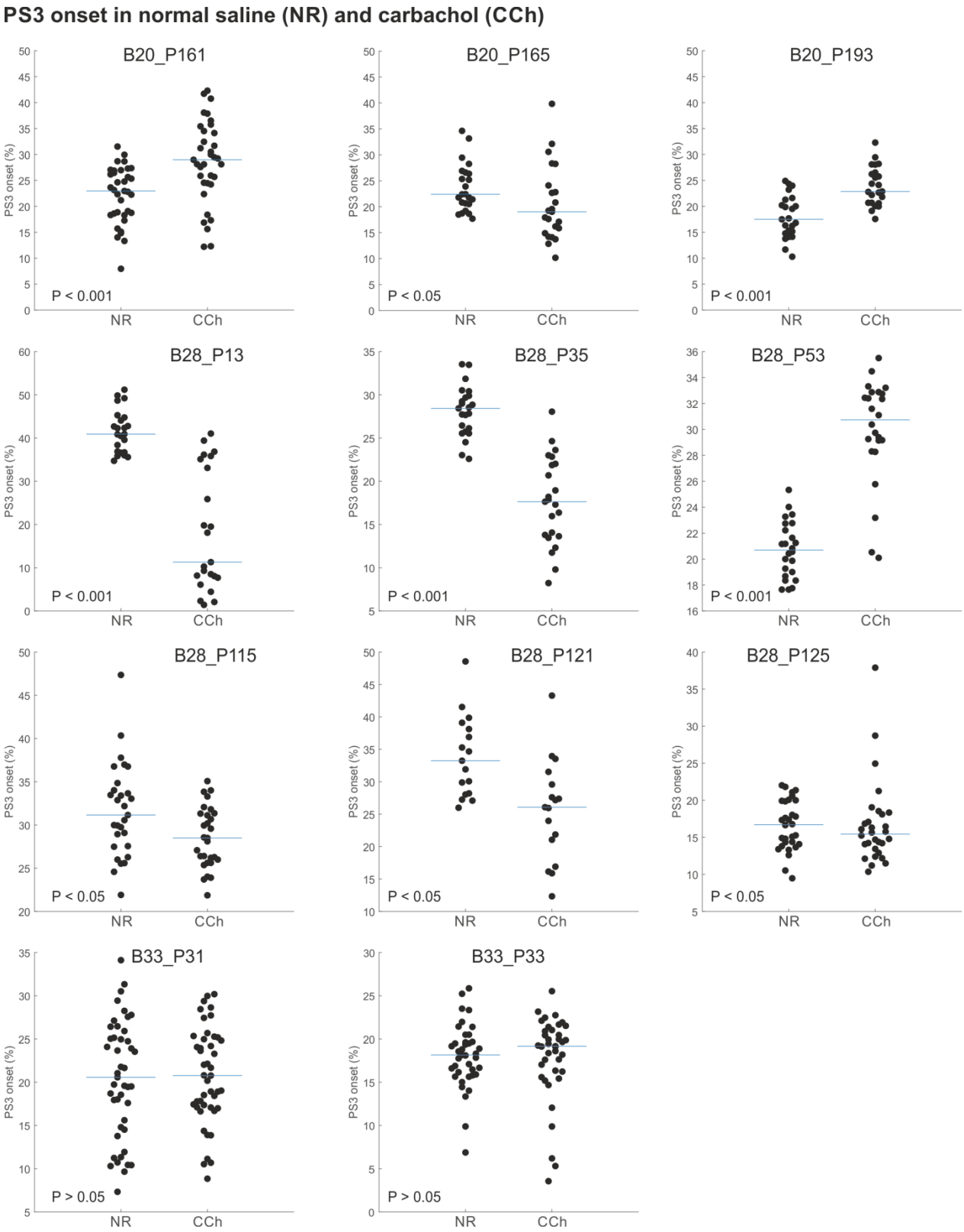

Supplementary Figure 19: PS3 onset in single experiments during NR and CCh application.

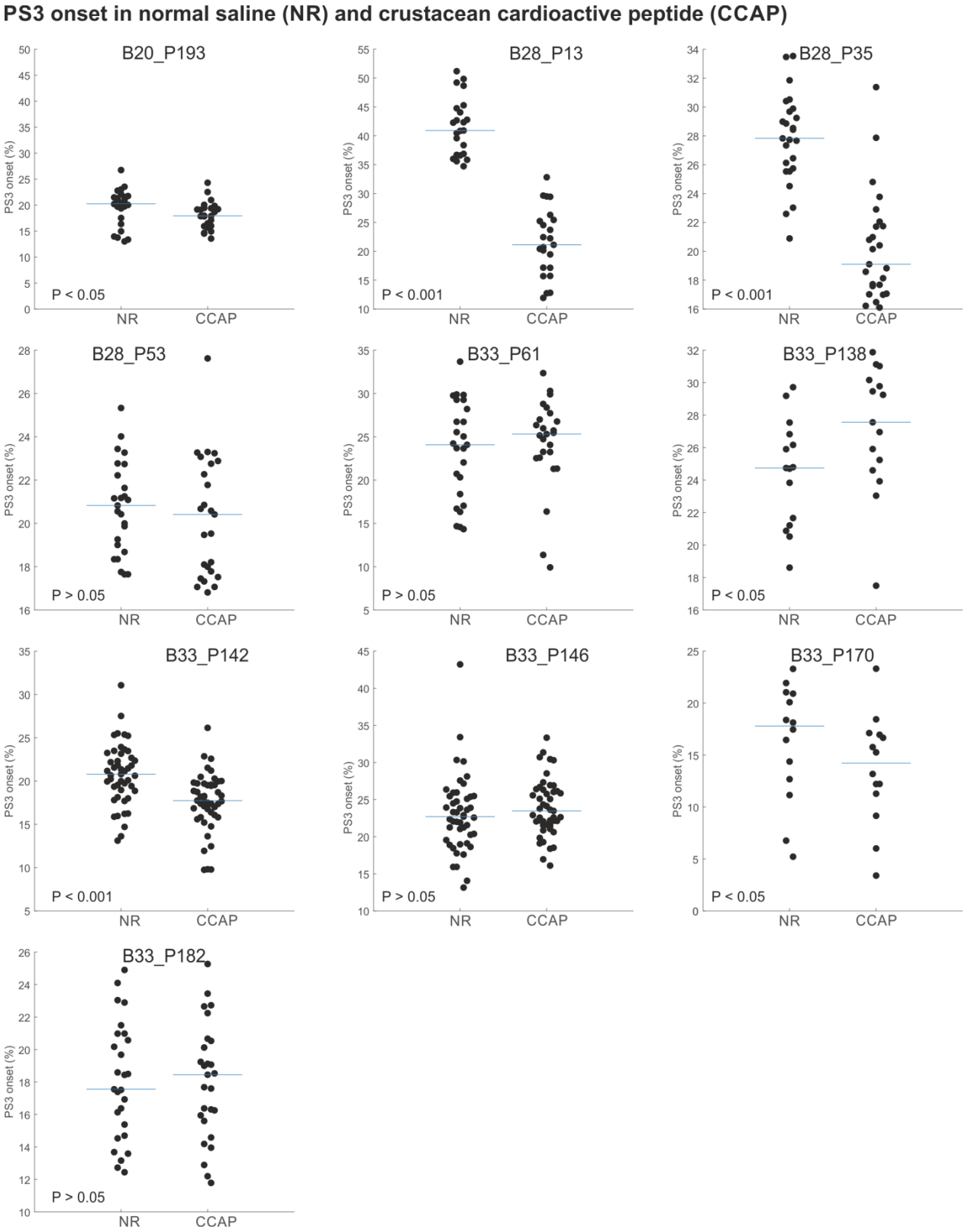

Supplementary Figure 20: PS3 onset in single experiments during NR and CCAP application.

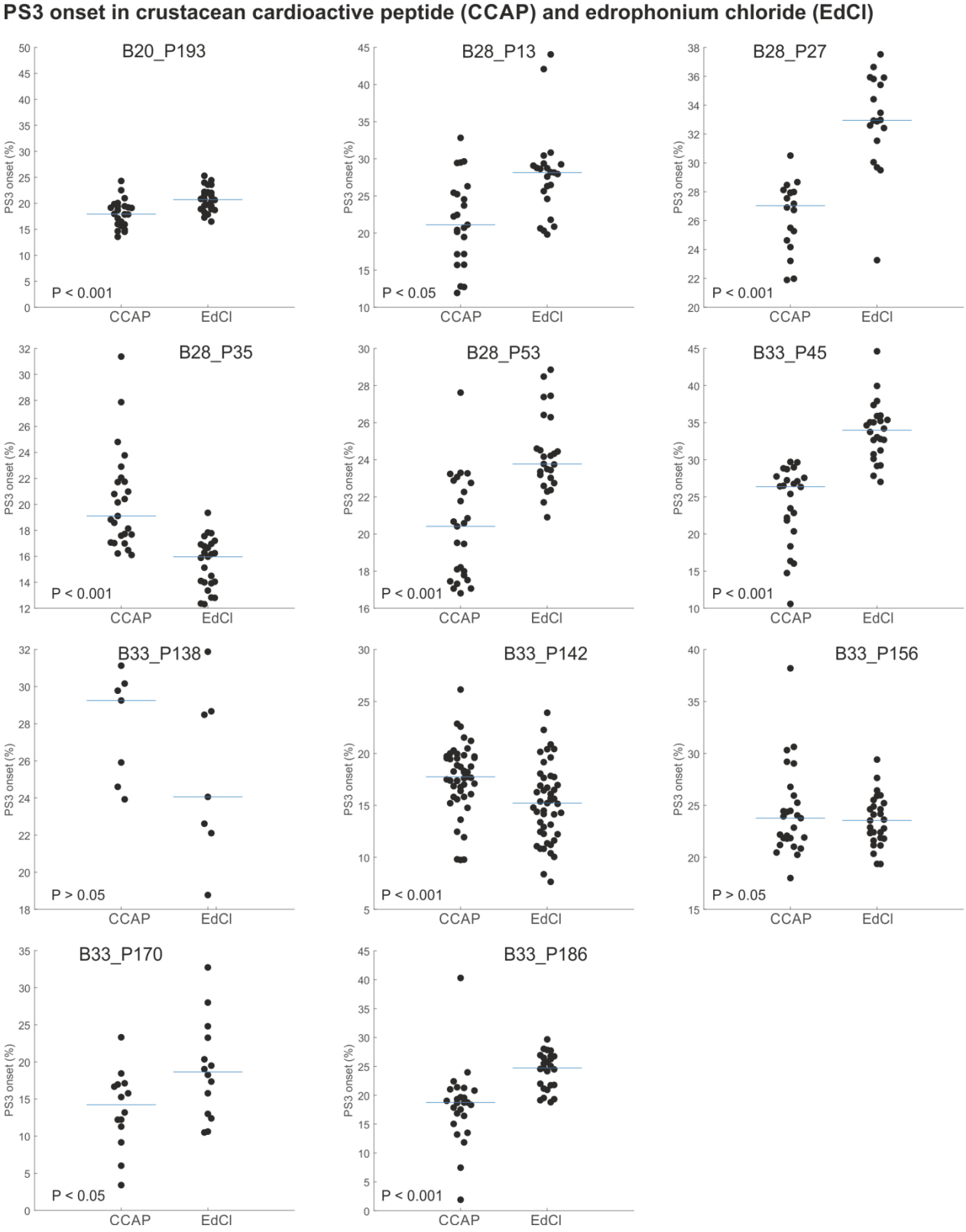

Supplementary Figure 21: PS3 onset in single experiments during CCAP and EdCl application.

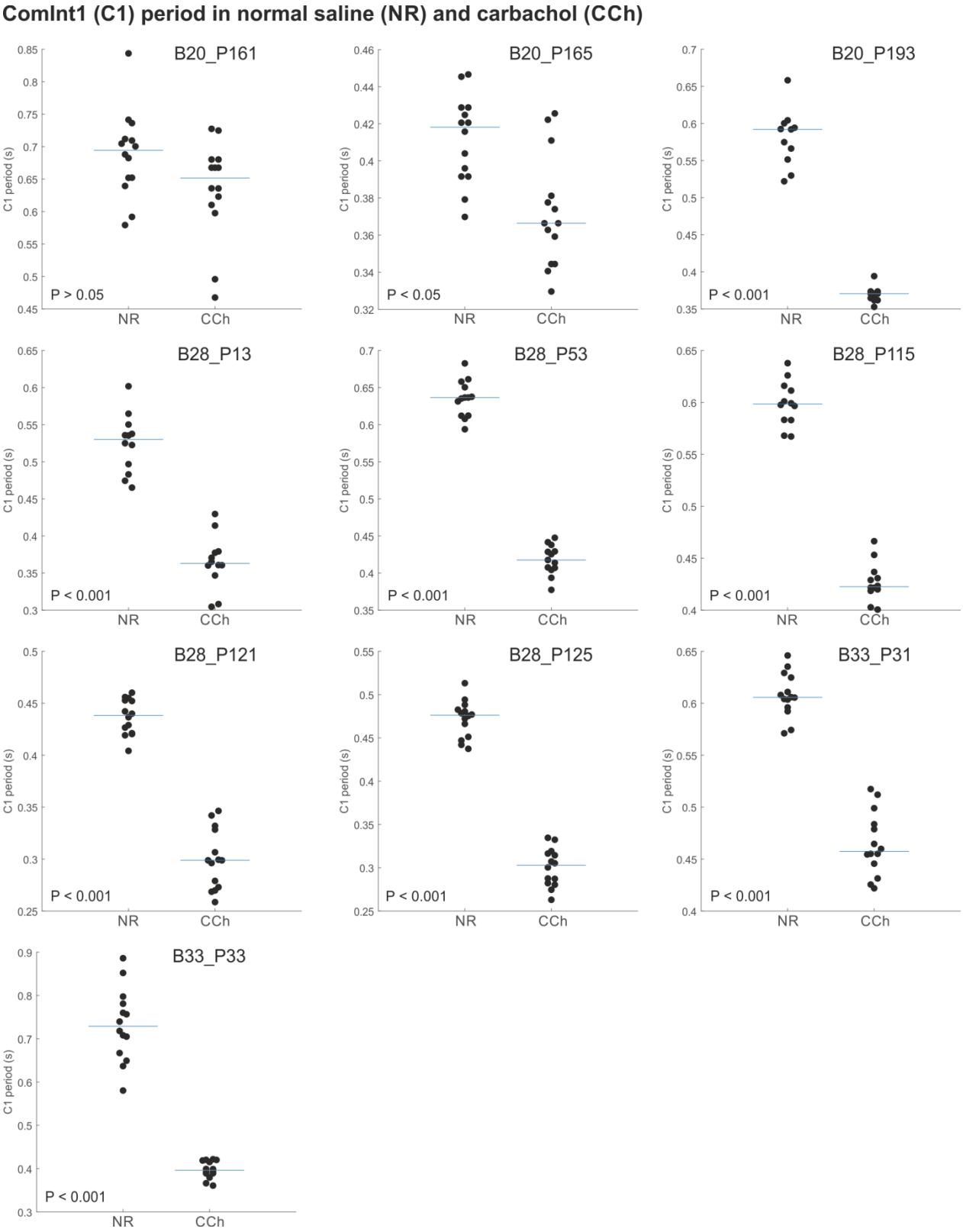

Supplementary Figure 22: ComInt1 period in single experiments during NR and CCh application.

ComInt1 (C1) period in normal saline (NR) and crustacean cardioactive peptide (CCAP)

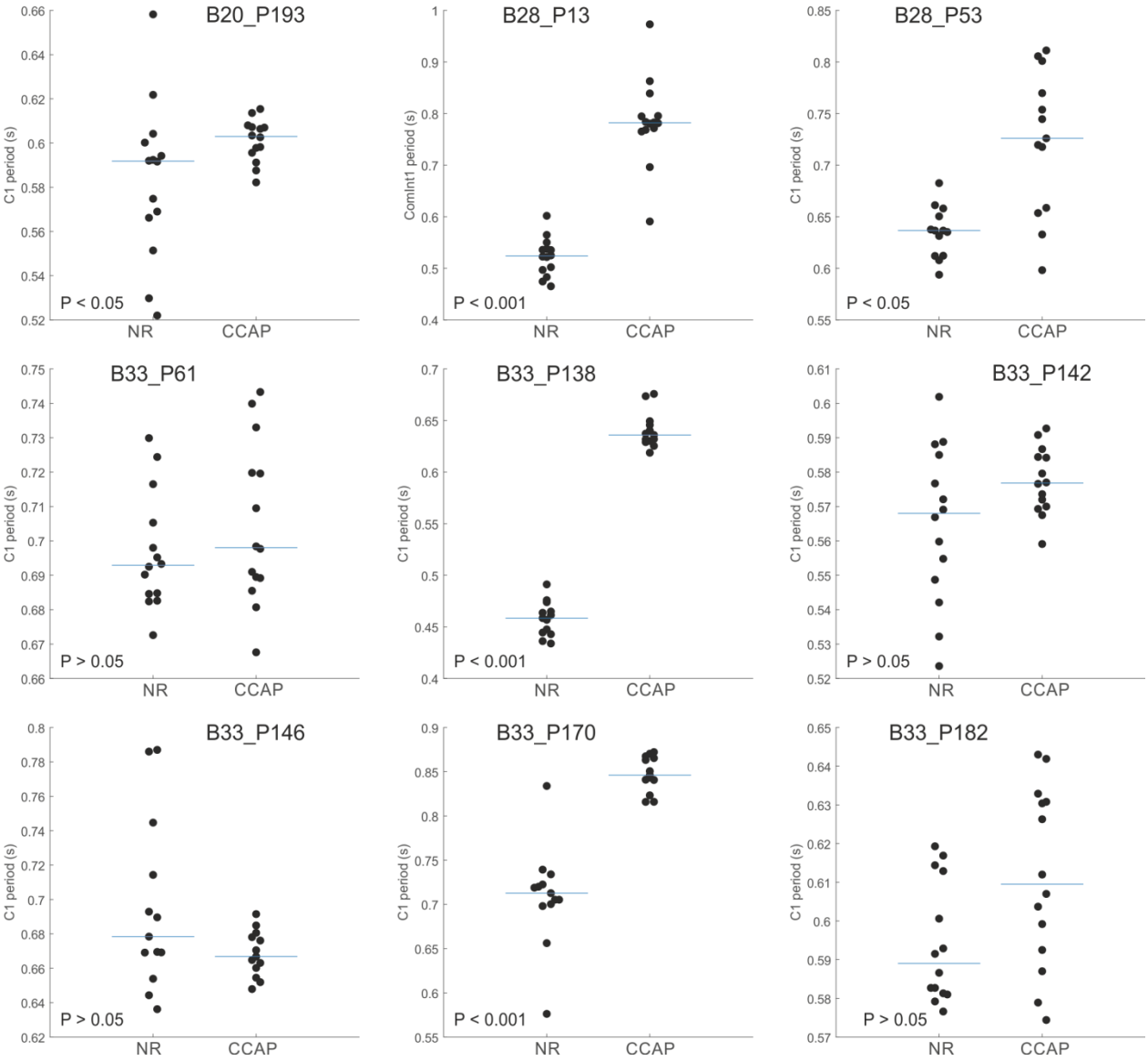

Supplementary Figure 23: ComInt1 period in single experiments during NR and CCAP application.

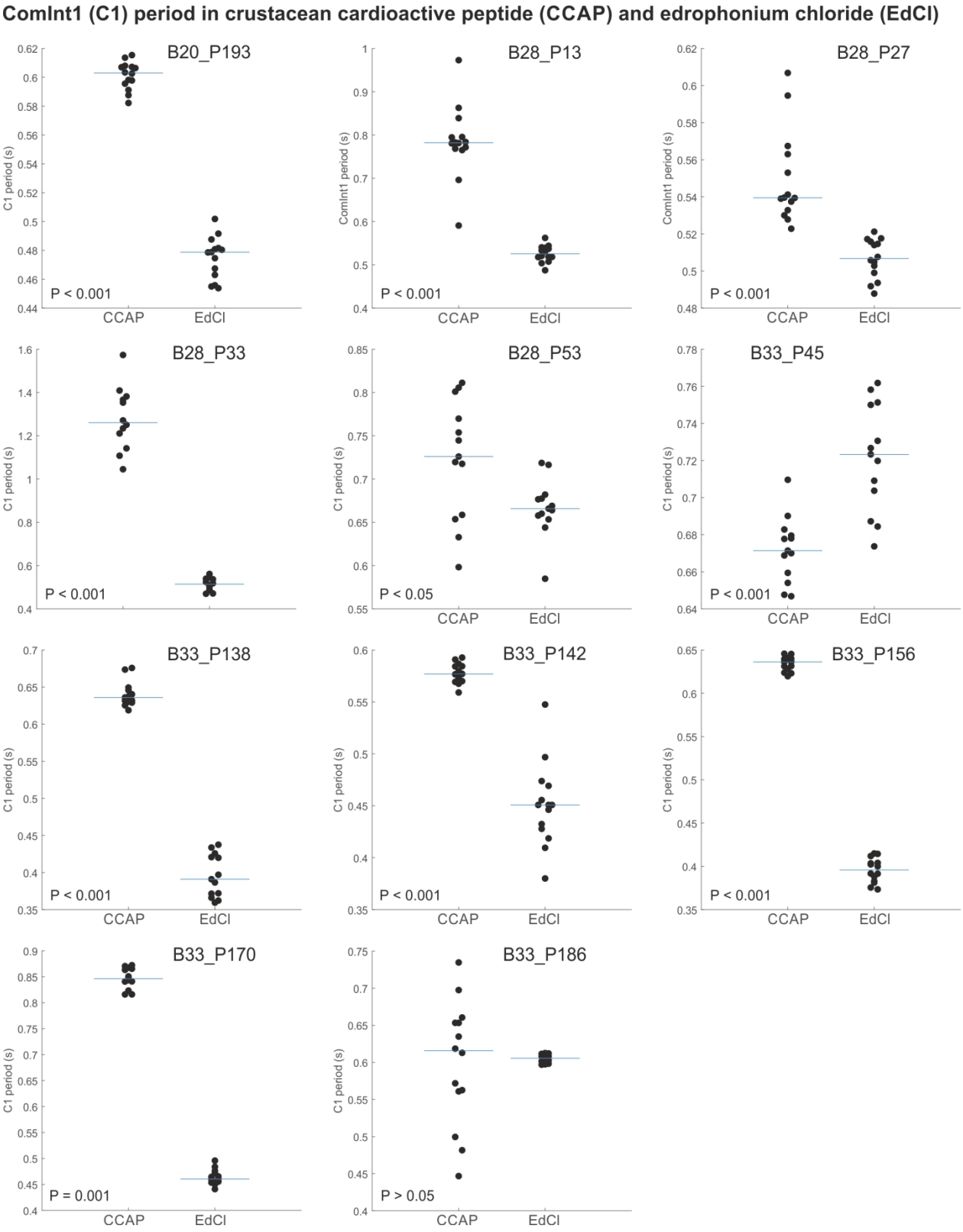

Supplementary Figure 24: ComInt1 period in single experiments during CCAP and EdCl application.

ComInt1 (C1) duration in normal saline (NR) and carbachol (CCh)

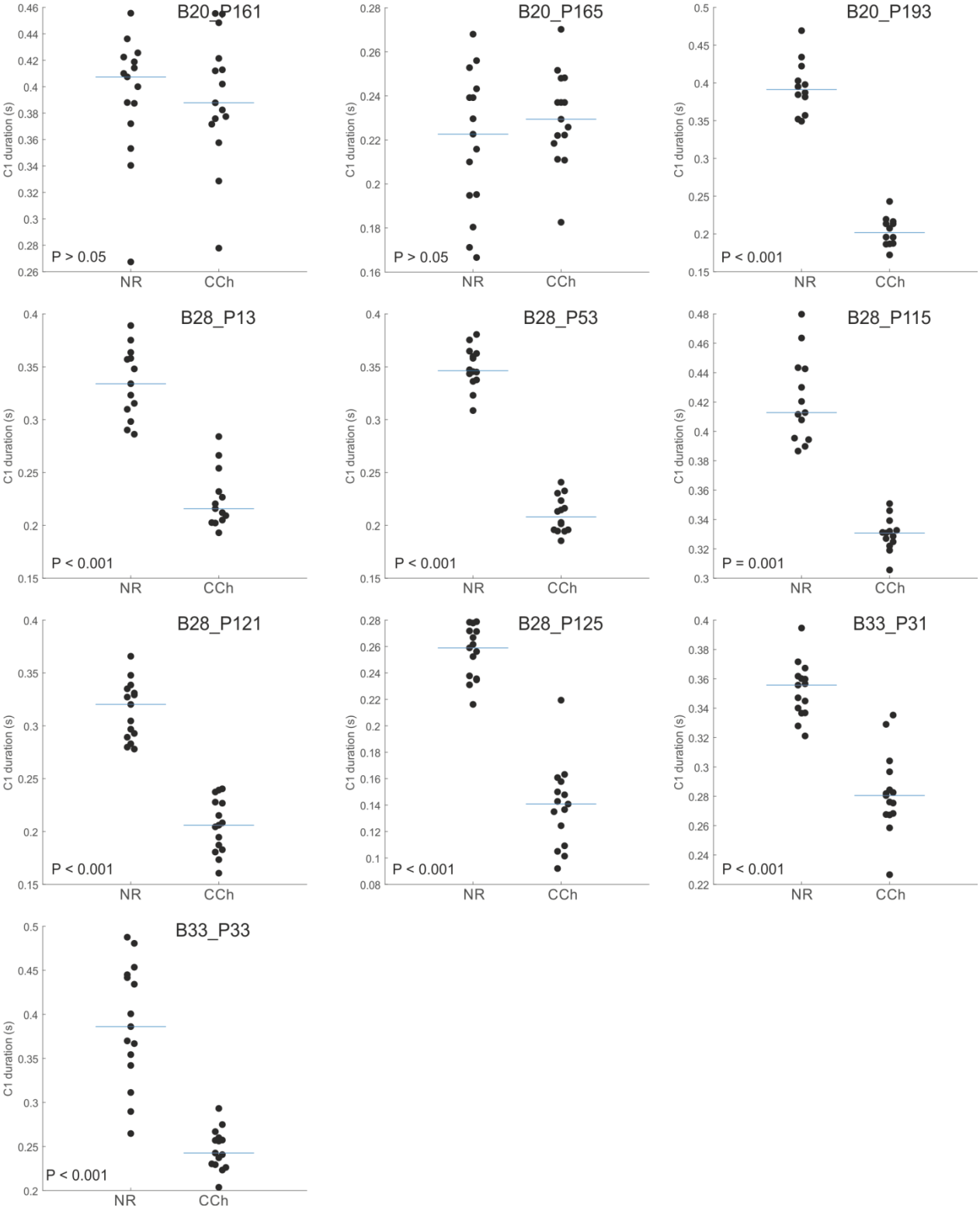

Supplementary Figure 25: ComInt1 duration in single experiments during NR and CCh application.

ComInt1 (C1) duration in normal saline (NR) and crustacean cardioactive peptide (CCAP)

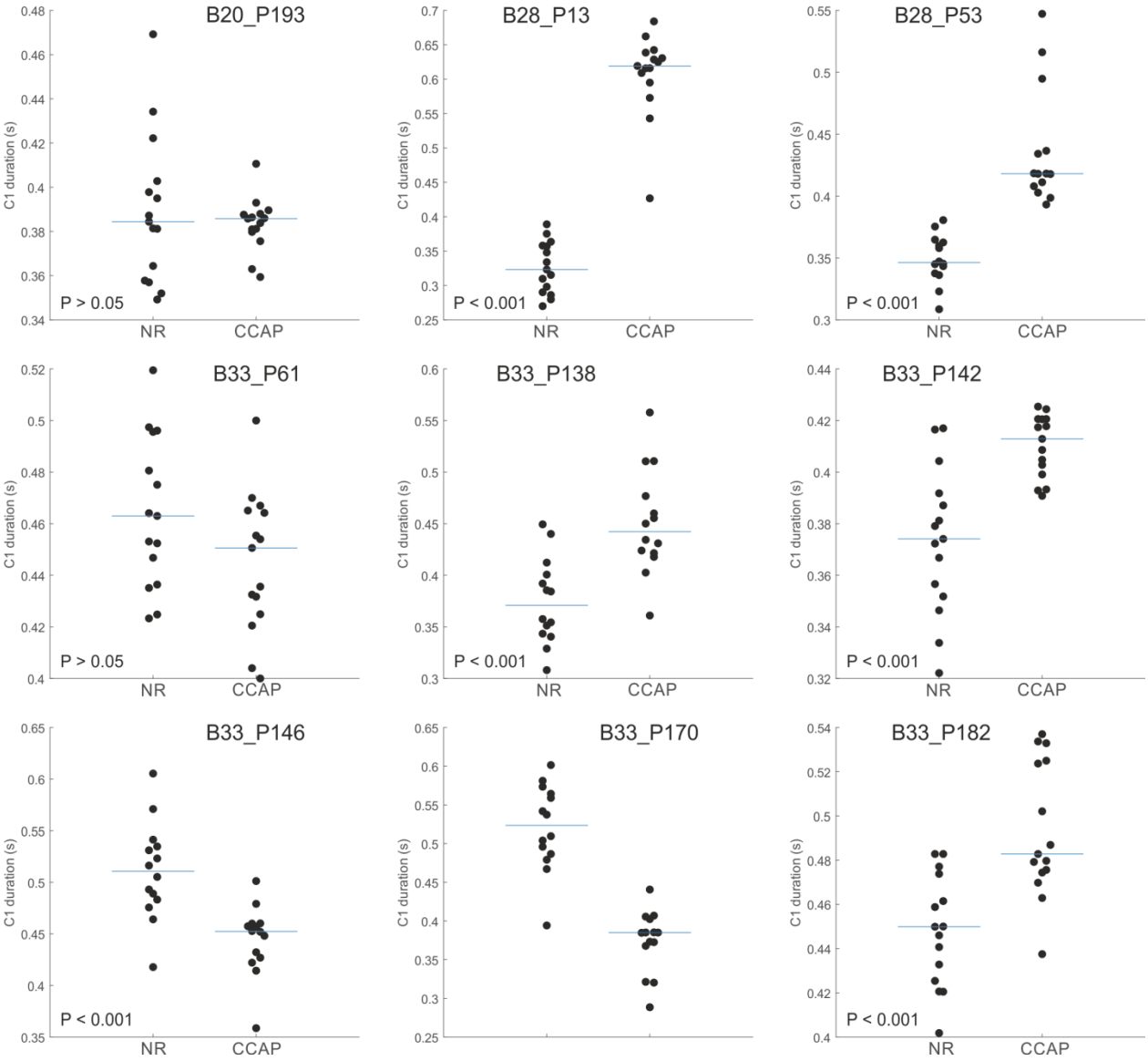

Supplementary Figure 26: ComInt1 duration in single experiments during NR and CCAP application.

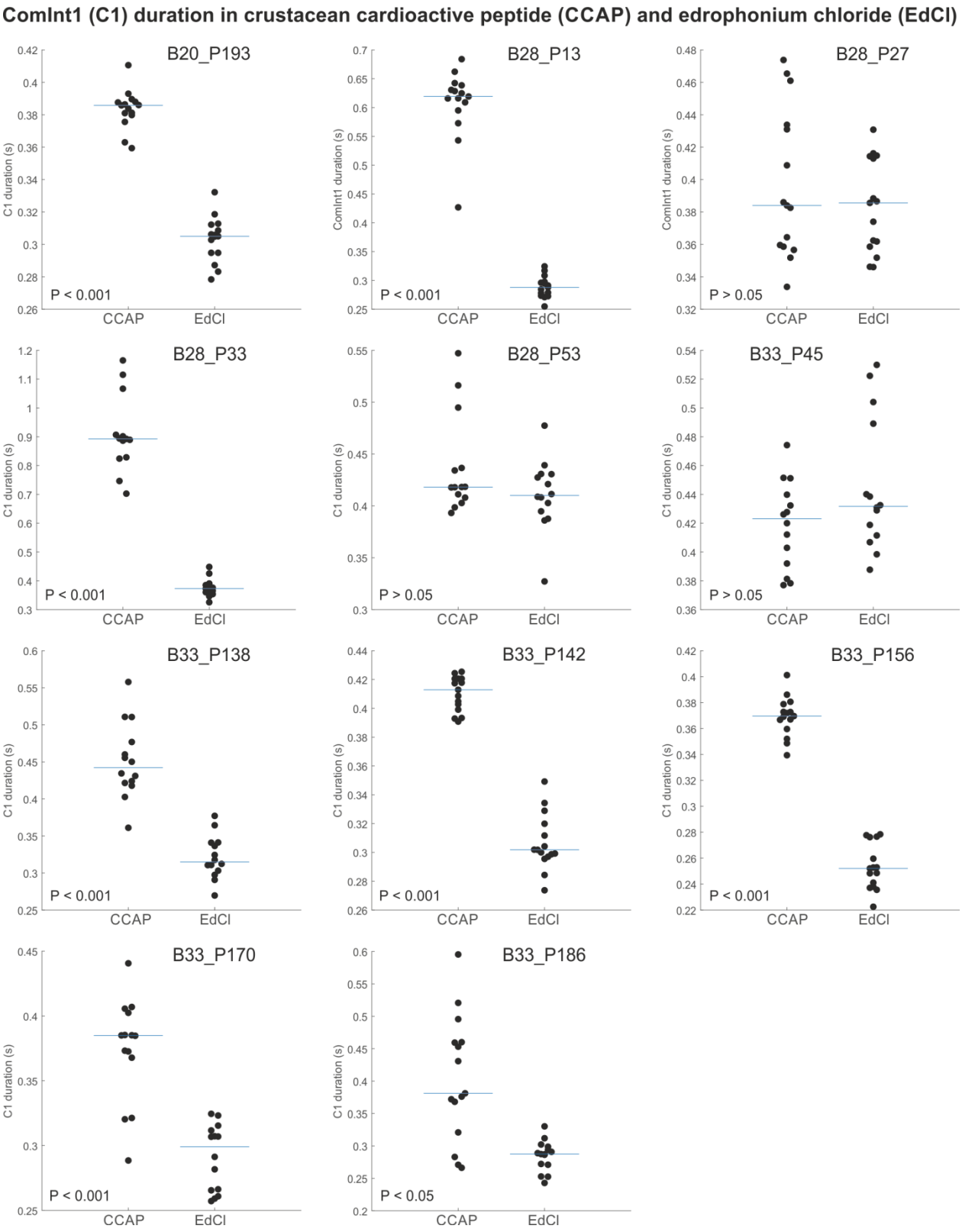

Supplementary Figure 27: ComInt1 duration in single experiments during CCAP and EdCl application.

ComInt1 (C1) duty cycle in normal saline (NR) and carbachol (CCh)

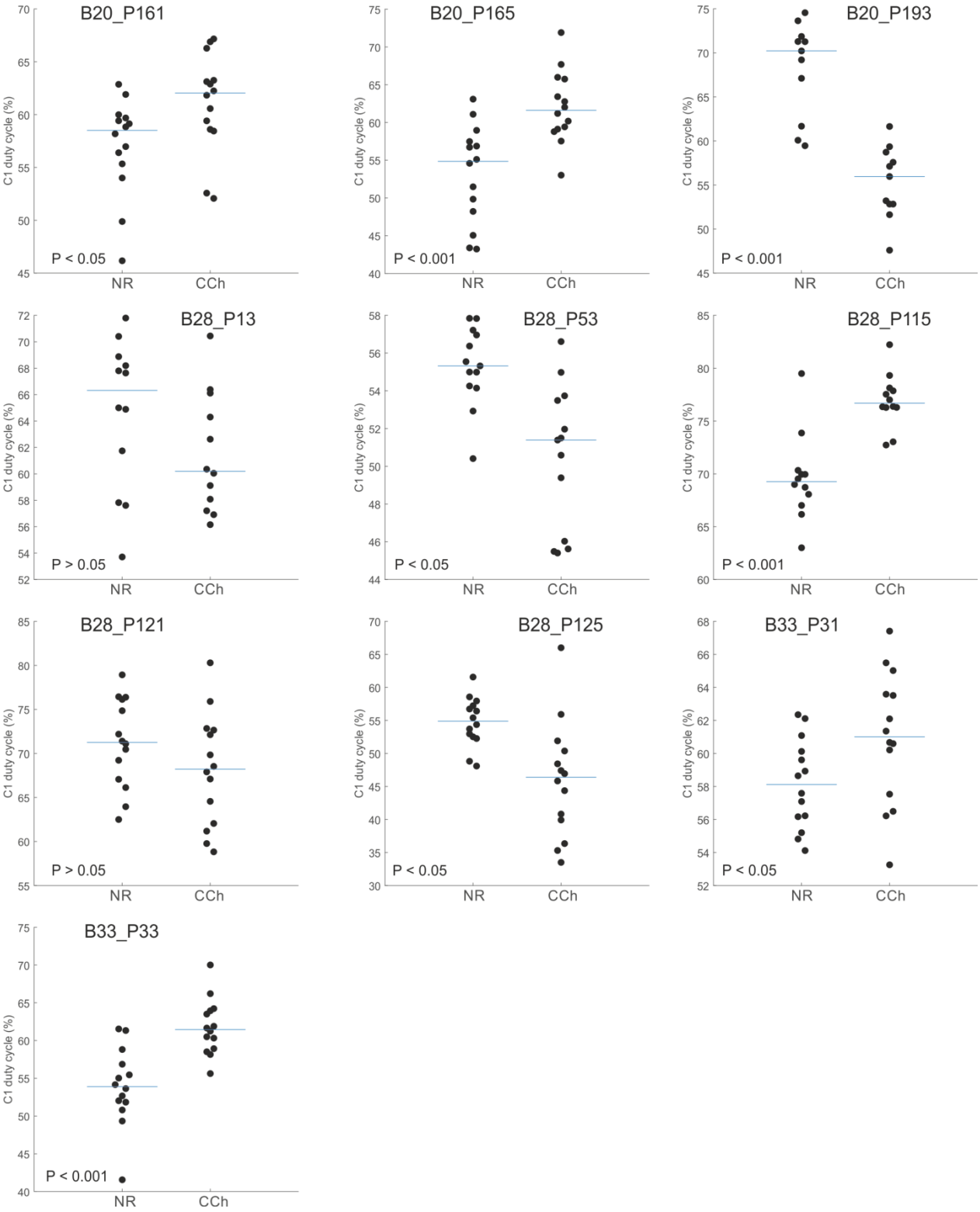

Supplementary Figure 28: ComInt1 duty cycle in single experiments during NR and CCh application.

ComInt1 (C1) duty cycle in normal saline (NR) and crustacean cardioactive peptide (CCAP)

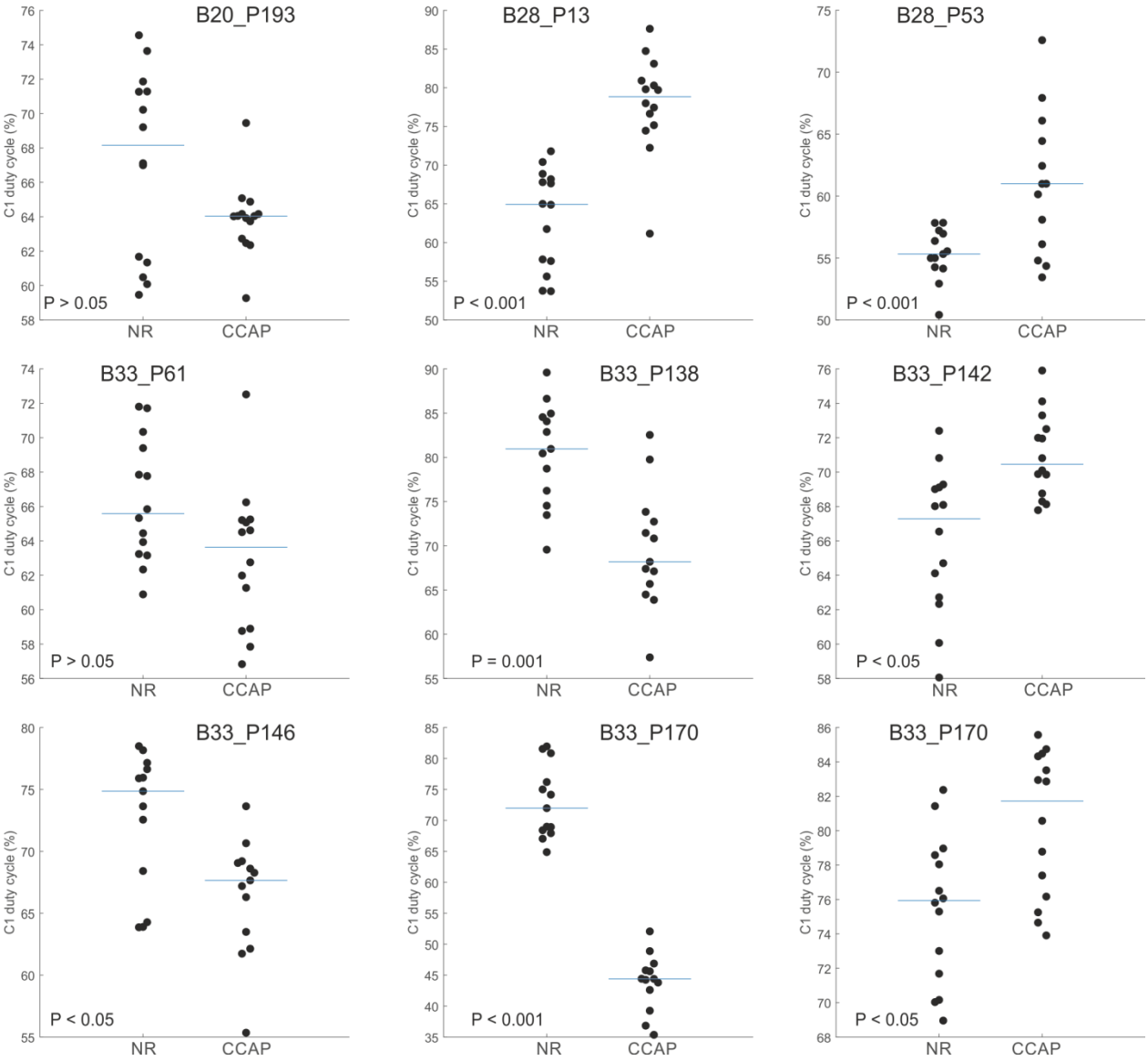

Supplementary Figure 29: ComInt1 duty cycle in single experiments during NR and CCAP application.

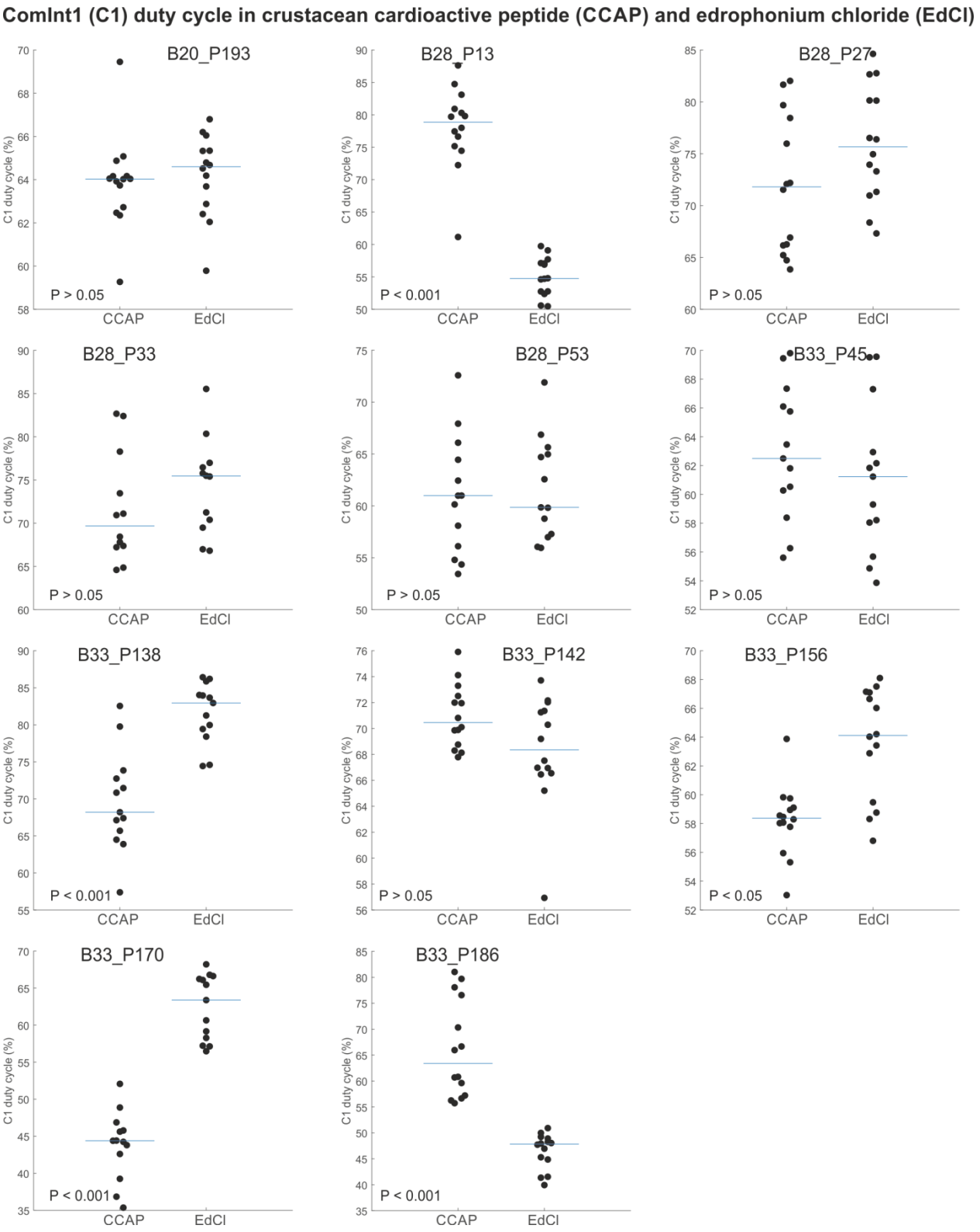

Supplementary Figure 30: ComInt1 duty cycle in single experiments during CCAP and EdCl application.

Membrane potential oscillation in normal saline (NR) and carbachol (CCh)

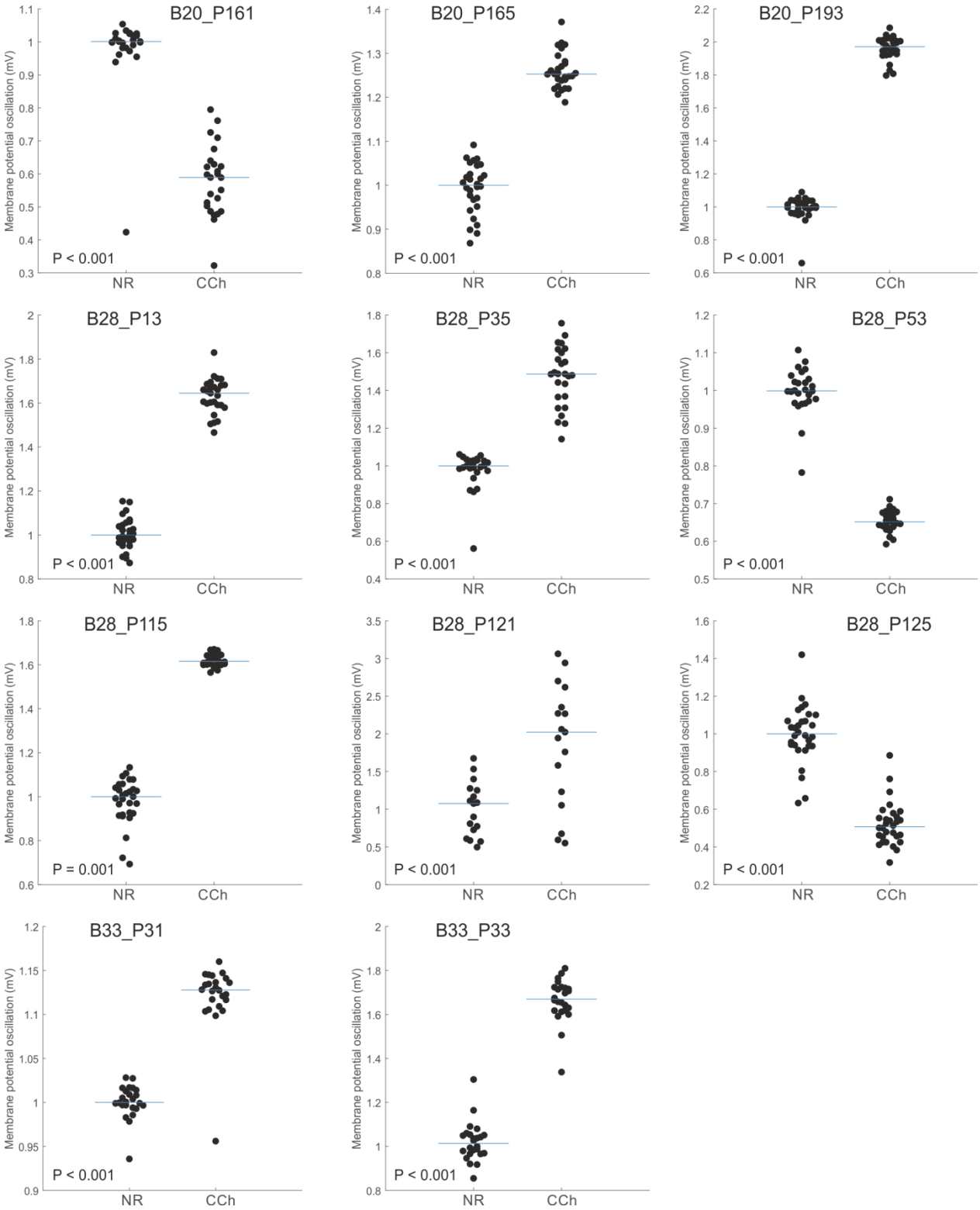

Supplementary Figure 31: Membrane potential oscillation amplitude in single experiments during NR and CCh application.

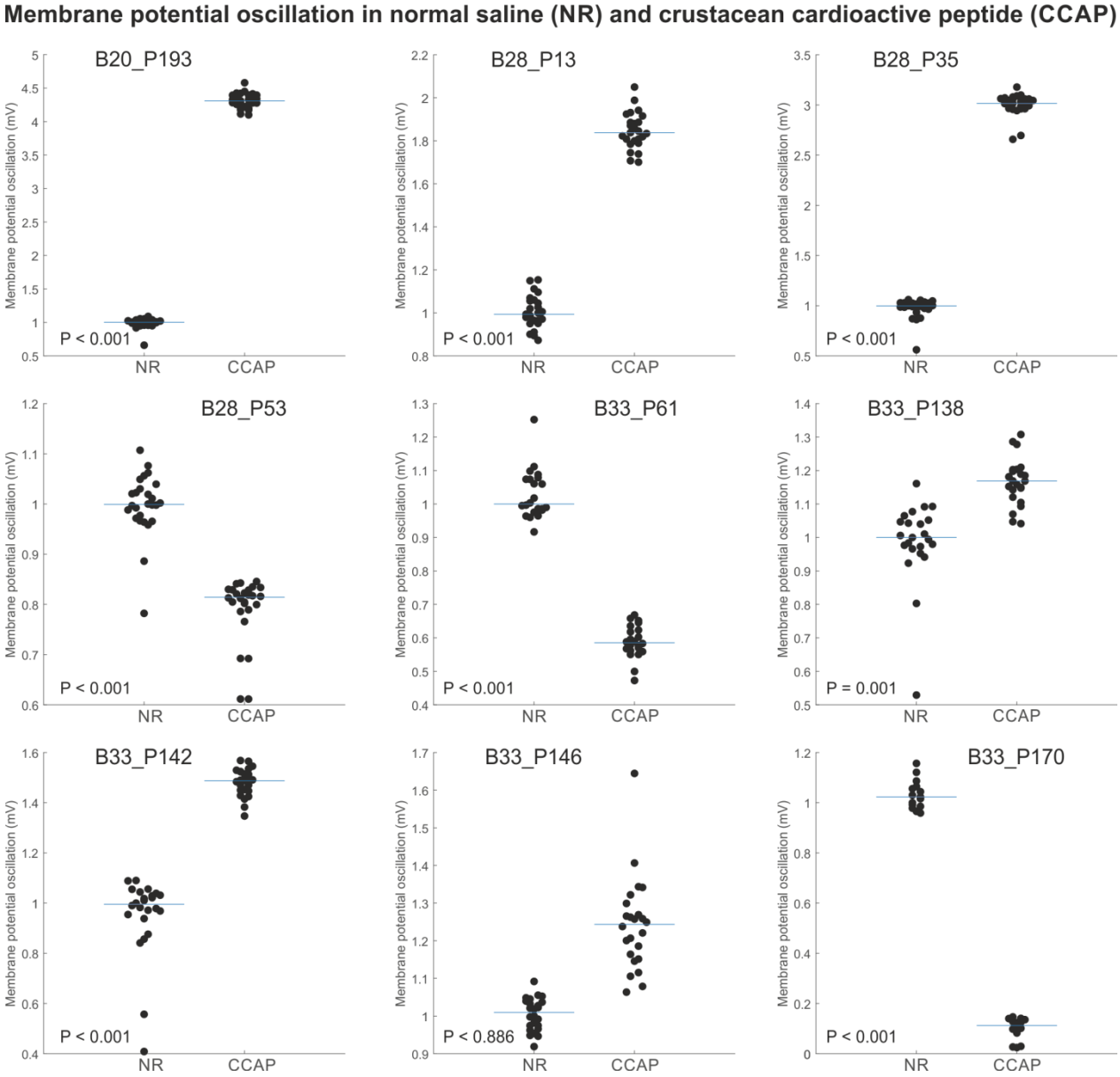

Supplementary Figure 32: Membrane potential oscillation amplitude in single experiments during NR and CCAP application.

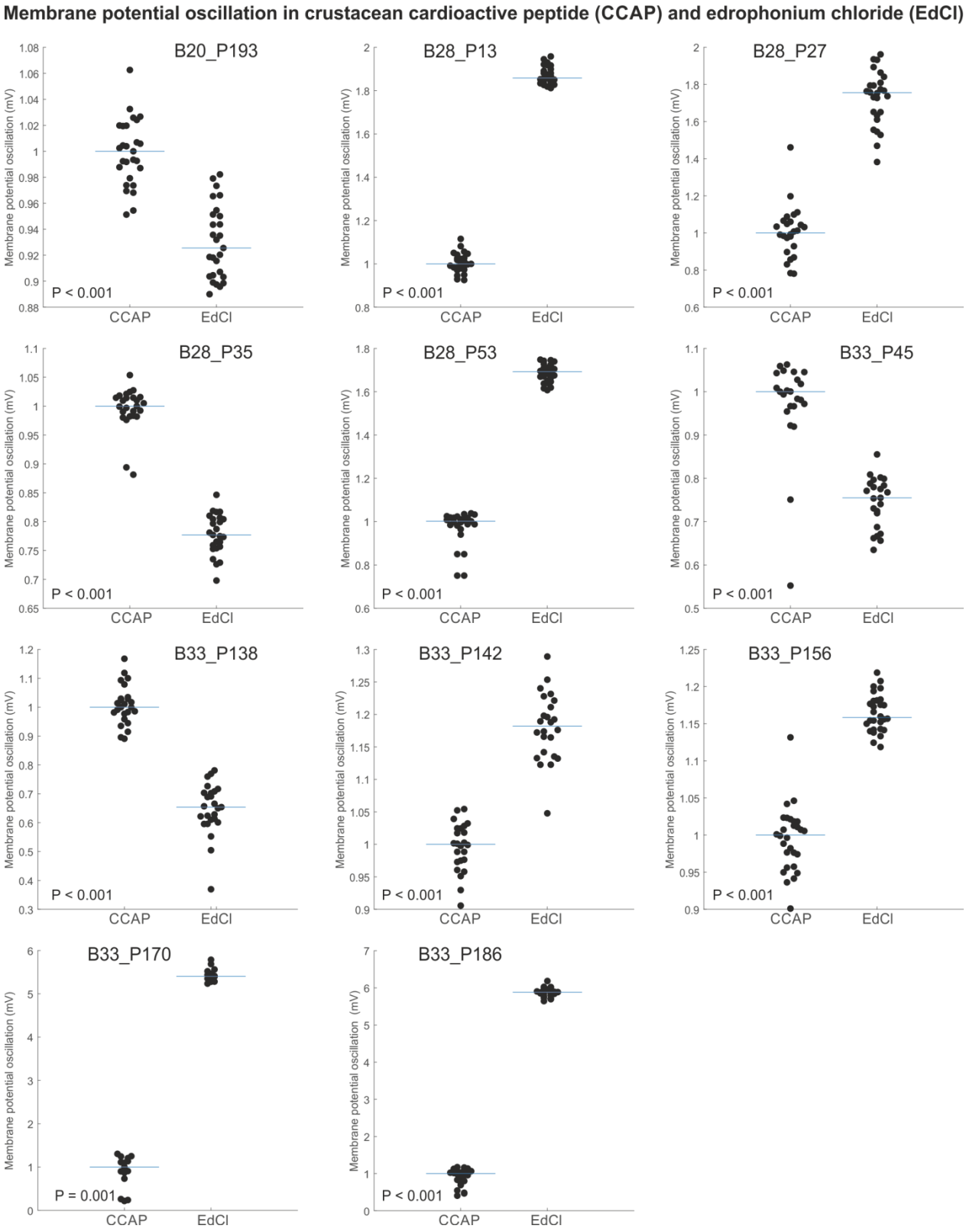

Supplementary Figure 33: Membrane potential oscillation amplitude in single experiments during CCAP and EdCl application.

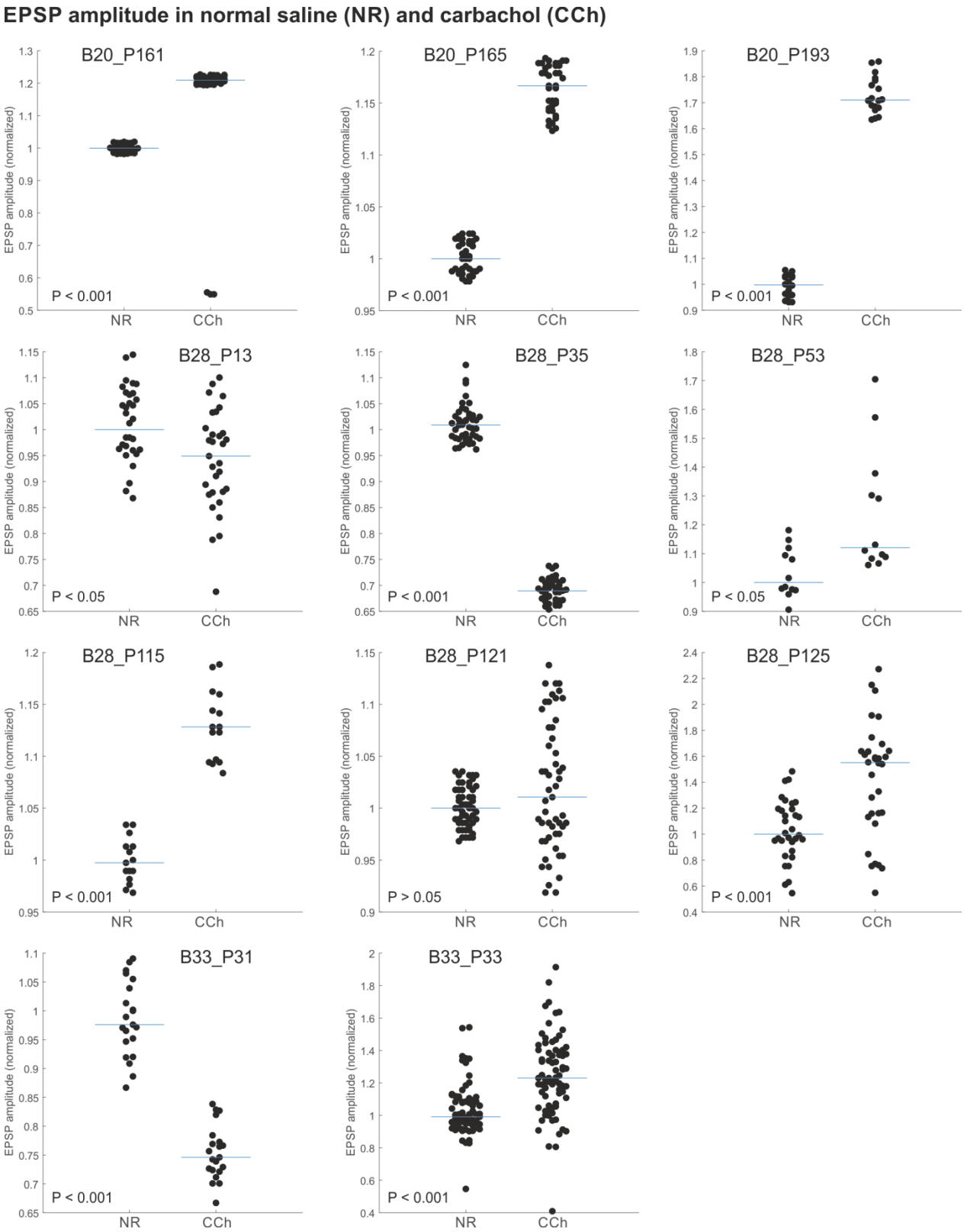

Supplementary Figure 34: Large EPSP amplitude in single experiments during NR and CCh application.

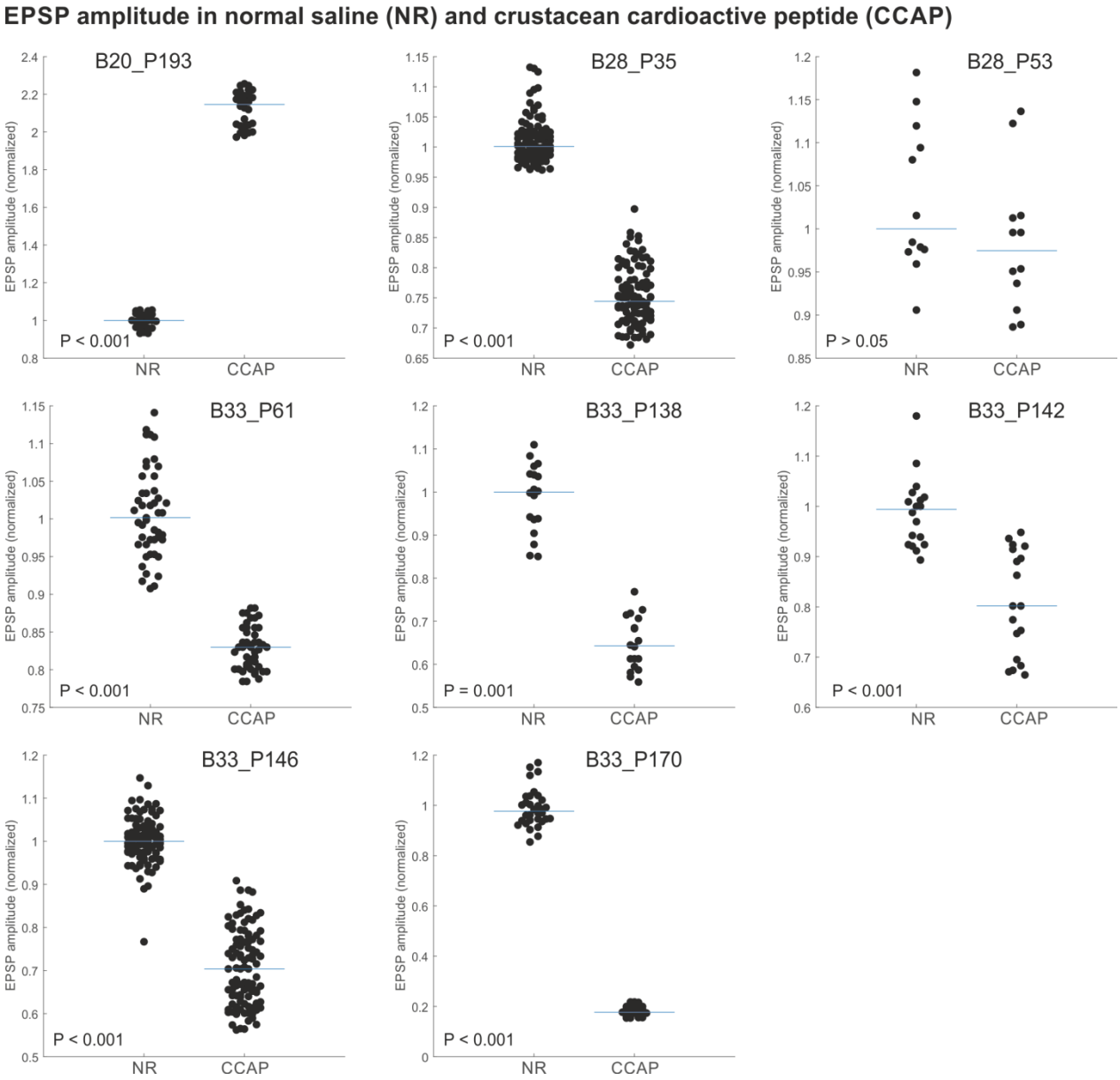

Supplementary Figure 35: Large EPSP amplitude in single experiments during NR and CCAP application.

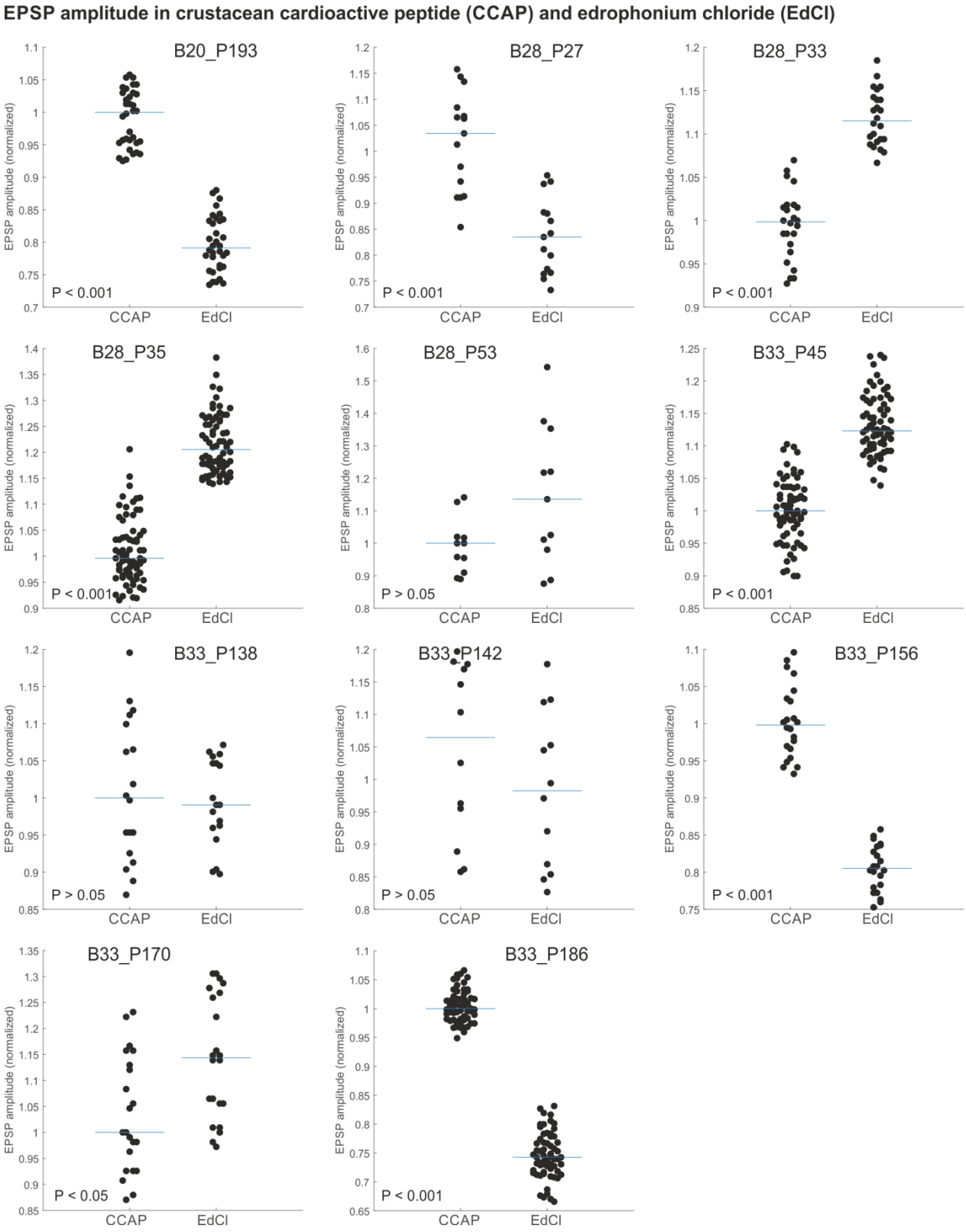

Supplementary Figure 36: Large EPSP amplitude in single experiments during CCAP and EdCl application.

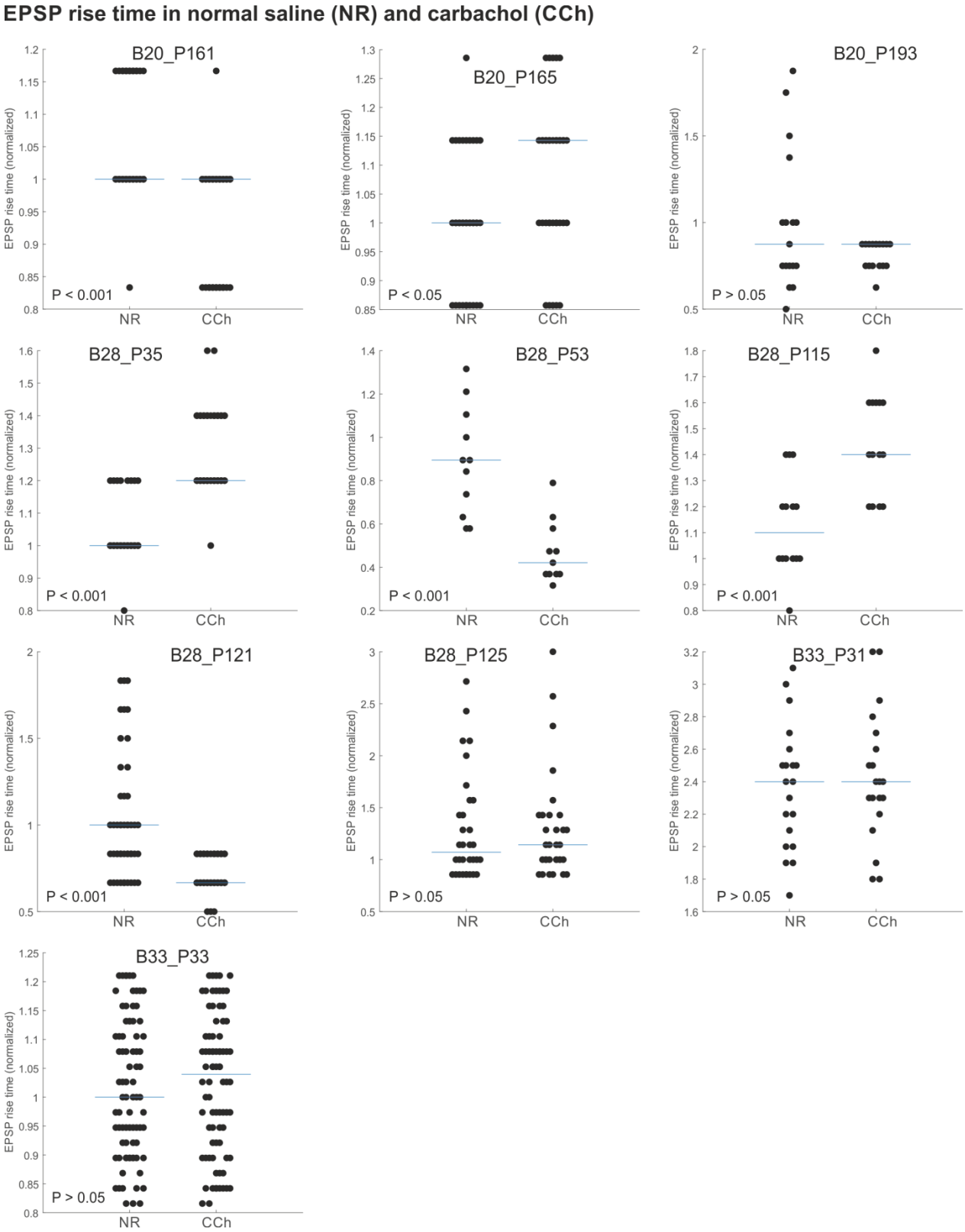

Supplementary Figure 37: Large EPSP rise time in single experiments during NR and CCh application.

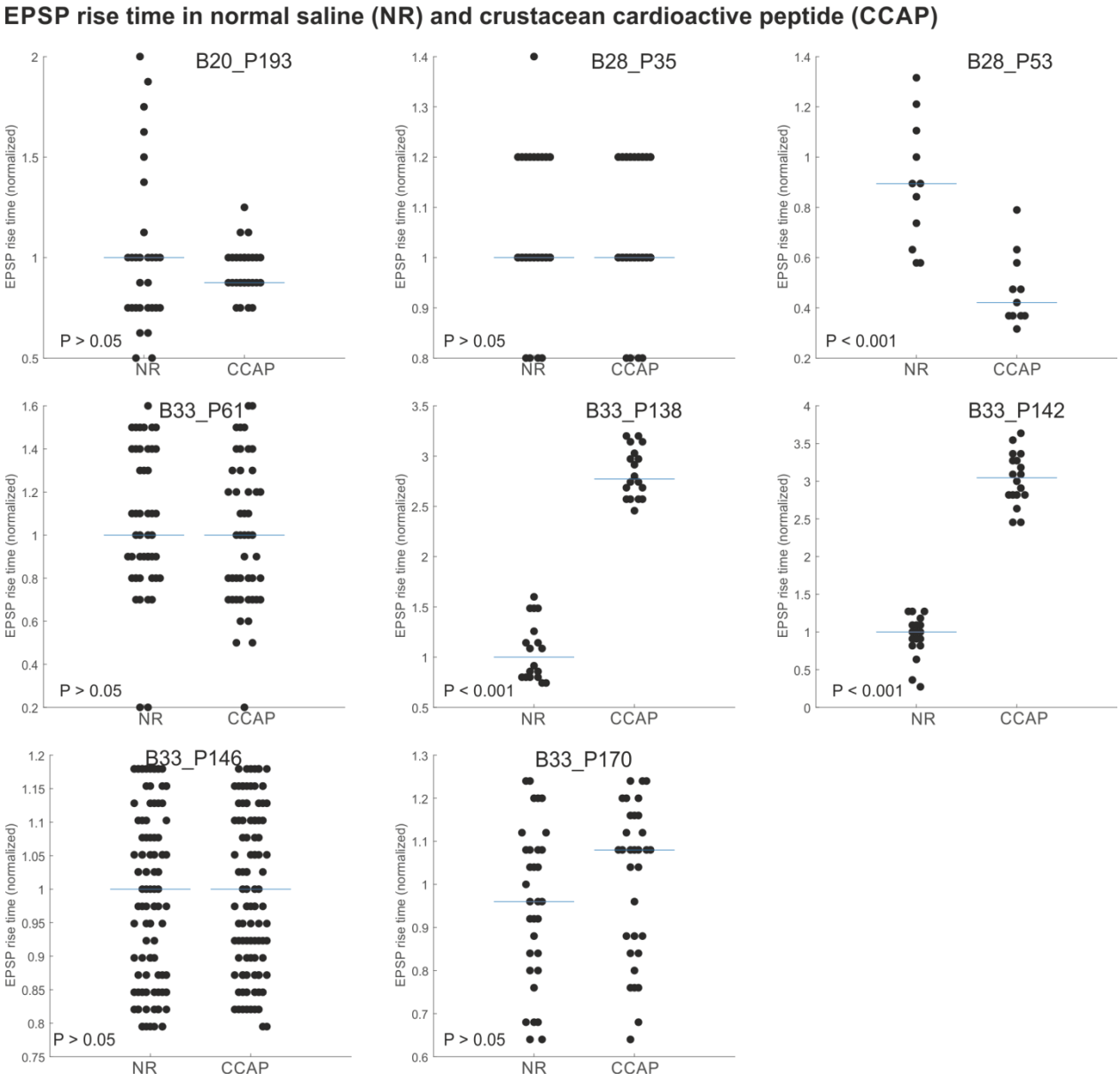

Supplementary Figure 38: Large EPSP rise time in single experiments during NR and CCAP application.

EPSP rise time in crustacean cardioactive peptide (CCAP) and edrophonium chloride (EdCl)

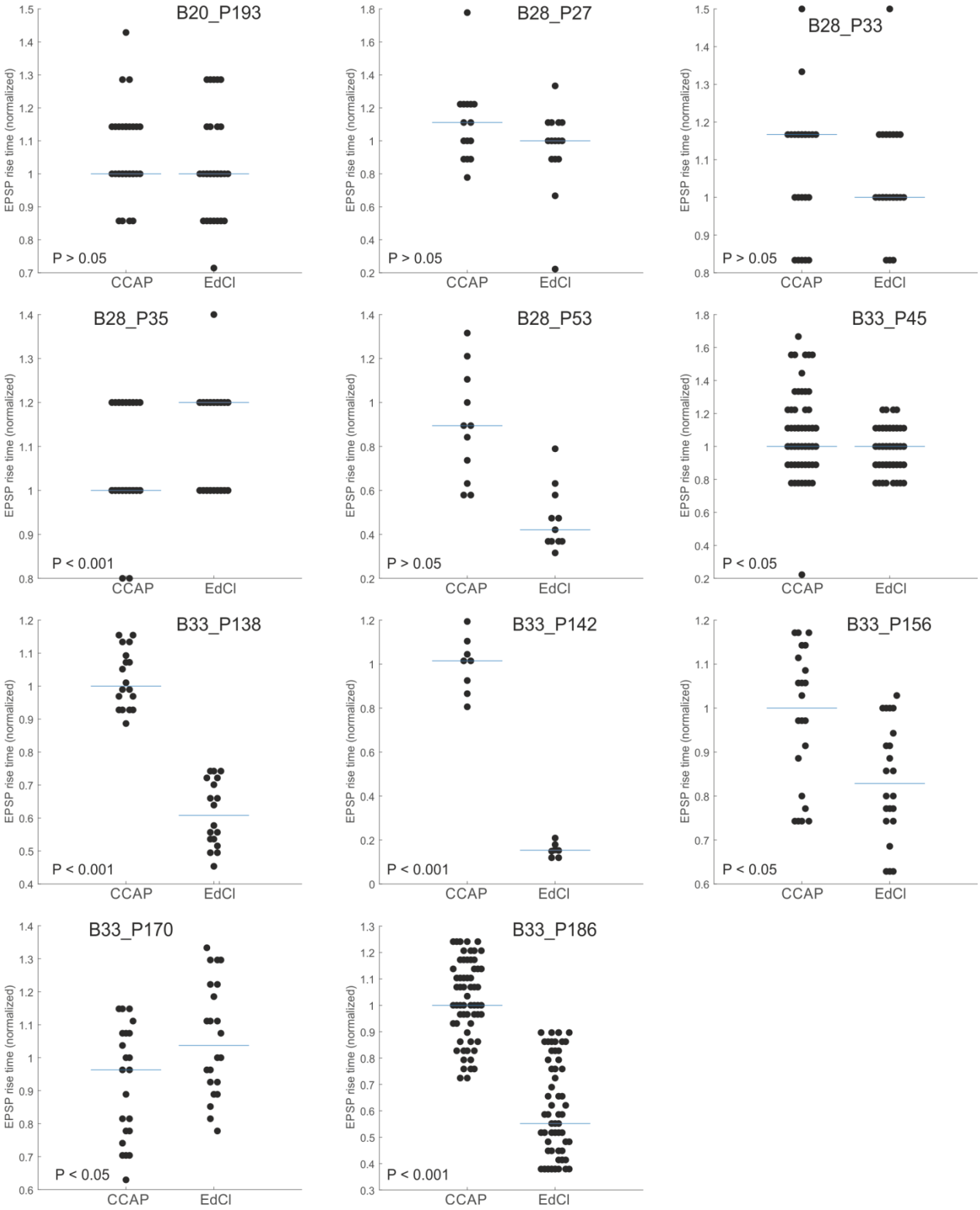

Supplementary Figure 39: Large EPSP rise time in single experiments during CCAP and EdCl application.

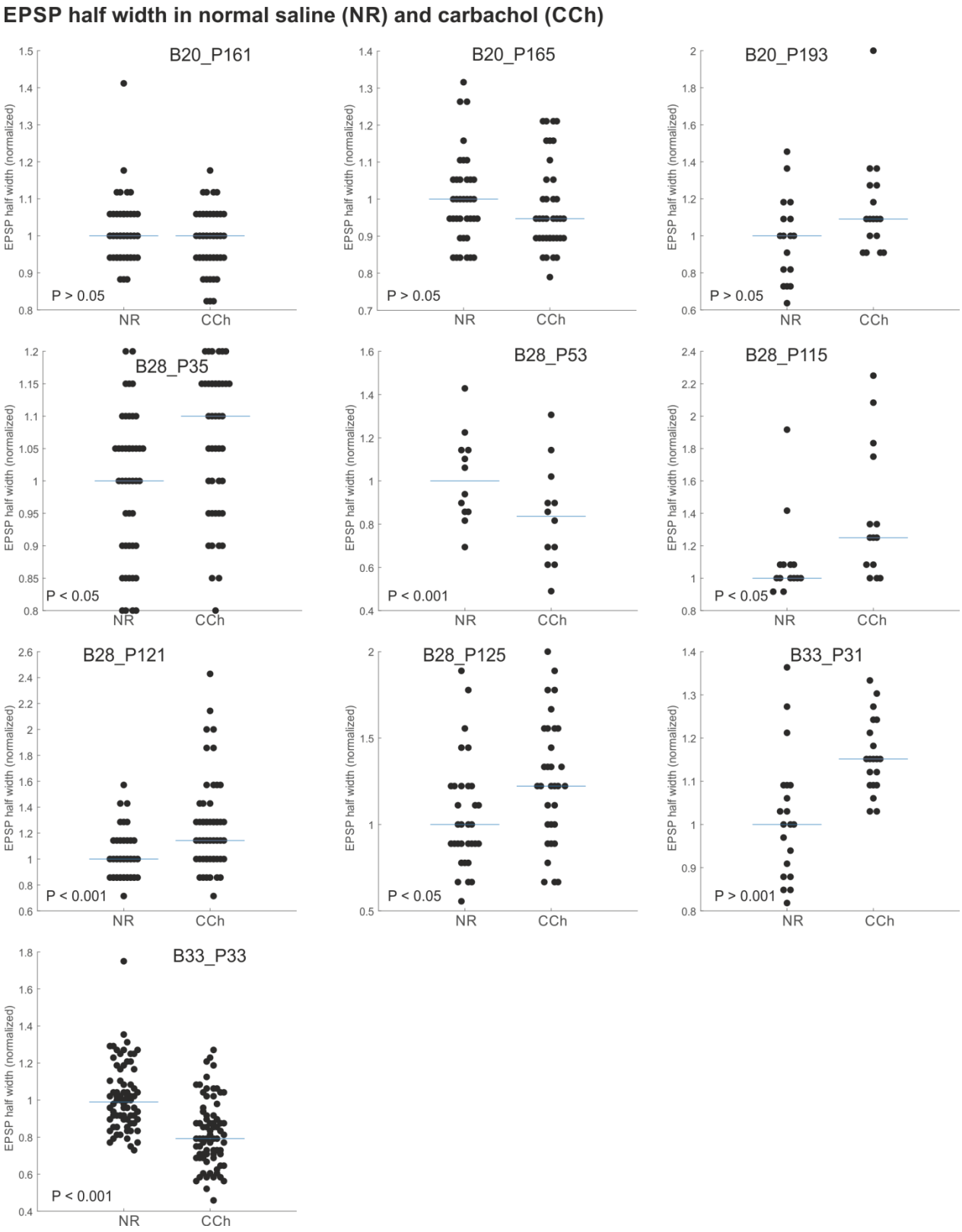

Supplementary Figure 40: Large EPSP half width in single experiments during NR and CCh application.

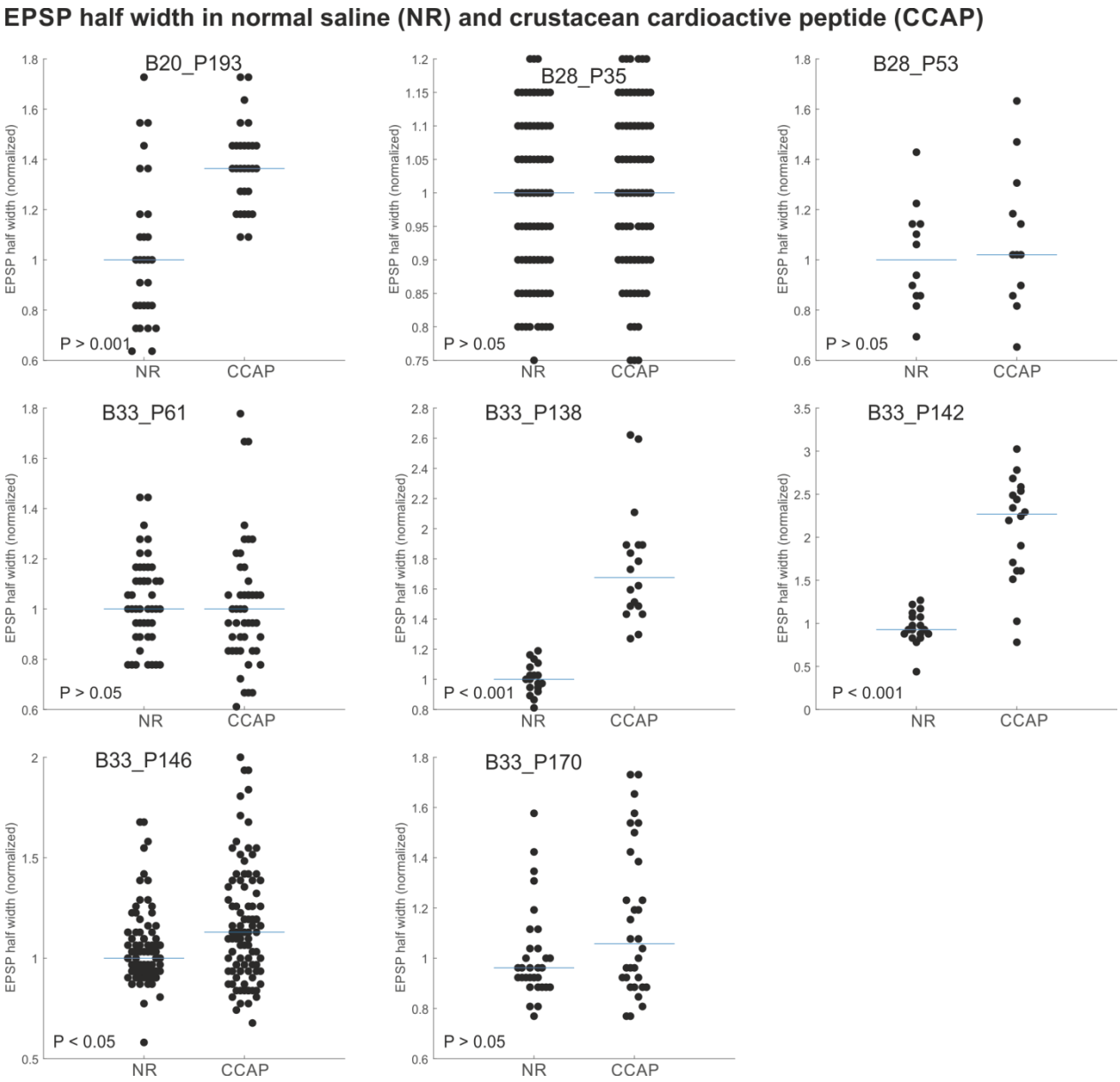

Supplementary Figure 41: Large EPSP half width in single experiments during NR and CCAP application.

EPSP half width in crustacean cardioactive peptide (CCAP) and edrophonium chloride (EdCl)

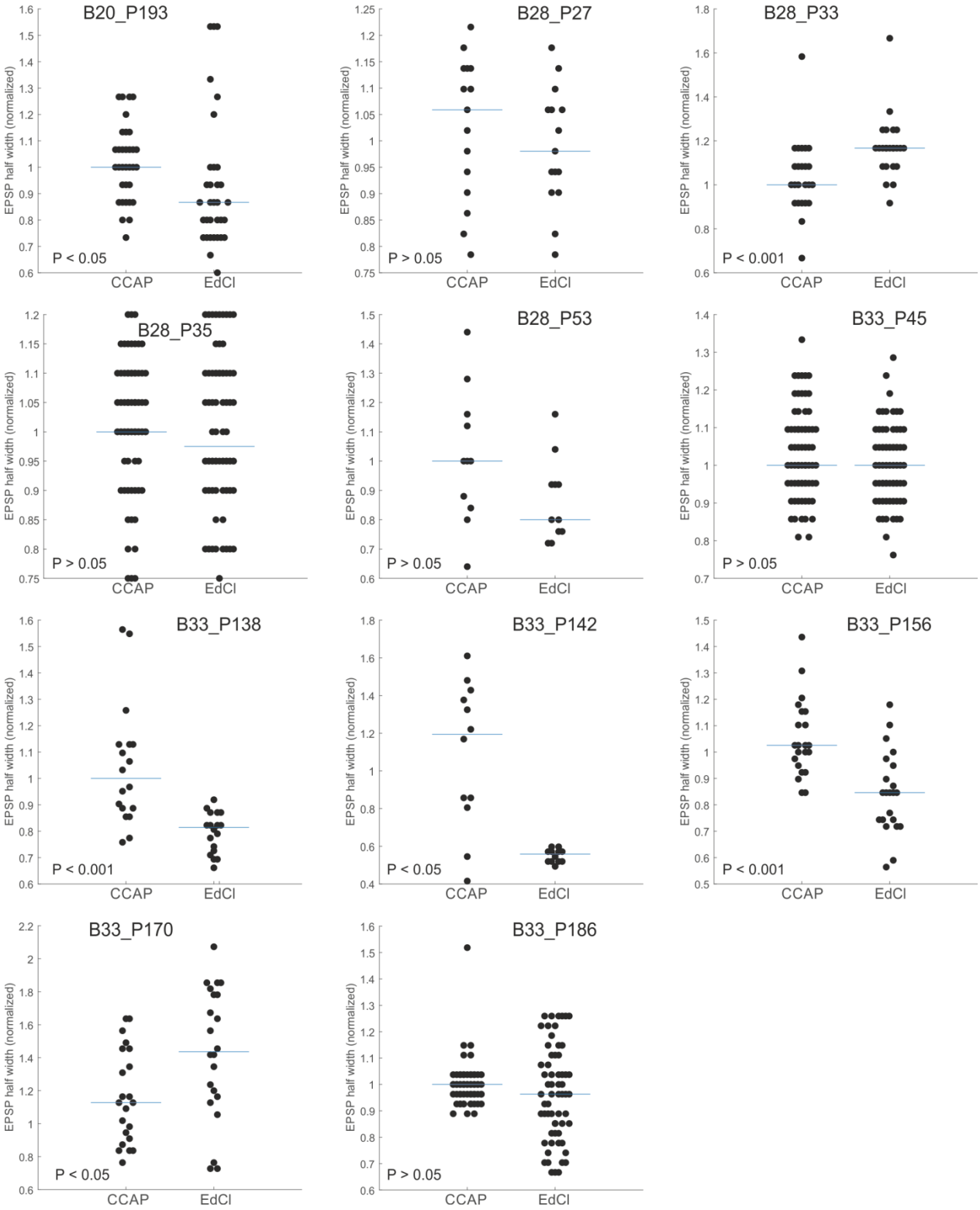

Supplementary Figure 42: Large EPSP half width in single experiments during CCAP and EdCl application.

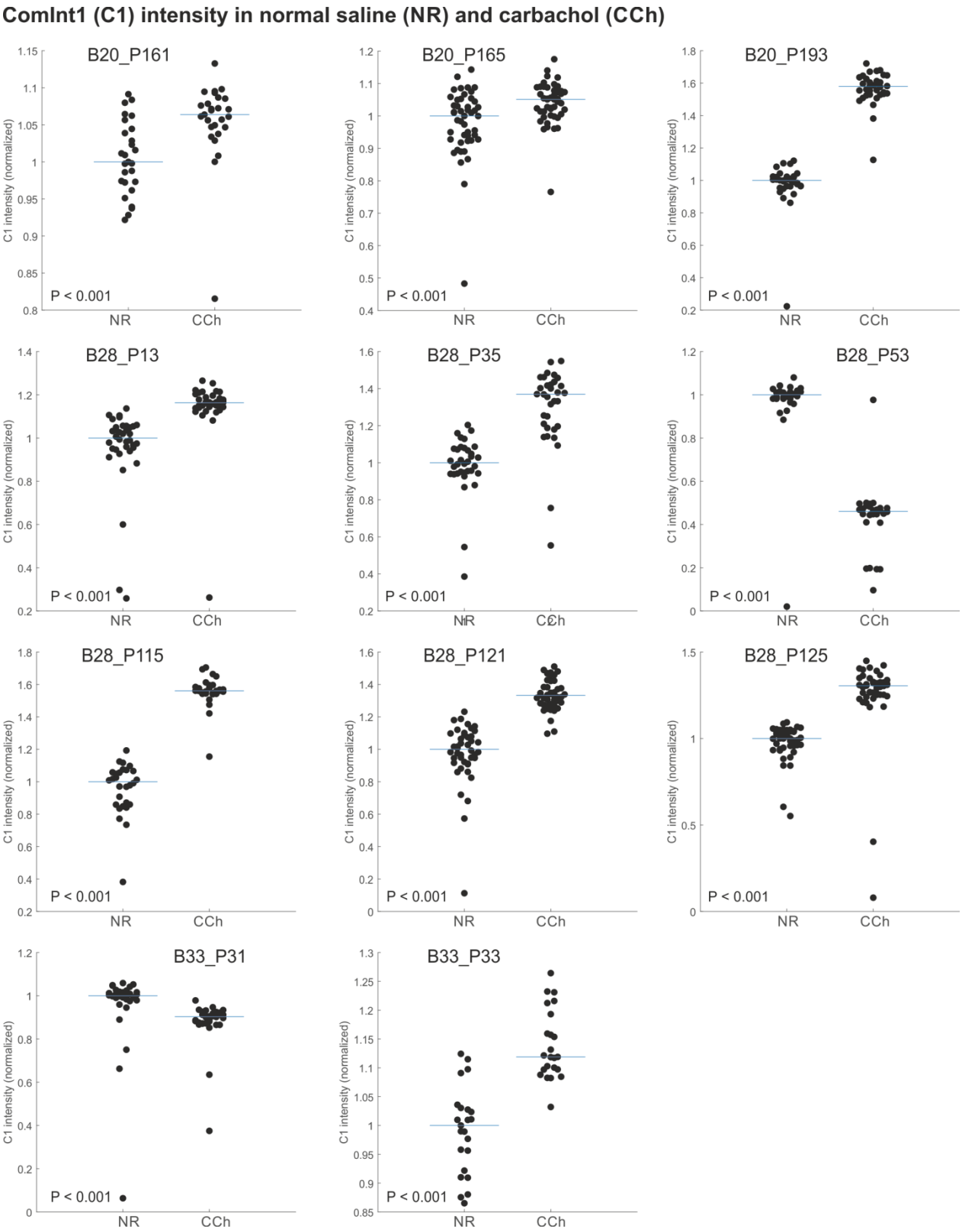

Supplementary Figure 43: C1 intensity in single experiments during NR and CCh application.

ComInt1 (C1) intensity in normal saline (NR) and crustacean cardioactive peptide (CCAP)

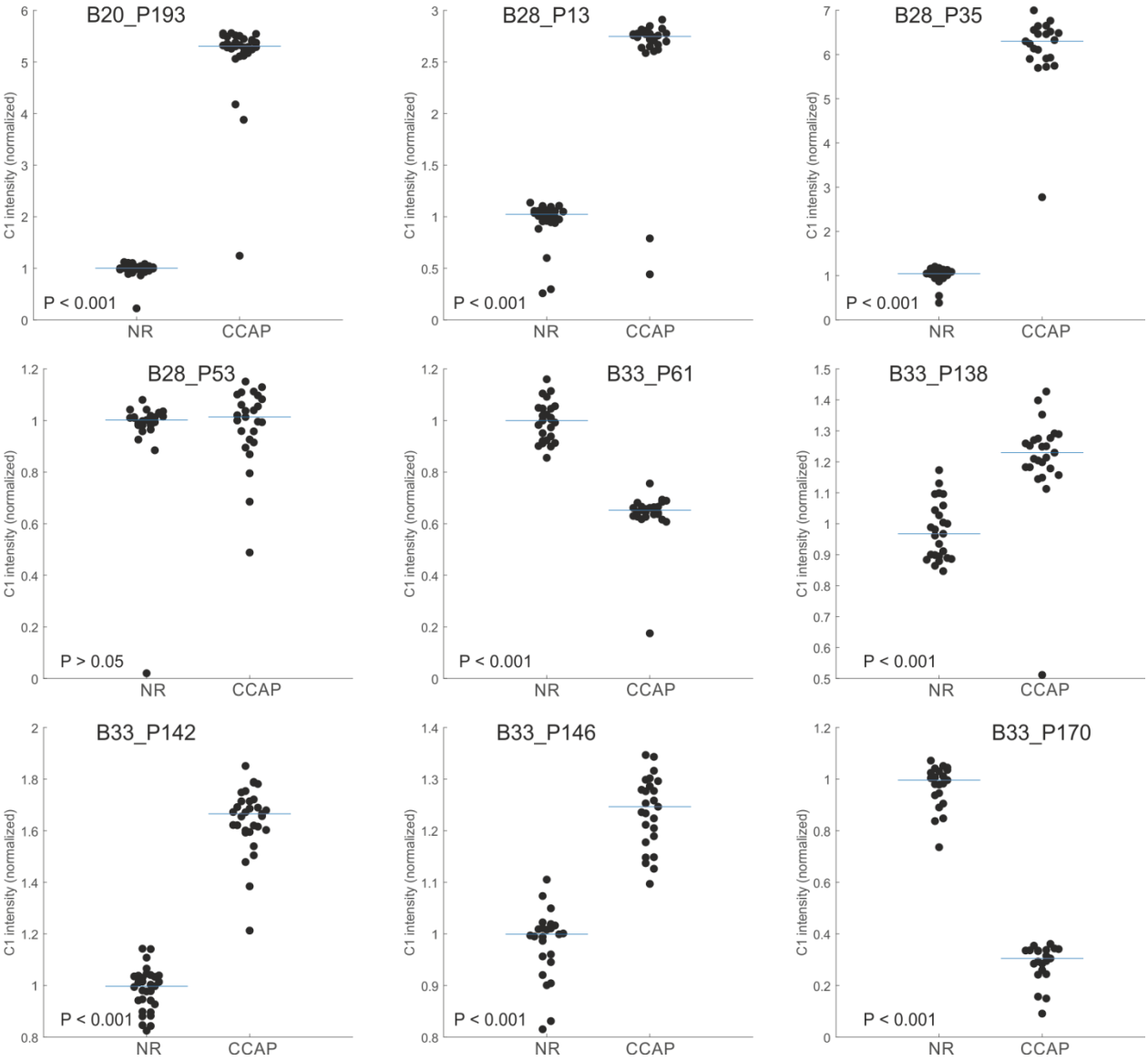

Supplementary Figure 44: C1 intensity in single experiments during NR and CCAP application.

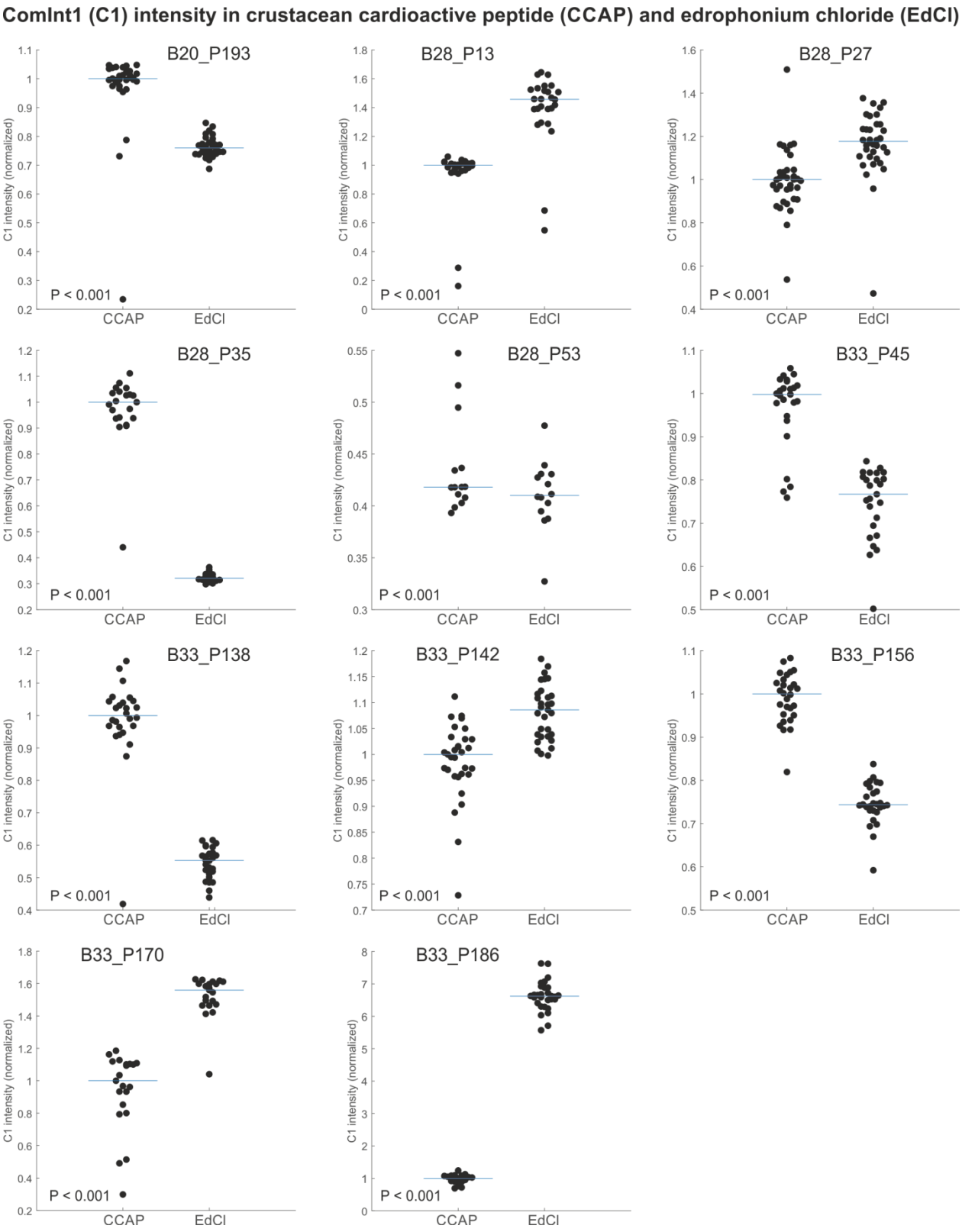

Supplementary Figure 45: C1 intensity in single experiments during CCAP and EdCl application.

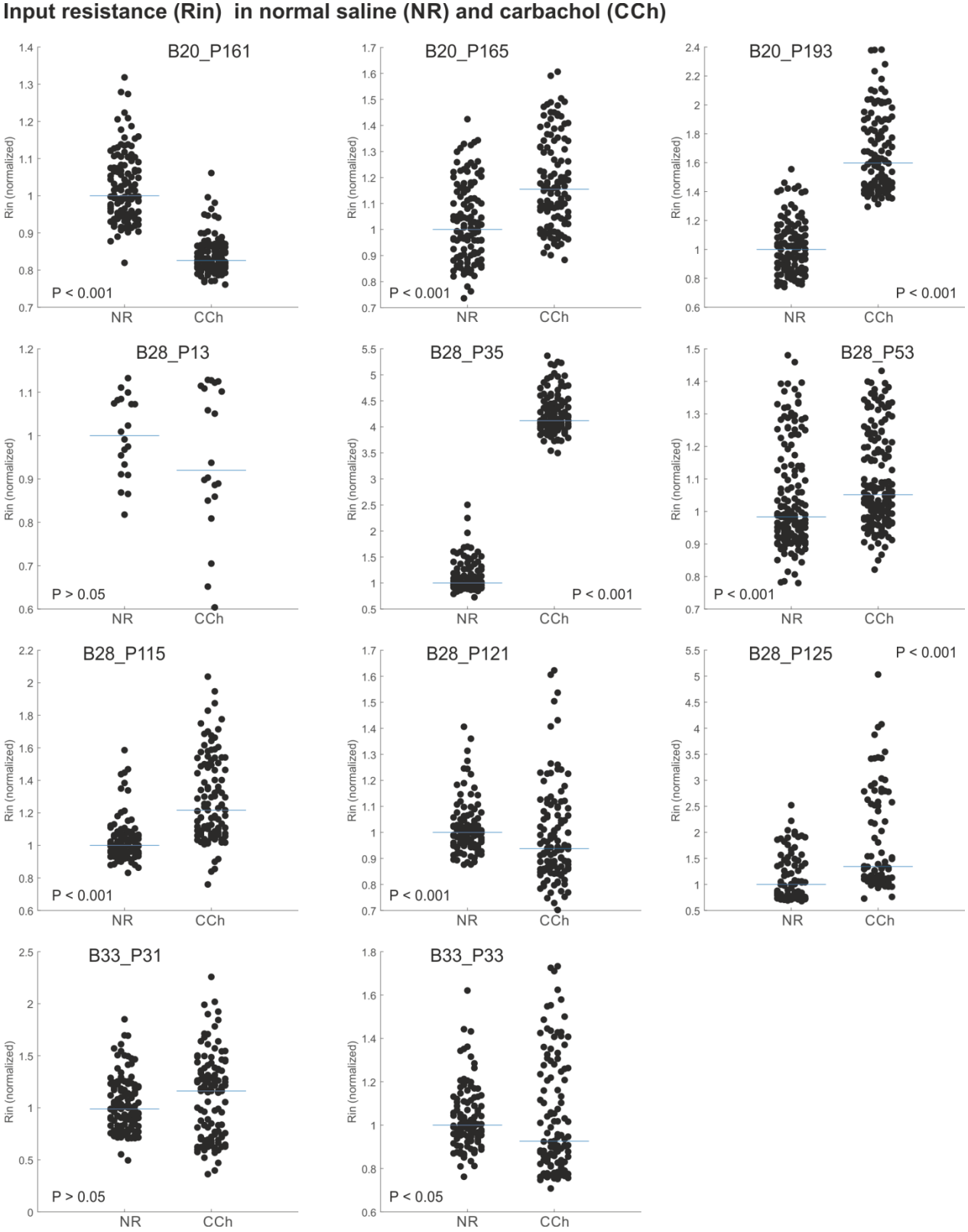

Supplementary Figure 46: Input resistance (R_{in}) in single experiments during NR and CCh application.

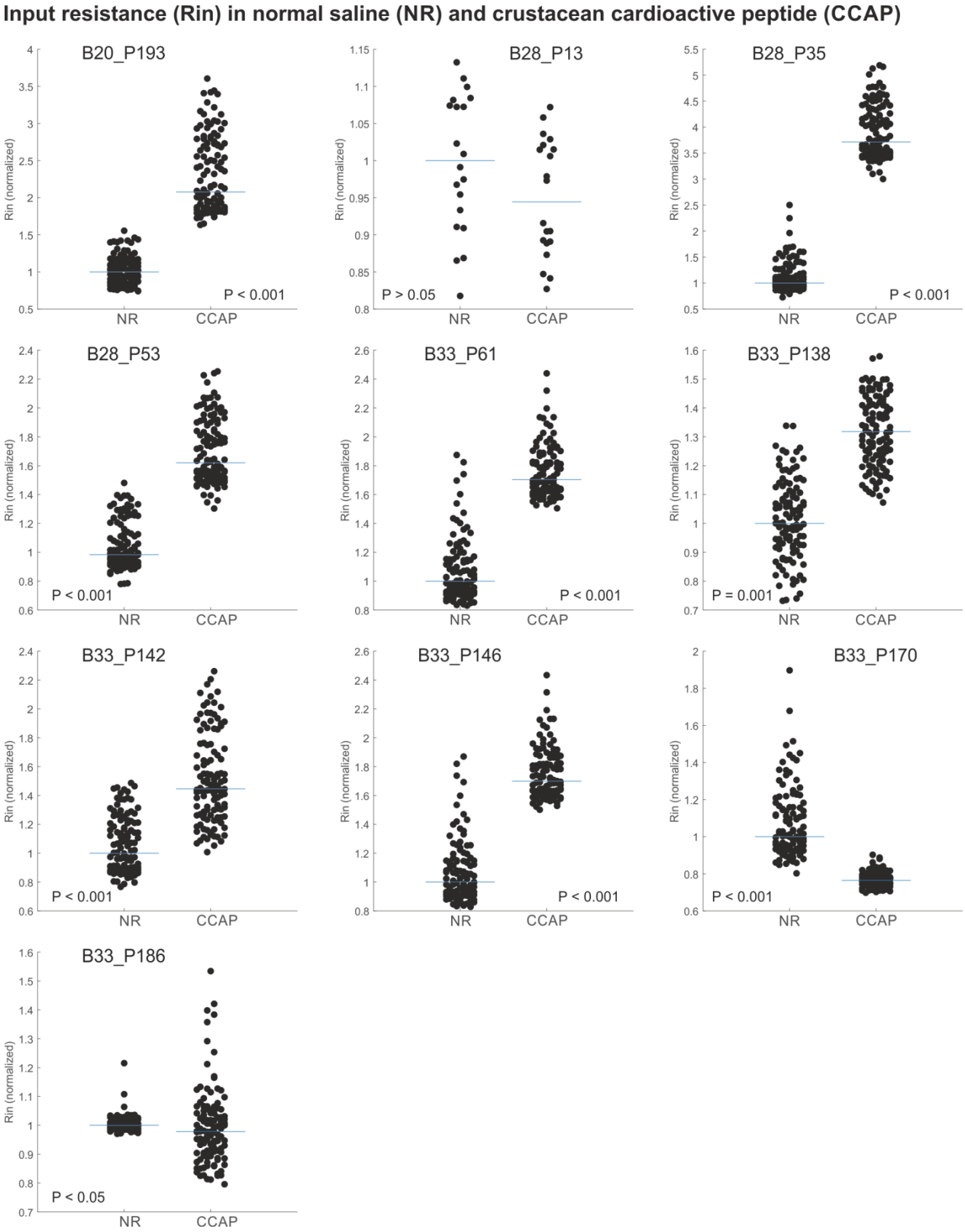

Supplementary Figure 47: Input resistance (R_{in}) in single experiments during NR and CCAP application.

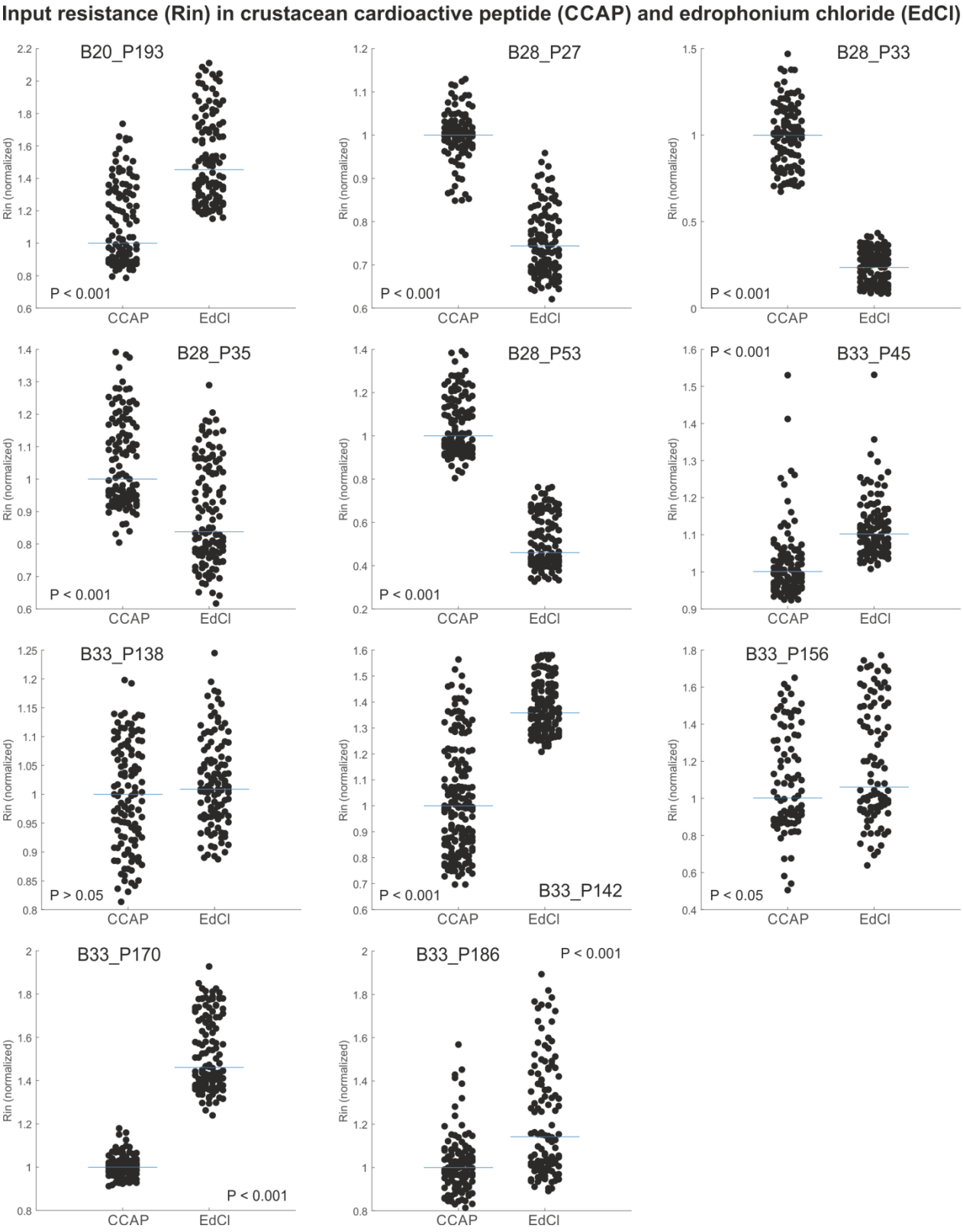

Supplementary Figure 48: Input resistance (R_{in}) in single experiments during CCAP and EdCl application.

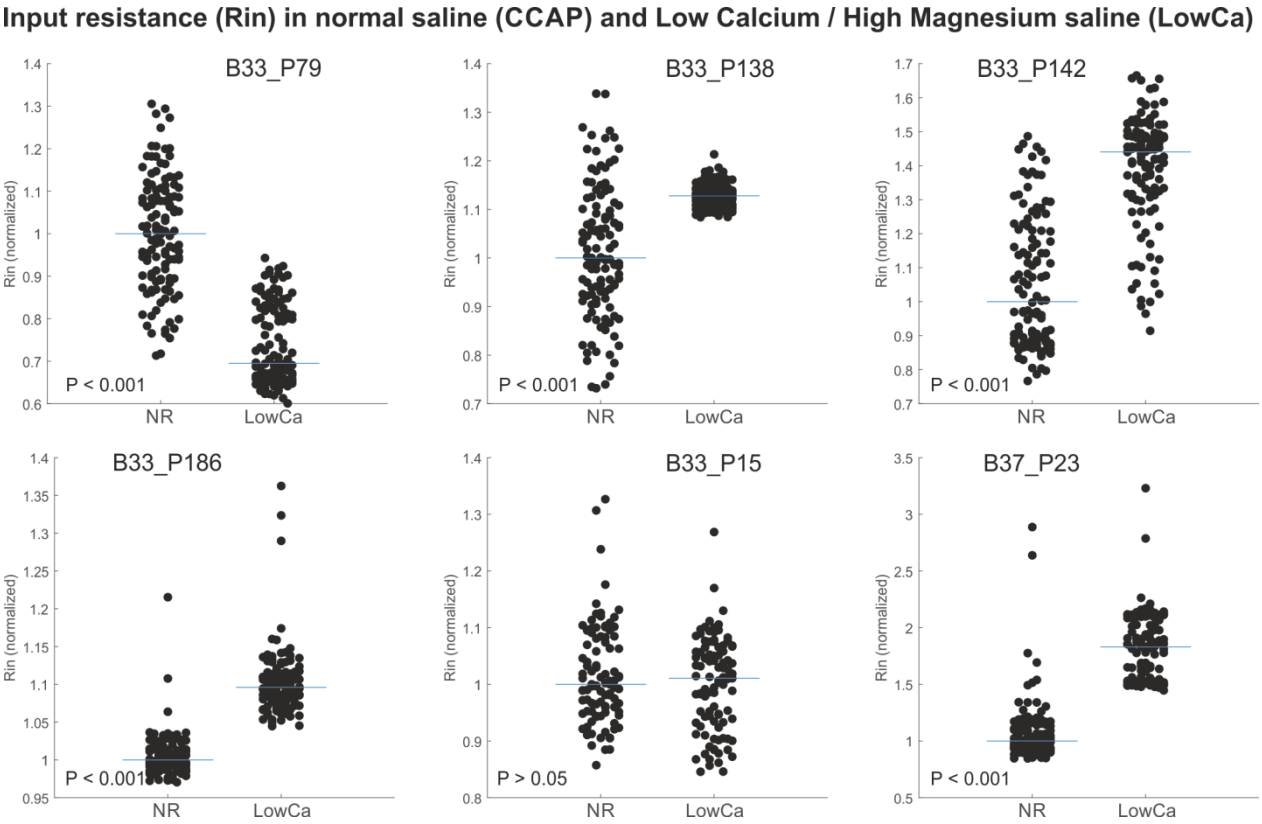

Supplementary Figure 49: Input resistance (R_{in}) in single experiments during NR and LowCa application.

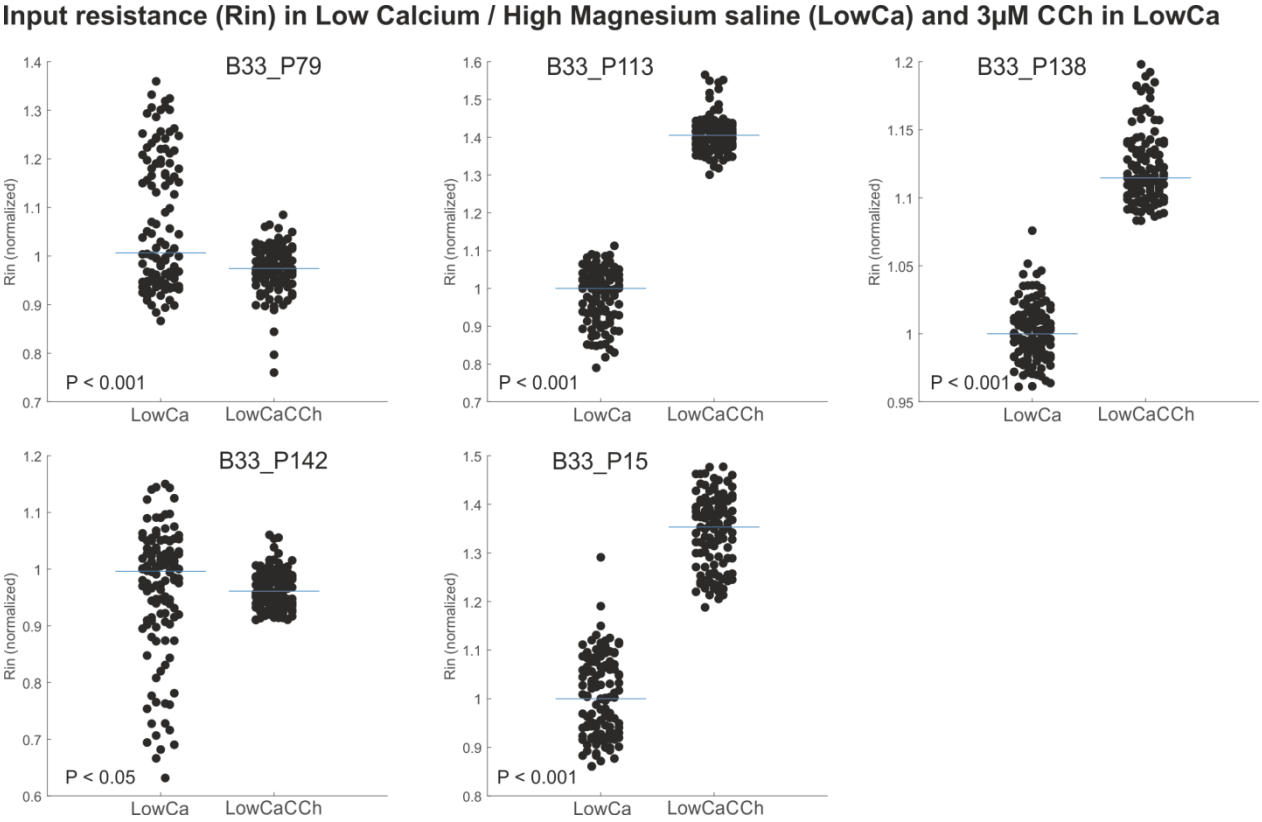

Supplementary Figure 50: Input resistance (R_{in}) in single experiments during LowCa and LowCaCCh application.

Acknowledgements

First and foremost, I have to thank Dr. Carmen Wellmann, the supervisor of my thesis and concurrently the person, who tolerated me for the last 7 and something years. She made this thesis possible, always supported me and had a lot of patience with me, even if things did not go so well… Thank you Carmen!!! It has been a pleasure to work in your research group.

Special thanks go to the other members of my thesis committee, Prof. Dr. Ansgar Büschges and Prof. Dr. Sigrun Korsching. Furthermore, I have to thank Ansgar Büschges for being second assessor of this thesis. Also he tolerated me for the last 7 and something years and he was always there when I needed him… Ansgar, thank you very much!!!

Moreover, I have to thank the world's best research group, AG Wellmann. Felix, Laura, Heike. Thank you for soothing each day in the office. Felix… thank you for supporting me and for the corrections of some parts of my thesis. Heike… thank you for providing all materials and solutions. Laura… thank you for everything, without you, everything would not have been possible. I also have to thank the former members of the world's best research group, especially Anna. She supported me in every sense (especially MATLAB and corrections), no matter where she lives… Newark, Cologne, Internet is the main thing.

I also thank all members of the research group of AG Büschges and AG Daun for the helpfulness, nice breaks and the nice work climate. In this context I have to highlight Tommi and Joschi… Thank you guys for supporting me and also for reading some pages of my thesis… Tommi… I know, it was hard.

Another thank goes to all my friends who were always there for me and also supported me during the course of my thesis. In this sense: "HIIIIYYYYYAAAAAHHH"

Mama und Papa… euch kann man ja nur danken und zwar für alles was ihr jemals für mich getan habt und ich zu dem geworden bin, was ich bin… Danke euch, dass ihr immer für mich da wart und auch sein werdet.

This work was funded by the DFG's Emmy Noether-Programm SM 206/2-1

Eigenständigkeitserklärung

Ich versichere, dass ich die von mir vorgelegte Dissertation selbständig angefertigt, die benutzten Quellen und Hilfsmittel vollständig angegeben und die Stellen der Arbeit − einschließlich Tabellen, Karten und Abbildungen −, die anderen Werken im Wortlaut oder dem Sinn nach entnommen sind, in jedem Einzelfall als Entlehnung kenntlich gemacht habe; dass diese Dissertation noch keiner anderen Fakultät oder Universität zur Prüfung vorgelegen hat; dass sie − abgesehen von unten angegebenen Teilpublikationen − noch nicht veröffentlicht worden ist, sowie, dass ich eine solche Veröffentlichung vor Abschluss des Promotionsverfahrens nicht vornehmen werde. Die Bestimmungen der Promotionsordnung sind mir bekannt. Die von mir vorgelegte Dissertation ist von Dr. Carmen Wellmann betreut worden.

Köln, den 23.01.2019